UNIVERSITÀ DI PARMA

UNIVERSITA' DEGLI STUDI DI PARMA

Dottorato di Ricerca in Scienze del Farmaco, delle Biomolecole e dei Prodotti per la Salute

Ciclo XXXII

Inhibition of FGFR and EGFR Signalling by Ligand Traps and Kinase Inhibitors for Anti-Cancer Drug Discovery

Coordinatore:

Chiar.mo Prof. Marco Mor

Tutore:

Chiar.mo Prof. Marco Mor

Dottorando

Giuseppe Marseglia

Anni 2016/2019

Acknowledgements

I would like to express my gratitude to Professor Marco Mor for having given me the chance to work in the field of medicinal chemistry. This experience allowed me to grow not only as a scientist but also as a person. I thank him for his enthusiasm and the sincere guidance.

I express my thankfulness to Professor Alessio Lodola and Professor Silvia Rivara for advice they have given me and for the stimulating conversations about our research work. I would like to thank all the members of the research group: Professor Federica Vacondio, Dr. Laura Scalvini, Dr. Donatella Callegari, Dr. Francesca Ferlenghi, Dr. Martina Maccesi, Andrea Ghidini and the former master students Monia Zerbini and Jennifer Ferrara.

I am deeply indebted with Dr. Riccardo Castelli, for the time he spent to guide me through the laboratory activities and for having taught me about organic chemistry.

I especially thank Nicole Bozza, the best lab-mate one could wish. I have really appreciated our scientific and non-scientific discussions and I thank her for having shared with me concerns, defeats, results and successes about our work.

I am also indebted with Professor Anders Bach for having given me the possibility to carry out a research period at the University of Copenhagen. I thank him for this great opportunity that allowed me to learn new things about medicinal chemistry in a really friendly atmosphere. This pleasant experience would have not been the same without my lab-mates: Jakob Staun Pallesen, Jie Zang, Kim Tai Tran, Dorleta González Chichón, Nanna Haap-anen, Amina Baig, Erik Bjørn Dampe and Martina Luchini. I really thank you all.

TABLE OF CONTENTS

1 Protein kinases

1.1 Introduction

Protein kinases are a large family of enzymes that catalyse the transfer of a phosphate group from a donor nucleoside triphosphate to an acceptor hydroxyl group on the target substrate (figure 1). [1]

The human genome encodes for more than 500 different protein kinases which can be classified on the basis of the acceptor amino acid: serine/threonine, tyrosine and mixed kinases. According to the sequence of the catalytic domain, protein kinases can be classified in seven main groups: AGC (including the family of Protein Kinases A and C), CAMK (Calcium Calmodulin-Dependent Kinases), CK1 (Casein Kinase1), CMGC (including the Cyclin-Dependent Kinases, Mitogen-Activated Protein Kinases and Glycogen Synthase Kinases), STE (homologs of yeast sterile kinases), TK (Tyrosine Kinases) and TKL (Tyrosine kinase-Like).[2] Tyrosine kinases represent 17% of the entire human kinome, and they catalyse the transfer of γ-phosphate from the adenosine triphosphate (ATP) to the hydroxyl group of a tyrosine residue of the target substrate.[3]

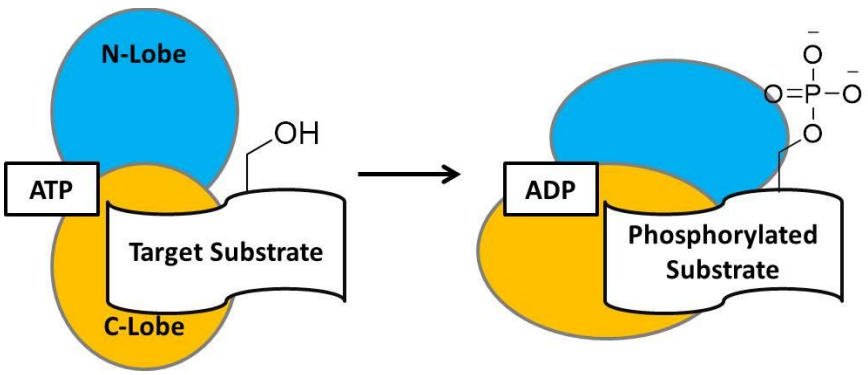

Figure 1: representation of phosphorylation reaction catalysed by protein kinase

Protein phosphorylation is a post-translational modification that serves as a switch for cellular components belonging to a wide range of signalling pathways. These pathways are strongly involved in many regulation mechanisms which affect the major physiological cell functions such as development, differentiation,

metabolism and survival.[4] Unsurprisingly, the phosphorylation process is highly regulated by different cell mechanisms including protein phosphatases, which play an essential role by catalysing the cleavage of phosphate.[5]

The protein kinases are also responsible for the transduction and amplification of a wide range of growth factors in different tissues, and the deregulation of this signalling represents a mechanism of uncontrolled proliferation.[6,7] Some of the identified oncogenes (genes primary involved in cancer development) encode for aberrant or amplified tyrosine protein kinases, such as the fusion gene BCR-ABL1[8], or encode for mutated and amplified EGFR (epidermal growth factor receptor)[9], FGFR (fibroblast growth factor receptor) and other kinase receptors.[10] On these basis, the kinase proteins represent an attractive target in medicinal chemistry for the development of targeted anti-cancer therapies.[11] Among these kinases FGFR and EGFR have been the subject of efforts aimed to develop new antiproliferative inhibitors which led to recent approvals for EGFR inhibitors such as afatinib[12] and osimertinib[13] in 2013 and 2017 respectively, and, more recently, for the FGFR-inhibitor erdafitinib.[14]

1.2 Structure and function of kinase domain

The intracellular catalytic domain of protein kinases consists of about 300 amino acids and its secondary structure is organized in stranded β-sheets and several helices. The tertiary structure of each kinase is distinguished in two structurally and functionally different lobes, which contribute to the catalytic and regulatory activity of the entire protein.[15] The smaller and flexible N-lobe consists of 80 amino acid residues and features a conserved C-helix and 5 stranded β-sheets (β1-β5). A glycine rich sequence (GxGxxG), called Gly-rich motif or ''P-loop'', connects together the β1- β2 strands which represent the binding site of the purine ring of the ATP.[16] The C-helix is a conserved subdomain located between the two lobes, and its right positioning is crucial for the activity of the catalytic site. The distance between the C-helix and the activation loop determines an open/closed conformational state adopted throughout the catalytic cycle. The C-helix contains a conserved glutamate residue which establishes a salt bridge with a lysine located on the β3-strand. This interaction, highly conserved through the kinome, determines the right positioning of the C-helix and features the active state of the

kinase domain.[17] This event also results in a loss of flexibility of the N-lobe which acts as a rigid body as a consequence of its activation.[18]

The larger C-lobe (about 200 amino acids) consists mainly of helices and a short β-sheet. The stable helical subdomains form the core of the catalytic site and represent also the binding site for the target substrate. The β-strand is flanked by a DFG motif (aspartic acid, phenylalanine and glycine) that coordinates the magnesium ion and stabilizes the ATP in the binding site, and the catalytic loop where the phosphate group of the ATP is transferred to the target tyrosine residue.[19] The activation loop extends from the conserved DFG motif to the APE motif (alanine, proline and glutamic acid). This portion is highly involved in the regulation of the kinase activity and substrate recognition, thereby its primary structure is the most variable of the kinase domain.[20] Finally, the GHI domain is constituted by three helices subdomains on the terminal portion of the C-lobe. This region is not only responsible for the recognition of the target substrates and regulatory proteins, but also stabilizes the catalytic site through a conserved interaction between an arginine residue positioned on the H-I loop, and an aspartate residue located on the activation loop.[21]

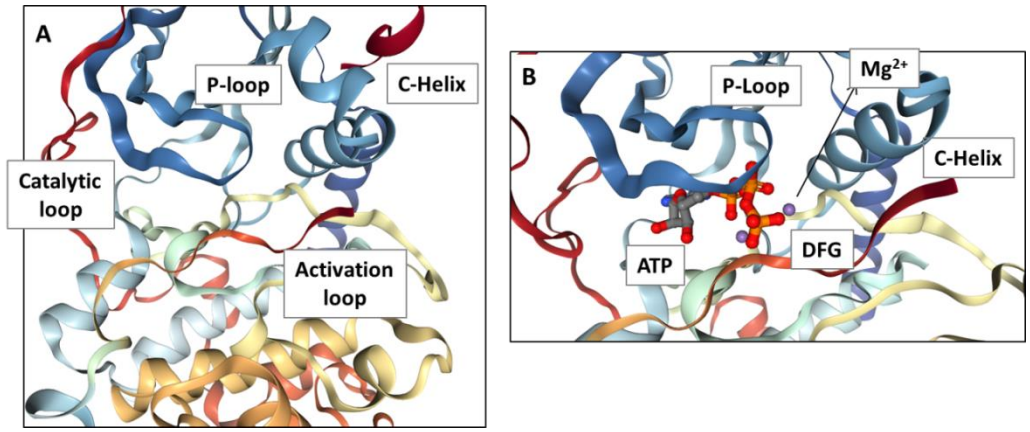

Figure 2: A) Structure of PKA kinase domain (PDBID: 1ATP). **B**) Crystal structure of ATP at the binding site.

Several conserved hydrophobic residues of the two lobes are involved in the formation of the ''regulatory spine'' and the ''catalytic spine''.[22,23] These spatial motifs are found throughout the entire kinase family and represent a hallmark of the active state of the kinase domain. The regulatory spine comprises residues

from the C-helix, the catalytic loop and the phenylalanine of the DFG motif, whereas the catalytic spine includes the adenine ring of the ATP.

The *trans* auto-phosphorylation of the activation loop is generally considered the first of the chain of events that leads to switching the kinase from the inactive to the active state.[24] The introduction of the phosphate group induces the formation of strong ionic interactions between the activation loop, the catalytic loop and the C-helix. This results in shifting the DFG motif in DFG-in conformation, that is able to coordinate the magnesium ion at the ATP binding pocket. Moreover, the orientation of the DFG-in residues makes the formation of the catalytic and the regulatory spines possible. The right positioning of the Glycine-rich region and the C-helix are also required to achieve an effective catalytic transfer of the γ-phosphate from the ATP to the target substrate.[25,26] Although the active kinases share common features such as the hydrophobic spine and the DFG conformation, the regulation of the processes needed to achieve the active catalytic state differ among the class of the kinase family. For example the CDKs (cyclin-dependent kinases) require the binding of cyclin proteins to switch to the active state[27] whereas the AGC kinases share a conserved C-tail with accessory phosphorylation sites that connects together the C-lobe and the N-lobe.[15] In Fes kinases the C-helix adopts the optimal conformation binding an SH2 domain which also provides a docking site for the target substrate.[28]

Once the catalytic process is over, the activation loop loses its activating phosphate residues and the DFG motif shift into the DFG-out conformation, where the phenylalanine residue occupies the ATP binding pocket and disrupt both the regulatory and the catalytic spines.[29] The DFG-out conformation is a clear signal of inactive kinase domain.

1.3 Receptor tyrosine kinases

Cell-surface receptors with kinase activity (RTKs, Receptor tyrosine kinases) are primary involved as regulators of cellular processes such as differentiation, proliferation, cell survival and metabolism.[30] They share common structural domains such as the extracellular binding site, the trans-membrane helix and the intracellular kinase domain.

Generally, the receptor monomers are in equilibrium with the active oligomer conformation (figure 3). The binding of growth factors to the extracellular region induces and stabilizes the dimers formation, which in turn leads to the activation (phosphorylation) of the kinase domain and the cytoplasmic signalling.[31] The formation of a stable dimer requires a tight binding between the extracellular regions of RTKs through the establishment of intermolecular interactions among the ligands, the binding domain of the receptors and other accessory molecules.[32]

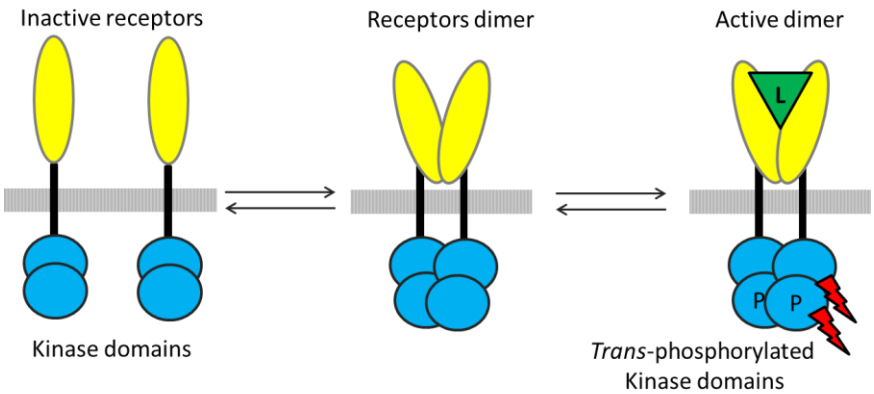

Figure 3: Schematic representation of receptors dimerization.

The *trans*-autophosphorylation of the RTKs increases the catalytic efficiency of the kinase domain and serves to create the binding sites for docking proteins.[33] The signalling molecules bearing the Src homology-2 (SH2) and phosphotyrosine-based binding (PTB) domains recognize selectively the phosphorylated residues on the RTKs. These molecules can be directly recruited by the phosphorylated receptors or they can bind docking proteins which in turn are phosphorylated by the RTKs.[34]

The activated RTKs expose multiple phosphorylation sites that can recruit different SH2/PTB domain containing proteins which in turn promote the interaction with multiple signalling proteins. The interconnection among the signalling mediators and the downstream amplification determines a complex cellular network where the RTKs represent the trigger point. The downstream pathway often consists of redundant second messengers and effectors, for example mitogen-activated protein kinase (MAPK), phosphatidylinositol 3-kinase (PI3K), protein kinase B (akt), signal transducer and activator of transcription

(STAT) and phospholipase C (PLC) are often activated by several RTKs. Therefore, the specificity of the signals, and the final effect on cellular processes, are defined not only by the signalling mediators but also by their concentration.[35,36] The regulation of the entire signalling involves also positive and negative feedback, which can increase or decrease the sensitivity of the system to the triggering signal.[37]

The negative feedback plays a key role in maintaining cellular homeostasis, and a tight regulation is required to terminate the signal.[38] The inactivation by protein tyrosine phosphatases (PTP) and endocytosis of RTKs are common downregulation processes.[39,40]

1.4 Targeting the protein kinases in cancer

The human genome encode for more than 500 kinase proteins which are virtually involved in every signal transduction process, and the modulation of their activity elicits deep physiological response.[19] Genetic mutation, amplification and translocations drive the expression of oncogenic kinase proteins that are directly involved in cancer development.[41] Fusion protein BCR-ABL, mutated PI3KCA and amplified EGFR represent a primary target in anti-cancer therapy.[42–44] MAPK, mTOR, RSK and other components of the downstream signalling constitute a second class of targeted kinases that are required for cancer cell survival, proliferation and migration.[45,46] Finally, other kinases expressed in the surrounding tumour tissue, such as VEGFR and FGFR, are involved in different stages of cancer development and progression.[47]

Three general strategies are available to target RTKs: Tyrosine Kinase Inhibitors (TKIs), monoclonal antibodies (mAbs) and extracellular agents able to interfere with the ligand-receptor interaction (peptides, mAbs and ligand traps).[11]

Tyrosine kinase	Tyrosine kinase inhibitors
EGFR	Gefitinib, erlotinib, lapatinib, afatinib, osimertinib
c-Met	Crizotinib, cabozantinib
BCR-ABL	Bosutinib, dasatinib, imatinib, nilotinib, ponatinib
ALK	Crizotinib, ceritinib, alectinib, brigatinib
PDGFR α/β	Axitinib, gefitinib, imatinib, lenvatinib, nintedanib, pazopanib, regorafenib, sorafenib
VEGFR	Axitinib, lenvatinib, nintedanib, regorafenib, pazopanib, sorafenib, sunitinib

FGFR	Erdafitinib
Src	Bosutinib, dasatinib, ponatinib, vandetanib

Table 1: Examples of approved TKIs

To date several small-molecules belonging to the class of TKIs have been approved, and they are available for the treatment of a wide range of cancers. TKIs prevent the signalling cascade, triggered by activated RTKs, by occupying the ATP binding pocket at the intracellular kinase domain. TKIs can be classified in three main classes.[48]

First generation of TKIs belongs to the type I inhibitors which were designed to bind the ATP binding site of the kinase domain during its active state conformation (DFG-in) by mimicking the adenine ring (figure 4). The general pharmacophore model is constituted by a nitrogen-containing heterocycle, able to establish one to three hydrogen bonds at the hinge region within ATP pocket, substituted by an aromatic portion which targets an adjacent hydrophobic cleft. This class of compounds recognizes a conserved conformation and despite being characterized by a broad spectrum of action, potent and selective compounds have been developed as in the case of the EGFR inhibitor gefitinib (Iressa®),[49] or the FGFR inhibitor Ly2874455[50]. Type II TKIs bind the ATP binding pocket when the kinase domain is in the inactive state conformation (DFG out) (figure 4). This conformation exposes an additional hydrophobic pocket, juxtaposed to the ATP binding site, which is occupied by type II inhibitors. These compounds share the pharmacophoric model of the type I class, featuring an additional hydrophobic group able to target the pocket displayed by the DFG out conformation. An example of type II TKIs is the BCR-ABL inhibitor imatinib (Gleevec®), which binds the hinge region establishing hydrogen bonds with the aspartate residue of the DFG motif and a glutamate residue on the C-helix.[51]

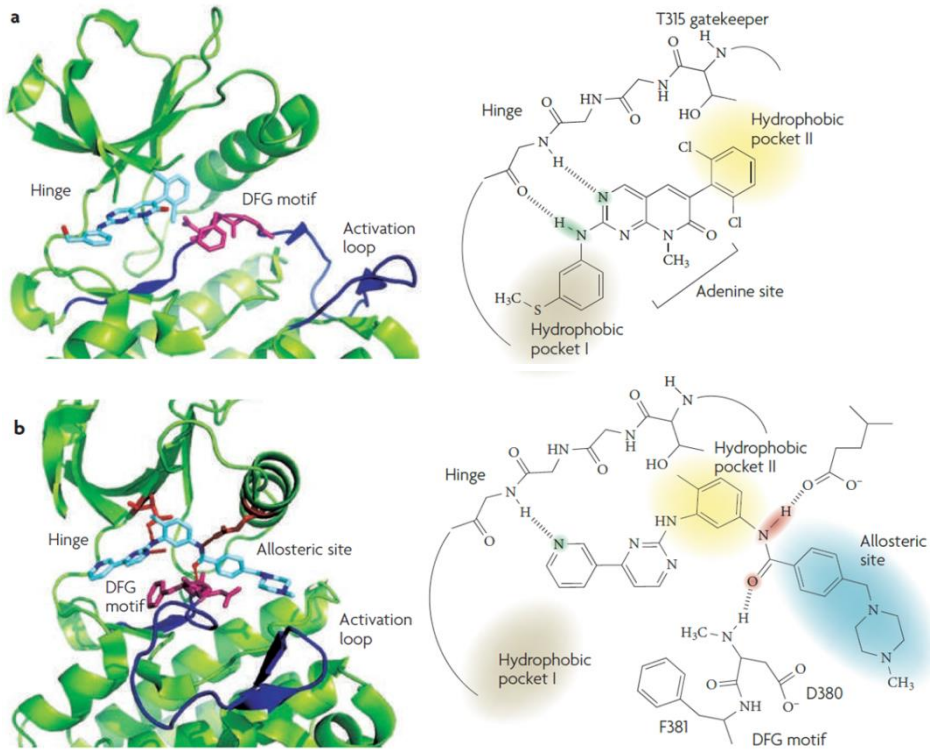

Figure 4: a) ABL1 (DFG-in conformation) in complex with type I inhibitor PD166326. **b**) ABL2 (DFG-out conformation) in complex with type II inhibitor imatinib. Figure adapted from ref. 48.

Finally, a third class of TKIs are able to bind irreversibly the kinase active site by targeting conserved nucleophilic residues.[52,53] These compounds feature an electrophilic group to a driver portion able to recognize the target site. Despite the concerns about off target toxicity, the interest toward this class of inhibitors is increased in the last years.[54] Covalent agents usually display higher potency compared to the reversible analogues, as their binding is non-competitive with ATP, and they represent a viable approach to overcome acquired resistance to available therapies.[55–57] The EGFR inhibitors afatinib (Giotrif®) and osimertinib (Tagrisso®) are example of approved covalent RTKIs.[12,13]

Monoclonal antibodies constitute a second therapeutic strategy.[58] They are able to bind the extracellular domain preventing the receptor dimerization induced by the natural ligand. Several mAbs have been authorized for the treatment of different cancer types, but generally the clinical efficacy as single agent therapy is limited and combination therapies mAbs/TKIs are preferred. Example of approved mAbs comprise the anti-ErbB2 trastuzumab (Herceptin®)[59], the anti-EGFR

antibodies cetuximab (Erbitux®)[60] and necitumumab (Portrazza®)[61] and the anti-PDGFRa antibody olaratumab (Lartruvo®)[62].

2 Fibroblast growth factors system

2.1 Function and structure

Fibroblast growth factors (FGFs) system regulates many physiological cell processes. FGFs signalling is strongly involved during embryogenesis and deeply affect angiogenesis, wound healing and tissue repair.[10] FGF system also contributes to maintaining the homeostasis of phosphates, bile acids, lipids and glucose.[63] The deregulation of FGF signalling has been linked to the development of congenital diseases such as craniosynostosis and dwarfism.[64] Aberrant FGF signalling contributes to the progression of metabolic disorders and it represents a leading cause to cancer development.[65]

There are 18 mammalian fibroblast growth factors classified in six families according to their homology[66]. The families FGF1 (including FGF1 and FGF2), FGF4 (FGF4, FGF5 and FGF6), FGF7 (FGF3, FGF7, FGF10 and FGF22), FGF8 (FGF8, FGF17 and FGF18) and FGF9 (FGF9, FGF16, FGF20) act as locally paracrine factors (canonical FGFs), whereas FGF19 group (FGF19, FGF21 and FGF23) act on long distance as endocrine factors. Additional four receptor-independent factors are FGF11-14 which act on voltage-gated sodium channels.[67]

The primary structure of fibroblast growth factors consist of 150-300 amino acids with a conserved core of ~120 amino acids residues organized in 12 β strands in paracrine factors, and 11 β strands in hormonal factors.[68] The amino- and carboxy-terminal regions are highly variable and contribute to ligand-receptor specificity. FGFs show discrete affinity for heparane sulphate (HS), which is essential for the formation of a stable FGF-FGFR complex and contributes to regulate FGFs diffusion in the extracellular environment.[69] Specifically canonical FGFs exhibit higher affinity to HS thus they can only act locally as paracrine factors, whereas hormonal FGFs, which show poor affinity to HS, can enter the bloodstream and act on longer distance.[70] The binding site of HS on endocrine FGFs is constituted by a conserved solvent-exposed basic region.[71]

The fibroblast growth factor receptors are a family of four proteins (FRGFR1-4) constituted by an extracellular region containing three immunoglobulin-like domains (D1-3) connected to the kinase domain by a single trans-membrane

helix.[72] An additional FGFR receptor, FGFRL1 or FGFR5, lack of the kinase domain and serve as a decoy receptor.[73]

The D2-D3 domains, and the linker chain between them, serve as a ligand binding site, whereas D1 domain and loop between D1 and D2 domains (containing a conserved region called ''acid box'') are involved in an auto-inhibiting mechanism.[68,74] Specifically, in absence of the FGFs, D1 region interacts with the ligand binding pocket between D2-D3 domains whereas the acid box occupies a positively charged region that serves to accommodate the HS cofactor, needed for the receptor dimerization.

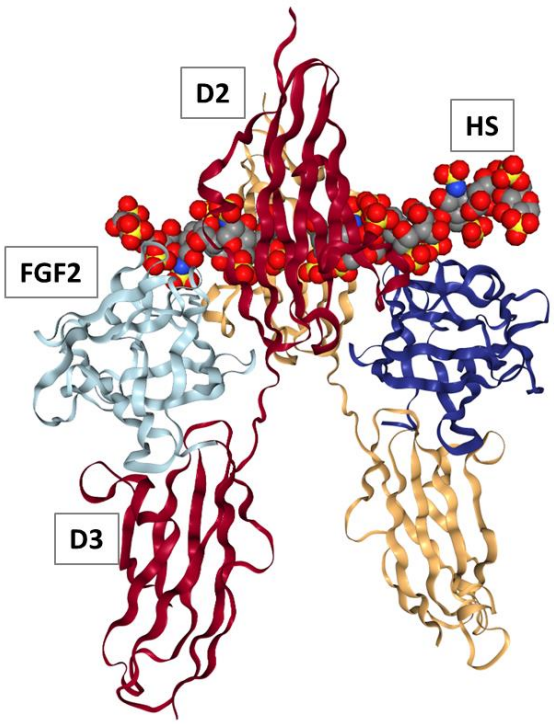

Figure 5: Symmetric ternary complex comprising FGFRs (magenta and white), FGFs (blu and pale blu) and HS (PDBID 1FQ9).

FGFR1-3, but not FGFR4, are expressed in different tissues as two distinct isoforms (b and c) resulting from the alternative splicing of D3 domain.[75] FGFR isoform b is mainly present in the epithelial tissue whereas isoform c is found in mesenchyme tissues. Canonical FGFs also exhibit tissue-specific expression, with FGFs binding isoform b being expressed in mesenchyme and FGFs binding isoform c expressed in epithelium. This results in a signalling loop between the mesenchyme and the epithelium that is decisive for tissue homeostasis.[63]

The formation of an active FGF-FGFR complex requires a stabilizing cofactor, which is represented by HS or other ancillary molecules, resulting in a 2:2:2 symmetrical ternary structure[76] (figure 5). FGF binds its receptor at D2-D3 domain and engage the D2 region of the neighbouring receptor. Additionally the FGFRs directly interact with each other at the bottom end of their D2 domains[77]. HS

stabilizes the transient FGF-FGFR complex by binding both ligands and receptors at their HS binding site, which are juxtaposed to one another resulting in a continuous canyon rich of basic residues.[69] Instead, the complex between hormonal FGFs and their receptors is stabilized by co-receptors belonging to the α and β Khloto family.[78] The affinity of receptor paralogs to different ligands combined to the tissue-specific expression of FGFs, receptors and cofactors determine an elevated FGF-FGFR signal specificity.

2.2 FGFR activation and signalling

The assembling of FGF-FGFR-HS (or Khloto co-receptor) in a 2:2:2 ternary complex leads to juxtaposition and the *trans*-autophosphorylation of the kinase domains. Specifically, the activation loop of one kinase domain serves as a substrate for the neighbouring FGFR kinase site.[68,79] A first phosphorylation (FGFR1 Y653 residue) activates the kinase site increasing the catalytic efficiency, then others phosphorylation at different tyrosine residues (Y583, Y463, Y 585 on FGFR1) serve to create the binding sites for the substrate proteins and further increase the catalytic activity of the kinase domain.[33]

The activated FGFR is recognized by the adaptor protein FRS2 (FGFR Substrate 2) which in turn is activated by phosphorylation at several tyrosine residues.[80] Phosphorylated FRS2 recruits different docking proteins among which SOS (Son Of Sevenless) and GRB2 (Growth factor Receptor-Bound 2) allow the activation of RAS-RAF-MAPK (Mitogen-Activated Protein Kinase) axis signalling.[10] GRB2 serves also as a docking site for GAB1 (GRB2-Associated binding Protein 1) which promotes the activation of PI3K-AKT (phosphatidylinositol 3-kinase) pathway.[81] The activated FGFR constitutes a recognition site for the SH2 domain protein PLCγ (phospholipase Cγ) that is responsible for the hydrolysis of PIP_2 to DAG and PIP_3 and the consequent effect on PKC and intracellular level of calcium.[82] Other pathways can be activated according to the cellular context, including JAK-STAT (Signal Transducer and Activator of Transcription) signalling, RSK2 (Ribosomal protein S6 Kinase 2) and p38.[83,84]

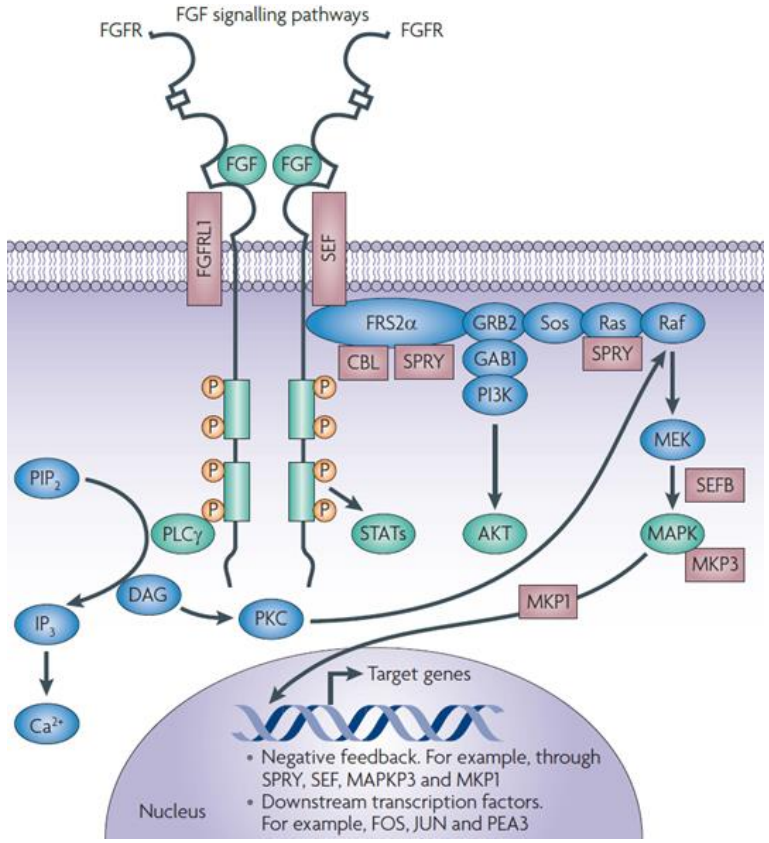

Figure 6: schematic representation of FGFR downstream signalling. Figure adapted from ref. 65.

The signalling axis is regulated by different negative feed-back including the MAPK-phosphatase MKP3, Sprouty and SEF protein families.[85–87] The receptor also undergoes internalization, and subsequent degradation or recycling, in a process regulated by ubiquitinylation.[88]

2.3 FGF/FGFR system in cancer

Cancer development mediated by FGF/FGFR system is well documented and occurs through receptor amplification and overexpression, activating mutations and aberrant fusion proteins.[89,90]

Amplification of FGFs and overexpression has been found in 15% of all triple negative breast cancer (TNBC) where FGFR1 amplification is one of the most common deregulation in 15% of all subtype of breast cancers.[91,92] FGFR1 overexpression has been also detected in 6% of lung cancers, in 17% of patients

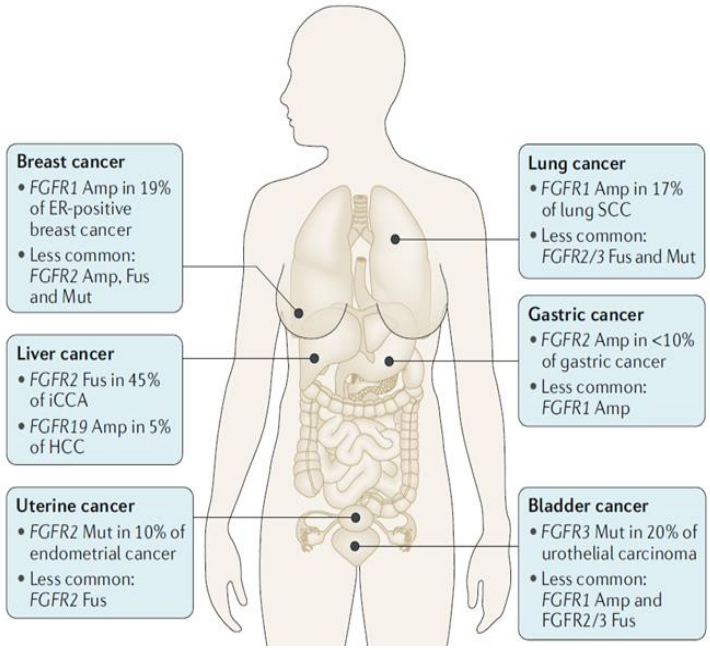

Figure 7: distribution of common aberrant FGFRs in cancers. Figure adapted from ref. 90.

with squamous cell carcinoma (SCC) and 12% of non-small cell lung cancer (NSCLC).[93,94] FGFR2 amplification is detected approximately in 10% of all patients with gastric cancer and is associated with invasiveness.[95] FGFR activating mutations are commonly observed on the extracellular domain leading to increased ligand binding affinity or even ligand independent activation.[96,97] Aberrant FGFR3 is a leading cause of bladder cancer being detected in 20-50% of all urothelial carcinoma. Specifically Y375C mutation at extracellular domain of FGFR3 induces ligand-independent signalling mediated by the formation of disulphide bonds between aberrant receptors.[98,99] Mutated FGFR2 expression has been found in gastric cancer and endometrial carcinoma.[100,101] Chromosomal rearrangement and translocation involving FGFR proteins have been detected in a wide range of malignancies.[102,103] FGFR3 fused protein have been also observed in bladder cancer and SCC.[104]

The establishment of paracrine loop of FGF stimulation in cancer proliferation have been identified in bladder, lung and breast cancers.[105,106] High plasma level of FGF2 has been identified in leukemia and lung cancer representing a poor prognosis factor[107], whereas FGF19/FGFR4 overexpression is associated to hepatocellular carcinoma (HCC) development.[108,109] FGFs play a key role also in stimulating angiogenesis in both cancer tissue and in the surrounding environment.[110] The upregulated FGF/FGFR downstream signaling is also involved in developing resistance to anti-VEGF therapy.[111]

2.4 FGFR Tyrosine kinase inhibitors

This class represents the most explored approach to target FGF/FGFR signalling in anti-cancer therapy.[112] FGFR TKIs can be classified either as multi-target or selective and ATP-competitive or covalent, according to their target specificity and mode of action.

The first generation of FGFR inhibitors is constituted by multi-target ATP-competitive inhibitors able to disrupt FGFR signalling and to inhibit a wide range of kinases such as Kit, Flt3, VEGFRs, RET and PDGFRs. Dovitinib[113], nintedanib[114], lenvatinib[115,116] and ponatinib[117] are example of approved drugs currently available for cancer treatment. These compounds show a therapeutic anti-cancer profile mainly dependent by VEGFRs and PDGFRs inhibition and a high toxicity rate, due to their anti-angiogenic effect.[112,118,119]

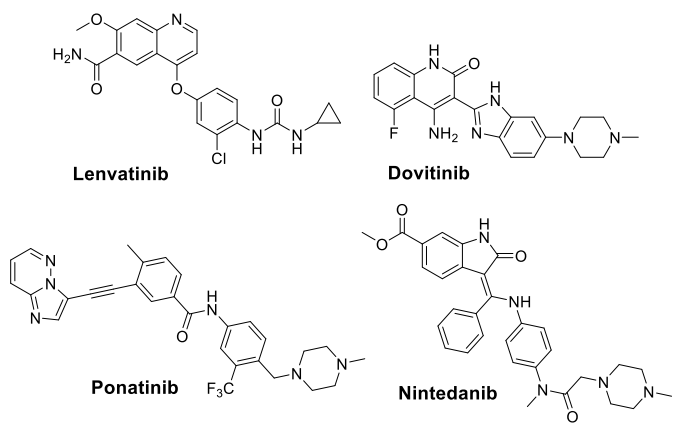

Figure 8: some examples of first generation of FGFR TKIs.

Thus, a second generation of ATP-competitive agents have been developed aiming to reduce the adverse effects by targeting selectively FGFRs. AZD4547[120], NVP-BGJ398[121] and LY2874455[50] are some of the selective FGFRs inhibitors currently under clinical investigation. These compounds have shown a favorable toxicity profile, mainly characterized by hyperphosphatemia as a result of inhibition of hormonal FGFs signaling, but the clinical efficacy appears confined to a small subsets of cancers.[112,122] Clinical evidences suggest that FGFR inhibition only affects a fraction of the malignancies characterized by FGFR alteration. Specifically, only cancers bearing FGFR2-3 fusion proteins or highly overexpressing FGFR1-2 appear sensitive to selective FGFR inhibitors.[89,122] Nevertheless, the ATP-

competitive and selective FGFR TKI erdafitinib has been approved this year (April 2019) by FDA for the treatment of FGFR2-3 aberrant bladder cancer.[14]

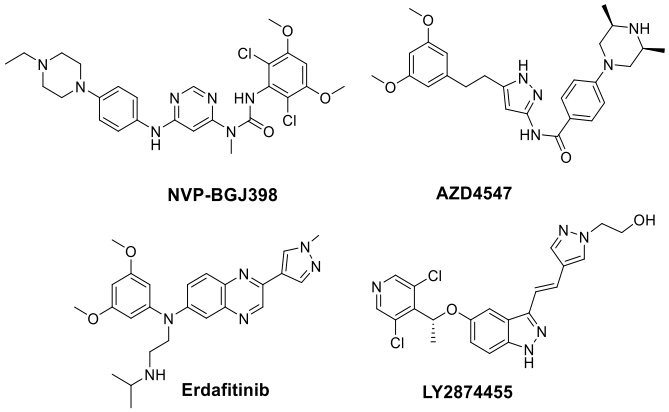

Figure 9: some example of second generation FGFR inhibitors.

The long-term efficacy of cancer therapies is hampered by acquired resistance, mainly represented by secondary FGFR mutations and activation of bypassing signaling.[90,123] Exposition of TKIs to cancer cell often results in expression of mutated kinase proteins. A commonly found kinase point mutation is the so-called ''gatekeeper'' mutation, at the ATP binding pocket.

The gatekeeper residue features a hydrophobic pocket exploited by many TKIs which become ineffective when this residues is replaced by bulky amino acids, as demonstrated by the reduced inhibitory potency of first and second generation of FGFR TKIs.[124] Case of resistant FGFR1-4 bearing mutated gatekeeper residues have already been reported, specifically the gatekeeper valine residue (wild type FGFR) has been found replaced by leucine, isoleucine and methionine. Examples of gatekeeper resistant FGFR forms are V565I FGFR2 resistant to dovitinib[124], V561L FGFR1 resistant to lucitanib[125] and V555M FGFR1 and FGFR3 resistant to PD173074 and AZD4547.[126]

Since covalent inhibition represents an effective approach to overcome gatekeeper mutations, a third generation of irreversible FGFR inhibitors has been developed.[127] The series of covalent compounds FIIN-1, FIIN-2 and FIIN-3 displayed inhibitory activity on WT-FGFR (wild-type receptor) and a wide range of mutated FGFRs.[55,128] These compounds were designed attaching a reactive acrylamide warhead on a driver portion, structurally related to PD173074. The

electrophilic acrylamide engages a cysteine residue (Cys486 in FGFR1) on the Gly-rich loop at the ATP binding site.[129] PRN1371[130] and TAS-120[131] are two example of covalent pan-FGFR TKIs currently under clinical evaluation.

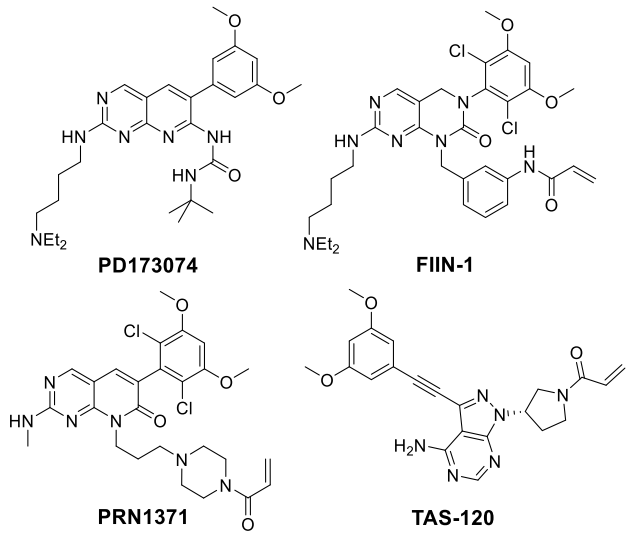

Figure 10: some examples of covalent FGFR inhibitors.

A further class of covalent and selective FGFR4 inhibitors has been recently disclosed.[109] These compounds show structural similarity with PD173074 and NVP-BGJ398, sharing the 2-oxo-3,4-dihydropyrimido[4,5-d]pyrimidine core as a driver portion. The high inhibition specificity is achieved by targeting the FGFR4-conserved cysteine residue (Cys554) at the hinge region.[132,133] Selective FGFR4 inhibitors exhibited anti-cancer activity on hepatic carcinoma (HCC) and currently FGFR4 TKIs BLU554 (fisogatinib)[134,135], H3B6527[136] and FGF401 (roblitinib)[137] are in clinical trials .

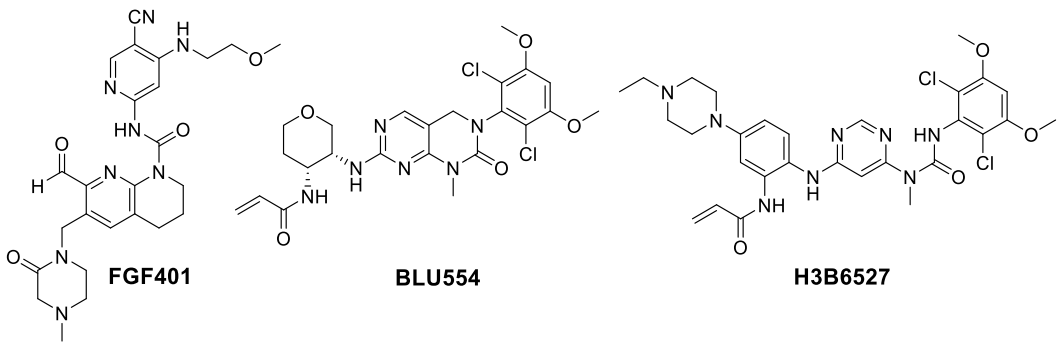

Figure 11: some example of selective and covalent FGFR4 inhibitors.

Despite an increasing interest toward covalent kinase inhibitors, the development of new electrophilic warheads remains an underexplored field[138]. The intrinsic reactivity of the acrylamide group, its metabolic instability and the risk of toxicity justify the development of alternative warheads and their potential application in clinic.[139,140] On this basis, the group at the University of Parma where I have carried out the doctoral research has recently disclosed a series of FGFR inhibitors aimed to target the conserved cysteine residue at the hinge region (Cys486 in FGFR1).[141] These compounds have been designed on the basis of the structure of FIIN-2, replacing its acrylamide function with different electrophilic groups (figure 12, panel D).

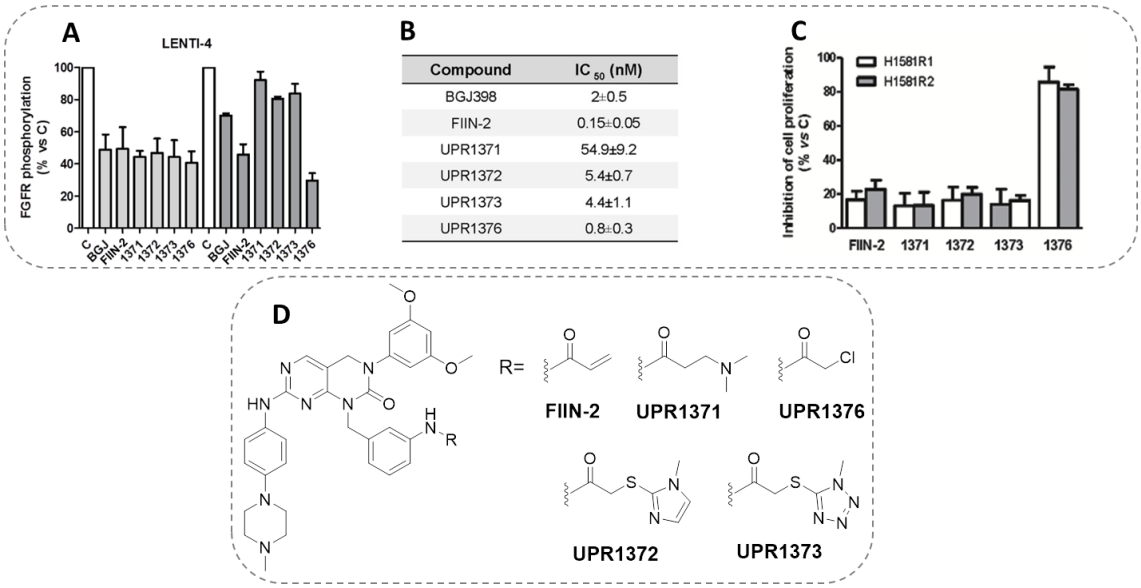

Figure 12: A) Inhibition of FGFR1 autophosphorylation in LENTI-4 cells incubated 1h with tested compound at 1µM. On the left (pale grey) is reported the measure of the inhibition *vs.* control after 1 h; on the right (grey) the cells were incubated 1 h then washed with PBS and the autophosphorylation was measured after 8 hrs. B) Inhibition of H1581 cell line proliferation exhibited by tested compounds, performed with MTT assay C) Inhibition of NVP-BGJ398-resistant H1581R1 and H1581R2 cell lines exhibited by tested compounds incubated for 72 hrs. Data obtained by MTT assay. Figures adapted from ref. 141. D) Molecular structures of synthesised compounds.

Among these compounds, UPR1376 has proved to bind irreversibly to FGFR preventing the phosphorylation of the receptor several hours after the washing (figure 12, panel A). This compound strongly affects the proliferation of FGFR1-overexpressing cells, proving its efficacy also on resistant cell lines (figure 12,

panel B and C). Interestingly, UPR1376 prevents the proliferation of resistant cells which are not affected by FIIN-2 (figure 12, panel C). These results demonstrate that the 2-chloroacetamide might serve as a potential covalent warhead and the development of different electrophilic groups could lead to new FGFR inhibitors.

2.5 FGF traps and NSC12

FGF traps represent an alternative approach to modulate FGF/FGFR signaling by sequestering FGFs thus preventing the binding with their receptors.[142] The first example of ligand trap is the peptide FGFR1-derived FP-1039.[143] This protein consists of the soluble extracellular domain of FGFR1 (isoform c) fused with the crystallizable fragment of human immunoglobulin. FP-1039 binds the paracrine and hormonal FGFs hampering the activation of FGFR signaling. This peptide exhibited anti-angiogenic and anti-proliferative activity, and early clinical outcomes have shown a favorable toxicity profile lacking of any sign of hyperphosphatemia. FP-1039 is currently under clinical evaluation for the treatment of different cancers bearing aberrant FGFR.[144,145]

At the University of Brescia, a group led by Professor Presta has identified the first small-molecule FGF trap. Starting from a human protein able to bind FGFs (PTX3),[146] a small penta-peptide (ARPCA) was found as the smallest recognition pattern.[147,148] A pharmacophoric interaction model between FGF2 and ARPCA and, a subsequent screening among a library of the National Cancer Institute, served to identify NSC12 (also known as NSC172285 or UPR1358).[148,149]

The structure of this steroidal compound was correctly established after its synthesis was performed in 2016, as it was at that time still undisclosed by their original authors. NSC12 display a pregnenolone core substituted at position 17 with a *bis*-(trifluoromethyl)propanediol chain bearing an ambiguous chiral center at position 20. Thus two different diastereoisomers were synthesized, UPR1358 (20*S*) and UPR1357 (20*R*), showing different physicochemical and pharmacological properties (figure 13).[150]

Whereas UPR1358 (NSC12) is able to disrupt the formation of the ternary FGF-FGFR-HS complex, UPR1357 is devoid of any biological activity. Additionally, UPR1358 exhibit anti-cancer activity in mice model of FGFR-dependent human

lung carcinoma when orally administered, without significant signs of toxicity (figure 13). UPR1357 was also characterized by a lower solubility when compared to UPR1358 (or NSC12). These evidences raised the question whether the different biological behavior of UPR1358 and UPR1357 derived from the stereochemistry, the solubility or both.

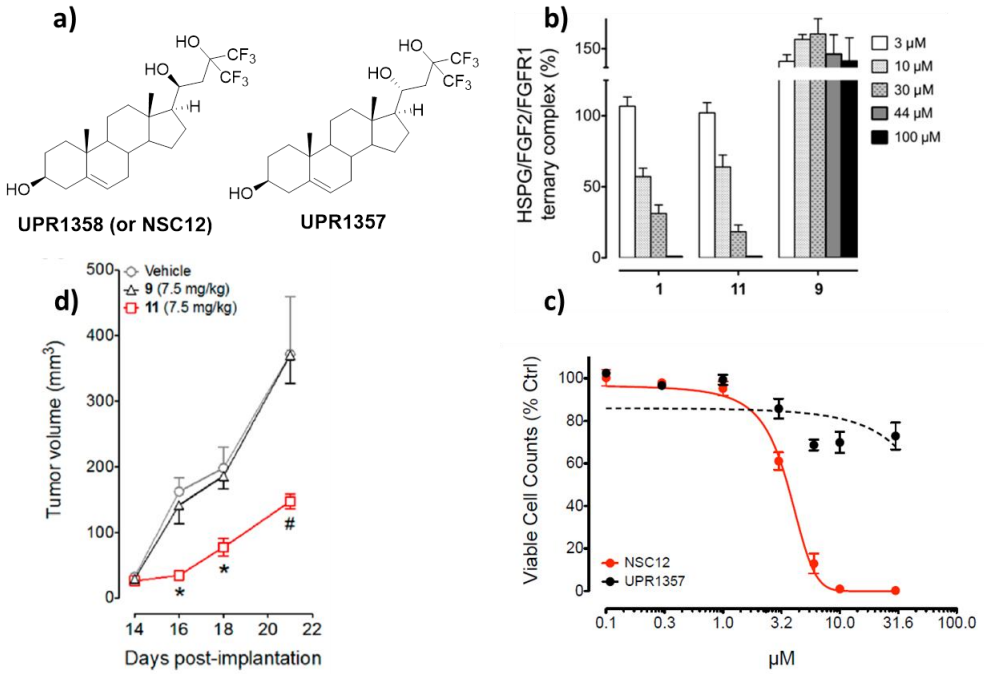

Figure 13: a) Chemical structure of diastereoisomers UPR1358 (NSC12) and UPR1357. **b)** Inhibition of FGFR-FGF-HS ternary complex formation displayed by UPR1358 (11 in the picture) and UPR1357 (9 in the picture). **c)** Inhibition of KMS-11 myeloma cell proliferation exerted by UPR1358. **d)** Inhibition of Lewis lung carcinoma growth after oral administration of UPR1357 (11 in the picture) and UPR1357 (9 in the picture). Figures b) c) and d) adapted from ref. 150.

Since a clear model of interaction of UPR1358 with its target is not available, a research work aimed at clarifying the role of the lateral *bis*-(trifluoromethyl)propanediol on the biological activity was carried out. The *bis*-(trifluoromethyl)propanediol chain was thus replaced with different bioisosteric derivatives leading to a panel of UPR1358 steroidal analogues (figure 14). Additionally, the role of the hydroxyl group at position 3 was investigated by synthesizing derivatives containing hydrophilic groups or oxidized analogues (figure 14).

The synthesized compounds have been tested to evaluate their ability to inhibit the proliferation of FGFR-dependent cells or the autophosphorylation of FGFR3 (table 1). Unfortunately the biological results gave us an unclear picture, showing how the stereochemistry appears a marginal factor for the anti-proliferative activity. Moreover, some compounds were able to affect the cell proliferation without interfere with FGFR phosphorylation, suggesting an alternative mechanism of action.

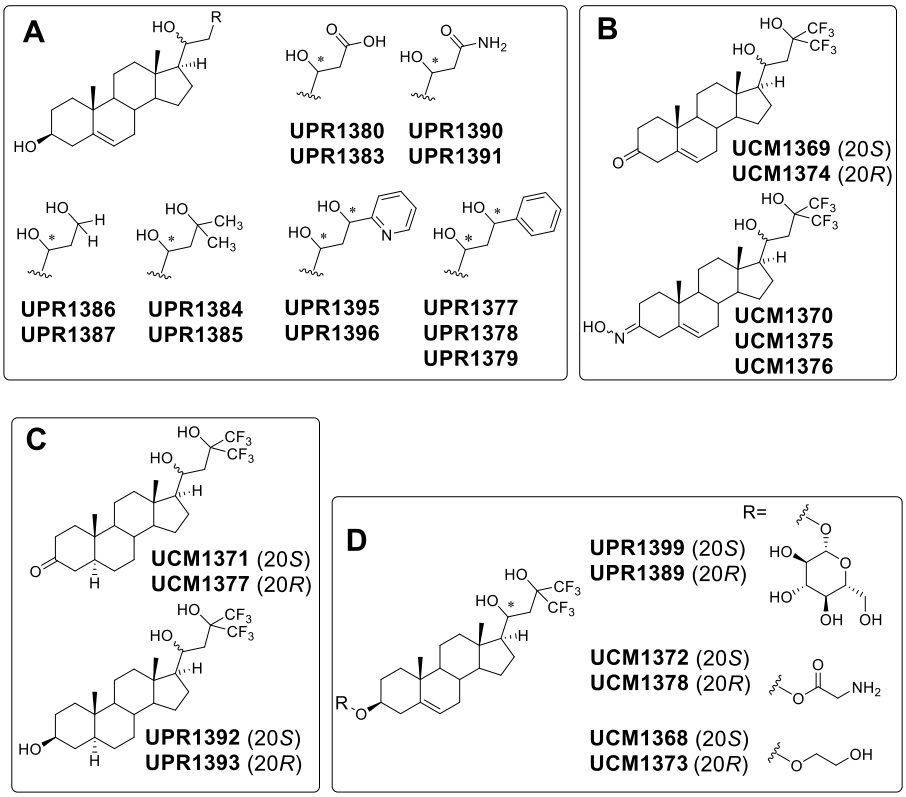

Figure 14: UPR1358 and UPR1357 and their derivatives. **A**) Lateral chain substitution. **B**) Oxidation at position 3. **C**) Pregnanolone derivatives. **D**) Substitution at position 3.

Compound	IC_{50} [a]	% Inhibition [b]
UPR1358	3.4	74.2
UPR1357	inactive	0
Lateral chain substitution		
UPR1383	26	65.5
UPR1380	inactive	34.2
UPR1391	inactive	16
UPR1390	inactive	0
UPR1385	26.6	0
UPR1384	12.2	13.9
UPR1387	13.3	0
UPR1386	22.8	48.6
UPR1377	5.5	40.3
UPR1378	inactive	20.3
UPR1379	inactive	54.8
UPR1395	7	51.2
UPR1396	9.4	53.1
Oxidation of position 3		
UCM1369 (20*S*)	3.4	85.2
UCM1374 (20*R*)	5.8	active
UCM1370 (20*S*)	7.2	41.5
UCM1375 (20*R*)	5.3	35
UCM1376 (20*R*)	6.2	67.4
Pregnanolone derivatives		
UCM1371 (20*S*)	7.0	75.9
UCM1377 (20R)	2.4	97.6
UPR1392 (20*S*)	2.9	63.3
UPR1393 (20R)	4.2	0
Substitution of position 3		
UCM1372 (20*S*)	5.6	87.9
UCM1378 (20R)	2.3	99.7
UCM1368 (20*S*)	3.3	57.1
UCM1373 (20R)	7.7	85.2
UPR1389 (20R)	4.5	0
UPR1399 (20*S*)	4.0	100

Table 1: biological results of tested compound classified according to their chemical scaffold. [a]: cell count viability on KMS-11 human myeloma cell line. [b]: inhibition of FGFR3 phosphorylation with tested compound at 6µM.

2.6 Aim of the work

UPR1358 (NSC12) is the first small-molecule FGF trap endowed with anti-proliferative activity in vivo, but the mechanism of interaction with its target is not fully understood yet. A first strategy to investigate such mechanism was aimed to clarify the structure-activity relationships by exploring the chemical space surrounding the lateral fluorinated chain and the steroidal nucleus. Early results have shown that the replacement of the *bis*-(trifluoromethyl)propanediol chain of UPR1358 with isosteres groups led to derivatives with negligible biological activity (figure 14 previous section). On the other hand, minor modifications of the steroid were tolerated, leading to compounds which retained the anti-proliferative activity. In some cases, the substitution and the oxidation of the secondary alcohol at position 3 of UPR1358 led to derivatives which not only maintained the anti-cancer activity (figure 15 panel A and C), but also exhibited strong inhibition of ligand-dependent activation (figure 15, panel B).

The biological evaluation of the steroidal derivatives have also shown how the anti-proliferative activity is marginally affected by the chiral configuration at *C*20 of the *bis*-(trifluoromethyl)propanediol chain, whereas the stereochemistry appears somehow involved in the inhibition of FGFR ligand-dependent activation.

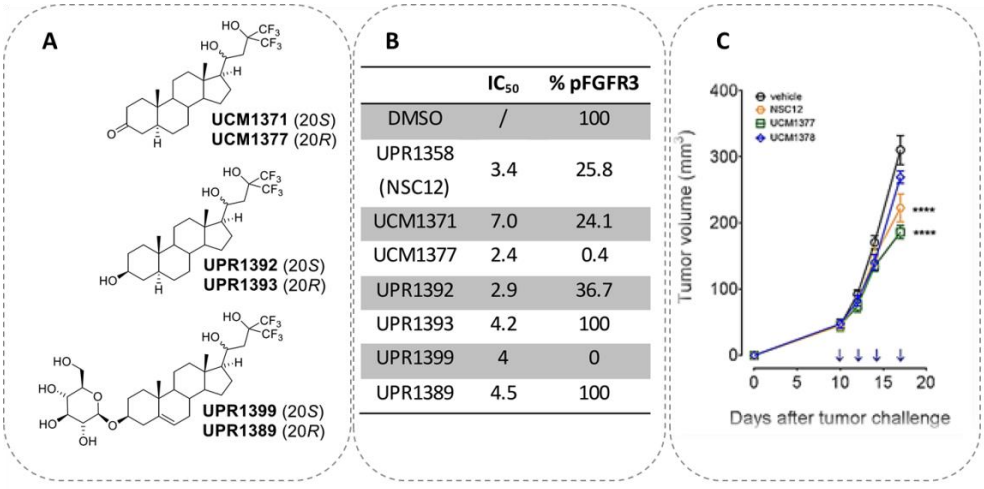

	IC_{50}	% pFGFR3
DMSO	/	100
UPR1358 (NSC12)	3.4	25.8
UCM1371	7.0	24.1
UCM1377	2.4	0.4
UPR1392	2.9	36.7
UPR1393	4.2	100
UPR1399	4	0
UPR1389	4.5	100

Figure 15: A) steroidal derivatives of UPR1358. **B)** Biological results of tested compounds. IC_{50} calculated on human myeloma KMS-11 cell count viability assay. %pFGFR: KMS-11 cells were incubated with 6 µM concentration of the tested compounds for 6 h. The cells were subsequently lysed and the receptors were quantified by immunoblot assay. %pFGFR represent the percentage of phosphorylated receptor. **C)** Anti-cancer activity of tested compound in human lung cancer xenografts in mice

As an example, two set of diastereomeric compounds UPR1399 (20*S*)/UPR1389 (20*R*) and UPR1392 (20*S*)/UPR1393 (20*R*) exhibit a comparable IC_{50} value when tested in cell viability assay, whereas the two isomers 20*S* show stronger autophosphorylation inhibition than isomers 20*R* (figure 15 panel B). Ambiguously, this stereochemical effect cannot be generalized, for example the diastereoisomers UCM1371 (20*S*) and UCM1377 (20*R*) display a similar level of autophosphorylation inhibition (figure 15 panel B).

These evidences suggest that the steroidal portion can be further subjected to structure-activity analysis aiming to clarify the mechanism of action and possibly increase the potency of UPR1358. On this basis, we have considered the replacement of the pregnenolone core of UPR1358 as a potential approach to obtain non-steroidal derivatives suitable for the investigation of the structure-activity relationships. Thus, we subjected UPR1358 to structural simplification without affecting the lateral *bis*-(trifluoromethyl)propanediol chain and replacing the pregnenolone core with mimetic biaryl scaffolds (figure 16).

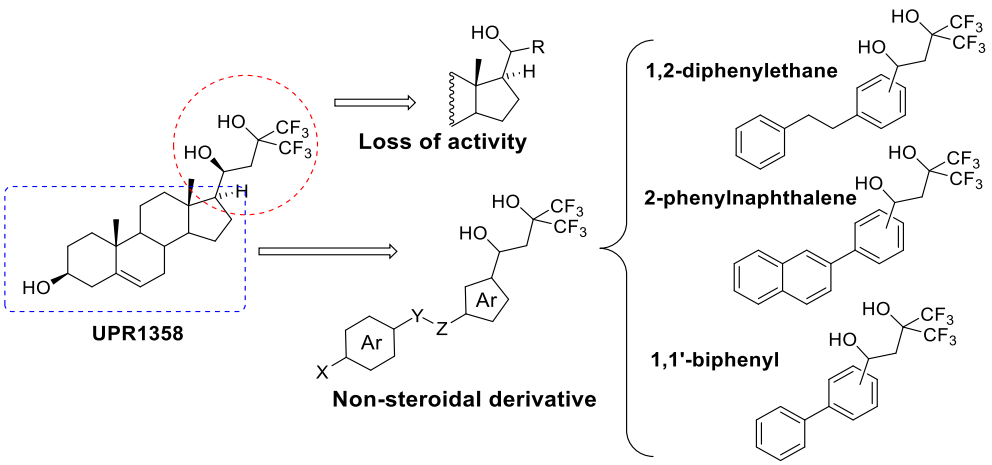

Figure 16: schematic representation of the research approach. Modifications of the lateral fluorinated chain lead to loss of activity. The aim of this work is exemplified by the replacement of the steroidal nucleus of UPR1358 with mimetic scaffolds.

Three class of steroidal mimetics have been explored: 1,2-diphenyl ethane, 2-phenylnaphtalene and 1,1'-biphenyl derivatives (figure 16). A unit of non-steroidal derivatives was obtained by attaching the *bis*-(trifluoromethyl)propanediol chain to the phenyl ring of the 1,2-diphenyl ethane scaffold (figure 17, panel A). The hydroxyl group at position 3 of the pregnenolone nucleus was replaced by

halogen atoms, whereas the chemical space between the rings A and D of the steroid nucleus was explored with an ethane chain, ethers groups, secondary and tertiary amides and a heterocycle ring. Finally, we investigated the position of the *bis*-(trifluoromethyl)propanediol chain on the phenyl ring. The class of 2-phenylnaphtalene derivatives consists of a β-naphthol ring, where the hydroxyl group superimpose the secondary alcohol of the pregnenolone core, and a phenyl ring where the *bis*-(trifluoromethyl)propanediol group has been attached in the *para* or *meta* position (figure 17, panel B). A third derivative was designed combining the 2-phenylnaphthalene core with a 4-fluoro-phenoxy group. The class of derivatives bearing a 1,1'-byphenyl core have been synthesized exploring the position 3 of the pregnenolone scaffold with an ester, a carboxylic acid, a ketone and alcohol groups (figure 17, panel C). Again, the *bis*-(trifluoromethyl)propanediol chain was attached at the *para* or *meta* position of the phenyl ring.

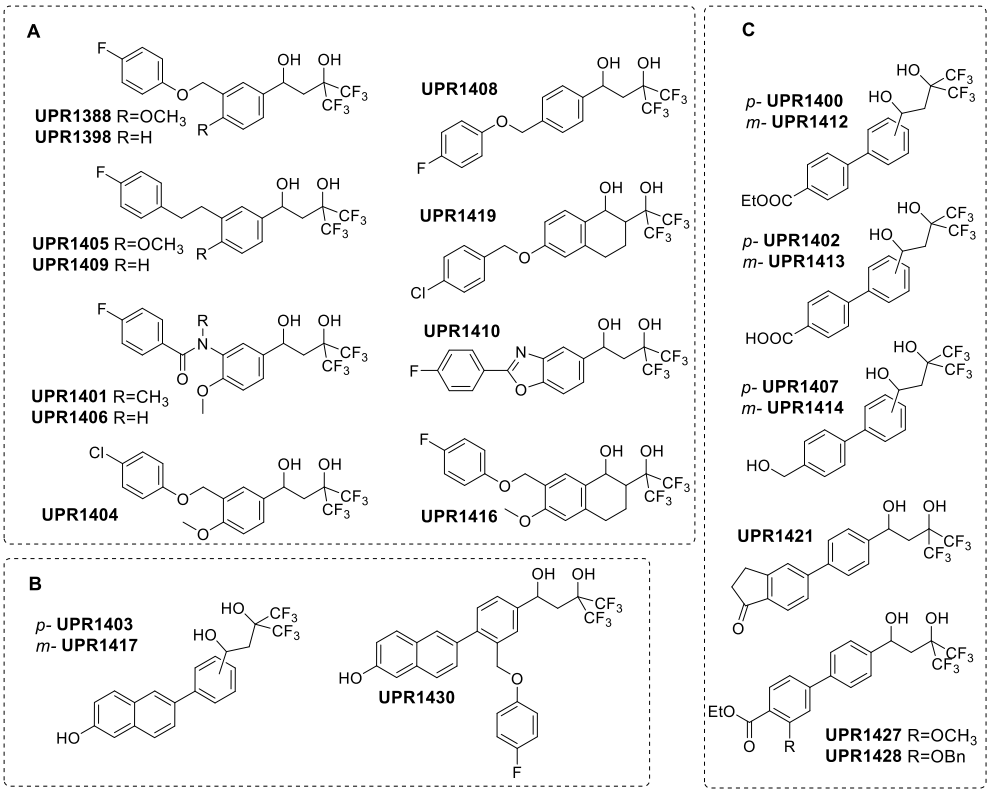

Figure 17: A) Non-steroidal derivatives with 1,2-diphenyl ethane scaffold. **B**) Non-steroidal derivatives with 2-phenylnaphtalene scaffold. **C**) Non-steroidal derivatives with 1,1'-biphenyl scaffold.

Since the role of the stereochemistry of the *bis*-(trifluoromethyl)propanediol group remained ambiguous, two enantiomers belonging to the 1,1'-byphenyl class (UPR1422 and UPR1426, figure 18) were isolated to evaluate their biological response (next section).

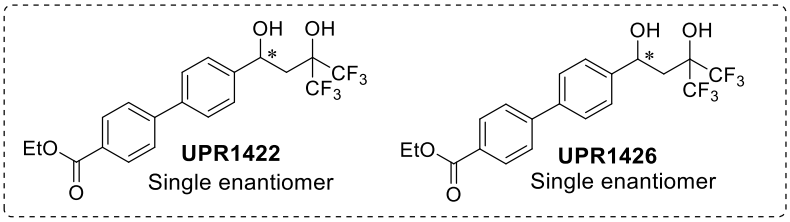

Figure 18: molecular structures of the isolated enantiomers.

2.7 Biological results

The biological evaluation of non-steroidal derivatives was performed at the University of Brescia in collaboration with the research group led by Professor Marco Presta.

The anti-proliferative activity was assessed by incubating the KMS-11 human myeloma cells with the designed compounds, performing a cell count viability assay (figure 19, C). Whether the inhibition of cell proliferation was to be ascribed to the suppression of FGF/FGFR signalling, it has been determined by measuring the inhibition of FGFR3 phosphorylation (figure 19 B).

The biological results were thus compared to that of the target compound UPR1358 and the negative probe UPR1420. The latter, constituted by the *bis*-(trifluoromethyl)propanediol group attached on a linear aliphatic chain, is a non-steroidal derivative with a negligible effect on FGF/FGFR system (figure 19 A, B and C).

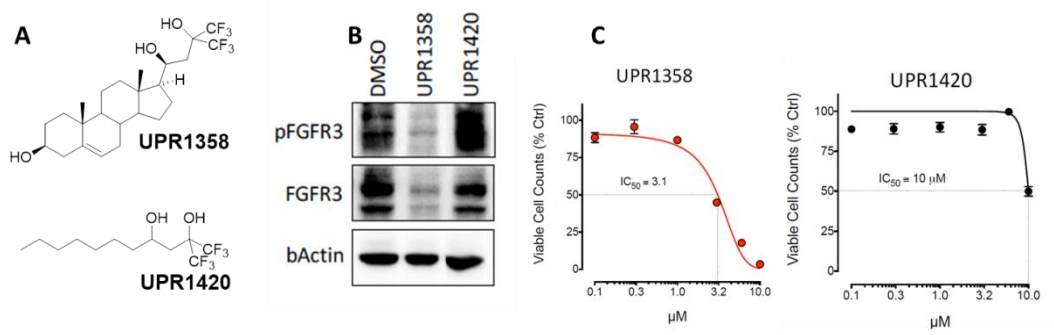

Figure 19: A) Chemical structure of target compound UPR1358 and the negative probe UPR1420. **B)** FGFR3 autophosphorylation assay. **C)** Cell count viability assay. UPR1358 $IC_{50} \approx 3.1$ µM. UPR1420 $IC_{50} \approx 10$ µM.

The biological results show that the substitution of the pregnenolone core with steroidal mimetic scaffolds generally leads to compounds with an anti-proliferative activity comparable to that of UPR1358. Nevertheless, the inhibition of cell proliferation appears in some cases unrelated to the inhibition of FGF/FGFR signalling, suggesting that different mechanisms of action can play a role for some of these compounds. Derivatives with polar moieties display a loss of activity, whereas the exploration of the surrounding space with hydrophobic groups is generally tolerated. Finally, the anti-proliferative activity and the inhibition of

FGFR3 phosphorylation appear favoured when the phenyl ring is substituted with the *bis*-(trifluoromethyl)propanediol group at the *para* position.

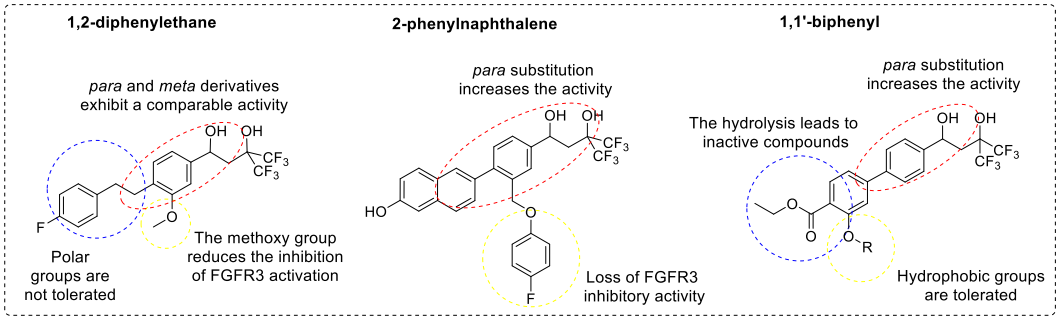

Figure 20: schematic representation of structure-activity relationships.

Compound UPR1398, belonging to class of 1,2-diphenyl ethane derivatives, shows a biological profile comparable to that of UPR1358, exhibiting a strong inhibition of FGFR3 phosphorylation. This is a remarkable result, demonstrating that the steroidal nucleus can be replaced by more versatile biomimetic scaffold, giving novel compounds still able to work as efficient FGF traps. The addition of a methoxy group on the phenyl ring leads to derivatives which maintain the inhibitory potency on cell viable assay, but exhibiting a decreased inhibition of FGFR3 phosphorylation (UPR1388, figure 21 panel B). The exploration of the steroid core with polar groups such as the amides and the heterocyclic ring resulted in a complete loss of activity (UPR1401, 1406 and 1410). The addition of an extra ring, as in case of the tetrahydronaphthalene derivatives UPR1419 and UPR1416, does not significantly change the antiproliferative activity. Finally, the position of the fluorinated group on the 1,2-diphenyl ethane scaffold marginally affects the biological activity.

The derivatives belonging to 2-phenylnaphtalene class share a similar inhibitory potency on cell proliferation. Nevertheless, only UPR1403 exhibits a strong inhibition of FGFR3 phosphorylation (figure 21, panel B). The lower potency of UPR1417 in inhibiting the FGFR3 activation suggests that the fluorinated chain lies in a sub-optimal position.

Within the 1,1'-biphenyl class, UPR1400 shows a biological profile comparable to that of UPR1358. Interestingly, the replacement of the ester group of UPR1400 with a carboxylic acid (UPR1402 and 1413), the benzyl alcohol (UPR1407 and UPR1414) or the ketone (UPR1421) strongly reduces the anti-proliferative activity

(figure 21, table A). The substitution of the phenyl ring also negatively affects the inhibition of FGFR3 phosphorylation as shown by UPR1427 and UPR1428. Again, the *meta*-substituted analogue UPR1412 is characterized by a lower anti-proliferative activity compared to that of UPR1400.

Finally, the biological evaluation of the enantiomers UPR1422 and UPR1426 has revealed that neither the anti-proliferative activity nor the inhibition of FGFR3 phosphorylation are affected by the stereochemical configuration of the secondary alcohol on the fluorinated chain (figure 21).

A

Non-steroidal derivatives	IC_{50} [1]	Inhibition of FGFR3 [2]
1,2-diphenyl ethane scaffold		
UPR1358 (NSC12)	4.6	74.2% [3]
UPR1388	7.2	-
UPR1404	5.1	-
UPR1405	5.2	-
UPR1406	>10	--
UPR1401	>10	--
UPR1410	>10	--
UPR1398	8.4	+
UPR1409	7.1	-
UPR1408	6.1	-
UPR1416	7.0	--
UPR1419	5.2	-
2-phenylnaphtalene scaffold		
UPR1403	4.2	+
UPR1417	4.6	--
UPR1430	3.9	--

Non-steroidal derivatives	IC_{50} [1]	Inhibition of FGFR3 [2]
1,1'-biphenyl scaffold		
UPR1400	6.0	+
UPR1402	>10	--
UPR1407	9.4	--
UPR1412	8.1	-
UPR1413	>10	--
UPR1414	>10	--
UPR1421	>10	--
UPR1427	5.3	-
UPR1428	6.9	-
Single enantiomers		
UPR1422	9.9	-
UPR1426	11.5	-

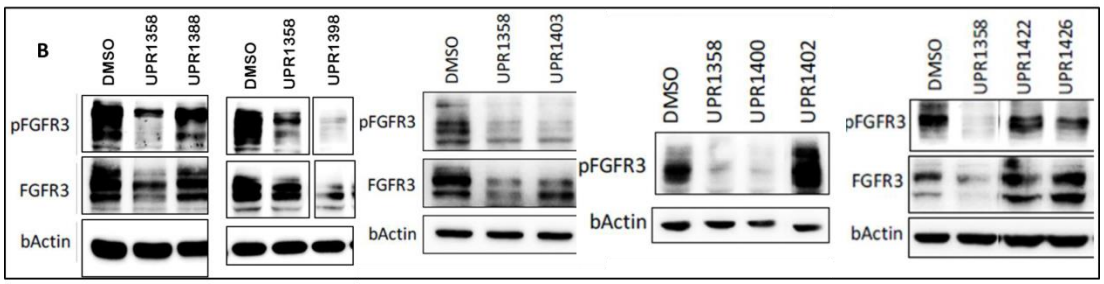

Figure 21: A) The table summarize the preliminary data of non-steroidal derivatives. Data are obtained after a single experiment.. [1] KMS-11 cells were incubated with increasing concentrations of tested compounds for 48 h and viable cells were quantified by flow cytometry (propidium iodide staining). [2] KMS-11 cells were incubated with 6 µM concentration of the tested compounds for 6 h. The cells were lysed and the receptors quantified by immunoblot assay. [3] Calculated inhibition ratio pFGFR3/FGFR3.''–'' indicates lower inhibition of FGFR3 phosphorylation compared to UPR1358.''+'' indicates higher inhibition of FGFR3 phosphorylation compared to UPR1358. **B)** Immunoblot detection of FGFR3 and phosphorylated FGFR3.

2.8 Synthesis of FGF traps

As a broadly defined strategy, the adopted synthetic approach consists of (i) the synthesis of the non-steroidal portion and then (ii) the synthesis of the *bis*-(trifluoromethyl)propanediol group (scheme 1, panel A). The latter is obtained following the same procedure adopted for the synthesis of UPR1358 and UPR1357[150]. The first step is an aldol-type condensation between a methyl-ketone, attached on the phenyl ring of the non-steroidal portion, and hexafluoroacetone (scheme 1, panel B). The resulting β-hydroxyketone is then reduced to afford the *bis*-(trifluoromethyl)propanediol.

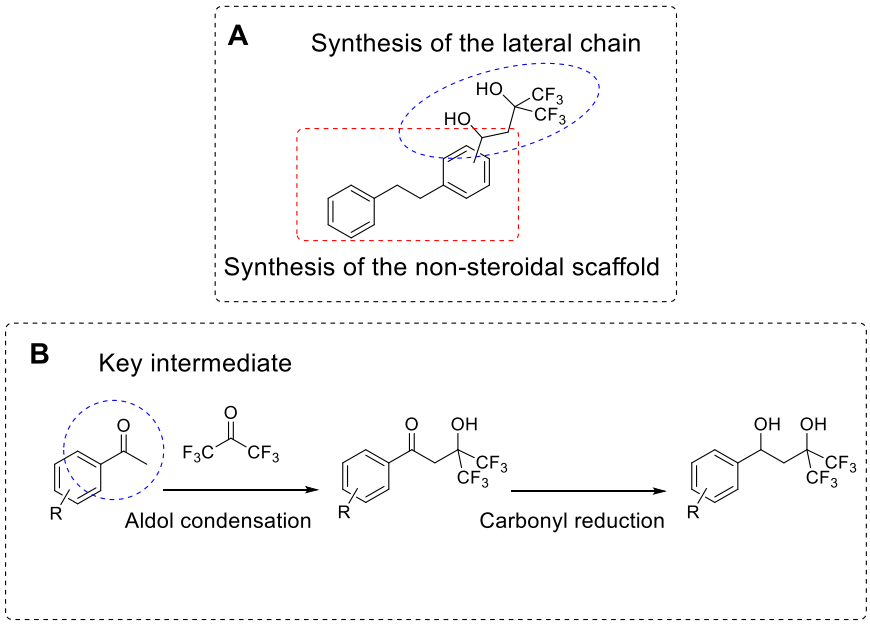

Scheme 1: A) general synthetic approach. **B)** Synthesis of the bis-(trifluoromethyl)propanediol group.

1,2-diphenyl ethane class

The multistep synthesis of UPR1398 and its isomer UPR1408 starts with the nucleophilic substitution of the proper bromomethyl benzoate with a 4-fluorophenol providing the aryl ether compounds **1** and **5** (scheme 2). These compounds were then converted in the corresponding ketones (**3** and **7**) using the Weinreb ketones synthesis (Weinreb-amide intermediate). Subsequently **3** and **7** served as the substrates for the aldol-type condensation affording to compounds **4** and **8** which were reduced to give the desired compounds.

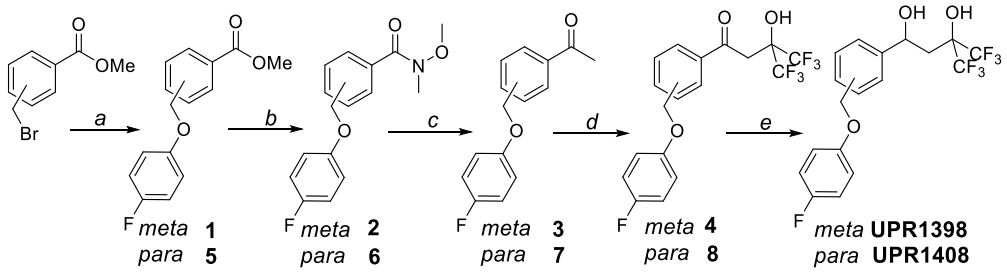

Scheme 2: *a) DMF, 4-fluorophenol, K_2CO_3, r.t,. 15 h. b) THF, N,O-dimethylhydroxylamine HCl, iBuMgCl, -40°C to r.t. c) THF, MeMgBr, 1 h. d) THF, LiHMDS, HFA, -60°C to r. t.. e) THF, MeOH, $NaBH_4$, 0°C, 30 min.*

A similar approach was followed to prepare UPR1409. The methyl-3-(bromomethyl) benzoate was converted in the corresponding organozinc reagent and used for the nucleophilic addition to the 4-fluorobenzaldehyde providing the intermediate **9** (scheme 3). This compound was reduced (**10**) and converted to the ketone **12** which served for the aldol condensation (**13**). Finally, the reduction of the β-hydroxyketone afforded UPR1409.

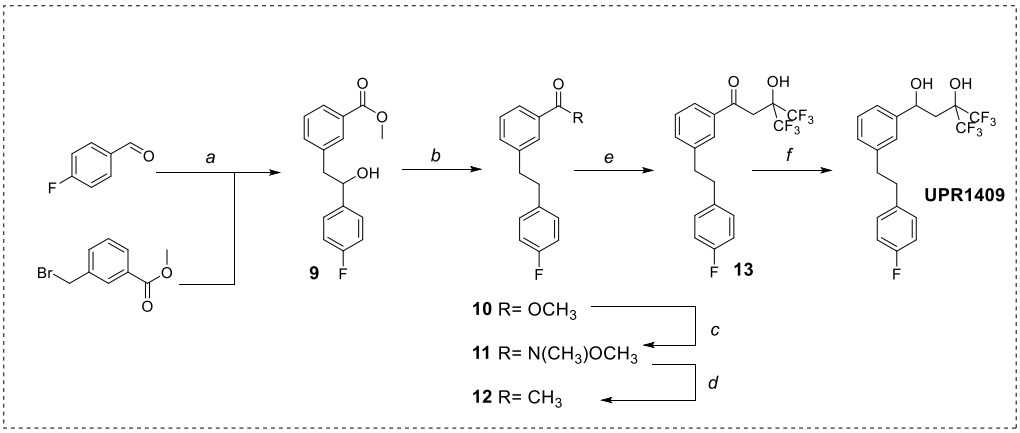

Scheme 3: *a) (i) THF, methyl 3-(bromomethyl)benzoate, Zn°, 80°C, 2 h. (ii) THF, 4-fluorobenzaldehyde, 0°C to r.t., 18 h, 25%. b) (i) HCl 37%, 50 min. (ii) AcOH, Zn°, 1 h, 33%. c) THF, N,O-dimethylhydroxylamine HCl, iBuMgCl, -40°C to r.t. 67% yield. d) THF, MeMgBr, 0°C, 1 h, 73%. e)* THF, *LiHMDS, HFA, -60°C to r. t.95%. f) THF, MeOH, $NaBH_4$, 0°C, 30 min, quantitative yield.*

The non-steroidal scaffold of UPR1410 was prepared from ethyl 4-hydroxybenzoate which was first subjected to an aromatic nitration and then converted to the corresponding aniline **15** (scheme 4). The acylation on amino group of **15** with 4-fluorobenzoyl chloride provided the amide **16**. This compound served as the precursor of **17** which was then converted to the corresponding ketone **19**. Finally, the *bis*-(trifluoromethyl)propanediol group was synthesised.

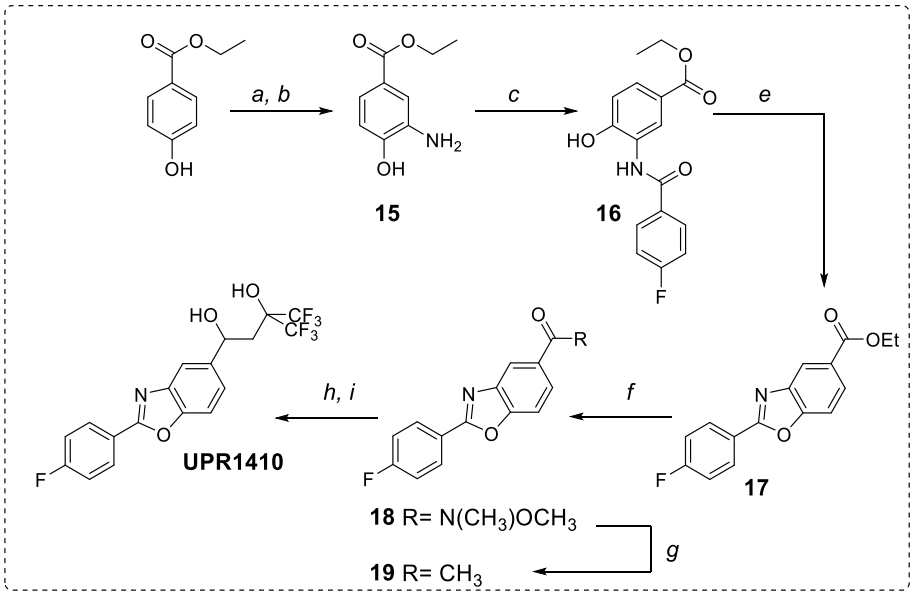

Scheme 4: *a) AcOH, HNO_3, 40°C, 3 h, quantitative yield. b) THF, water, 10% Pd/C, HCOONa, 50°C, 4 h, 98%. C) (i) $SOCl_2$, 4-fluorobenzoic acid, 90°C, 1,5 h. (ii) THF,* **15**, *Net_3, 0°C, 1 h, 65%. e) Toluene, pTSA, 110°C, 2 h, 66%. f) THF, N,O-dimethylhydroxylamine HCl, iBuMgCl, -40°C to -20°C. 80%. g) THF, MeMgBr, 0°C, 30min, 94%. h) THF, LiHMDS, HFA, -60°C to r. t. 3h, 60%. i) THF, MeOH, NaBH4, 0°C, 30 min, quantitative yield.*

A different approach was pursued in case of UPR1388. Here the *bis*-(trifluoromethyl)propanediol group has been synthesised by a nucleophilic addition of 2-(bromomethyl)-hexafluoropropan-2-ol, converted *in situ* to the corresponding organolithium reagent, to the aldehyde **22** (scheme 5). This represents an effort to explore a different synthetic route for the preparation of the fluorinated chain, but the organolithium intermediate appeared incompatible with different functional groups, rendering this approach albeit very straightforward, of limited synthetic utility.

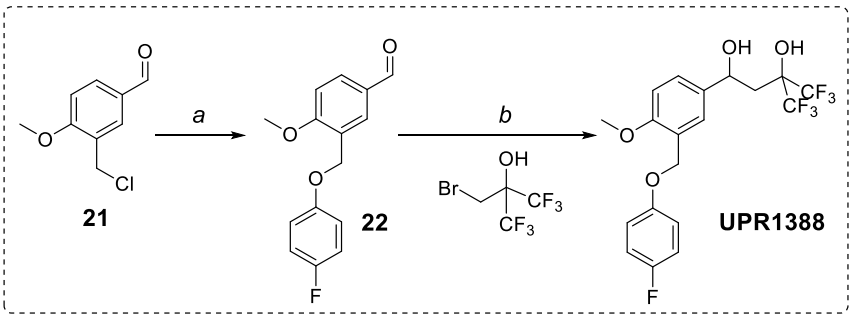

Scheme 5: *a) DMF, 4-fluorophenol, K_2CO_3, r.t., 18 h, 65%. b) THF, nBuLi, -78°C, 1 h, 35%.*

UPR1404, the chloro-analogues of UPR1388, was thus synthesised following the usual procedure (scheme 6). The aldehyde **24** was converted in the secondary alcohol **25** and then oxidized to the corresponding ketone **26** by means of a

modified Oppenauer oxidation, employing trimethylaluminum as the alcohoxide precursor. Finally, the *bis*-(trifluoromethyl)propanediol chain was obtained *via* aldol condensation and β-hydroxyketone reduction.

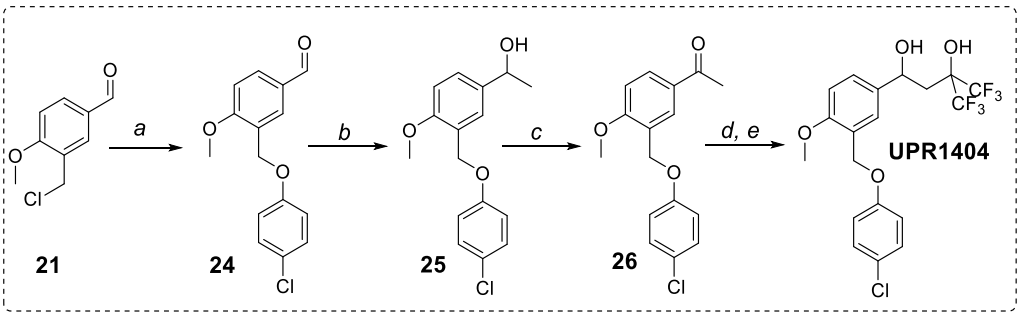

Scheme 6: *a) DMF, 4-chlorophenol, K2CO3, r.t., 18 h, 82%. b) THF, MeMgBr, 0°C, 20min, 97%. c) (i) Toluene, $Al(CH_3)_3$, 0°C, 20min. (ii) Toluene, ciclohexanone, 130°C, 2 h, 72%. d) THF, LiHMDS, HFA, -60°C to r. t. 4h, 30%. e) THF, MeOH, NaBH4, 0°C, 1 h, 75%.*

The synthesis of the scaffold of UPR1405 started from the conversion *in situ* of the 2-chloromethylanisole **28** in the corresponding organomagnesium compound and its addition to the *para*-fluorobenzaldehyde. The resulting secondary alcohol **29** was then reduced and subjected to a Friedel-Craft acylation providing the methyl ketone **31**. This compound served as the substrate for the aldol condensation and the following β-hydroxyketone reduction.

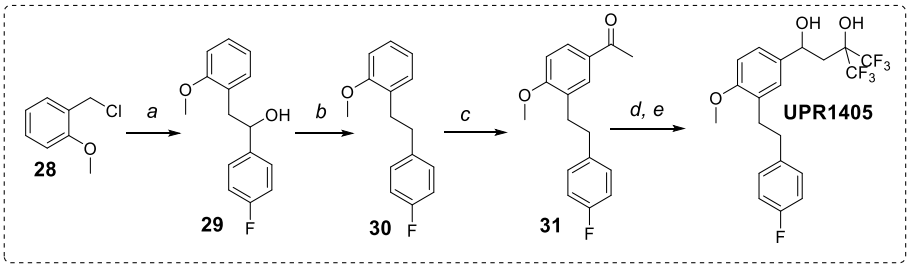

Scheme 7: *a) (i) THF, **28**, Mg°, 80°C, 30 min. (ii) THF, 4-fluorobenzaldehyde, 0°C, 30 min, 15%. b) (i) HCl 37%, 30 min, r.t. (ii) AcOH, Zn°, 110°C, 60 min, 60%. c) DCM, $AlCl_3$, Ac_2O, 0°C, 20 min, 68%. d) THF, LiHMDS, HFA, -60°C to r. t. 4h, 92%. e) THF, MeOH, $NaBH_4$, 0°C, 30 min, 81%.*

The 4-methoxy-3-nitro-acetophenone **33** served as the starting material for both derivatives UPR1406 and UPR1401 (scheme 8), which despite differing only for the methylation at the nitrogen atom, required to distinct synthetic routes, for some functional group incompatibilities (pKa values and very similar nucleophilicities). In case of UPR1406 the acetophenone **33** served as the substrate for the aldol condensation, providing the β-hydroxyketone derivative **34.** This was reduced in two steps to give the aniline/propanediol **36** which was acylated to provide the final compound UPR1406. On the other hand, for UPR1401, the nitro compound **33** was reduced as the first step to the corresponding aniline **37** and acylated with

4-fluorobenzoyl chloride to give the amide **38**. This was methylated (**39**) and then the *bis*-(trifluoromethyl)propanediol was synthesised affording UPR1401.

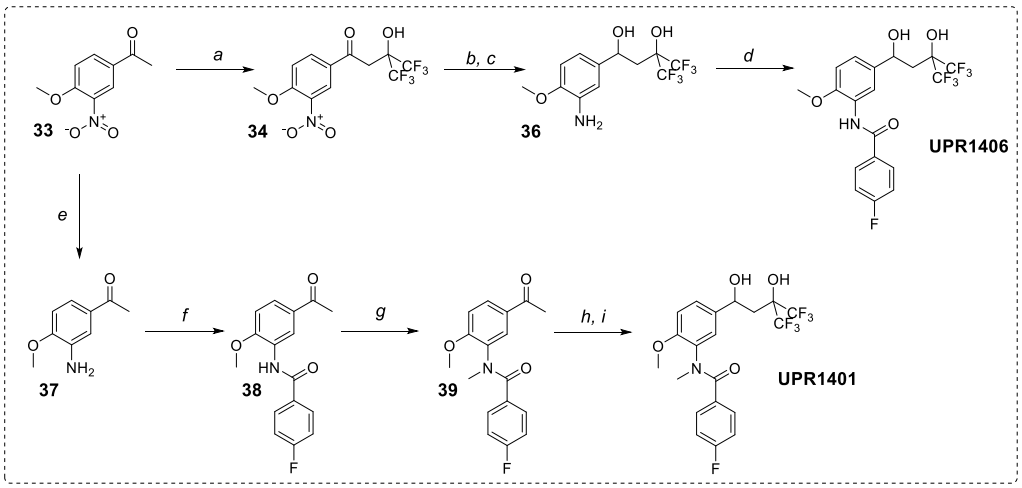

Scheme 8: *a) THF, LiHMDS, HFA, -78°C, 1 h, 31%. b) MeOH, $NaBH_4$, 0°C, 30 min, 65%. c) EtOH, water, AcOH, Fe°, r.t. 3 h, 70%. d) (i) $SOCl_2$, 4-fluorobenzoic acid, DMF, 1.5 h, r.t. (ii) Pyridine,* **36**, *30 min, r.t. 82%. e) EtOH, water, AcOH, Fe°, 3 h, 62%. f) (i) THF, 4-fluorobenzoic acid, pivaloyl chloride, DiPEA, 0°C, 30 min. (ii) THF,* **37**, *0°C to r.t., 18 h, 66%. g) THF, NaH, MeI, 0°C, 2.5 h, 95%. h) THF, LiHMDS, HFA, -78°C, 1 h, 31%. i) MeOH, $NaBH_4$, 0°C, 20 min, 90%.*

The synthesis of UPR1416 features a nucleophilic substitution at the benzylic position of compound **41** which provided aryl ether **42**. This was then converted in the desired product through the usual route (scheme 9). Analogously, UPR1419 was obtained by aldol-type condensation and the β-hydroxyketone reduction from the aryl ether **44**.

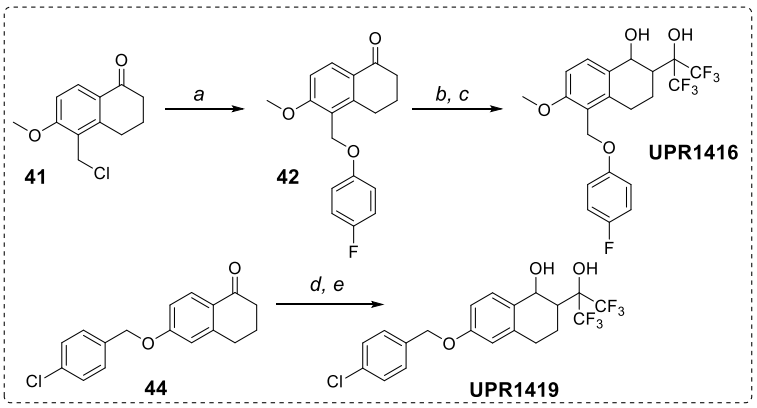

Scheme 9: *a) DMF, 4-fluorophenol, K_2CO_3, r.t., 18 h 37%. b) THF, LiHMDS, HFA, -60°C, 3 h, 43%. c) MeOH, $NaBH_4$, 0°C, 30 min, 53%. d) THF, LiHMDS, HFA, -60°C, 3 h, 32%. e) MeOH, $NaBH_4$, 0°C, 30 min, 36%.*

2-phenylnaphtalene class

To obtain the compounds of this class, the central C-C bond was planned to be obtained through a Suzuki-Miyaura Pd-catalyzed cross coupling reaction. The derivative UPR1403 and its regioisomer UPR1417 were obtained from the TBS-protected aryl-halide **47** (scheme 10). This compound served as a partner for the Suzuki-Miyaura coupling which provided ketone intermediates **48** and **51**. The target compounds were obtained by deprotecting the phenol group after condensation and the reduction of the resulting β-hydroxyketone intermediates (**49** and **52**).

The 6-bromonaphth-2-ol **46** was converted to the corresponding boronic ester **54** which served, together with the aryl-halide **56**, for the carbon-carbon bond formation providing the intermediate **57**. The nucleophilic substitution at the benzylic position of **57**, and the aldol condensation gave compound **58** which was reduced to afford UPR1430.

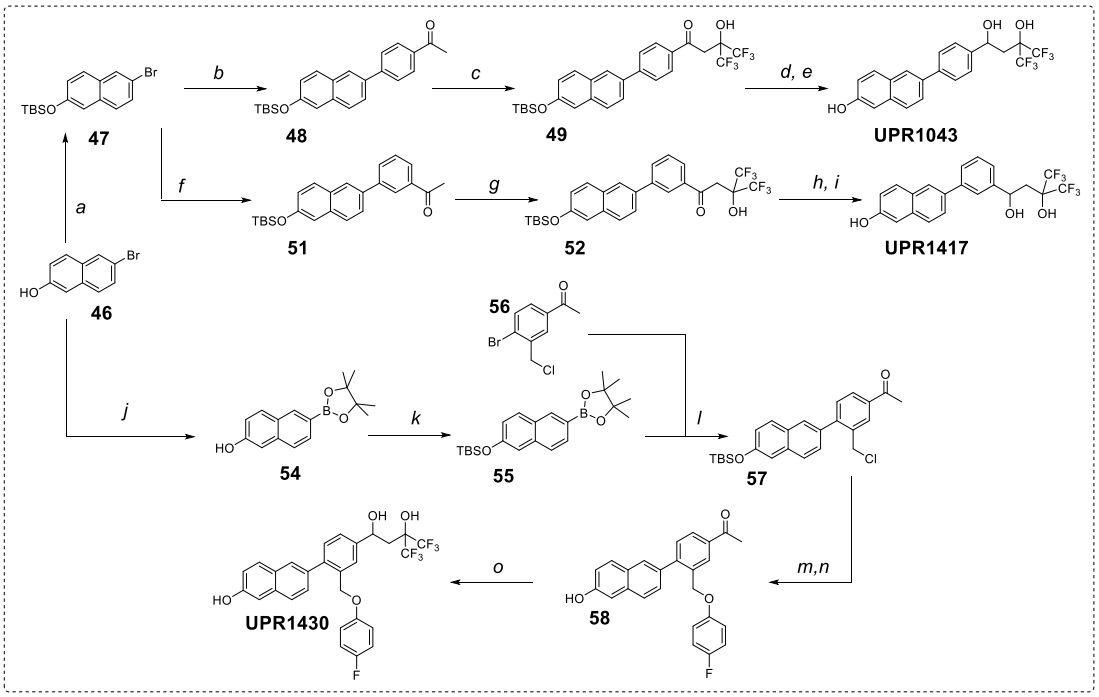

Scheme 10: *a) DMF, TBDMSiCl, NEt_3, 0°C, 24 h, 66%. b) 1,4-dioxane, water, 4-acetylphenylboronic acid pinacol ester, $Pd(PPh_3)_2Cl_2$, K_2CO_3, 100°C, 5 h, 66%. c) THF, LiHMDS, HFA, -60°C,3 h, 71%. d) THF, MeOH, $NaBH_4$, 0°C, 2 h, 96%. e) THF, TBAF, 3 h, 85%. f) 1,4-dioxane, water, 3-acetylphenylboronic acid pinacol ester, $Pd(PPh_3)_2Cl_2$, K_2CO_3, 100°C, 5 h, 62%. g) THF, LiHMDS, HFA, -60°C, 30%. h) THF, MeOH, $NaBH_4$, 0°C, 2 h, 86%. i) THF, TBAF, 3 h, 97%. j) 1,4-dioxane, B_2Pin_2, $Pd(Dppf)Cl_2$, AcOK, 90°C, 6 h, 55%. k) DMF, TBDMSiCl, imidazole, 0°C, 18 h, 83%. l) 1,4-dioxane, water, $Pd(PPh_3)_2Cl_2$, K_2CO_3, 90°C, 7 h, 73%. m) DMF, 4-fluorophenol, K_2CO_3, r.t. 18 h, 25%. n) THF, LiHMDS, HFA, -60°C, 3 h. (ii) THF, TBAF, 3 h, 58%. o) THF, MeOH, $NaBH_4$, 0°C, 1 h, 90%.*

Biphenyl class

The derivatives belonging to the biphenyl class share a similar synthetic route where the biphenyl scaffold is provided by a carbon-carbon bond formation between two functionalized phenyl rings under Suzuki-Miyaura conditions. The *bis*-(trifluoromethyl)propanediol group is then synthesised through the usual aldol condensation and the subsequent β-hydroxyketone reduction.

UPR1400, UPR1402 and UPR1407 were obtained from the common ketone intermediate **62** which served as the substrate for the aldol condensation (scheme 11). From **63**, the simultaneous reduction of the ester and carbonyl groups led to UPR1407 whereas the selective reduction of β-hydroxyketone provided UPR1400. Finally its hydrolysis gave UPR1402.

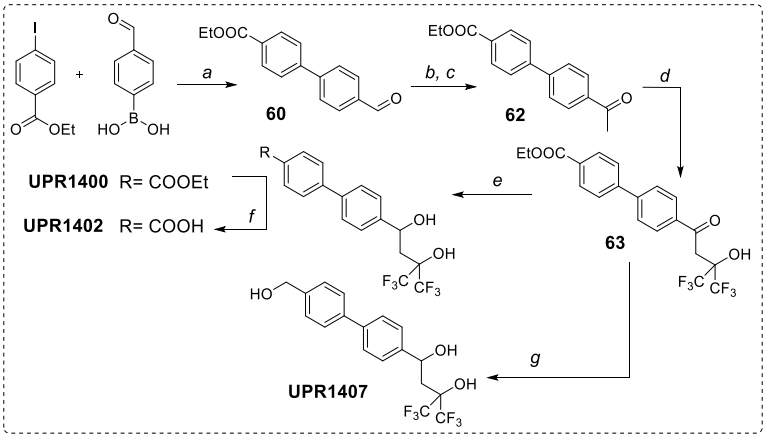

Scheme 11: *a) 1,4-dioxane, water, $Pd(PPh_3)_2Cl_2$, K_2CO_3, 100°C, 3 h, 87%. b) THF, MeMgBr, 0°C, 1min, 99%. c) (i) Toluene, $Al(CH_3)_3$, 0°C, 20min. (ii) Toluene, ciclohexanone, 130°C, 3 h, 77%. d) THF, LiHMDS, HFA, -60°C, 3 h, 95%. e) THF, MeOH, $NaBH_4$, 0°C, 30 min, 75%. F) H_2O, THF, NaOH, r.t., 18 h, 70%. g) THF, $LiAlH_4$, 0°C, 1 h, 58%.*

The same synthetic approach was followed to obtain the regioisomers UPR1412, UPR1413 and UPR1414, as depicted in scheme 12.

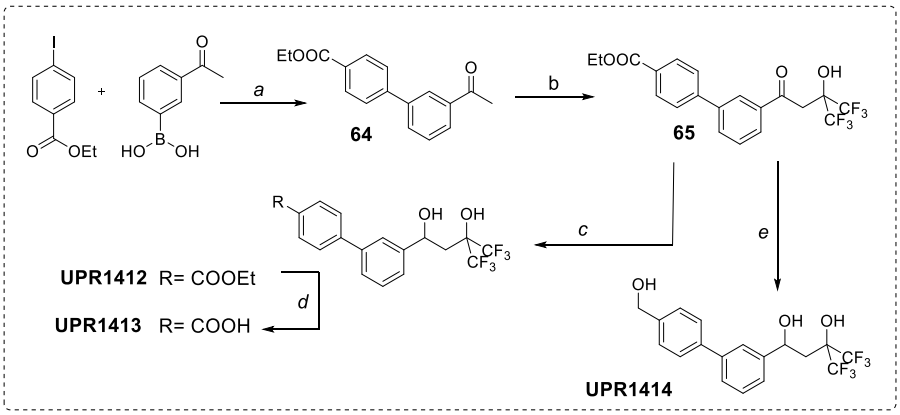

Scheme 12: *a) 1,4-dioxane, water, $Pd(PPh_3)_2Cl_2$, K_2CO_3, 100°C, 3 h, 83%. b) THF, LiHMDS, HFA, -60°C,3 h, 58%. c) HF, MeOH, $NaBH_4$, 0°C, 30 min, 99%. d) Water, THF, NaOH, r.t., 18 h, 73%. e) THF, $LiAlH_4$, 0°C, 1 h, 70%.*

In a similar fashion, the biphenyl scaffold of UPR1427 and UPR1428 was obtained through a Suzuki-Miyaura coupling between the substituted ethyl 4-iodobenzoate (**66** and **69**) and the corresponding boronic acid (scheme 13). The resulting ketones (**67** and **70**) served as the substrate for the synthesis of the *bis*-(trifluoromethyl)propanediol group. In case of UPR1421, the Suzuki reaction was performed between the aryl-halide **73**, already equipped with the fluorinated chain, and the boronic ester **74**. This procedure prevented the aldol condensation with the indanone moiety of **74**, and additionally served to prove the stability of the *bis*-(trifluoromethyl)propanediol group under the conditions of Suzuki-Miyaura coupling.

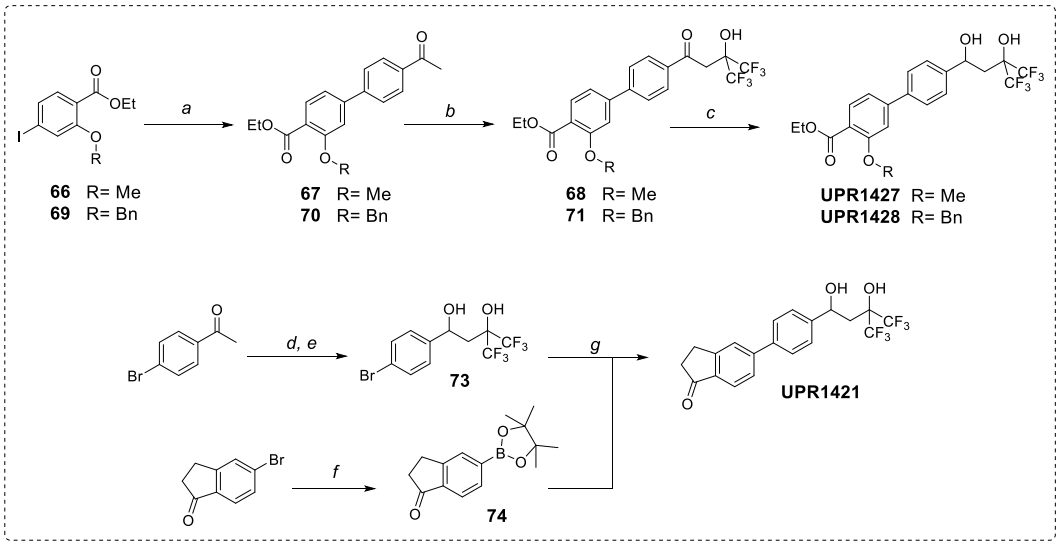

Scheme 13: *a) 1,4-dioxane, water, $Pd(PPh_3)_2Cl_2$, K_2CO_3, 100°C. b) THF, LiHMDS, HFA, -60°C. c) THF, MeOH, $NaBH_4$, 0°C. d) THF, LiHMDS, HFA, -60°, 3 h, 58%. e) THF, MeOH, $NaBH_4$, 0°C, 2 h, quantitative yield. f) DMF, B_2Pin_2, $Pd(OAc)_2$, AcOK, 90°C, 6 h, 15%. g) 1,4-dioxane, water, $Pd(PPh_3)_2Cl_2$, K_2CO_3, 100°C, 6 h, 15%.*

The chiral derivatization of racemic mixture **73** with *N*-Boc-L-alanine allowed the chromatographic separation of diastereoisomers **75a** and **75b** (scheme 14). These were hydrolysed to give isolated enantiomers **76a** and **76b** which were coupled with **77** to provide UPR1422 and UPR1426.

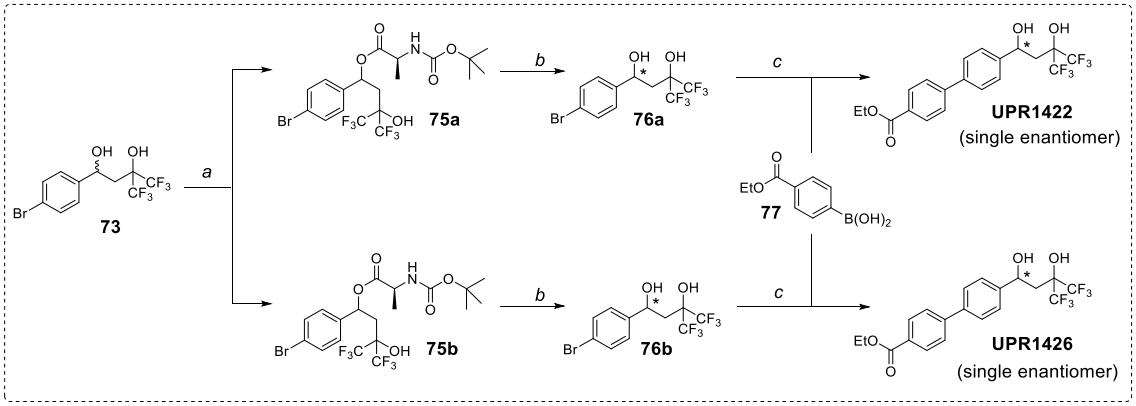

Scheme 14: a) *DCM, N-Boc-L-Alanine, DMAP, EDC, 0°C to r.t., 18 h. 36%* **75a***; 11%* **75b***. b) MeOH, Na°, 0°C 24 h. 82%* **76a***; 91%* **76b***. c) 1,4-dioxane, water, $Pd(PPh_3)_2Cl_2$, K_2CO_3, 100°C, 5 h. 69%* UPR1422*; 35%* UPR1426*.*

The negative probe UPR1420 was obtained by converting the octanoic acid **78** to the corresponding ketone **80** (scheme 15). This served as the substrate for the aldol condensation and the following reduction of the β-hydroxyketone.

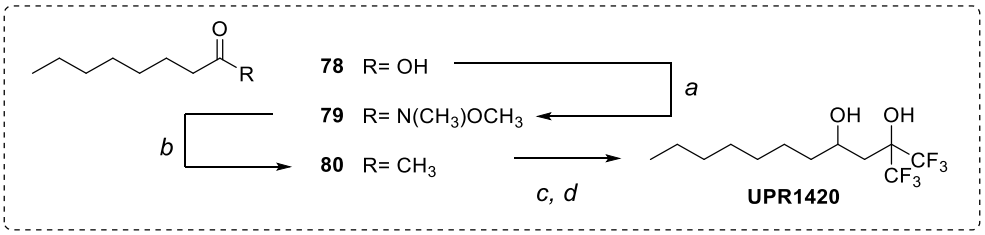

Scheme 15: *a) (i) DMF, NEt_3, ethyl chloroformate, 0°C, 30 min. (ii) N,O-dimethyl hydroxylamine hydrochloride, r.t. 8 h, 76%. b) THF, MeLi, 0°C, 20 min, 91%. c) THF, LiHMDS, HFA, -60°, 3 h, 29%. d) THF, MeOH, $NaBH_4$, 0°C, 2 h, 58%.*

3 Epidermal growth factor receptor

3.1 Overview on ErbB family

ErbB is a family of tyrosine kinases constituted by four receptors: the epidermal growth factor receptor (EGFR, or ErbB1 also known as HER1), which represents the first identified RTK, ErbB2, ErbB3 and ErbB4 (also called HER2-4).[151] Belonging to the class of receptor tyrosine kinases, ErbB receptors share common structural features such as an extracellular region, a trans-membrane helix and a cytosolic kinase domain. The receptor ErbB3 lacks the intracellular domain and is devoid of any catalytic activity. Their ligands can be divided in four groups according to their receptor specificity. EGFs (Epidermal Growth Factors), TGF-α (Transforming Growth Factor-α) and amphiregulin bind specifically to EGFR, betacellulin, epiregulin and heparin-binding EGF show affinity for EGFR and ErbB4 whereas neuregolins (NRGs) are able to bind specifically to ErbB3 and ErbB4 (NRG1 and NRG2) or only to ErbB4 (NRG3 and NRG4).[44,152,153] Most of the ErbB factors are exposed as precursors on the cell membrane, and they are released, under proper stimuli, by enzymatic cleavage by cell surface proteases.[154] This mechanism serves to regulate the ligand concentration on the extracellular environment.

The extracellular region is organized in four domains (D1-D4) where domain D1 and D3 are constituted by several LRR-like (Leucine Rich Repeat) β-helices capped by a α-helix, and domains D2 and D4, consisting of ~150 amino acids, which contains cysteine rich regions.[36,155] In its inactive state the extracellular region is assembled in a gathered conformation where D2 region is buried between D1 and D3 domains.[156,157] When the ErbB ligand approaches its receptor, D1 and D3 domains act as a pincer to accommodate the ligand disclosing the D2 domain which is now able to exposes its dimerization arm.[158] The dimerization can occur between two identical ErbB receptors (homo-dimer) or between two different members of the family (hetero-dimer). In both cases the interface of the dimer is constituted by the D2 domains (they interact each other) whereas the ligands serves only to disrupt the auto-inhibited gathered conformation.[159] ErbB2, lacking of the extracellular domains D1 and D3, has a fixed structure where the dimerization arm is always exposed, resembling the active conformation.[160] This is

consistent with the fact that ErbB2 is often found as a hetero-dimerization partner with other ligand-activated receptors.[44,161]

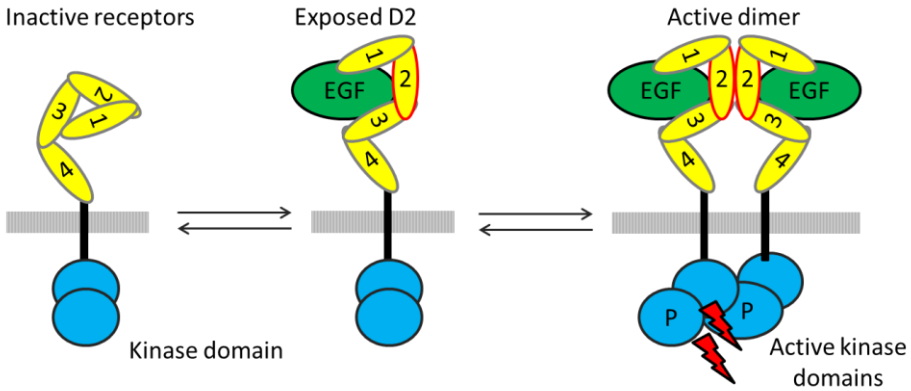

Figure 22: schematic representation of EGFR dimerization.

Generally, the mechanism of activation of the RTKs involves a key phosphorylation event at the activation loop. The EGFR/ErbB family represents an exception showing a unique mechanism of kinase activation.[151,162] The assembly of ErbB dimer leads to the formation of an asymmetric cytoplasmic complex where the C-lobe of one kinase domain serves as an ''activator'' for the ''receiver'' N-lobe of the neighbouring kinase domain. This interaction induces the rotation of the C-helix of the receiver, followed by the formation of the conserved ionic bridges between the residue Glu762 (on the C-helix of the N-lobe) and the Lys745 (on the β3-strand of the N-lobe). As a consequence of these conformational changes, the receiver kinase adopts the usual configuration of the active catalytic state without having phosphorylated its activation loop.[163] The juxtamembrane region of the receiver kinase also promote the interaction between the receiver and the activator kinases.[164]

Once the cytoplasmic domain is activated, the recruitment of adaptor proteins allow the signalling transduction.[165] The activated pathway includes RAS-RAF-MAPK PI3K-AKT-mTOR (Mammalian Target Of Rapamycin), PLCγ-PKC and the transcription factors activator JAK-STAT signalling which affect the proliferation, the differentiation and the cell survival.[166,167]

3.2 ErbB family and cancer

ErbB signalling contributes to cell proliferation, differentiation and survival in several tissues. The entire process from the expression to the activation of the receptors, as well as the expression and release of EGF ligand family is highly regulated.[151] The deregulation of ErbB family signalling has been found in many cancers, where it represents a poor prognosis factor or even an oncogenic driver.[44,168,169,170] The gene amplification and overexpression of mutated ErbB family occur in 35% of glioblastoma cases, where the expression of aberrant EGFR-(vIII) is a well-known mutation[9]. EGFR-(vIII) exhibits an aberrant extracellular region, which lacks domain I and part of domain II, with an impaired auto-inhibitory mechanism resulting in a constitutively activated conformation.[171]

EGFR also plays a key role in lung cancer development, where its mutated forms appear in 20-80% cases of NSCLC (non-small cell lung cancer).[172] One of the most common mutations found in NSCLC is L858R, a point mutation which affects the kinase domain and promotes a ligand-independent signalling.[173].

3.3 EGFR Tyrosine kinase inhibitors

EGFR is a validate target in anti-cancer therapy as demonstrated by the different kinase inhibitors approved for clinic use.[44,169] The first generation of EGFR TKIs comprises the reversible compounds gefitinib and erlotinib, which have been approved in 2003 and 2004 respectively, for the treatment of NSCLC.

These agents have achieved high clinical response rate by targeting specifically L858R mutated EGFR.[174–177] Aberrant $EGFR^{L858R}$ displays lower affinity to ATP compared to the wild-type receptor, nevertheless this mutation promotes a ligand-independent signalling and represents an oncogenic factor for NSCLC development.[178] The different affinity to ATP provides an advantage factor to selectively target the mutated receptor.[179]

X-ray diffraction data show how erlotinib and gefitinib bind the kinase domain establishing a hydrogen bond between *N*1 of the 4-amino-quinazoline ring and backbone residues at the ATP binding pocket.[180,181] The aniline ring is involved in a key interaction with a hydrophobic pocket, at the gatekeeper position, which is

not exploited by ATP (figure 23). Moreover, the lateral substituents extend in a solvent exposed region.

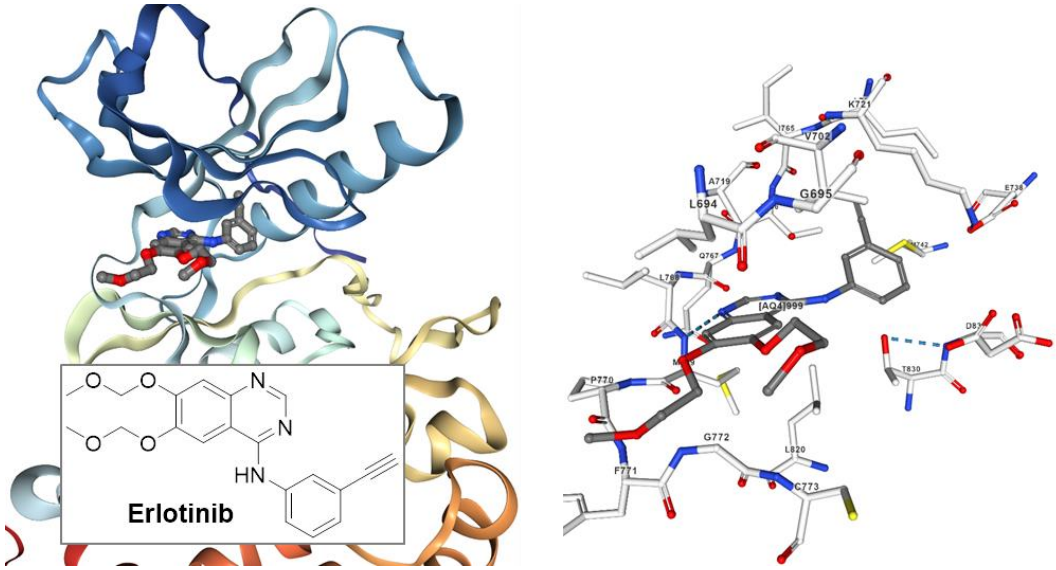

Figure 23: crystal structure of EGFR and first generation inhibitor erlotinib (PDBID:1M17).

The clinical efficacy of first generation TKIs is limited to 10-14 months of therapy, when the development of resistance, often due to secondary mutations, induces resistance to these inhibitors.[182] One of the best characterized secondary point mutations is the replacement of the gatekeeper threonine with a methionine residue (T790M).[183] This event hampers the hydrophobic interaction of the aniline ring of the first generation agents at the gatekeeper position. Additionally, this mutation restores the affinity of $EGFR^{L858R/T790M}$ to ATP, further limiting the efficacy of TKIs due to an increased competition with intracellular ATP.[184] $EGFR^{T790M}$ has been reported in almost 70% of patients with acquired resistance to EGFR TKIs, and thus represents a case of mutation induced by first generation EGFR inhibitors.[185]

A second generation of irreversible TKIs was designed to overcome the gatekeeper mutation and restore the clinical efficacy.[186–188] Afatinib has been approved in 2013 for the treatment of advanced lung cancer.[12] This compound targets the ATP binding pocket interacting with its 4-amino-quinazoline ring and the acrylamide warhead reacts with a conserved cysteine residue (Cys797) at the hinge region.[189,190] The irreversible inhibition avoids the binding competition with

cellular ATP thus increasing the potency and the clinical efficacy of TKIs. This class of agents exhibits a low maximum tolerated dose due to a low selectivity and the inhibition of the wild-type EGFR.[191] This on-target toxicity is characterized by diarrhea, fatigue and adverse skin reactions.[192,193]

A third generation of EGFR TKIs has been recently disclosed to target selectively the mutated EGFR thus avoiding the related adverse effects.[194–196] Osimertinib[197], rociletinib[198], olmutinib[199] and WZ4002[57] are some of third-generation inhibitors (figure 24). Among these compounds osimertinib has been approved by FDA in 2015 for the treatment of NSCLC expressing EGFR^{T790M}.

These compounds adopt a U-shaped conformation at the ATP binding site allowing the target of the Cys797. They share a common 2-amino-pyrimidine ring which establishes key hydrogen bonds with the backbone residues of the hinge region.[57] The pyrimidine core is substituted by a small hydrophobic moiety, constituted by 5-membered heterocyclic moieties or halogen atoms that interact hydrophobically with the mutated gatekeeper residue (Met790), thus corroborating the selectivity over the wild-type receptor.

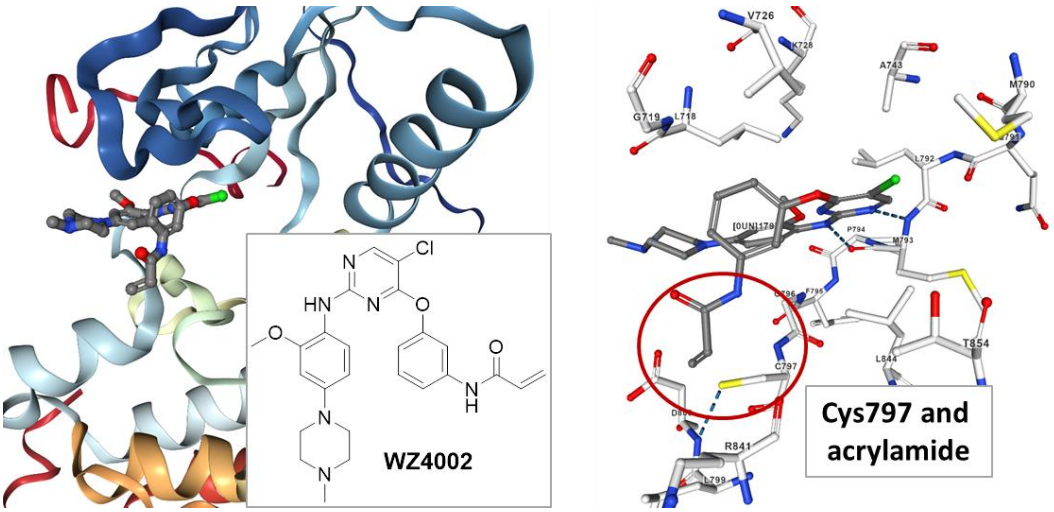

Figure 24: crystal structure of EGFR and third generation covalent inhibitor WZ4002 (PDBID3LKA).

The long term therapy with second and third generation EGFR TKIs has been correlated to the insurgence of secondary mutations,[200–202] among which the targeted cysteine (Cys797) has been found mutated in a less nucleophilic serine (C797S)[203,204] or glycine (C797G), excluding the option of the irreversible inhibition

as a strategy.[205] Thus, the selection of a triple mutant EGFR$^{L858R/T790M/C797S}$, or the activation of bypassing signalling pathways lead to a dramatic reduction of therapeutic options.[206,207]

3.4 Aim of the work

A class of 2,4-diaminopyrimidine based inhibitors were synthesised with the aim of targeting EGFR receptors characterized by the mutation of the Cys797 residue. Being the target for acrylamide warheads of covalent inhibitors, its mutation led to loss of clinical efficacy of therapies based on third generation of EGFR inhibitors (figure 25)[208]. The mutation of the cysteine residue with a serine (C797S) demands developing covalent agents bearing new electrophilic warheads. Additionally, the mutation of the cysteine residue into a glycine (C797G) has been already detected, thus rendering ineffective any strategy based on covalent inhibitors that address residue 797. It becomes therefore necessary to identify different residues as the target for covalent inhibition as alternative strategy.

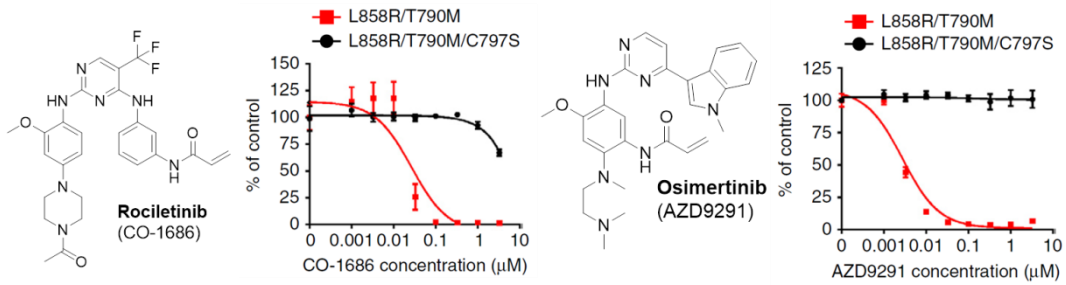

Figure 25: inhibition of proliferation exerted by third generation EGFR inhibitors rociletinib and osimertinib in Ba/F3 lines harbouring EGFR with double mutation (L858R/T790M) or triple mutation (L858R/T790M/C797S). Figure adapted from [208]

We focused our attention on a lysine residue (Lys745), spatially close to the P-loop, which is involved in the formation of a conserved salt bridge with Glu762, located on the C-helix. This crucial interaction allows the kinase to adopt an active catalytic state, thus the risk of casual point mutation of Lys745 is reasonably low.
A 2,4-diaminopyrimidine ring shared by third generation EGFR inhibitor rociletinib was chosen on the basis of computational modelling analysis and synthetic feasibility. The steric arrangement of the U-shaped structure of rociletinib appeared to be favourable to reach the proximity of the lysine residue and it was designed to bind selectively to EGFRT790M over the wild-type EGFR, providing a solid base for the selectivity towards the receptor. Lastly, the few synthetic operation involved in its preparation made its synthesis particularly appealing, with minor modifications.

With a suitable scaffold in our hand, we focused our attention on the exploration of electrophilic warheads able to react with the lysine residue. On this basis five different compounds were initially synthesized: a negative control UPR1423 with a non-reactive acetamide and four compounds UPR1424, UPR1425, UPR1432 and UPR1433 each with a different reactive group (figure 26).

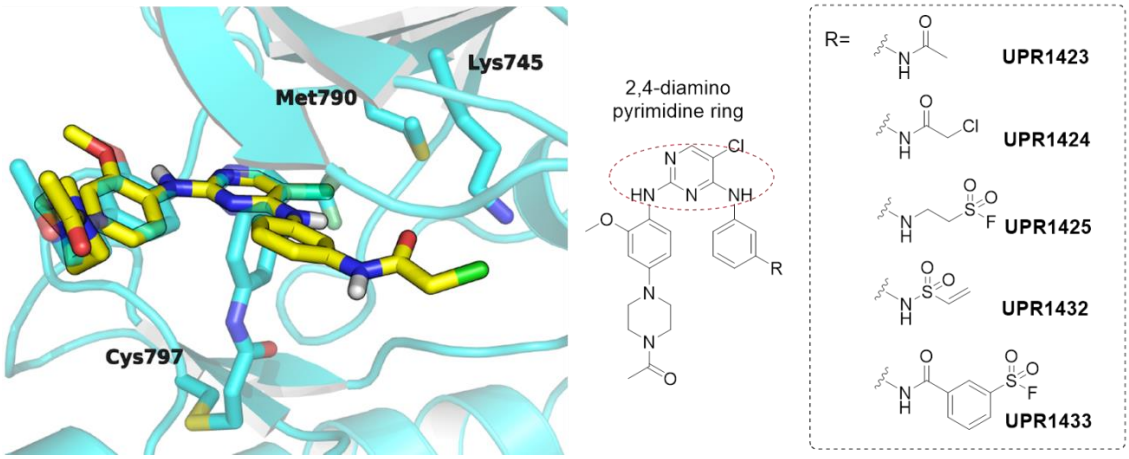

Figure 26: left side, docket pose of UPR1424 (yellow) superimposed to crystal structure of rociletinib (light blue) in complex with EGFR^{T790M} (PDBID: 5XDK). Right side, molecular structure of synthesised 2,4-diaminopyrimidine compounds.

The 2-chloroacetamide derivative UPR1424 was designed for its high reactivity toward nucleophiles and thus the reasonable ability to give a covalent adduct with the target lysine. The sulfonyl fluoride group of UPR1425 and UPR1433 was selected as a suitable warhead able to target the lysine residue, since this class of electrophiles has been exploited in chemical biology to obtain covalent probes that bind lysines. A recent example is provided by the multi-target kinase inhibitor XO44, that in complex with the kinase Src or EGFR confirms the chemoselective reaction between its sulfonyl fluoride warhead and the target lysine, proved by X-ray diffraction crystallography.[209] The vinyl sulphonamide group was selected as a possible lysine-targeting warhead in UPR1432. This electrophilic moiety was found to bind irreversibly the lysine residue as exemplified by CDK2 inhibitor NU6300.[210] As geometrical requirements play a role in the early phases of adduct formation, an additional derivative decorated with a sulfonyl fluoride warhead was designed (UPR144), in order to reproduce as much as possible the conformation adopted by the chemical probe XO44 in the adduct with EGFR (figure 27).

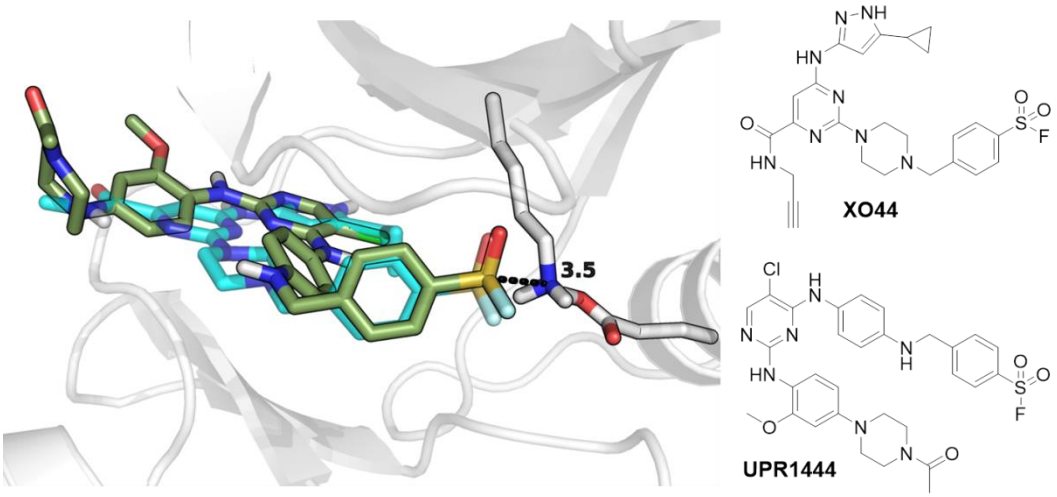

Figure 27: docket pose of UPR1444 (green) superimposed to the crystal structure of XO44 (light blue) in complex with EGFR (PDBID: 5U8L).

3.5 Biological results

The synthesised derivatives were tested to evaluate (i) their activity on triple mutant $EGFR^{L858R/T790M/C797S}$, (ii) their mechanism of inhibition and (iii) their anti-proliferative effect assessed *in vitro* on different cell lines.

The inhibitory activity on triple mutant EGFR isoform has been measured quantifying the amount of phosphorylated product by Time Resolved Fluorescence Energy Transfer (TR-FRET). The FRET-based assay served to obtain an IC_{50} value of the kinase inhibition performing the measure with ATP and pre-incubating (3 hours) the inhibitor and the receptor in absence of ATP. The two different IC_{50} measures collected for each compound gave us preliminary information on the nature of the binding between the triple mutant EGFR and the tested compound. In particular, for slow-binding covalent inhibitors pre-incubation causes a decrease in IC_{50} values (i.e. an increase of potency). Along with the synthesised 2,4-diaminopyrimidine derivatives, the FRET based assay was performed also to measure the inhibitory potency of three reference compounds: brigatinib[211] (a non-covalent inhibitor able to inhibit EGFR with C797S mutation) as a positive control, osimertinib as a negative control and XO44 as a positive control given its reported ability to bind the Lys745 covalently.

As expected, the covalent probe XO44 displays two different IC_{50} values, with a ≈ 40 fold potency increase when tested after pre-incubation, whereas brigatinib exhibit a high inhibitory potency with an IC_{50} value of ≈ 9nM (figure 28). Compound UPR1424 displayed a high IC_{50} value comparable to that of osimertinib and UPR1423, thus indicating that the 2-chloroacetamide appears an unsuitable electrophilic group for the targeted lysine. Compound UPR1432, with a vinyl sulphonamide warhead, exhibited a low inhibitory potency and its pre-incubation with the target gave a negligible potency improvement. Similar results were observed for the derivative with the aliphatic sulfonyl fluoride warhead UPR1425, where the pre-incubation with its target did not result in an appreciable potency improvement. On the other hand the derivative bearing the 4-carbamoylbenzensulfonyl fluoride showed a lower potency compared to that of UPR1425, but the pre-incubation with the receptor led to ≈ 6 folds increase of the IC_{50} value. Finally, UPR1444, bearing a sulfonyl fluoride group on a different scaffold, exhibited an inhibitory potency 100 fold lower than that of brigatinib but

its pre-incubation gave a ≈ 67 folds potency improvement The nature of the binding between UPR1444 with triple mutant $EGFR^{L858R/790M/C797S}$ isoform was further investigated by a rapid dilution assay, which revealed irreversible inhibition. The results of this test corroborated the hypothesis of a covalent interaction between the aromatic sulfonyl fluoride group of the inhibitor and the target receptor (figure 28).

Compound	IC_{50} (nM) EGFR t_0	IC_{50} (nM) EGFR t_{3h}	Ratio t_0/t_{3h}
Brigatinib	9 ± 3	N/D	N/A
Osimertinib	952 ± 523	N/D	N/
XO44	253 ± 14	6	42
UPR1423	661 ± 434	487	1.4
UPR1424	954	N/D	N/A
UPR1432	679	449	1.5
UPR1425	454	329	1.4
UPR1433	845 ± 405	146	5.8
UPR1444	111 ± 23	1.6	67

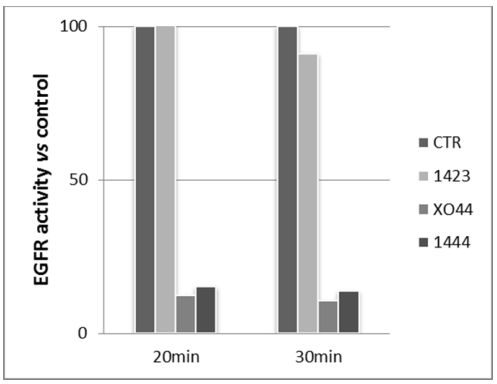

Figure 28: left side, IC_{50} values of tested compounds on triple mutated EGFR L858R/790M/C797S measured by FRET-based activity assay. When showed, mean ± SD (n=3), N/D not available, N/A not applicable. Right side, rapid dilution assay. UPR1444 was incubated with EGFR L858R/790M/C797S for 3h with the UPR1423 (negative control), XO44 (positive control) and UPR144compounds. The treated samples were diluted (x100) and the activity of the enzyme was measured by quantification of the phosphorylation of a reference peptide with a FRET-based technique. Activity is reported as % of the untreated enzyme (CTR).

The antiproliferative effect of UPR1444 was assessed by evaluating the inhibition of EGFR phosphorylation and the inhibition of cell proliferation in different lines harbouring the wild-type EGFR (A459), double mutant $EGFR^{L858R/T790M}$ (H1975) , del19EGFR (PC9) and the triple mutant isoform $EGFR^{L858R/790M/C797S}$ (PC9M) (figure 29, A and B). These results show how the activation of the receptor, among the different cell lines including the one harbouring $EGFR^{L858R/790M/C797S}$, is affected by UPR1444, nevertheless its inhibitory activity on cell proliferation appear extremely low. On this basis a stability assay was performed to evaluate the lability of the UPR1444 in the cell medium (figure 29, C).

A

	% of inhibition of EGFR at 1 µM after 1h treatment			
	A549	H1975	PC9	PC9M
Osimertinib	30	100	100	0
UPR1444	80	60	90	30

B

	IC_{50} (nM) measured 72h after treatment			
	A549	H1975	PC9	PC9M
Osimertinib	~ 500	*N.A*	< 10	> 3,000
UPR1444	> 3,000	1,000 -3,000	~ 3,000	> 3,000

C

	Cell Medium
Osimertinib	66.4%[a]
X044	$t_{1/2}$ = 65.6 ± 2.0 min[b]
UPR1444	$t_{1/2}$ = 48.8 ± 2.3 min[b]

Figure 29: A) % of inhibition of EGFR activity on lung cancer lines. **B**) Inhibition of cell proliferation of lung cancer lines. **C**) Stability of tested compound. [a] % of compound remaining in medium (t= 4h, 37°C). Mean ± SD (n=3). [b] The formation of the corresponding sulfonic acid is observed.

3.6 Synthesis of EGFR inhibitors

The synthetic strategy adopted to obtain the EGFR inhibitors is based on a convergent approach where the aniline **88** (scheme 1) served as the common precursor for the synthesis of UPR1423, UPR1424, UPR1425, UPR1432 and UPR1433.

The synthetic route toward the aniline **88** has been optimized in our group and is illustrated in scheme 16. The 2,4-diaminopyrimidine core of **88** is provided through two subsequent nucleophilic aromatic substitutions of 2,4,5-trichloropyrimidine **85**[212]. The first aromatic substitution involves a 3-nitroaniline that replaces the chlorine regioselectively in the position 4 of the trichloropyrimide **85**, affording to the intermediate **86** exclusively. The aniline **84**, which is used as the nucleophile for the aromatic substitution of **86**, has been prepared by substituting the fluorine atom of **82** with 1-acetyl-piperazine and reducing its nitro group. Finally, the nitro derivative **87** is reduced to afford **88**.

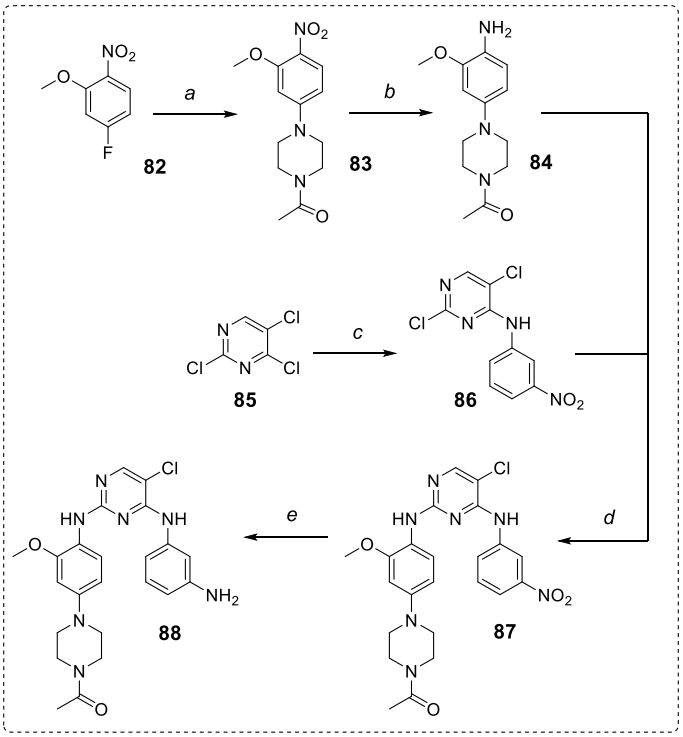

Scheme 16: *a) 1-acetyl-piperazine, 70°C, 8 h, neat, 98% b) THF, NH_4Cl, Zn°, 75°C, 8 h, 52% c) iPrOH, 3-nitroaniline, DiPEA, 80°C, 18 h, 72%. d) iPrOH, pTSA, 50°C, 18 h, 50%. e) EtOH, Fe°, HCl, 90°C, 2 h, 93%.*

The acetylation of aniline **88** provided UPR1423, whereas its acylation with the mixed anhydride of chloroacetic acid and trimethylacetic (pivalic) acid gave UPR1424 (scheme 17). UPR1425 has been prepared through a hetero-Michael reaction between aniline **88** and the vinyl sulfonyl fluoride **91**. The 2-bromoethane-1-sufonyl chloride **89**[213] served to obtain UPR1432: the aniline gave the nucleophilic substitution to the sulfonyl chloride whereas the elimination of hydrobromic acid gave the corresponding vinyl sulphonamide. Finally, UPR1433 was obtained by coupling aniline **88** with 3-fluorosulfonyl-benzoyl chloride **90**[214].

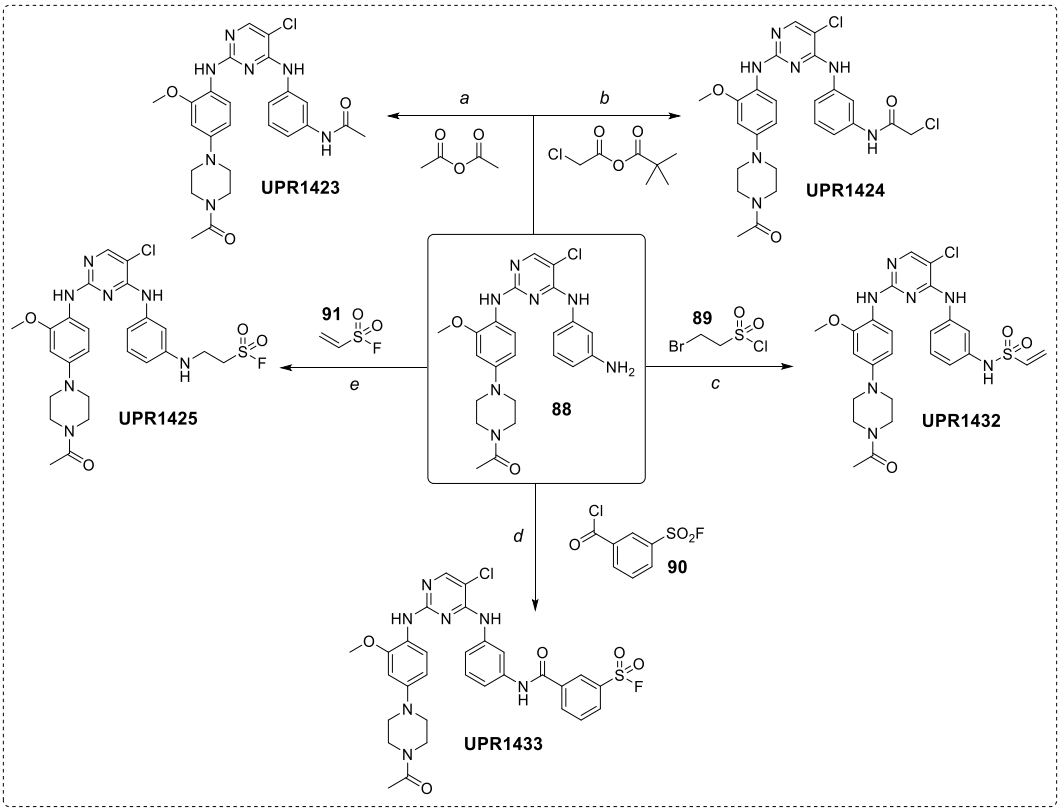

Scheme 17: *a) Pyridine, Ac_2O, 30 min, 82%. b) (i) THF, 2-chloroacetic acid, pivaloyl chloride, DiPEA, 20 min. (ii) Toluene,* **88***, 1 h, 55%. c) Pyridine, toluene, NEt_3,* **89***, 0°C, 24 h, 14%. d) THF, pyridine,* **90***, 0°C, 10 min, 21%. e) Chloroform, MeOH,* **91***, 3 h, 13%.*

A similar synthetic strategy has been adopted to prepare UPR1444 (scheme 18). Analogously, the 2,4,5-trichloropyrimide **85** served as the precursor for the 2,4-diaminopyrimidine core of UPR1444, where its chlorine atoms replacement with a 4-nitroaniline and then with aniline **84** afforded to the nitro derivative **93**. The

reduction of the nitro group gave the aniline **94** which was alkylated with the 4-(bromomethyl)-benzen sulfonyl fluoride **95**[215] providing UPR1444.

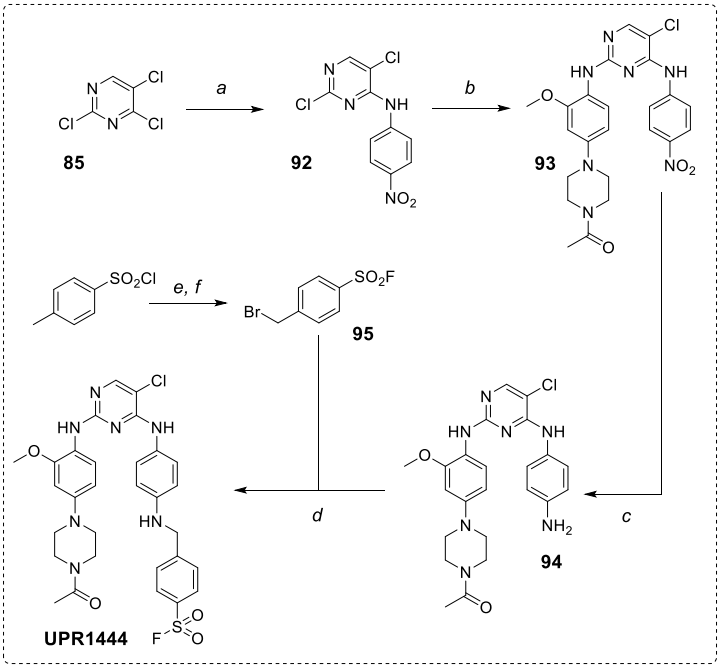

Scheme 18: *a) Water, 4-nitroaniline, HCl, 100°C, 7 h, 80%. b) iPrOH,* **84**, *pTSA, 90°C, 18 h, 45%. c) EtOH, Fe°, HCl, 90°C, 2 h, 43%. d) DMF, K_2CO_3, 40°C, 2 h, 35%. e) ACN, KF, 85°C, 18 h, 70%. f) CCl_4, NBS, BPO, 80°C, 18%.*

4 Conclusion

Signal transduction is a crucial process by which an extracellular signal triggers a cascade of intracellular molecular events that eventually result in an appropriate cell response. Protein kinase receptors represent the first step of the transduction pathway serving as a key adaptor between extracellular signals and intracellular messengers. Cell responses such as cell survival and proliferation are largely affected by growth factors which bind their kinase receptors triggering the intracellular signalling. Deregulation of this process drives uncontrolled cell proliferation and cancer development thus growth factors and their receptors represent a primary target for developing antiproliferative therapies. To date several agents targeting the growth factors and their receptors are already available in clinic, and kinase inhibitors represent one of the most explored class.

This thesis describes the design and the development of antiproliferative agents against the tyrosine kinase receptors FGFR and EGFR.

In case of FGFR we have explored a different approach by developing small-molecules able to bind extracellular FGFs and thus prevent the transduction of FGF/FGFR signalling. Based on the promising biological activity of NSC12 we decided to investigate the structure-activity relationships in order to find new active compounds with improved properties and to clarify its mechanism of action. Early results have shown that the replacement of the fluorinated chain of NSC12 led to a loss of activity whereas modifications of its steroid core gave compounds which retain the antiproliferative effect. On this basis we planned to replace the pregnenolone core of NSC12 with mimetic non-steroidal scaffolds with the aim of further extend the investigation of the structure-activity relationships. Three classes of non-steroidal derivatives have been synthesised showing that the pregnenolone core can be successfully replaced by mimetic biaryl scaffolds. These compounds thus represent an accessible starting point for further investigations of the mechanism of action of this class of agents. Additionally, we addressed the role of the stereochemistry of the *bis*-(trifluoromethyl)propanediol group by isolating two enantiomers UPR1422 and UPR1426. The biological evaluation of these compounds revealed that the antiproliferative activity and the inhibition of FGFR signalling are not affected by the configuration of the secondary alcohol of the fluorinated chain.

In case of EGFR the research work was focused on the design of tyrosine kinase inhibitors targeting EGFR harbouring T790M/C797S mutation. The replacement of the cysteine residue with less nucleophilic residues hampers the effectiveness of third generation EGFR inhibitors. Thus the discovery of new chemotypes targeting different residues appears as a potential approach to overcome mutated resistant isoforms. Here is described the design of derivatives based on suitable driving portion bearing diverse electrophilic groups aimed to target the Lys745. Among the synthesised derivatives the sulfonyl-fluoride UPR1444 exhibited promising *in vitro* activity suggesting a covalent interaction with its target. Despite the inhibitory potency of UPR1444 on the isolated receptor, the evaluation in cellular assays revealed a suboptimal antiproliferative profile. The different inhibitory potency exhibited by UPR1444 could be ascribed to its instability in the cell environment. The optimization of reactivity and physicochemical properties of sulfonylfluoride-based derivatives is thus required for the development of potential fourth generation inhibitors.

5 Keap1-Nrf2 protein-protein interaction inhibitors

5.1 Introduction

Nrf2 (Nuclear Factor Erythroid 2-Related Factor 2) is the transcription factor of more than 200 genes that contain, within their promote region, the antioxidant response element (ARE).[216,217] Nrf2 is constituted by six conserved Nrf2-Ech homology (Neh) domains where Neh1, Neh4 and Neh5 regions are crucial for assembling an effective transcription complex, Neh6 plays a role in regulating the protein half-life whereas Neh2 contains two conserved motif responsible for the binding to Keap1.[218,219]

Keap1 (Kelch-like ECH-Associated Protein 1) is the natural repressor of NRF2 and regulates its concentration in the cellular environment.[220] Under basal condition Keap1 binds NRF2 and acts as the adaptor substrate of E3 ubiquitin ligase allowing its proteasomal degradation. Keap1 consists of three functional domains (i) Broad complex, Tramtrack and Bric-à-brac (BTB), (ii) intervening region (IVR) and (iii) Kelch domain (figure 1, A).[221] Specifically, Keap1 is present in the cellular environment as a homodimer where the BTB domains serve as the linker point between two Keap1 proteins. This region also constitutes the anchor point for the assembly of the CRL3 complex (Cullin-Ring Ligase 3) which in turn determines the ubiquitylation of Nrf2 and its degradation.[222] The Keap1 homodimer associates with a single Nrf2 molecule through two interaction sites constituted by the Kelch domains of Keap1, and two conserved motifs (called ETGE and DLG on the basis of their amino acids sequence) of the Neh2 domain of Nrf2 (figure 30, A).[223] These conserved motifs located within Neh2 domain show different binding affinity constants where the ETGE motif binds the Kelch domain ≈50 fold more strongly compared to DLG. Nevertheless ETGE and DLG motifs are both required for the right positioning of Nrf2 within Keap1 homodimer and its consequent ubiquitylation (figure 30, B).

It has been proposed that the cysteine residues located on the surface of Keap1 act as sensors of the cellular environment, and in case of stressed condition they serve to ''activate'' Nrf2 pathway (figure 30, C).[224] The modification of such

reactive residues, due to oxidizing or electrophilic agents, triggers the cascade of events that eventually hampers the degradation of Nrf2. Finally, the reduced degradation rate of Nrf2 combined to its *de novo* synthesis lead to an increased intracellular concentration of Nrf2 and, upon translocation into the nucleus, the activation of target ARE-dependent genes.[225]

The genes activated by NRF2 encode a wide set of enzymes, among others superoxide dismutase (SOD), heme oxygenase 1 (HO-1), NAD(P)H:quinone oxidoreductase 1 (NQO1), and glutathione S-transferase which are mainly involved in defence mechanisms against oxidative stress.[216] Additionally, NRF2 induces enzymes that regulate the metabolism of xenobiotics and endogenous substances, as well as protein degradation and iron catabolism. The beneficial effect of Nrf2 in protecting against oxidative stress contributes to the maintenance of a stable cellular environment.

On this basis the modulation of Nrf2 activity has been explored as a potential approach to discover therapeutic agents against pathologies where the oxidative stress plays a key role.[226] Particularly, Nrf2 has shown to play a crucial role in central nervous system (CNS) diseases. Since the high oxygen consumption the brain is susceptible to oxidative stress and activation of Nrf2 was found to protect the nervous tissue against neurodegenerative diseases and acute events such as ischemic and haemorrhagic stroke.[227–229]

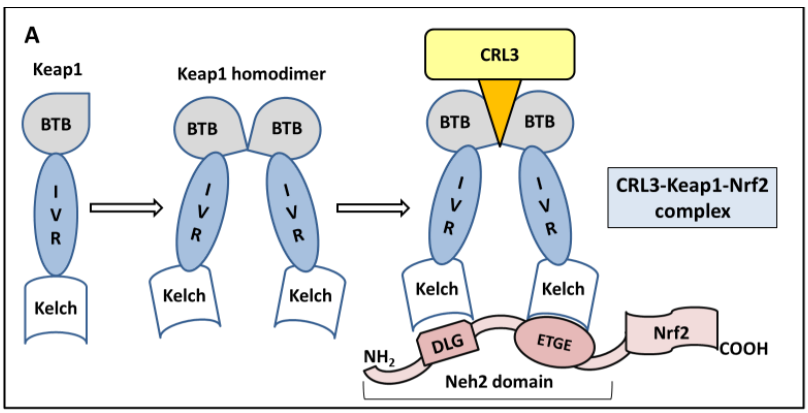

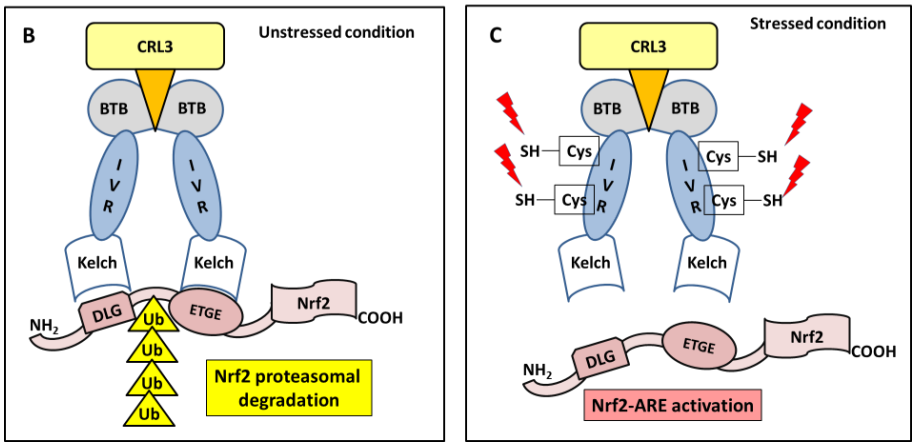

Figure 30: A) Schematic representation of Keap1 and its complex with Nrf2. **B)** Keap1 mediates Nrf2 ubiquitylation under basal condition. **C)** Upon stressed condition Nrf2 is ''activated''.

5.2 Modulation of Keap1-Nrf2 axis

The pharmacological modulation of Nrf2 activity has been explored by employing two different classes of agents: (i) electrophilic Keap1 binders and (ii) Keap1-Nrf2 protein-protein interactions (PPIs) inhibitors (figure 31, A).[230] The first class comprises small-molecules bearing electrophilic groups able to induce covalent modifications within the cysteine residues located on Keap1 surface.[231] The modifications of these residues lead to conformational changes in Keap1 which eventually triggers the transduction of Nrf2-dependent genes. This mode of action closely resembles the endogenous activation of Keap1-Nrf2 axis. Dimethyl fumarate (DMF, Tecfidera)[232] is an example of this class of compounds (figure 31, B). Upon administration the DMF is converted to the monomethyl fumarate which in turn binds covalently the cysteine residues (Cys151) of Keap1 leading to Nrf2 activation. This compound has been approved for the treatment of psoriasis and multiple sclerosis. Other examples of covalent agents under clinical evaluation are bardoxolone, omaveloxolone and CXA10 (figure 2, B). The intrinsic reactivity of these compounds represents the main drawback since their unspecific interaction within the biological environment determines an increased risk of side effects and a narrow therapeutic window.[226]

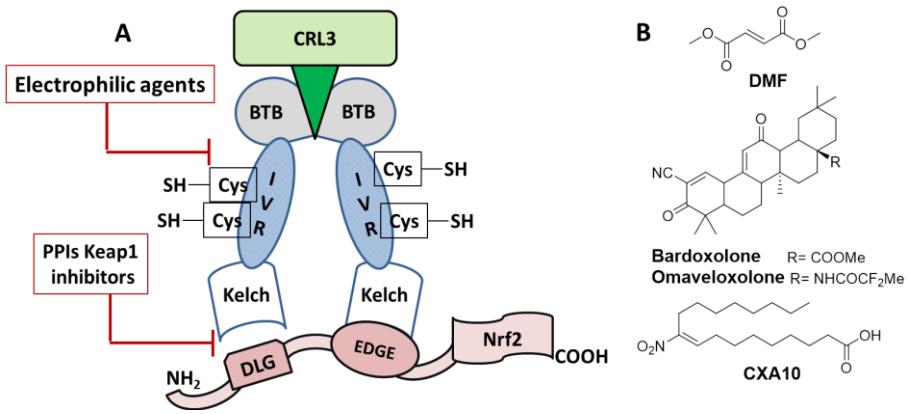

Figure 31: A) Modulation of Nrf2 activity by electrophilic agents and PPIs inhibitors. **B)** Example of electrophilic compounds.

On this basis the inhibition of Keap1-Nrf2 PPIs raised as promising strategy for the development of selective and safer agents.[226] The inhibition of PPIs with small-molecules is generally considered a challenging task given their extended surface area and the shape of the interaction sites. However, the X-ray crystallography of Keap1 bound to the Neh2 domain of Nrf2 has given crucial structure information encouraging the research of potential inhibitors (figure 32).[233] The interface area between Kelch-ETGE and Kelch-DLG extent for 550-750 Å which compared to the surface of other PPIs is a relatively small area. The binding site located on the Kelch domain can be divided in five subpockets (P1-P5) that together adopt a bowl-shaped conformation to accommodate ETGE and DLG motifs. Additionally, subpockets P1 and P2 are characterized by polar and basic residues (Arg483, Arg415 and Arg380) involved in the formation of salt bridges with carboxylic acid residues located on ETGE and DLG motifs.[234]

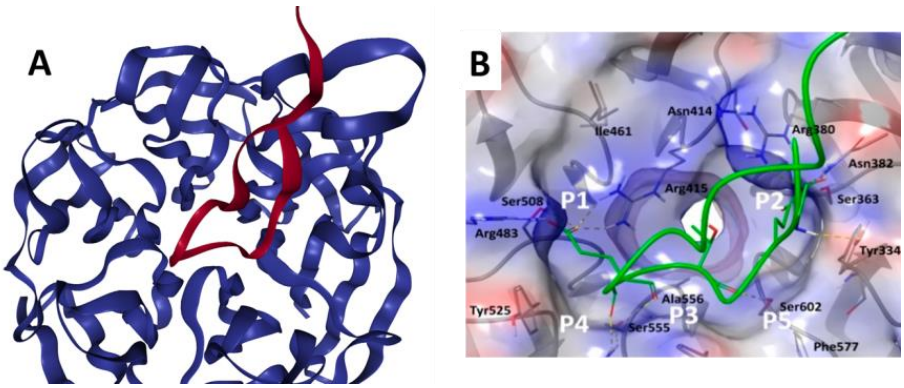

Figure 32: A) Crystal structure of Keap1 Kelch domain (blue) with truncated Neh2 domain (red) of Nrf2 (PDBID: 2FLU). **B)** Detail of Kelch domain and the ETGE motif (adapted from ref. [230]).

Starting from this information, different research groups from academia and pharmaceutical companies have reported several non-covalent Keap1-Nrf2 PPIs inhibitors.[230,235] These compounds have been designed to target the Kelch domain by exploiting the polar subpockets P1 and P2, considered as hot spot sites. Despite the different chemical scaffolds these compounds share common molecular features such as the presence of a carboxylic acid group which serves to establish key interaction with basic residues within P1 and P2 subpockets (figure 33).

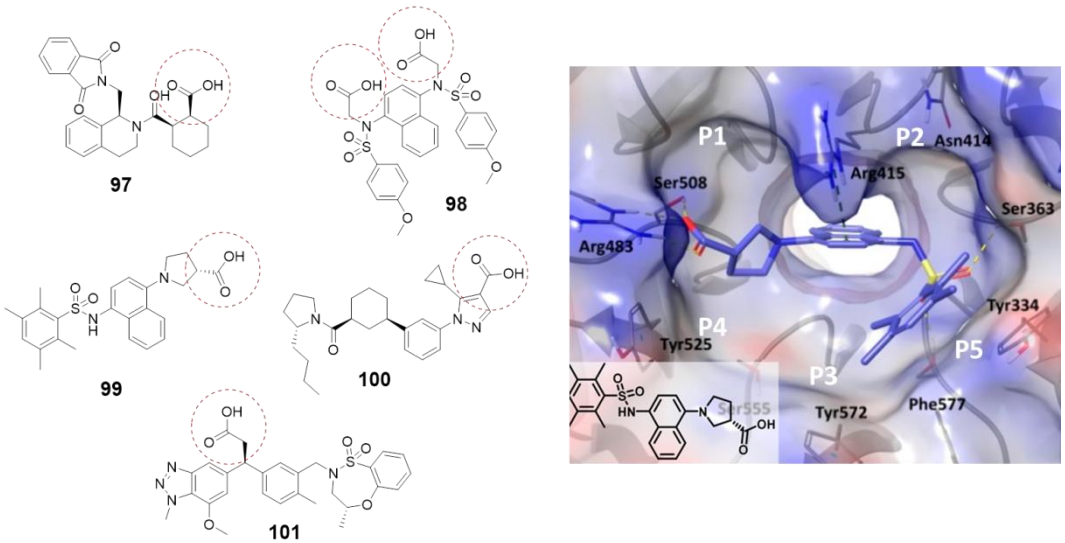

Figure 33: Molecular structures of Keap1 PPIs inhibitors. On the right the crystal structure of compound **99** bound to the Kelch domain (PDBID 5CGJ9, adapted from ref[230]).

The evaluation of these compounds has shown their ability to displace Neh2-based peptides from Keap1 with a binding affinity to the Kelch domain ranging from the low micromolar to nanomolar level (table 2).[230] Despite their promising *in vitro* activity, these agents lack of a favourable pharmacokinetics profile as demonstrated by their high metabolic turnover in cells and animal models.[236,237] Additionally, their physicochemical properties make the penetration of the BBB (blood brain barrier) an unlikely event for these compounds (table 2).[230,238] The molecular weight higher than 450 Da, the total polar surface area larger than 50 $Å^2$ and, particularly, the presence of a negatively charged carboxy group prevent the passive diffusion across the BBB.

	IC_{50}	K_d	MW (Da)	tPSA (Å^2)	HBD[4]
97	2.3 mM (FP)[1]	1.0 mM (SPR)[2]	446.5	95.0	1
98	29 nM (FP)	5.2 nM (SPR)	614.6	167.8	2
99	0.14 mM (FP)	6.0 mM (ITC)[3]	452.6	88.7	2
100	10-100 nM (FP)	ND	463.6	73.2	1
101	<15 nM (FP)	1.3 nM (ITC)	550.6	121.1	1

Table 2: the IC50 and the Kd measured by biophysics assays. [1] Fluorescence polarization. [2] Surface plasmon resonance. [3] Isothermal calorimetry. [4] Hydrogen bond donor.

5.3 Optimization of Keap1 PPIs inhibitors

This section describes the research work carried out during a secondment period within the group of Associate Professor Anders Bach at the department of Drug Design and Pharmacology at University of Copenhagen.

In the last years the Bach Group has been active on researching novel Keap1 PPIs inhibitors by the means of fragment based drug discovery (FBDD).[235] Briefly, this technique consist of (i) screening fragment libraries evaluating the binding affinity with proper biophysics assays and (ii) the optimization of promising fragments into lead compounds. Thus, different known Keap1 PPIs inhibitors have been deconstructed in fragments, which have been reconstructed affording new Keap1 inhibitors. The merging of two fragments, obtained from deconstruction of compounds **98** and **100**, provided UCAB#310 which displayed low micromolar affinity to Keap1 in an FP assay (figure 34, A).

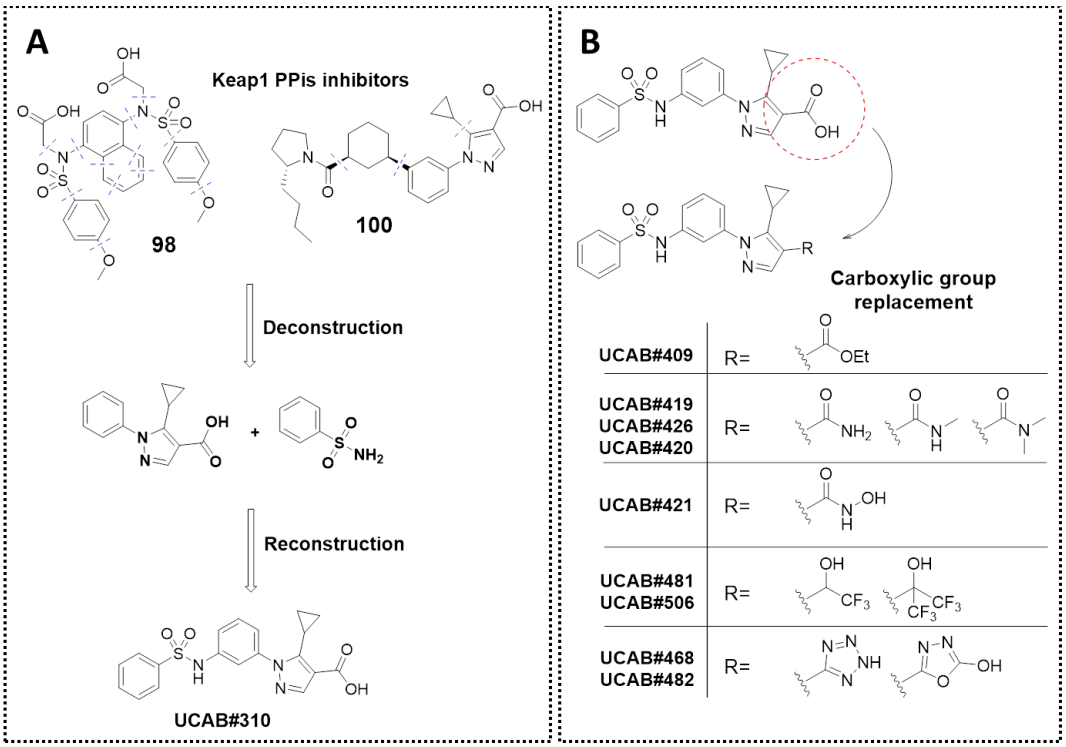

Figure 34: A) Schematic representation of the discovery of UCAB#310. **B)** Representation of the present work.

Nevertheless this compound exhibits the common carboxy group which likely prevents the penetration of the BBB. On this basis, the replacement of the

carboxylic acid with different isosteres groups has been considered as a potential approach to provide derivatives of UCAB#310 endowed with improved cellular permeability.[239]

In this project, we have selected bioisosteric groups considering their physicochemical properties (MW, tPSA and PKa), literature examples[240,241] and the synthetic feasibility. Ester and amide derivatives (UCAB#409, UCAB#419, UCAB#426 and UCAB#420) were synthesised for their polar properties and the lack of an acid centre, whereas the hydroxamic acid and the fluorinated secondary and tertiary alcohol derivatives (UCAB#421, UCAB#481 and UCAB#506) were chosen for their different Pka strength. Finally, UCAB#468 and UCAB#482 were synthesized to explore polar and acid heterocycles groups.

The evaluation of Keap1 binding affinity, of the designed compounds, has been measured by competitive FP assay using a modified Neh2 peptide containing the ETGE motif (fluorescent Cy5-LDEETGEFL-NH_2).

A

Name	Activity in FP (Ki)
UCAB#310	17.1 µM ± 1
UCAB#409	> 1mM
UCAB#419	> 1mM
UCAB#420	> 1mM
UCAB#426	> 1mM
UCAB#421	> 1mM
UCAB#481	> 1mM
UCAB#506	> 1mM
UCAB#482	577 µM ± 56
UCAB#468	13.3 µM ± 0.1

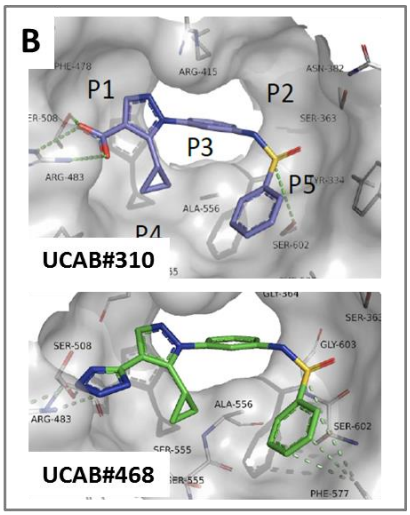

Figure 35: A) Results of competitive FP assay of isosteres derivative of UCAB#310. **B**) X-ray structure of UCAB#310 and UCAB#468 in complex with Kelch domain (X-ray data to be deposited in the PDB bank).

The replacement of the carboxy group with neutral (uncharged) isosteres groups (ester, amides and alcohols) led to a dramatic loss of the binding affinity (figure 35, A). Among the heterocycles derivatives, UCAB#482, bearing a 5-hydroxy-1,3,4-oxadiazole ring, partially retained the affinity to Keap1 whereas UCAB#468 with a tetrazole ring has displayed a binding affinity comparable to that of UCAB#310 (figure 35, A). This result, combined with X-ray crystallography data of UCAB468

(figure 35, B), suggests that the acid moiety is required to establish a proper interaction with basic residues (Arg483) at P1 subpocket.

On the other hand, the investigation of structure-activity relationship (SAR) of UCAB#310 carried out by other members from the Bach group, has revealed that addition of methyl groups at the phenyl ring, or polar chains at the nitrogen of the sulphonamide moiety, lead to compounds with a binding affinity ≈ 10 to 30 fold higher than that of UCAB#310 (figure 36). On this basis we combined these modifications, including the replacement of the carboxy group with the tetrazole ring, affording four derivatives (figure 36) in an effort to further improve the binding affinity of the lead compound.

The evaluation of the affinity by competitive FP has shown that the combination of methyl groups with the polar chain (acid or amide group) on the sulphonamide portion do not lead to a cumulative effect (figure 36). Similar results were observed when the carboxy group was replaced by the tetrazole ring.

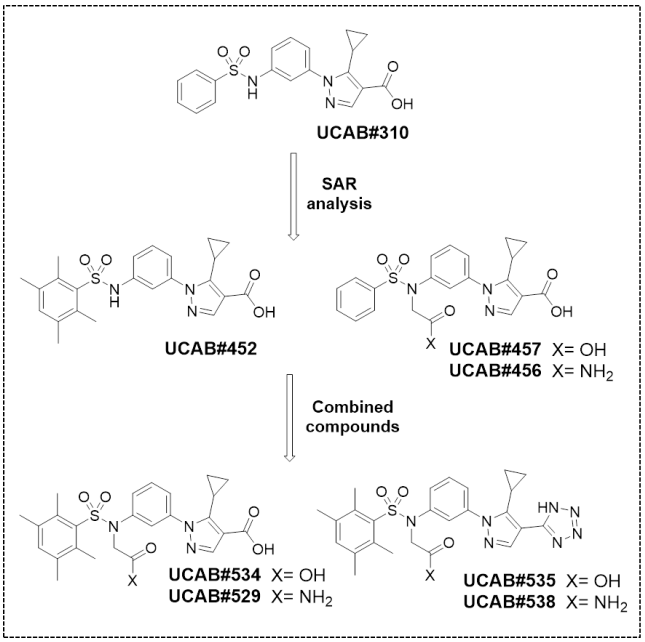

Name	Activity in FP (Ki)
UCAB#310	17.1 µM ± 1
SAR analysis	
UCAB#452	2.4 µM ± 0.1
UCAB#457	0.55 µM ± 0.01
UCAB#456	0.61 µM ± 0.02
Combined compounds	
UCAB#534	0.79 µM ± 0.08
UCAB#529	1.4 µM ± 0.1
UCAB#535	0.66 µM ± 0.03
UCAB#538	1.49 µM ± 0.2

Figure 36: schematic representation of SAR investigation of UCAB#310 and combined compounds. The table on the right shows the binding affinity of the corresponding compounds measured in FP assay.

5.4 Synthesis of Keap1 PPIs inhibitors

This section describes the synthetic strategy adopted to prepare the compounds previously presented. The synthetic route toward UCAB#310 and its derivatives comprises three key steps: the synthesis of the 1-phenylpyrazole core, the Ullmann-type condensation for the N-C bond formation between the sulphonamide and the phenylpyrazole core, and the manipulation of the carboxy group (scheme 19).

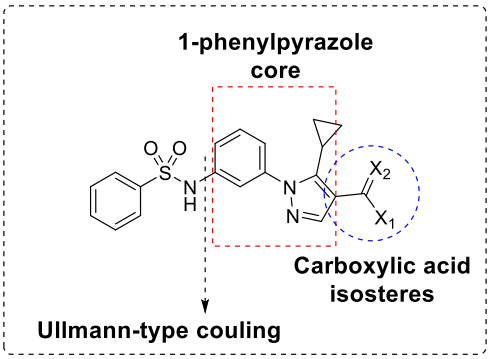

Scheme 19: synthetic approach.

UCAB#310 has been prepared from substituted β-ketoester **102** which has been condensed with a 3-bromo-phenylhydrazine to provide the 1-phenylpyrazole core (**103**) (scheme 20). This compound served as the substrate for the Ullmann-type coupling with benzenesulfonamide affording UCAB#409.

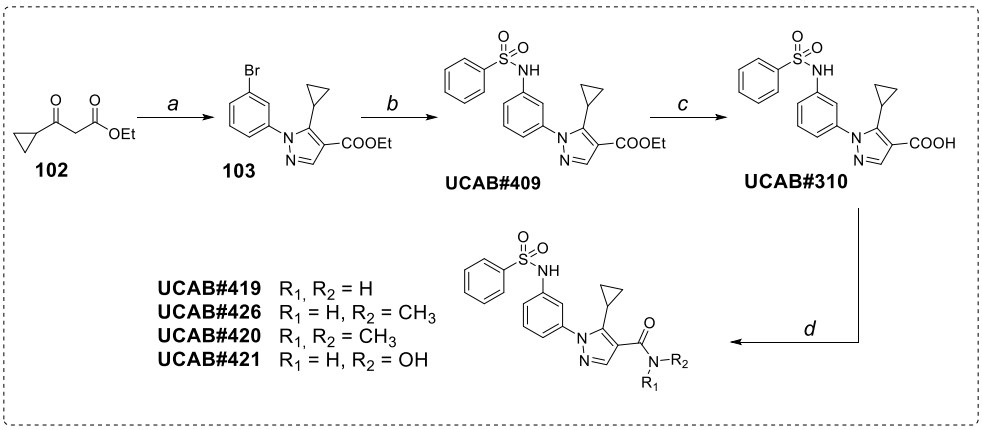

Scheme 20: (a) (i) DMF-dimethylacetal, MW 130°C, 15min. (ii) EtOH, 3-Bromo-phenylhydrazine hydrochloride, Et_3N, 24 h, r.t., 72%. (b) DMF, Benzenesulfonamide, CuI, N,N-dimethyl-Glycine, K_3PO_4, 160°C, 24 h, 80%. (c) EtOH, water, NaOH, r.t., 18 h, 95%. (d) DMF, HATU, DiPEA, amine hydrochloride, r.t., up to 24 h, 14-100%.

The hydrolysis of the ester gave UCAB#310 and then the coupling between its carboxy group and the proper amine afforded UCAB#419, UCAB#420, UCAB#426 and UCAB#421.

The Weinreb amide **105**, prepared from the carboxylic acid **104** using EDC as the coupling agent with *N,O*-dimethyl-hydroxylamine, served as the substrate for the nucleophilic addition of the Ruppert-Prakash reagent (TMS-CF_3) providing the trifluoromethylketone **106** (scheme 21). This compound served as common intermediate toward the synthesis of UCAB#481 and UCAB#506. Thus the reduction of trifluoromethylketone **106** afforded to the trifluoromethylacohol **107** which was coupled with the benzenesulfonamide to provide UCAB#481. In case of UCAB#506 the trifluoromethylketone **106** served as the substrate for the nucleophilic addition of TMS-CF_3. The resulting *bis*-trifluoromethylacohol **108** was then coupled with the benzenesulfonamide under Ullmann coupling condition. Unfortunately, the only product observed was the trifluoromethylketone **109** resulting from the elimination of a fluoroform molecule. Thus UCAB#506 was prepared from **109** through an additional nucleophilic addition of TMS-CF_3.

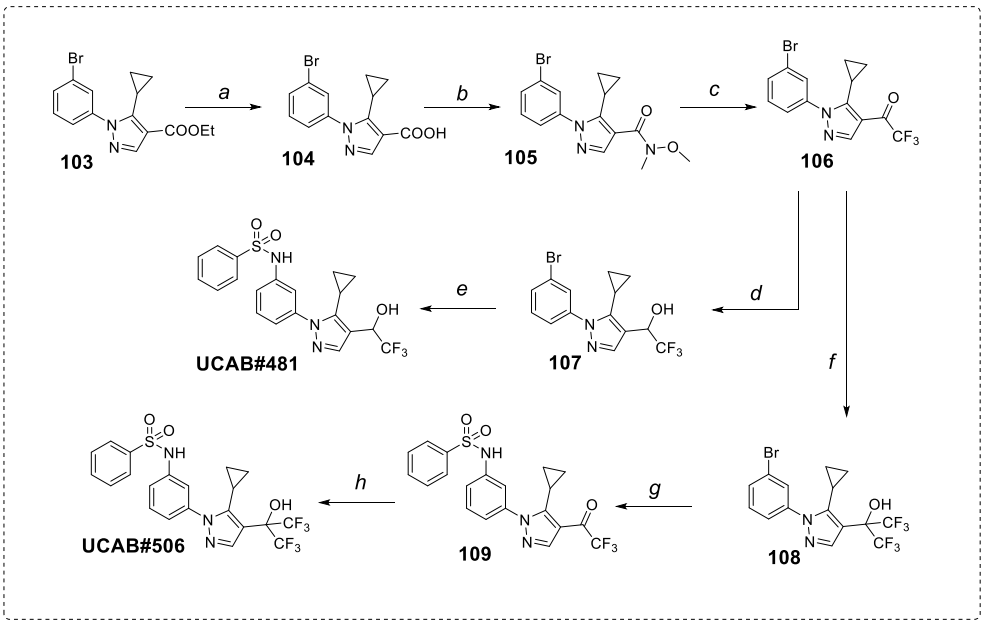

Scheme 21: (a) EtOH, water, NaOH, r.t., 18 h, quantitative yield. (b) DMF, EDC hydrochloride, HOBt, DiPEA, *N,O*-dimethylhydroxylamine hydrochloride, r.t., 18 h, 94%. (c) THF, TMS-CF_3, CsF, HCl, r.t., 18 h, 73%. (d) THF, EtOH, $NaBH_4$, 0°C, 4 h, 88%.. (e) DMF, Benzenesulfonamide, CuI, *N,N*-dimethylGlycine, K_3PO_4, 160°C, 4 h, 42%. (f) THF, TMS-CF_3, CsF, HCl, r.t., 1 h, 60% (g) DMF, Benzenesulfonamide, CuI, *N,N*-dimethyl-Glycine, K_3PO_4, 160°C, 4 h, 39%. (h) THF, TMS-CF_3, CsF, HCl, r.t., 1 h, 41%.

The 5-hydroxy-1,3,4-oxadiazole ring of UCAB#482 was prepared by condensing the hydrazide **110** with triphosgene (scheme 22). Then the Ullmann-type coupling between **111** and the benzenesulfonamide gave UCAB#482.

In case of tetrazole isostere UCAB#468, the amide UCAB#419 was dehydrated to the corresponding nitrile **112** and then treated with TMS-azide at neat condition affording UCAB#468 (scheme 22).

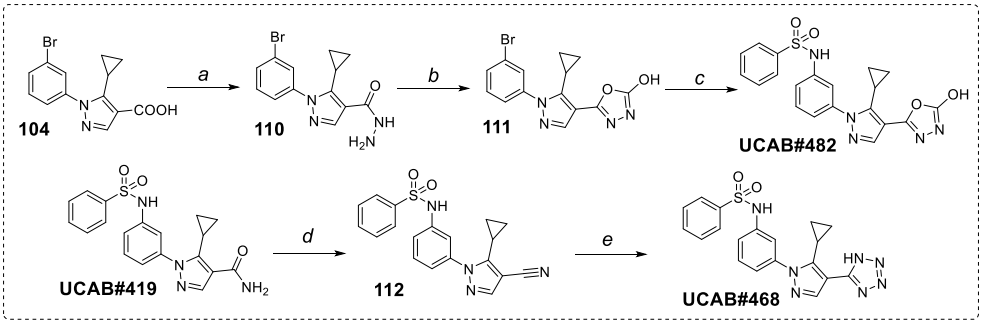

Scheme 22: (a) DMF, EDC hydrochloride, HOBt, DiPEA, hydrazine HCl, r.t., 1.5 h, 72%. (b) DCM, triphosgene, 0°C to r.t., 18 h, 54%. (c) DMF, Benzenesulfonamide, CuI, *N,N*-dimethyl-Glycine, K_3PO_4, 160°C, 24 h, 7%. (d) DMF, thionylchloride, 0°C, 30 min, 94%. (e) TMS-N_3, TBAF, 100°C, neat, 22 h, 29%.

The synthetic route adopted to obtain both UCAB#529 and UCAB#534 started from the common intermediate **103** (scheme 23). This was hydrolysed and then coupled with the 2,3,5,6-tetramethyl-benzenesulphonamide under Ullmann condition.

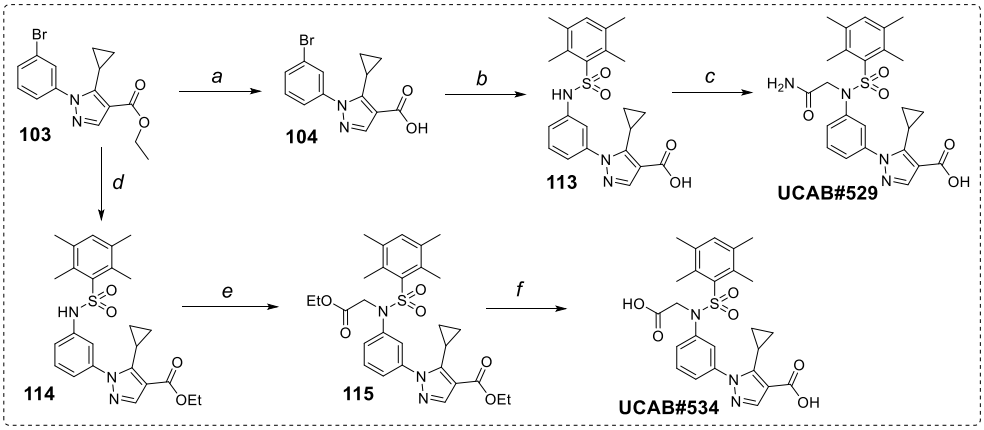

Scheme 23: a) EtOH, water, NaOH, r.t., 18 h, quantitative yield. b) DMF, 2,3,5,6-tetramethyl-benzenesulfonamide, CuI, *N,N*-dimethyl-Glycine, K_3PO_4, DMF, 150°C, 24 h, 27%. c) (i) DMF, TBDMSiCl, imidazole, r.t., 20h. (ii) 2-bromoacetamide, NaH, THF, 0°c to r.t., 3 h, 18%. d) DMF, 2,3,5,6-tetramethyl-benzenesulfonamide, CuI, *N,N*-dimethyl-Glycine, K_3PO_4, 150°C, 24 h, 99%. e) Ethyl 2-bromoacetate, NaH, THF, 0°C to r.t., 20 h, 70%. f) EtOH, water, NaOH, r.t., 18 h, 18%.

The resulting sulphonamide **113** was then alkylated with the 2-bromo-acetamide to provide UCAB#529. In case of UCAB#534, the 1-(3-bromo)-phenylpyrazole served as the substrate for the Ullmann-type coupling affording the sulphonamide **114**. This intermediate was alkylated with ethyl 2-bromo-acetate obtaining the ester **115**. The hydrolysis of the ethyl ester groups of **115** provided UCAB#534. This step suffered of low yield due to chemical instability of the secondary sulphonamide moiety.

UCAB#535 and UCAB#538 share the same synthetic route (scheme 24). The carboxylic acid **104** was converted to the corresponding nitrile **117** and then coupled with the 2,3,5,6-tetramethyl-benzenesulphonamide under Ullmann condition. The resulting sulphonamide **118** was alkylated with ethyl 2-bromo-acetate affording the ester **119** and then was treated with TMS-azide under neat condition providing the tetrazole intermediate **120**. This compound was hydrolized affording UCAB#535 whereas its subsequent amination gave UCAB#538.

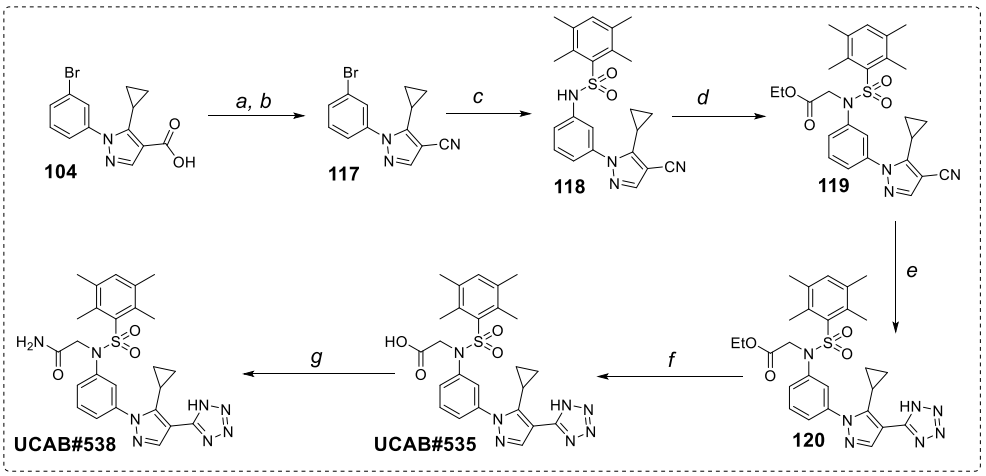

Scheme 24: a) DMF, EDC hydrochloride, HOBt, DiPEA, ammonium chloride, r.t., 1.5 h, 85% b) DMF, Thionylchloride, 0°C, 30 min, 93%. c) DMF, 2,3,5,6-tetramethyl-benzenesulfonamide, CuI, *N,N*-dimethylGlycine, K_3PO_4, 150°C, 24 h, 84%. d) THF, ethyl 2-bromoacetate, NaH, 0°C to r.t., 20 h, 95%. e) TMS-N_3, TBAF, neat, 100°C, 24 h, 53%. f) EtOH, water, NaOH, r.t., 8 h, 27%. g) DMF, EDC hydrochloride, HOBt, DiPEA, ammonium chloride, r.t., 22 h, 38%.

5.5 Summary

The inhibition of Keap1-Nrf2 PPI, and thus the transcription of Nrf2-dependent genes, represents a therapeutic strategy against diseases where inflammation and oxidative stress play a key role. Non-covalent small-molecule PPIs inhibitors have been proposed as potential therapeutic agents for the treatment of chronic CNS diseases and acute events such as ischemic and haemorrhagic strokes. X-ray crystallography data of Keap1-Nrf2 interface has encouraged the research of novel non-covalent PPI inhibitors and several of them have been disclosed by academia and pharmaceutical companies. Despite these compounds have shown promising *in vitro* activity, they suffer of suboptimal physicochemical properties which affect the pharmacokinetic profile. Particularly, Keap1 PPI inhibitors share a carboxy group which is required to achieve a high binding affinity, but on the other hand the presence of a negatively charged group drastically reduces the penetration to the CNS.

On this basis, we have synthesised derivatives of UCAB#310, a Keap1 PPI inhibitor discovered by the means of FBDD, where its carboxylic acid moiety has been replaced by isosteres groups in an effort to (i) explore the SAR and (ii) potentially improve the permeation of the BBB. However, the evaluation of the designed analogues has shown that the replacement of the carboxy group with neutral groups dramatically reduces the binding affinity to Keap1. Conversely, the replacement of the carboxy group with a tetrazole ring led to a derivative with a Keap1 binding affinity comparable to that of UCAB#310. These results suggest that an acid and polar group is required in order to maintain PPI inhibitory activity. Finally, the addition of methyl groups to the phenyl ring and polar chains to the nitrogen atom of the sulphonamide moiety led to compounds with an improved Keap1 binding affinity. Despite these chemical modifications likely reduces the penetration of the BBB, the increased Keap1 affinity makes these compounds a good starting point for future optimization.

6 Experimental section

Reagents were obtained from commercial suppliers and used without further purification. Solvents were purified and stored according to standard procedures. Anhydrous reactions were conducted under a positive pressure of dry N2 or Ar, and using standard syringe/septa techniques. Reactions were monitored by TLC, on Kieselgel 60F 254 (DC-Alufolien, Merck). Final compounds and intermediates were purified by flash chromatography (SiO2 60, 40–63 μm). Melting points were determined with a Gallenkamp melting point apparatus and are uncorrected. NMR spectra were recorded on a Bruker 300 MHz Avance, Bruker 400 MHz Avance or Jeol 600 MHz spectrometer; chemical shifts (δ scale) are reported in parts per million relative to the central peak of the solvent. 1H NMR spectra are reported in the following order: multiplicity, approximate coupling constant (J value) in hertz, and number of protons; signals are characterized as s (singlet), d (doublet), dd (doublet of doublets), t (triplet), dt (doublet of triplets), q (quartet), m (multiplet), and br s (broad signal). All 13C NMR spectra were measured with complete proton decoupling. All tested compounds (herein reported with UPR-code) were > 95% pure by HPLC/UV or HPLC/MS analysis.

HPLC-MS purity of key target compounds: Analytical Method
10 mM stock solutions of test compounds were freshly prepared in HPLC grade MeOH and serially diluted in MeOH to get a standard solution in the □M concentration range, which was directly analyzed by LC-MS. For the majority of compounds a 20 □M solution was analyzed, while for those compounds displaying a very low or a very high ionization yield, concentration was increased to 50 or decreased to 10 □M respectively. A Thermo Accela UHPLC gradient system (Thermo, USA) coupled to a heated electrospray ionization (H-ESI) ion source and a Thermo TSQ Quantum Access Max triple quadrupole mass analyzer was employed for data acquisition. Mass spectra were acquired either in positive (ESI+) or in negative (ESI-)polarity and in full scan mode. For positive polarity, H-ESI interface parameters were set as follows: probe middle (D) position; capillary temperature: 270 °C; spray voltage: 3.5 kV. Nitrogen was used as nebulizing gas at the following pressure: sheath gas: 35 psi; auxiliary gas: 15 arbitrary units (a.u.). Argon was used as the collision gas at a pressure of approximately 1.5 mtorr (1 torr = 133.3 Pa). For negative polarity, spray voltage: 2.5 kV. Compound separation was achieved on a Phenomenex Synergi Fusion C18 column (100 × 2.1 mm i.d., 4 □m particle size; Phenomenex, USA). Mobile phases consisted of MeCN (eluent A) and water (eluent B), both added with 0.1% v/v formic acid, at a flow rate of 350□L min-1. Injection volume was 10 □L. Linear gradient elution was employed for each target compound. Elution conditions employed for each compound are reported after the corresponding HPLC

traces. Thermo Xcalibur v. 2.2 SP1 software (Thermo, USA) was employed for data acquisition and processing.

6.1 Experimental procedures: FGF traps.

Methyl 3-((4-fluorophenoxy)methyl)benzoate (1). Methyl-3-Bromomethyl Benzoate (1.15gr, 5.05 mmol), 4-Fluoro phenol (0.79 gr, 7.01 mmol) and potassium carbonate (1.75 gr, 12.6 mmol) are placed in a bottom flask with DMF. The mixture is stirred at room temperature overnight (15 hrs). Reaction diluted with toluene and solvent removed under reduced pressure. Crude product dissolved in diethyl ether and washed with water. Organic layer dried over sodium sulphate and filtered. Crude product then purified with gel silica column chromatography (petroleum ether/ DCM 6:4) to afford the desired product as white solid (1.31 gr, 100%). ^{1}H NMR (300 MHz, Methanol-d4) δ 6.58 (s, 1H), 6.45 (d, J = 7.9 Hz, 1H), 6.15 (d, J = 7.7 Hz, 1H), 5.97 (td, J = 7.8, 1.7 Hz, 1H), 5.52 – 5.44 (m, 4H), 3.57 (s, 2H), 2.40 (d, J = 1.9 Hz, 3H).

3-((4-fluorophenoxy)methyl)-N-methoxy-N-methylbenzamide (2). Methyl 3-((4-fluorophenoxy)methyl) benzoate (**1**) (1.31 gr, 5.05 mmol) and N,O dimethyl hydroxylamine hydrochloride (1.4 gr, 14.4 mmol) are dissolved in anhydrous THF at -40°C under nitrogen atmosphere then isopropyl magnesium chloride (14 ml, 28 mmol) is added dropwise. Reaction mixture stirred at room temperature overnight. Reaction quenched with ammonium hydrochloride saturated water solution and extracted with diethyl ether. Organic layer dried over sodium sulphate, filtered and solvent removed to give the desired clean product (1.28 gr, 88%). ^{1}H NMR (300 MHz, DMSO-d6) δ 7.64 (t, J = 1.8 Hz, 1H), 7.55 (tt, J = 7.9, 1.6 Hz, 2H), 7.51 – 7.43 (m, 1H), 7.13 (t, J = 8.8 Hz, 2H), 7.07 – 6.98 (m, 2H), 5.14 (s, 2H), 3.52 (s, 3H), 3.25 (s, 3H).

1-(3-((4-fluorophenoxy)methyl)phenyl)ethan-1-one (3). 3-((4-fluorophenoxy)methyl)-N-methoxy-N-methyl benzamide (**2**) (1.28 gr, 4.43 mmol) is dissolved in anhydrous 10ml THF at 0°C under nitrogen atmosphere, then methyl magnesium bromide (2.60 ml, 7.87 mmol) was added dropwise. The reaction is stirred 40min then is quenched with few drops of glacial acetic acid. The mixture is diluted with water and extracted with AcOEt, organic layer dried over sodium sulphate, filtered and solvent removed under reduced pressure. Crude product purified with gel silica column chromatography (DCM/petroleum ether 1:1) to afford the desired product as yellowish solid (0.75 gr, 70%). ^{1}H NMR (400 MHz, Chloroform-d) δ 8.02 (t, J = 2.1 Hz, 1H), 7.92 (dt, J = 7.7, 1.5 Hz, 1H), 7.67 – 7.60 (m, 1H), 7.49 (t, J = 7.7 Hz, 1H), 7.04 – 6.86 (m, 4H), 5.08 (s, 2H), 2.62 (s, 3H).

4,4,4-trifluoro-1-(3-((4-fluorophenoxy)methyl)phenyl)-3-hydroxy-3-(trifluoromethyl)butan-1-one (4). 1-(3-((4-fluorophenoxy)methyl)phenyl)ethan-1-one (**3**) (0.74 gr, 3.01 mmol) placed at -60°C in anhydrous THF under nitrogen atmosphere then LiHMDS (4.5 ml, 4.52 mmol) is added dropwise and stirred for 30min. In a separate two neck flask concentrated H2SO4 (10 ml) is warmed to 50 °C and linked through a cannula with the enolate flask then a trihydrate hexafluoroacetone (0.84 ml, 6.02 mmol) is dropped inside the H2SO4 and the formed gaseous HFA is cannulated inside the enolate solution. The mixture is stirred 1 hr, then the reaction is quenched with glacial acetic acid (few drops). Mixture diluted with ACOEt and washed with water and brine. Organic layer collected and dried over sodium sulphate, filtered and solvent removed under reduced pressure. Crude product purified with gel silica column chromatography (petroleum ether/DCM 7:3) to afford the desired product (370 mg, 30%). ^{1}H NMR (300 MHz, Chloroform-d) δ 8.01 (d, J = 1.8 Hz, 1H), 7.92 (dt, J = 7.8, 1.5 Hz, 1H), 7.81 – 7.72 (m, 1H), 7.58 (t, J = 7.7 Hz, 1H), 7.10 – 6.87 (m, 4H), 5.10 (s, 2H), 3.47 (s, 2H).

4,4,4-trifluoro-1-(3-((4-fluorophenoxy) methyl) phenyl)-3-(trifluoromethyl)butane-1,3-diol (UPR1398). Starting material (**4**) (365 mg, 0.89 mmol) is dissolvd in methanol (10 ml) at 0°C then sodium boron hydride (100 mg, 2.66 mmol) was added. Reaction stirred 20 min then is quenched with sodium bicarbonate overnight.). Mixture diluted with ACOEt and washed with water and brine. Organic layer collected and dried over sodium sulphate, filtered and solvent removed Crude residue purified with gel silica column chromatography (DCM/petroleum ether 1:1) to afford **UPR1398** (300 mg, 82%). ^{1}H NMR (300 MHz, Chloroform-d) δ 7.54 – 7.32 (m, 4H), 7.08 – 6.88 (m, 4H), 6.13 (s, 1H), 5.34 (d, J = 11.4 Hz, 1H), 5.06 (s, 2H), 2.41 (ddq, J = 15.6, 11.5, 2.1 Hz, 1H), 2.24 (dd, J = 15.6, 2.2 Hz, 1H). HPLC-MS (ESI): m/z calcd for $C_{18}H_{15}F_7O_3$ [$(M+H)^-$]: 411.08; found: 411.00.

Methyl 4-((4-fluorophenoxy)methyl)benzoate (5). Methyl-3-(bromomethyl) benzoate (1.23 gr, 5.7 mmol), 4-fluorophenol (0.81 gr, 7.0 mmol) and potassium carbonate (1.49 gr, 10.9 mmol) were dissolved in 15 ml of DMF. The mixture is stirred overnight 17hrs then it is diluted with diethyl ether and washed with water and brine. Organic layer collected and dried over sodium sulphate, filtered and solvent removed under reduced pressure. Crude residue recrystallized with isopropyl ether to afford the clean product (1.10 gr, 79%). ^{1}H NMR (400 MHz, Chloroform-d) δ 8.09 – 8.02 (m, 2H), 7.52 – 7.46 (m, 2H), 7.03 – 6.85 (m, 4H), 5.09 (s, 2H), 3.92 (s, 3H).

4-((4-fluorophenoxy)methyl)-N-methoxy-N-methylbenzamide (6). Methyl4-((4-fluorophenoxy) methyl) benzoate (**5**) (1.05 gr, 4.0 mmol) and N,O-dimethyl hydroxylamine hydrochloride (1.18 gr, 12.1 mmol) are stirred in 10 ml of anhydrous THF and placed at -40°C under nitrogen for 10 min the iso-butyl magnesium bromide (11 ml,

5.5 mmol) is added dropwise . Reaction allowed to warm to room temperature and stirred overnight. Reaction quenched with few drops of glacial acetic acid and mixture diluted with diethyl ether and washed with water, NaHCO3 and brine. Organic layer collected and dried over sodium sulphate, filtered. Solvent removed under reduced pressure to give the clean product (1.20 gr, 100%). ^{1}H NMR (300 MHz, Chloroform-d) δ 7.76 – 7.67 (m, 2H), 7.45 (d, J = 8.0 Hz, 2H), 7.04 – 6.85 (m, 4H), 5.07 (s, 2H), 3.56 (s, 3H), 3.37 (s, 3H).

1-(4-((4-fluorophenoxy)methyl)phenyl)ethan-1-one (7). Weinreb amide (**6**) (1.16 gr, 4.0 mmol)) was placed in anhydrous THF at 0°C under nitrogen atmosphere, and then methyl magnesium bromide (2.0 ml, 6.0 mmol) was added dropwise. Reaction quenched with acetic acid after 1 hr. Mixture diluted with diethyl ether and washed with water, NaHCO3 and brine Organic layer collected and dried over sodium sulphate, filtered. Solvent removed under reduced pressure to give the clean product (0.84 gr, 86%). ^{1}H NMR (400 MHz, Chloroform-d) δ 7.98 (d, J = 8.1 Hz, 2H), 7.52 (d, J = 8.0 Hz, 2H), 6.98 (t, J = 8.6 Hz, 2H), 6.90 (dd, J = 9.2, 4.3 Hz, 2H), 5.10 (s, 2H), 2.61 (s, 3H).

4,4,4-trifluoro-1-(4-((4-fluorophenoxy)methyl)phenyl)-3-hydroxy-3-(trifluoromethyl)butan-1-one (8). 1-(4-((4-fluorophenoxy)methyl)phenyl)ethan-1-one (**7**) (0.2 gr, 0.9 mmol) placed at -60°C in anhydrous THF under nitrogen atmosphere then LiHMDS (1.3 ml, 1.3 mmol) is added dropwise and stirred for 30min. In a separate two neck flask concentrated H2SO4 (10 ml) is warmed to 50 °C and linked through a cannula with the enolate flask then a trihydrate hexafluoroacetone (0.5 ml, 3.5 mmol) is dropped inside the H2SO4 and the formed gaseous HFA is cannulated inside the enolate solution. The mixture is stirred 3 hrs, and then the reaction is quenched with glacial acetic acid (few drops). Mixture diluted with ACOEt and washed with water and brine. Organic layer collected and dried over sodium sulphate, filtered and solvent removed under reduced pressure. Crude product purified with gel silica column chromatography (hexane/DCM 7:3) to afford the desired product (220 mg, 62%%). ^{1}H NMR (300 MHz, Chloroform-d) δ 8.03 – 7.94 (m, 2H), 7.60 (d, J = 8.1 Hz, 2H), 7.12 (s, 1H), 7.05 – 6.85 (m, 4H), 5.13 (s, 2H), 3.46 (s, 2H).

4,4,4-trifluoro-1-(4-((4-fluorophenoxy) methyl) phenyl)-3-(trifluoromethyl) butane-1,3-diol (UPR1408). Starting material (X) (0.14 gr, 0.3 mmol) is placed in methanol at 0°C, then sodium boron hydride (15 mg, 0.4 mmol) is added. Mixture stirred 30 min, then the reaction is quenched with NaHCO3. Mixture diluted with diethyl ether and washed with water and brine. Organic layer collected and dried over sodium sulphate, filtered and solvent removed. Crude residue purified by a silica gel column chromatography (hexane/DCM 7:3) to afford **UPR1408** as a white solid (105 mg, 77%). ^{1}H NMR (400 MHz,

Chloroform-d) δ 7.47 (d, J = 7.9 Hz, 2H), 7.40 (d, J = 8.0 Hz, 2H), 6.98 (t, J = 8.6 Hz, 2H), 6.89 (dd, J = 9.2, 4.2 Hz, 2H), 6.10 (s, 1H), 5.32 (d, J = 11.5 Hz, 1H), 5.04 (s, 2H), 2.56 (s, 1H), 2.44 – 2.32 (m, 1H), 2.21 (d, J = 15.5 Hz, 1H). HPLC-MS (ESI): m/z calcd for $C_{18}H_{15}F_7O_3$ [(M+H)$^-$]: 411.08; found: 411.34.

Methyl 3-(2-(4-fluorophenyl)-2-hydroxyethyl)benzoate (9). Methyl-3-(bromomethyl) benzoate (4.7 gr, 20.5 mmol) is stirred 2 hrs in refluxing THF with activated metallic zinc (6.0 gr, 91.8 mmol) under nitrogen atmosphere. Then the reaction mixture is cooled to 0°C and 4-fluoro benzaldehyde (2.5 gr, 20.5 mmol) is added. Reaction stirred overnight at room temperature under nitrogen atmosphere. Mixture filtered on celite pad, then diluted with DCM and washed with water, NaHCO3 and brine. Organic layer collected and dried over sodium sulphate, then filtered and solvent removed. Crude residue purified by a silica gel column chromatography (hexane/AcOEt 7:3) to give the clean product (1.4 gr, 25%). ^{1}H NMR (300 MHz, Chloroform-d) δ 7.97 – 7.83 (m, 2H), 7.43 – 7.27 (m, 4H), 7.02 (t, J = 8.7 Hz, 2H), 4.92 (t, J = 6.7 Hz, 1H), 3.91 (s, 3H), 3.04 (d, J = 6.7 Hz, 2H).

Methyl 3-(4-fluorophenethyl)benzoate (10). Methyl 3-(2-(4-fluorophenyl)-2-hydroxyethyl)benzoate (**9**) (1.12 gr, 4.1 mmol) is dissolved in 10ml HCl 37% and stirred at room temperature 50 min. The reaction mixture is diluted with diethyl ether and washed with water. Organic layer collected and solvent removed under reduced pressure. The crude intermediate is then dissolved in acetic acid (glacial, 10 ml) and zinc powder (1 gr, 15.3 mmol) is added. Mixture stirred 1 hr at room temperature then is filtered on a celite pad and diluted with toluene. Solvent removed under reduced pressure, crude residue purified by a silica gel column chromatography (hexane/AcOEt 10:1) to afford the desired product (0.35 gr, 33%). ^{1}H NMR (300 MHz, Chloroform-d) δ 7.90 – 7.80 (m, 2H), 7.38 – 7.28 (m, 2H), 7.11 – 7.05 (m, 2H), 6.95 (t, J = 8.7 Hz, 2H), 3.92 (s, 3H), 2.92 (q, J = 2.9 Hz, 4H).

3-(4-fluorophenethyl)-N-methoxy-N-methylbenzamide (11). Methyl 3-(4-fluorophenethyl)benzoate (**10**) (0.33gr, 1.3 mmol) and N,O-dimethyl hydroxylamine (0.37 gr, 3.8 mmol) are stirred in 10 ml of anhydrous THF and placed at -40°C under nitrogen for 10 min the iso-butyl magnesium bromide (3.2 ml, 6.4 mmol) is added dropwise . The reaction is quenched with few drops of glacial acetic acid after 4 hrs. Mixture diluted with diethyl ether and washed with water, NaHCO3 and brine. Organic layer collected and dried over sodium sulphate, filtered and solvent removed under reduced pressure. Crude residue purified by a silica gel column chromatography (hexane/DCM 6:1) to give the clean product (250 mg,67%). ^{1}H NMR (400 MHz, Chloroform-d) δ 7.52 – 7.42 (m, 2H), 7.30 (t, J = 7.6 Hz, 1H), 7.24 – 7.19 (m, 1H), 7.09 (dd, J = 8.3, 5.5 Hz, 2H), 6.94 (t, J = 8.6 Hz, 2H), 3.53 (s, 3H), 3.33 (s, 3H), 2.92 (s, 4H).

1-(3-(4-fluorophenethyl)phenyl)ethan-1-one (12). Weinreb amide (**11**) (0.16 gr, 0.56 mmol) was placed in anhydrous THF at 0°C under nitrogen atmosphere, and then methyl magnesium bromide (0.3 ml, 0.84 mmol) was added dropwise. Reaction quenched with acetic acid after 1 hr. Mixture diluted with diethyl ether and washed with water, NaHCO3 and brine. Organic layer collected and dried over sodium sulphate, filtered and solvent removed under reduced pressure. Crude residue purified by a silica gel column chromatography (hexane/DCM 9:1) to give the clean product (100 mg, 73%). ^{1}H NMR (300 MHz, Chloroform-d) δ 7.83 – 7.71 (m, 2H), 7.41 – 7.30 (m, 2H), 7.14 – 7.04 (m, 2H), 6.95 (t, J = 8.7 Hz, 2H), 3.02 – 2.84 (m, 4H), 2.58 (s, 3H).

4,4,4-trifluoro-1-(3-(4-fluorophenethyl)phenyl)-3-hydroxy-3-(trifluoromethyl)butan-1-one (13). 1-(3-(4-fluorophenethyl)phenyl)ethan-1-one (**12**) (0.10 gr, 0.4 mmol) placed at -60°C in anhydrous THF under nitrogen atmosphere then LiHMDS (0.8 ml, 0.8 mmol) is added dropwise and stirred for 30min. In a separate two neck flask concentrated H2SO4 (10 ml) is warmed to 50 °C and linked through a cannula with the enolate flask then a trihydrate hexafluoroacetone (0.3 ml, 2.1 mmol) is dropped inside the H2SO4 and the formed gaseous HFA is cannulated inside the enolate solution. The mixture is stirred 3 hrs, then the reaction is quenched with glacial acetic acid (few drops). Mixture diluted with ACOEt and washed with water and brine. Organic layer collected and dried over sodium sulphate, filtered and solvent removed under reduced pressure. Crude product purified with gel silica column chromatography (hexane/DCM 7:3) to afford the desired product (160 mg, 96%). ^{1}H NMR (300 MHz, Chloroform-d) δ 7.78 (td, J = 4.7, 3.6, 1.9 Hz, 1H), 7.66 (s, 1H), 7.48 – 7.38 (m, 2H), 7.16 (d, J = 3.1 Hz, 1H), 7.08 (dd, J = 8.4, 5.5 Hz, 2H), 7.02 – 6.90 (m, 2H), 3.40 (s, 2H), 3.06 – 2.86 (m, 4H).

4,4,4-trifluoro-1-(3-(4-fluorophenethyl)phenyl)-3-(trifluoromethyl)butane-1,3-diol (UPR1409). Starting material (**13**) (0.12 gr, 0.3 mmol) is placed in methanol at 0°C, then sodium boron hydride (15 mg, 0.4 mmol) is added. Mixture stirred 30 min, then the reaction is quenched with NaHCO3. Mixture diluted with diethyl ether and washed with water and brine. Organic layer collected and dried over sodium sulphate, filtered nd solvent removed. Crude residue purified bya silica gel column chromatography (hexane/DCM 7:3) to afford **UPR1409** as a white solid (82 mg, 71%). ^{1}H NMR (300 MHz, Chloroform-d) δ 7.33 (t, J = 7.6 Hz, 1H), 7.28 – 7.15 (m, 2H), 7.14 – 7.04 (m, 3H), 6.96 (t, J = 8.7 Hz, 2H), 6.20 (d, J = 5.0 Hz, 1H), 5.24 (d, J = 11.5 Hz, 1H), 2.91 (q, J = 2.8 Hz, 4H), 2.60 (s, 1H), 2.32 (ddt, J = 15.6, 11.5, 2.1 Hz, 1H), 2.15 (dd, J = 15.5, 2.2 Hz, 1H). HPLC-MS (ESI): m/z calcd for $C_{19}H_{17}F_7O_2$ $[(M+H)^-]$: 409.10; found: 409.10.

Ethyl 4-hydroxy-3-nitrobenzoate (14). Ethyl-4-hydroxy benzoate (5.5 gr, 33.0 mmol) is dissolved in 50 ml of glacial acetic and then 2.5 ml of concentrated nitric acid was added. Reaction stirred at 40°C 3 hrs. The mixture is poured in cold water and the precipitate is recovered by suction filtration. Solid product is washed with water and dried to under reduced pressure to remove traces of water (6.9 gr, 100%). ^{1}H NMR (300 MHz, Chloroform-d) δ 10.90 (s, 1H), 8.83 (d, J = 2.1 Hz, 1H), 8.26 (dd, J = 8.8, 2.1 Hz, 1H), 7.24 (d, J = 8.8 Hz, 1H), 4.42 (q, J = 7.1 Hz, 2H), 1.43 (t, J = 7.1 Hz, 3H).

Ethyl 3-amino-4-hydroxybenzoate (15). Ethyl 4-hydroxy-3-nitrobenzoate (**14**) (1.8 gr, 8.5 mmol) and palladium 10% on charcoal (0.5 mol%) were placed in 50 ml of THF under nitrogen atmosphere then sodium formate (2.8 gr, 42.6 mmol) and 15 ml of water were added. The mixture is heated to 50°C and stirred for 4 hrs then the reaction is cooled to room temperature and filtered on alumina pad. Mixture diluted with AcOAEt and washed with water and brine. Organic layer collected and dried over sodium sulphate, filtered and solvent removed. Crude residue recrystallized with acetic acid to give the clean product as pink crystals (1.5 gr, 98%). ^{1}H NMR (400 MHz, Chloroform-d) δ 7.49 – 7.41 (m, 2H), 6.75 (d, J = 8.2 Hz, 1H), 4.34 (p, J = 7.0 Hz, 2H), 1.37 (td, J = 7.2, 3.4 Hz, 4H).

Ethyl 4-(4-fluorobenzamido)-3-hydroxybenzoate (16). 4-fluoro benzoic acid (0.5 gr, 3.6 mmol) is dissolved in 5 ml of thionyl chloride and refluxed for 1.5 hrs. The mixture is cooled to room temperature and then the excess of thionyl chloride is removed under reduced pressure. In a separate flask Ethyl 3-amino-4-hydroxybenzoate (**15**) (0.5 gr, 2.8 mmol) and triethylamine (0.55 ml, 3.9 mmol) were placed in 15 ml of anhydrous THF at 0°C then a solution of the previously prepared chloride in 5ml of THF was added dropwise. The reaction is stirred 1 hrs to completion. Mixture diluted in AcOEt and washed with water, HCl 1M and brine. Organic layer collected and dried over sodium sulphate then filtered and solvent removed to give desired product as a white solid (0.55 gr, 65%). ^{1}H NMR (300 MHz, DMSO-d6) δ 9.63 (s, 1H), 8.28 (d, J = 2.1 Hz, 1H), 8.11 – 8.00 (m, 2H), 7.69 (dd, J = 8.5, 2.1 Hz, 1H), 7.37 (t, J = 8.8 Hz, 2H), 7.01 (d, J = 8.5 Hz, 1H), 4.27 (q, J = 7.1 Hz, 2H), 1.30 (t, J = 7.1 Hz, 3H).

Ethyl 2-(4-fluorophenyl)benzo[d]oxazole-5-carboxylate (17). Ethyl 4-(4-fluorobenzamido)-3-hydroxy benzoate (**16**) (0.25 gr, 0.8 mmol) and 4-toluen sulfonic acid (0.1 gr, 0.5 mmol) were dissolved in 20 ml of toluene and refluxed at 110°C for 2 hrs to completion. The mixture is then cooled to room temoperature and washed with NaHCO3 and brine. . Organic layer collected and dried over sodium sulphate then filtered and solvent removed. Crude residue purified by a silica gel column chromatography (hexane/DCM 7:3) to afford the desired product as a white solid (150 mg, 66%). ^{1}H NMR (300 MHz, Chloroform-d) δ 8.47 (d, J = 1.6 Hz, 1H), 8.33 – 8.22 (m, 2H), 8.12 (dd, J = 8.6,

1.7 Hz, 1H), 7.61 (d, J = 8.5 Hz, 1H), 7.27 – 7.18 (m, 3H), 4.43 (q, J = 7.1 Hz, 2H), 1.43 (t, J = 7.1 Hz, 3H).

2-(4-fluorophenyl)-N-methoxy-N-methylbenzo[d]oxazole-5-carboxamide (18). Ethyl 2-(4-fluorophenyl) benzo[d]oxazole-5-carboxylate (**17**) (0.15gr, 0.5 mmol) and N,O-dimethyl hydroxylamine hydrochloride (0.15 gr, 1.6 mmol) are stirred in 10 ml of anhydrous THF and placed at -40°C under nitrogen for 10 min the iso-butyl magnesium bromide (1.3 ml, 2.6 mmol) is added dropwise . Reaction allowed to warm to -20°C. Reaction quenched with few drops of glacial acetic acid and mixture diluted with AcOEt and washed with water, HCL 1M and brine. Organic layer collected and dried over sodium sulphate, filtered. Solvent removed under reduced pressure to give the clean product (0.12 gr, 80%). ^{1}H NMR (300 MHz, Chloroform-d) δ 8.33 – 8.22 (m, 2H), 8.15 (d, J = 1.6 Hz, 1H), 7.76 (dd, J = 8.5, 1.6 Hz, 1H), 7.60 (d, J = 8.4 Hz, 1H), 7.26 – 7.18 (m, 3H), 3.57 (s, 3H), 3.41 (s, 3H).

1-(2-(4-fluorophenyl)benzo[d]oxazol-5-yl)ethan-1-one (19). Weinreb amide (**18**) (0.17 gr, 0.5 mmol) was placed in 10 ml of anhydrous THF at 0°C under nitrogen atmosphere, and then methyl magnesium bromide (0.3 ml, 0.8 mmol) was added dropwise. Reaction quenched with acetic acid after 30 min. Mixture diluted with AcOEt and washed with water, NaHCO3 and brine Organic layer collected and dried over sodium sulphate, filtered. Solvent removed under reduced pressure to give the clean product (0.12 gr, 94%). ^{1}H NMR (400 MHz, Chloroform-d) δ 8.39 (d, J = 1.8 Hz, 1H), 8.31 (ddq, J = 8.5, 5.1, 3.0 Hz, 2H), 8.09 (dd, J = 8.5, 1.8 Hz, 1H), 7.66 (dd, J = 8.5, 2.0 Hz, 1H), 7.31 – 7.22 (m, 3H), 2.72 (d, J = 2.1 Hz, 3H).

4,4,4-trifluoro-1-(2-(4-fluorophenyl)benzo[d]oxazol-5-yl)-3-hydroxy-3-(trifluoromethyl)butan-1-one (20). Starting material (**19**) (0.11 gr, 0.4 mmol) placed at -60°C in anhydrous THF under nitrogen atmosphere then LiHMDS (0.8 ml, 0.8 mmol) is added dropwise and stirred for 30min. In a separate two neck flask concentrated H2SO4 (10 ml) is warmed to 50 °C and linked through a cannula with the enolate flask then a trihydrate hexafluoroacetone (0.2 ml, 1.2 mmol) is dropped inside the H2SO4 and the formed gaseous HFA is cannulated inside the enolate solution. The mixture is stirred 3 hrs, and then the reaction is quenched with glacial acetic acid (few drops). Mixture diluted with ACOEt and washed with water and brine. Organic layer collected and dried over sodium sulphate, filtered and solvent removed under reduced pressure. Crude product purified with gel silica column chromatography (petroleum ether/AcOEt 7:3) to afford the desired product (100 mg, 60%). ^{1}H NMR (300 MHz, Chloroform-d) δ 8.37 (d, J = 1.8 Hz, 1H), 8.34 – 8.24 (m, 2H), 8.06 (dd, J = 8.6, 1.8 Hz, 1H), 7.71 (d, J = 8.6 Hz, 1H), 7.26 (t, J = 8.6 Hz, 2H), 7.15 (s, 1H), 3.56 (s, 2H).

4,4,4-trifluoro-1-(2-(4-fluorophenyl)benzo[d]oxazol-5-yl)-3-(trifluoromethyl)butane-1,3-diol (UPR1410). Starting material (**20**) (0.1 gr, 0.2 mmol) is placed in methanol at 0°C, then sodium boron hydride (25mg, 0.6 mmol) is added. Mixture stirred 30 min, and then the reaction is quenched with NaHCO3. Mixture diluted with diethyl ether and washed with water and brine. Organic layer collected and dried over sodium sulphate, filtered and solvent removed. Crude residue purified by a silica gel column chromatography (petroleum ether/AcOEt 7:3) to afford **UPR1410** as a white solid (100 mg, 99%). ^{1}H NMR (300 MHz, Chloroform-d) δ 8.28 – 8.17 (m, 2H), 7.74 (s, 1H), 7.52 (d, J = 8.4 Hz, 1H), 7.26 – 7.10 (m, 3H), 6.37 (s, 1H), 5.38 (d, J = 11.4 Hz, 1H), 2.48 – 2.38 (m, 1H), 2.23 (dd, J = 15.6, 2.2 Hz, 1H). HPLC-MS (ESI): m/z calcd for $C_{18}H_{12}F_7NO_3$ [$(M+H)^-$]: 422.03; found: 422.08.

3-(chloromethyl)-4-methoxybenzaldehyde (21). 4-methoxybenzaldehyde (16.64 gr, 122.22 mmol), formaldehyde (6.68 gr, 224.4 mmol), zinc chloride (19.4 gr, 14.23 mmol) are dissolved in HCl (37%, 80 ml) and heated to 75°C for 30 min. The solution is coled to room temperature and poured in cold/ice water, then the precipitate is recovered by filtration to give the desired product as yellowish solid. (20 gr, 89%). 1H NMR (300 MHz, Chloroform-d) δ 9.88 (s, 1H), 7.94 – 7.77 (m, 2H), 7.01 (d, J = 8.5 Hz, 1H), 4.66 (s, 2H), 3.96 (s, 3H).

3-((4-fluorophenoxy)methyl)-4-methoxybenzaldehyde (22). 3-(chloromethyl)-4-methoxybenzaldehyde (**21**) (0.50 gr, 2.71 mmol), 4-fluoro phenol (0.32 gr, 2.85 mmol) were dissolved in degased DMF (30 ml) then potassium carbonate (0.70 gr, 5.07 mmol) and potassium iodide (0.11 gr, 0.66 mmol) are added. The solution is stirred at room temperature overnight (18 hrs). The solution is diluted with water and extracted with DCM. Organic layer collected and dried over sodium sulphate, filtered and solvent removed under reduced pressure. Crude product purified with silica gel column chromatography (hexane/AcOEt 10:2) to afford the desired compound as colourless oil (0.36 gr, 65%). 1H NMR (300 MHz, Chloroform-d) δ 10.93 (s, 1H), 9.06 (d, J = 2.2 Hz, 1H), 8.88 (dd, J = 8.5, 2.2 Hz, 1H), 8.15 – 7.86 (m, 5H), 6.10 (s, 2H), 4.98 (s, 3H).

4,4,4-trifluoro-1-(3-((4-fluorophenoxy)methyl)-4-methoxyphenyl)-3-(trifluoromethyl)butane-1,3-diol (UPR1388). A solution of 2-(bromomethyl)-1,1,1,3,3,3-hexafluoropropan-2-ol (0.46 ml, 2.88 mmol) in anhydrous THF 10ml is placed a -78°C then n-butyl lithium (3.8 ml, 6.05 mmol) is added dropwise at -78°C under nitrogen atmosphere. The solution is stirred for 30min then a solution of 3-((4-fluorophenoxy)methyl)-4-methoxybenzaldehyde (**22**) (0.25 gr, 0.96 mmol) in THF (10ml) is added dropwise. The reaction is stirred at -78°C under nitrogen atmosphere for additional 30min then the reaction is quenched with few drops of glacial acetic acid. Solvent

removed under reduced pressure then the crude product is dissolved in DCM and washed with sodium carbonate solution. The organic layer is dried over sodium sulphate, filtered and solvent removed under reduced pressure. The crude product is then purified with silica gel column chromatography (hexane/AcOEt 10:2) to afford **UPR1388** ad colourless oil (150mg, 35%).^{1}H NMR (300 MHz, Chloroform-d) δ 7.46 (d, J = 2.3 Hz, 1H), 7.35 – 7.26 (m, 2H), 7.07 – 6.88 (m, 4H), 5.06 (s, 2H), 3.88 (s, 3H), 2.55 (q, J = 2.1 Hz, 1H), 2.37 (ddd, J = 15.5, 11.4, 2.1 Hz, 1H), 2.16 (d, J = 15.4 Hz, 1H). HPLC-MS (ESI): m/z calcd for $C_{19}H_{17}F_7O_4$ [$(M+H)^-$]: 441.09; found: 441.01.

3-((4-chlorophenoxy)methyl)-4-methoxybenzaldehyde (24). 3-(chloromethyl)-4-methoxybenzaldehyde (**21**) (1.63 gr, 8.8 mmol), 4-clorophenol (1.23 ml, 12.5 mmol) and potassium carbonate (1.66 gr, 12.0 mmol) were dissolved in DMF and stirred overnight (18 hrs). The reaction is diluted with AcOEt and washed with HCl 1M and brine. Organic layer collected and solvent removed. Crude residue purified by silica gel column chromatography (hexane/AcOEt 8:1) to give the desired clean product (1.98 gr, 82%). ^{1}H NMR (400 MHz, Chloroform-d) δ 9.91 (s, 1H), 8.01 (dd, J = 2.1, 1.0 Hz, 1H), 7.87 (dd, J = 8.5, 2.2 Hz, 1H), 7.25 (d, J = 7.7 Hz, 2H), 7.03 (d, J = 8.5 Hz, 1H), 6.98 – 6.90 (m, 2H), 5.09 (s, 2H), 3.96 (s, 3H).

1-(3-((4-chlorophenoxy) methyl)-4-methoxyphenyl) ethan-1-ol (25). 3-((4-chlorophenoxy) methyl)-4-methoxy benzaldehyde (**24**) (0.32 gr, 1.2 mmol) was dissolved in anhydrous THF and placed at 0°C under nitrogen, then methyl magnesium bromide (0.8 ml, 0.3 mmol) was added dropwise. The reaction was stirred 20min then was quenched with few drops of glacial acetic acid. The mixture is is diluted with AcOEt and washed with HCl 1M and brine. Organic layer collected and fried over sodium sulphate, filtered and solvent removed to give the desired product (0.34 gr, 97%). ^{1}H NMR (300 MHz, Chloroform-d) δ 7.46 (d, J = 2.3 Hz, 1H), 7.34 (dd, J = 8.4, 2.3 Hz, 1H), 7.29 – 7.23 (m, 2H), 6.97 – 6.88 (m, 3H), 5.08 (s, 2H), 4.88 (q, J = 6.4 Hz, 1H), 3.87 (s, 3H), 1.49 (d, J = 6.5 Hz, 3H).

1-(3-((4-chlorophenoxy) methyl)-4-methoxyphenyl) ethan-1-one (26). 1-(3-((4-chlorophenoxy) methyl)-4-methoxyphenyl) ethan-1-ol (**25**) (0.34 gr, 1.2 mmol) was dissolved in 20 ml of toluene and placed at 0°C under nitrogen, then trimethyl aluminium (0.2 ml, 0.1 mmol) was added dropwise. The mixture is allowed to warm to room temperature then ciclohexanone (0.7 ml, 6.8 mmol) was added and the reaction was stirred at reflux at 130°C under nitrogen for 2 hrs. The reaction is quenched with NaHCO3 saturated water solution and extracted with AcOEt. Organic layer washed with HCl 1M and brine then it is dried over sodium sulphate, filtered and solvent removed. Crude residue purified by a silica gel column chromatography (petroleum ether/ AcOEt 10:3) to

afford the clean product as a white solid (0.24 gr, 72%). ^{1}H NMR (300 MHz, Chloroform-d) δ 8.08 (d, J = 2.4 Hz, 1H), 7.97 (dd, J = 8.7, 2.4 Hz, 1H), 7.25 – 7.20 (m, 2H), 7.00 – 6.89 (m, 3H), 5.08 (s, 2H), 3.93 (d, J = 1.7 Hz, 3H), 2.56 (d, J = 1.7 Hz, 3H).

1-(3-((4-chlorophenoxy)methyl)-4-methoxyphenyl)-4,4,4-trifluoro-3-hydroxy-3-(trifluoromethyl)butan-1-one (27). 1-(3-((4-chlorophenoxy) methyl)-4-methoxyphenyl) ethan-1-one (**26**) (0.22 gr, 0.8 mmol) is placed at -55°C in anhydrous THF under nitrogen atmosphere then LiHMDS (1.5 ml, 1.5 mmol) is added dropwise and stirred for 30min. In a separate two neck flask concentrated H2SO4 (10 ml) is warmed to 50 °C and linked through a cannula with the enolate flask then a trihydrate hexafluoroacetone (0.4ml, 2.9 mmol) is dropped inside the H2SO4 and the formed gaseous HFA is cannulated inside the enolate solution. The mixture is stirred 4 hr, and then the reaction is quenched with glacial acetic acid (few drops).). Mixture diluted with ACOEt and washed with water and brine. Organic layer collected and dried over sodium sulphate, filtered and solvent removed Crude product purified with gel silica column chromatography (petroleum ether/AcOEt 8:2) to afford the desired product (0.11 gr, 30%). ^{1}H NMR (300 MHz, Chloroform-d) δ 8.01 (d, J = 2.4 Hz, 1H), 7.88 (dd, J = 8.7, 2.4 Hz, 1H), 7.21 – 7.12 (m, 2H), 6.92 (d, J = 8.7 Hz, 1H), 6.88 – 6.80 (m, 2H), 4.98 (s, 2H), 3.88 (s, 3H), 3.30 (s, 2H).

1-(3-((4-chlorophenoxy)methyl)-4-methoxyphenyl)-4,4,4-trifluoro-3-(trifluoromethyl)butane-1,3-diol (UPR1404). Ketone (**27**) (100 mg, 0.2 mmol) is dissolved in methanol (5 ml) at 0°C then sodium boron hydride (15 mg, 0.4 mmol) was added. Reaction stirred 20 min then is quenched with sodium bicarbonate overnight. Mixture diluted with water and extracted with AcOEt, organic layer dried over sodium sulphate, filtered and solvent removed. Crude residue purified with gel silica column chromatography (petroleum ether/ AcOEt 8:1) to afford **UPR1404** as a white solid (70 mg, 75%). ^{1}H NMR (300 MHz, Chloroform-d) δ 7.46 (d, J = 2.3 Hz, 1H), 7.37 – 7.21 (m, 3H), 6.99 – 6.90 (m, 3H), 6.29 (s, 1H), 5.24 (d, J = 11.5 Hz, 1H), 5.07 (s, 2H), 3.89 (s, 3H), 2.74 (t, J = 2.3 Hz, 1H), 2.45 – 2.30 (m, 1H), 2.17 (d, J = 15.4 Hz, 1H). HPLC-MS (ESI): m/z calcd for $C_{19}H_{17}ClF_6O_4$ [$(M+H)^-$]: 457,07; found: 457.16.

1-(chloromethyl)-2-methoxybenzene (28). 2-hydroxy methyl anisole (2.05 gr, 14.9 mmol) stirred at room temperature with 5 ml of HCl 37%. Reaction mixture extracted with diethyl ether, organic layer washed with brine and dried over sodium sulphate then filtered and solvent removed to give the desired product (2.07 gr, 89%).

1-(4-fluorophenyl)-2-(2-methoxyphenyl)ethan-1-ol (29). 1-(chloromethyl)-2-methoxybenzene (**28**) (1.59 gr, 10.1 mmol) is stirred with activated magnesium (450 mg,

18.5 mmol) in THF at reflux under nitrogen atmosphere for 30min then is cooled to room temperature and is added dropwise to a solution of 4-fluoro-benzaldehyde (0.37 gr, 26.6 mmol) in THF. The reaction 30 min a 0°C then is quenched with ammonium chloride and water. Extraction with AcOEt, organic layer washed with NaHCO3, brine, dried over sodium sulphate and filtered. Solvent removed and crude product is purified with silica gel column chromatography (hexane/DCM 1:1) to afford the desired product as a white solid (340 mg, 14%). ^{1}H NMR (400 MHz, Chloroform-d) δ 7.37 – 7.28 (m, 2H), 7.25 – 7.19 (m, 1H), 7.02 (dtd, J = 8.8, 6.5, 1.9 Hz, 3H), 6.89 (t, J = 7.1 Hz, 2H), 4.95 (dd, J = 8.5, 4.1 Hz, 1H), 3.85 (s, 3H), 3.09 (dd, J = 13.6, 4.2 Hz, 1H), 2.95 (dd, J = 13.6, 8.5 Hz, 1H).

1-(4-fluorophenethyl)-2-methoxybenzene (30). 1-(4-fluorophenyl)-2-(2-methoxyphenyl)ethan-1-ol (29) (0.23 gr, 0.92 mmol) is stirred 30min with 5 ml of HCl 37%. The mixture is then extracted with diethyl ether and washed with brine. Organic layer diluted with glacial acetic acid (8 ml) then metallic zinc is added (265 mg, 4 mmol) and the mixture is heated to reflux for 60 min. The reaction is cooled to room temperature and filtered over celite pad. Crude product is purified with silica gel column chromatography (hexane) to afford the desired product as colourless oil (0.13 gr, 60%). ^{1}H NMR (300 MHz, Chloroform-d) δ 7.13 (dddd, J = 24.0, 18.4, 7.7, 1.7 Hz, 4H), 7.00 – 6.82 (m, 4H), 3.82 (s, 3H), 2.86 (q, J = 2.6 Hz, 4H).

1-(3-(4-fluorophenethyl)-4-methoxyphenyl)ethan-1-one (31). 1-(4-fluorophenethyl)-2-methoxybenzene (**30**) (0.13 gr, 0.57 mmol) dissolved in DCM (8 ml) is placed at 0°C then aluminium trichloride (0.15 gr, 1.14 mmol) and acetic anhydride (0.1 ml, 1.1 mmol) were added under nitrogen atmosphere. The reaction is stirred 20 min then is quenched with cold water. The mixture is extracted with DCM, organic layer washed with NaHCO3 and brine. Solvent removed and crude residue purified with silica gel column chromatography (petroleum ether/DCM 1:1) to afford the desired compound (105 mg, 68%). ^{1}H NMR (300 MHz, Chloroform-d) δ 7.84 (dd, J = 8.6, 2.3 Hz, 1H), 7.70 (d, J = 2.3 Hz, 1H), 7.17 – 7.07 (m, 2H), 7.02 – 6.82 (m, 3H), 3.88 (s, 3H), 2.88 (qq, J = 8.5, 5.0 Hz, 4H), 2.52 (s, 3H).

4,4,4-trifluoro-1-(3-(4-fluorophenethyl)-4-methoxyphenyl)-3-hydroxy-3-(trifluoromethyl)butan-1-one (32). 1-(3-(4-fluorophenethyl)-4-methoxyphenyl)ethan-1-one (**31**) (0.11 gr, 0.4 mmol) is placed at -55°C in anhydrous THF under nitrogen atmosphere then LiHMDS (0.58 ml, 0.6 mmol) is added dropwise and stirred for 30min. In a separate two neck flask concentrated H2SO4 (10 ml) is warmed to 50 °C and linked through a cannula with the enolate flask then a trihydrate hexafluoroacetone (0.22 ml, 1.6 mmol) is dropped inside the H2SO4 and the formed gaseous HFA is cannulated inside the enolate solution. The mixture is stirred 4 hr, and then the reaction is quenched with glacial acetic acid (few drops).). Mixture diluted with ACOEt and washed with water and

brine. Organic layer collected and dried over sodium sulphate, filtered and solvent removed Crude product purified with gel silica column chromatography (petroleum ether/DCM 8:2) to afford the desired product (138 mg, 92%). ^{1}H NMR (300 MHz, Chloroform-d) δ 7.85 (dd, J = 8.7, 2.4 Hz, 1H), 7.64 (d, J = 2.3 Hz, 1H), 7.15 – 7.05 (m, 2H), 6.95 (td, J = 8.7, 2.3 Hz, 3H), 3.92 (s, 3H), 3.32 (s, 2H), 2.99 – 2.79 (m, 4H).

4,4,4-trifluoro-1-(3-(4-fluorophenethyl)-4-methoxyphenyl)-3-(trifluoromethyl)butane-1,3-diol (UPR1405). Starting material (**32**) (118 mg, 0.31 mmol) is dissolved in methanol (5 ml) at 0°C then sodium boron hydride (15 mg, 0.4 mmol) was added. Reaction stirred 20 min then is quenched with sodium bicarbonate overnight. Mixture diluted with water and extracted with AcOEt, organic layer dried over sodium sulphate, filtered and solvent removed. Crude residue purified with gel silica column chromatography (petroleum ether/ AcOEt 9:1) to afford **UPR1405** (110 mg, 81%). ^{1}H NMR (300 MHz, Chloroform-d) δ 7.22 – 7.03 (m, 3H), 7.00 – 6.81 (m, 4H), 6.21 (s, 1H), 5.17 (d, J = 11.6 Hz, 1H), 3.84 (s, 3H), 2.96 – 2.77 (m, 4H), 2.29 (ddd, J = 15.5, 11.5, 2.0 Hz, 1H), 2.14 – 2.03 (m, 1H). HPLC-MS (ESI): m/z calcd for $C_{20}H_{19}F_7O_3$ [$(M+H)^-$]: 439,11; found: 439.25.

1-(4-methoxy-3-nitrophenyl)ethan-1-one (33). 4-metoxy acetophenone (5 gr, 33.3 mmol) is dissolved in concentrated sulphuric acid (20 ml) and placed at 0°C then concentrated nitric acid (3 ml) is added dropwise. Reaction stirred and allowed to warm to room temperature then stirred for 20 min. Reaction mixture is then poured in cold/ice water and the precipitate recovered by filtration. Crude product crystallized from ethanol to afford the desired product (4.0 gr, 62%). ^{1}H NMR (300 MHz, Chloroform-d) δ 8.42 (d, J = 2.2 Hz, 1H), 8.17 (dd, J = 8.8, 2.2 Hz, 1H), 7.16 (d, J = 8.8 Hz, 1H), 4.04 (s, 3H), 2.60 (s, 3H).

4,4,4-trifluoro-3-hydroxy-1-(4-methoxy-3-nitrophenyl)-3-(trifluoromethyl)butan-1-one (34). 4-methoxy-3-nitrophenyl)ethan-1-one (**33**) (0.55 gr, 2.8 mmol) is placed at -78°C in anhydrous THF under nitrogen atmosphere then LiHMDS (4.2 ml, 4.2 mmol) is added dropwise and stirred for 30min. In a separate two neck flask concentrated H2SO4 (10 ml) is warmed to 50 °C and linked through a cannula with the enolate flask then a trihydrate hexafluoroacetone (0.78 ml, 5.6 mmol) is dropped inside the H2SO4 and the formed gaseous HFA is cannulated inside the enolate solution. The mixture is stirred 1 hr then the reaction is quenched with glacial acetic acid and water (2 ml 1:1).). Mixture diluted with ACOEt and washed with water and brine. Organic layer collected and dried over sodium sulphate, filtered and solvent removed Crude product purified with gel silica column chromatography (petroleum ether/ AcOEt 4:1) to afford the desired product (320 mg, 31%). ^{1}H NMR (300 MHz, Chloroform-d) δ 8.47 (d, J = 2.3 Hz, 1H), 8.20 (dd, J = 8.9, 2.3 Hz, 1H), 7.30 – 7.20 (m, 1H), 6.87 (s, 1H), 4.11 (s, 3H), 3.45 (s, 2H).

4,4,4-trifluoro-1-(4-methoxy-3-nitrophenyl)-3-(trifluoromethyl)butane-1,3-diol (35). Starting material (**34**) (0.32 gr, 0.9 mmol) is dissolved in 10 ml of methanol and placed at 0°C then sodium boron hydride (50 mg,1.33 mmol) is added. Reaction stired for 20 min then is is quenched with sodium bicarbonate overnight. Mixture diluted with water and extracted with AcOEt, organic layer dried over sodium sulphate, filtered and solvent removed. Crude residue purified with gel silica column chromatography (petroleum ether/ AcOEt 5:1) to afford the desired product (210 mg, 65%). ^{1}H NMR (300 MHz, Chloroform-d) δ 7.87 (d, J = 2.3 Hz, 1H), 7.56 (dd, J = 8.7, 2.3 Hz, 1H), 7.13 (d, J = 8.7 Hz, 1H), 5.93 (s, 1H), 5.32 (d, J = 11.4 Hz, 1H), 3.98 (s, 3H), 2.34 (ddd, J = 15.4, 11.4, 2.0 Hz, 1H), 2.24 – 2.13 (m, 1H).

1-(3-amino-4-methoxyphenyl)-4,4,4-trifluoro-3-(trifluoromethyl)butane-1,3-diol (36). Starting material (**35**) (0.28 gr, 0.8 mmol) is dissolved in 10 ml of ethanol with water and acetic acid (7 ml, 1.5 ml, 1.5 ml) then metallic iron powder (0.43 gr, 7.7 mmol) is added. Reaction stirred at room temperature for 3 hrs then mixture filtere on a celite pad. Organic layer dried over sodium sulphate, filtered and solvent removed. Crude residue purified by silica gel column chromatography (petroleum ether/AcOEt 1:1) to afford the clean product (232 mg, 70%). ^{1}H NMR (300 MHz, Methanol-d4) δ 6.87 – 6.76 (m, 2H), 6.69 (dd, J = 8.2, 2.1 Hz, 1H), 5.03 (d, J = 11.0 Hz, 1H), 3.84 (s, 3H), 2.32 – 2.17 (m, 1H), 2.08 (dd, J = 15.3, 2.4 Hz, 1H).

4-fluoro-N-(2-methoxy-5-(4,4,4-trifluoro-1,3-dihydroxy-3-(trifluoromethyl)butyl)phenyl)benzamide (UPR1406).4-fluoro benzoic acid (0.1 gr, 0.7 mmol) is dissolved in thionyl chloride (2 ml) and DMF (0.05ml). Reaction stirred for 1.5 hrs then the excess of thionyl chloride is removed under reduced pressure.
In a separate flask starting material **36** (50 mg, 0.2mmol) is dissolved in pyridine then a solution of the previously prepared chloride (0.1 Mol in pyridine, 0.08ml, 0.08 mmol) is added. Mixture stirred 30 min then the reaction is diluted with toluene. Solvent removed under reduced pressure, crude residue dissolved in AcOEt and washed with NaHCO3 saturated solution and brine. Organic layer dried over sodium sulphate, filtered and solvent removed. Crude product purified by silica gel column chromatography (petroleum ether/ AcOEt 3:1) to afford **UPR1406** (30mg, 82%). ^{1}H NMR (400 MHz, DMSO-d6) δ 9.53 (s, 1H), 8.07 – 7.99 (m, 2H), 7.77 (d, J = 2.2 Hz, 1H), 7.40 – 7.31 (m, 2H), 7.20 (dd, J = 8.5, 2.2 Hz, 1H), 7.08 (d, J = 8.5 Hz, 1H), 5.00 (d, J = 9.9 Hz, 1H), 3.83 (s, 3H), 2.23 (dd, J = 15.2, 10.1 Hz, 1H), 2.15 – 2.07 (m, 1H). HPLC-MS (ESI): m/z calcd for $C_{19}H_{16}F_7NO_4$ [$(M+H)^-$]: 454.09; found: 454.23.

1-(3-amino-4-methoxyphenyl)ethan-1-one (37). 1-(4-methoxy-3-nitrophenyl)ethan-1-one (**33**) (2.07 gr, 10.6 mmol) is dissolved in 35 ml of ethanol and acetic acid (7 ml) then

metallic iron powder (5.91 gr,106.0 mmol) is added. Reaction stirred at room temperature for 3 hrs then mixture filtered on a celite pad. Organic layer dried over sodium sulphate, filtered and solvent removed. Crude residue purified by silica gel column chromatography (petroleum ether/AcOEt 4:1) to afford the clean product (1.08 gr, 62%). ^{1}H NMR (300 MHz, DMSO-d6) δ 7.25 – 7.19 (m, 2H), 6.92 – 6.83 (m, 1H), 4.93 (s, 2H), 3.84 (s, 3H), 2.44 (s, 3H).

N-(5-acetyl-2-methoxyphenyl)-4-fluorobenzamide (38). 4-fluoro benzoic acid (1.67 gr, 9.8 mmol) and pivaloyl chloride (1.0 ml, 8.5 mmol) were dissolved in THF and placed at 0°C then DiPEA (3.4 ml, 19.52 mmol) was added and the reaction stirred 30min. A solution of starting material (**37**) (1.08 gr, 6.51 mmol) in anhydrous THF is added dropwise at 0°C. Mixture stirred overnight (18 hrs). Reaction quenched with water and extracted with AcOEt. Organic layer washed with NaHCO3 and brine, dried over sodium sulphate and filtered. Solvent removed, the crude residue is purified by a silica gel column chromatography (petroleum ether/AcOEt 4:1) to affor the clean compound (1.23 gr, 66%). ^{1}H NMR (300 MHz, Chloroform-d) δ 9.16 (d, J = 2.2 Hz, 1H), 8.46 (s, 1H), 7.98 – 7.87 (m, 2H), 7.82 (dd, J = 8.6, 2.2 Hz, 1H), 7.20 (t, J = 8.6 Hz, 2H), 7.00 (d, J = 8.7 Hz, 1H), 4.02 (s, 3H), 2.63 (s, 3H).

N-(5-acetyl-2-methoxyphenyl)-4-fluoro-N-methylbenzamide (39). Starting material (**38**) (0.58 gr, 2.0 mmol)was dissolved in anhydrous THF at 0°C then sodium hydride (60 mg, 2.4 mmol) and imidazole (15 mg, 0.2 mmol) were added. Reaction is stirred at 0°C under nitrogen 20 min then methyl iodide (0.4 ml, 6.06 mmol) is added dropwise. Reaction stirred 2.5 hrs the is quenched with few drops of glacial acetic acid. Mixture diluted in AcOEt and washed with brine, organic layer ollected and solvent removed under reduced pressure. Crude residue purified by a silica gel column chromatography (petroleum ether/AcOEt 3:1) to afford the desired compound (0.58 gr, 95%). ^{1}H NMR (300 MHz, Chloroform-d) δ 7.80 (dd, J = 8.6, 2.2 Hz, 1H), 7.72 (d, J = 2.2 Hz, 1H), 7.30 (t, J = 7.1 Hz, 2H), 6.82 (dt, J = 8.6, 4.3 Hz, 3H), 3.78 (s, 3H), 3.36 (s, 3H), 2.49 (s, 3H).

4-fluoro-N-(2-methoxy-5-(4,4,4-trifluoro-3-hydroxy-3-(trifluoromethyl) butanoyl) phenyl)-N-methyl benzamide (40). Starting material (**39**) (0.58 gr, 1.9 mmol) placed at -78°C in anhydrous THF under nitrogen atmosphere then LiHMDS (3.0 ml, 3.0 mmol) is added dropwise and stirred for 30min. In a separate two neck flask concentrated H2SO4 (10 ml) is warmed to 50 °C and linked through a cannula with the enolate flask then a trihydrate hexafluoroacetone (0.55 ml, 3.84 mmol) is dropped inside the H2SO4 and the formed gaseous HFA is cannulated inside the enolate solution. The mixture is stirred 1 hr the reaction is quenched with glacial acetic acid (few drops).). Mixture diluted with AcOEt and washed with water and brine. Organic layer collected and dried over sodium

sulphate, filtered and solvent removed. Crude product purified with gel silica column chromatography (petroleum ether/AcOEt 1:1) to afford the desired product (0.76 gr, 85%). ^{1}H NMR (300 MHz, Chloroform-d) δ 7.82 (dd, J = 8.7, 2.3 Hz, 1H), 7.70 (d, J = 2.3 Hz, 1H), 7.34 – 7.28 (m, 2H), 7.01 (s, 2H), 6.94 – 6.78 (m, 3H), 3.85 (s, 3H), 3.37 (s, 3H).

4-fluoro-N-(2-methoxy-5-(4,4,4-trifluoro-1,3-dihydroxy-3-(trifluoromethyl) butyl) phenyl)-N-methyl benzamide (UPR1401). Starting material (**40**) (0.35 gr, 0.76 mmol) is dissolved in methanol (10 ml) at 0°C then sodium boron hydride (90 mg, 2.3 mmol) was added. Reaction stirred 20 min then is quenched with sodium bicarbonate overnight. Mixture diluted with water and extracted with AcOEt, organic layer dried over sodium sulphate, filtered and solvent removed. Crude residue purified with gel silica column chromatography (petroleum ether/AcOEt 3:1) to afford **UPR1401** (320 mg, 90%). ^{1}H NMR (300 MHz, Chloroform-d) δ 7.14 (d, J = 8.5 Hz, 2H), 6.93 (s, 1H), 6.82 (d, J = 8.3 Hz, 3H), 6.12 (s, 1H), 5.08 (d, J = 11.1 Hz, 1H), 3.80 (s, 3H), 3.33 (s, 3H), 2.32 – 1.99 (m, 0H), 1.89 (s, 1H). HPLC-MS (ESI): m/z calcd for $C_{20}H_{18}F_7NO_4$ [$(M+H)^-$]: 468.10; found: 468.17.

5-(chloromethyl)-6-methoxy-3,4-dihydronaphthalen-1(2H)-one (41). 6-methoxy-3,4-dihydronaphthalen-1(2H)-one (1.50 gr, 8.5 mmol) and formaldehyde (0.34 gr, 11.01 mmol) were dissolved in 8 ml of HCl 37%. Mixture stirred at room temperature for 2 hrs the reaction diluted with water and washed with DCM. Organic collected and dried over sodium sulphate, filtered and solvent removed. Crude residue purified by a silica gel column chromatography (petroleum ether/AcOEt 7:3) to give the clean product as a white solid (0.6 gr, 31%). ^{1}H NMR (300 MHz, Chloroform-d) δ 8.06 (d, J = 8.9 Hz, 1H), 6.88 – 6.73 (m, 1H), 4.70 (s, 2H), 3.89 (s, 3H), 2.99 (t, J = 6.1 Hz, 2H), 2.57 (t, J = 6.5 Hz, 2H), 2.10 (h, J = 6.5 Hz, 2H).

5-((4-fluorophenoxy)methyl)-6-methoxy-3,4-dihydronaphthalen-1(2H)-one (42). Starting material (**41**) (0.6 gr, 2.7 mmol), 4-fluoro phenol (0.43 gr, 3.5 mmol) and potassium carbonate (0.9 gr, 7 mmol) were dissolved in 30 ml of degassed DMF. Reaction stirred overnight (18 hrs) the mixture diluted with AcOEt and washed water and brine. Organic layer collected and dried over sodium sulphate, filtered and solvent removed. Crude residue purified by a silica gel column chromatography (petroleum ether/Et2O 10:3) to give the clean product as a white solid (0.3 gr, 37%). ^{1}H NMR (300 MHz, Chloroform-d) δ 8.15 (d, J = 8.8 Hz, 1H), 7.06 – 6.87 (m, 5H), 5.11 (s, 2H), 3.91 (s, 3H), 3.01 (t, J = 6.1 Hz, 2H), 2.61 (dd, J = 7.4, 5.7 Hz, 2H), 2.12 (p, J = 6.4 Hz, 2H).

5-((4-fluorophenoxy)methyl)-2-(1,1,1,3,3,3-hexafluoro-2-hydroxypropan-2-yl)-6-methoxy-3,4-dihydro naphthalen-1(2H)-one (43). Starting material (**42**) (0.15 gr, 0.5 mmol) placed at -60°C in anhydrous THF under nitrogen atmosphere then LiHMDS (2.0

ml, 2.0 mmol) is added dropwise and stirred for 30min. In a separate two neck flask concentrated H2SO4 (10 ml) is warmed to 50 °C and linked through a cannula with the enolate flask then a trihydrate hexafluoroacetone (0.4 ml, 3 mmol) is dropped inside the H2SO4 and the formed gaseous HFA is cannulated inside the enolate solution. The mixture is stirred 3 hrs, and then the reaction is quenched with glacial acetic acid (few drops). Mixture diluted with ACOEt and washed with water and brine. Organic layer collected and dried over sodium sulphate, filtered and solvent removed under reduced pressure. Crude product purified with gel silica column chromatography (petroleum ether/Et2O 10:2) to afford **43** as a white solid (150 mg, 43%). ^{1}H NMR (300 MHz, Chloroform-d) δ 8.19 (d, J = 8.9 Hz, 1H), 7.08 – 6.89 (m, 5H), 5.19 (d, J = 10.5 Hz, 1H), 5.06 (d, J = 10.5 Hz, 1H), 3.97 (s, 3H), 3.29 (dt, J = 17.1, 3.6 Hz, 1H), 3.20 – 3.08 (m, 1H), 2.92 (ddd, J = 17.2, 13.2, 4.0 Hz, 1H), 2.54 (dd, J = 13.5, 3.9 Hz, 1H), 2.27 – 2.08 (m, 1H). HPLC-MS (ESI): m/z calcd for $C_{21}H_{17}F_7O_4$ [(M+H)$^-$]: 465.09; found: 465.12.

5-((4-fluorophenoxy) methyl)-2-(1,1,1,3,3,3-hexafluoro-2-hydroxypropan-2-yl)-6-methoxy-1,2,3,4-tetrahydro naphthalen-1-ol (UPR1416). 43 (0.1 gr, 0.2 mmol) is placed in methanol at 0°C, then sodium boron hydride (40mg, 0.9 mmol) is added. Mixture stirred 30 min, and then the reaction is quenched with NaHCO3. Mixture diluted with diethyl ether and washed with water and brine. Organic layer collected and dried over sodium sulphate, filtered and solvent removed. Crude residue purified by a silica gel column chromatography (petroleum ether/Et2O 10:3) to afford **UPR1416** as a white solid (50 mg, 53%). ^{1}H NMR (300 MHz, Chloroform-d) δ 7.34 – 7.25 (m, 1H), 7.12 – 6.81 (m, 5H), 6.20 (s, 1H), 5.09 (s, 2H), 3.88 (s, 3H), 3.20 (dt, J = 17.9, 4.4 Hz, 1H), 2.87 (ddd, J = 18.1, 11.1, 7.3 Hz, 1H), 2.40 (dd, J = 19.2, 6.9 Hz, 2H), 2.32 – 2.13 (m, J = 5.7 Hz, 2H). HPLC-MS (ESI): m/z calcd for $C_{21}H_{19}F_7O_4$ [(M+H)$^-$]: 467.09; found: 467.14.

6-((4-chlorobenzyl)oxy)-3,4-dihydronaphthalen-1(2H)-one (44). 6-hydroxy-3,4-dihydronaphthalen-1(2H)-one (1.0 gr, 6.2 mmol), 4-chloro benzyl bromide (1.0 gr, 5.0 mmol) and potassium carbonate (1.8 gr, 12.5 mmol) were dissolved in 20 ml of degassed DMF. Reaction stirred at room temperature overnight (18 hrs) then the mixture is diluted with DCM and washed with water and brine. Organic layer collected and dried over sodium sulphate, filtered and solvent removed. Crude residue purified by a silica gel column chromatography (petroleum ether/Et2O 10:4) to afford the product as a yellowish solid (1.1 gr, 77%). ^{1}H NMR (300 MHz, Chloroform-d) δ 8.01 (d, J = 8.7 Hz, 1H), 7.36 (s, 4H), 6.88 (dd, J = 8.7, 2.5 Hz, 1H), 6.76 (d, J = 2.5 Hz, 1H), 5.08 (s, 2H), 2.92 (t, J = 6.1 Hz, 2H), 2.61 (dd, J = 7.2, 5.8 Hz, 2H), 2.12 (td, J = 12.5, 11.6, 5.3 Hz, 2H).

6-((4-chlorobenzyl)oxy)-2-(1,1,1,3,3,3-hexafluoro-2-hydroxypropan-2-yl)-3,4-dihydronaphthalen-1(2H)-one (45). 6-((4-chlorobenzyl)oxy)-3,4-dihydronaphthalen-

1(2H)-one (**44**) (1.0 gr, 3.5 mmol) placed at -60°C in anhydrous THF under nitrogen atmosphere then LiHMDS (7.0 ml, 7.0 mmol) is added dropwise and stirred for 30min. In a separate two neck flask concentrated H2SO4 (10 ml) is warmed to 50 °C and linked through a cannula with the enolate flask then a trihydrate hexafluoroacetone (1.5 ml, 11.5 mmol) is dropped inside the H2SO4 and the formed gaseous HFA is cannulated inside the enolate solution. The mixture is stirred 3 hrs, and then the reaction is quenched with glacial acetic acid (few drops). Mixture diluted with ACOEt and washed with water and brine. Organic layer collected and dried over sodium sulphate, filtered and solvent removed under reduced pressure. Crude product purified with gel silica column chromatography (petroleum ether/Et2O 10:2) to afford **45** as a white solid (0.50 gr, 32%). ^{1}H NMR (300 MHz, Chloroform-d) δ 8.65 (d, J = 1.4 Hz, 1H), 8.04 (d, J = 8.9 Hz, 1H), 7.43 – 7.30 (m, 4H), 6.93 (dd, J = 8.8, 2.5 Hz, 1H), 6.77 (d, J = 2.5 Hz, 1H), 5.11 (s, 2H), 3.16 – 3.05 (m, 1H), 2.97 (dd, J = 7.2, 3.2 Hz, 2H), 2.48 (dd, J = 13.5, 3.9 Hz, 1H), 2.29 – 2.06 (m, 1H). HPLC-MS (ESI): m/z calcd for $C_{20}H_{15}ClF_6O_3$ [$(M+H)^-$]: 451.05; found: 451.09.

5-((4-fluorophenoxy)methyl)-2-(1,1,1,3,3,3-hexafluoro-2-hydroxypropan-2-yl)-6-methoxy-1,2,3,4-tetrahydronaphthalen-1-ol (UPR1419). 45 (0.4 gr, 0.9 mmol) is placed in methanol at 0°C, and then sodium boron hydride (120 mg, 3.0 mmol) is added. Mixture stirred 30 min, and then the reaction is quenched with NaHCO3. Mixture diluted with diethyl ether and washed with water and brine. Organic layer collected and dried over sodium sulphate, filtered and solvent removed. Crude residue purified by a silica gel column chromatography (petroleum ether/Et2O 10:2) to afford **UPR1419** as a white solid (150 mg, 36%). ^{1}H NMR (300 MHz, Chloroform-d) δ 7.35 (s, 4H), 7.19 (d, J = 8.5 Hz, 1H), 6.83 (dd, J = 8.5, 2.6 Hz, 1H), 6.74 (d, J = 2.6 Hz, 1H), 6.13 (s, 1H), 5.24 (d, J = 3.0 Hz, 1H), 5.03 (s, 2H), 2.98 (dt, J = 17.4, 4.1 Hz, 1H), 2.84 (dt, J = 17.5, 9.0 Hz, 1H), 2.41 (t, J = 7.8 Hz, 1H), 2.23 (dd, J = 9.4, 4.4 Hz, 2H), 2.06 (d, J = 4.6 Hz, 1H). HPLC-MS (ESI): m/z calcd for $C_{20}H_{17}ClF_6O_3$ [$(M+H)^-$]: 453.07; found: 453.16.

6-bromonaphthalen-2-ol (46). 2-naphthol (6.0 gr, 41.7 mmol) was dissolved in 15ml of glacial acetic acid, then bromine (4.3 ml, 83.1 mmol) diluted with 5 ml of glacial acetic acid was added dropwise over 30 min. The mixture is heated to 130°C then metallic tin (13.0 gr, 110.2 mmol) was added. Reaction stirred overnight (20 hrs) then is filtered and cooled to room temperature. Mixture diluted with DCM and washed HCl 1M and brine. Organic layer collected and dried over sodium sulphate, filtered and solvent removed. Crude residue purified with gel silica column chromatography (toluene/hexane 10:2) to afford the clean product as a white solid (4.5 gr, 48%). ^{1}H NMR (300 MHz, DMSO-d6) δ 8.03 (d, J = 2.7 Hz, 1H), 7.80 – 7.71 (m, 1H), 7.66 (d, J = 8.8 Hz, 1H), 7.48 (dd, J = 8.8, 1.9 Hz, 1H), 7.16 – 7.03 (m, 2H).

((6-bromonaphthalen-2-yl)oxy)(tert-butyl)dimethylsilane (47). 6-bromoaphthol (**46**) (1 gr, 4.5 mmol) and TBDMSiCl (0.80 gr, 5.5 mmol) were placed in degassed DMF at 0°C then triethyl amine (1.0 ml, 6.5 mmol) was added. Reaction stirred 24 hrs then is diluted with AcOEt and washed with water and brine. Organic layer collected and dried over sodium sulphate, filtered and solvent removed. Crude residue purified by a silica gel column chromatography (petroleum ether) to afford the clean product as a white solid (1.0 gr, 66%). ^{1}H NMR (300 MHz, Chloroform-d) δ 7.96 – 7.86 (m, 1H), 7.68 – 7.43 (m, 3H), 7.19 – 7.04 (m, 2H), 1.02 (s, 9H), 0.25 (s, 6H).

1-(4-(6-((tert-butyldimethylsilyl)oxy) naphthalen-2-yl) phenyl) ethan-1-one (48). ((6-bromonaphthalen-2-yl)oxy) (tert-butyl) dimethylsilane (**47**) (0.40 gr, 1.2 mmol), 1-(4-(4,4,5,5-tetramethyl-1,3,2-dioxaborolan-2-yl) phenyl) ethan-1-one (0.35 gr, 1.4 mmol), potassium carbonate (0.65 gr, 5.0 mmol) and bis(triphenylposphine) palladium dichloride (0.5% mol) were dissolved in 20ml of 1,4-dioxane and 3 ml of water. The mixture is heated to 100°C and the reaction is stirred at reflux under nitrogen atmosphere for 5 hrs, and then is cooled to room temperature. The mixture is diluted with AcOEt and washed with NaHCO3 saturated water solution and brine. Organic layer collected and dried over sodium sulphate, filtered and solvent removed under reduced pressure. Crude residue purified by a silica gel column chromatography (toluene/hexane 10:3) to give the desired product as a white solid (300 mg, 66%). ^{1}H NMR (300 MHz, Chloroform-d) δ 8.15 – 7.97 (m, 3H), 7.80 (dd, J = 8.6, 3.2 Hz, 4H), 7.71 (dd, J = 8.6, 1.8 Hz, 1H), 7.24 – 7.08 (m, 2H), 2.66 (s, 3H), 1.03 (s, 9H), 0.27 (s, 6H).

1-(4-(6-((tert-butyldimethylsilyl) oxy) naphthalen-2-yl) phenyl)-4,4,4-trifluoro-3-hydroxy-3-(trifluoromethyl) butan-1-one (49). Methyl ketone starting material (**48**) (0.25 gr, 0.7 mmol) placed at -60°C in anhydrous THF under nitrogen atmosphere then LiHMDS (1.4 ml, 1.4 mmol) is added dropwise and stirred for 30min. In a separate two neck flask concentrated H2SO4 (10 ml) is warmed to 50 °C and linked through a cannula with the enolate flask then a trihydrate hexafluoroacetone (0.3 ml, 2.1 mmol) is dropped inside the H2SO4 and the formed gaseous HFA is cannulated inside the enolate solution. The mixture is stirred 3 hrs, and then the reaction is quenched with glacial acetic acid (few drops). Mixture diluted with AcOEt and washed with water and brine. Organic layer collected and dried over sodium sulphate, filtered and solvent removed under reduced pressure. Crude product purified by a silica gel column chromatography (hexane/toluene 10:5) to afford the clean product as a white solid (0.27 gr,71%). ^{1}H NMR (300 MHz, Chloroform-d) δ 8.11 – 8.02 (m, 3H), 7.91 – 7.77 (m, 4H), 7.71 (dd, J = 8.6, 1.8 Hz, 1H), 7.25 (d, J = 8.5 Hz, 1H), 7.21 – 7.10 (m, 2H), 3.50 (s, 2H), 1.04 (s, 9H), 0.28 (s, 6H).

1-(4-(6-((tert-butyldimethylsilyl) oxy) naphthalen-2-yl phenyl)-4,4,4-trifluoro-3-(trifluoromethyl) butane-1,3-diol (50). Ketone starting material (**49**) (0.25 gr, 0.42 mmol) is placed in methanol at 0°C, and then sodium boron hydride (50 mg, 1.3 mmol) is added. Mixture stirred 2 hrs, and then the reaction is quenched with NaHCO3. Mixture diluted with DCM and washed with water and brine. Organic layer collected and dried over sodium sulphate, filtered and solvent removed to afford the desired product as a white solid (240 mg, 96%). ^{1}H NMR (300 MHz, Chloroform-d) δ 7.95 (d, J = 1.9 Hz, 1H), 7.83 – 7.62 (m, 5H), 7.47 (d, J = 8.3 Hz, 2H), 7.22 (d, J = 2.3 Hz, 1H), 7.12 (dd, J = 8.8, 2.4 Hz, 1H), 6.26 (s, 1H), 5.41 – 5.31 (m, 1H), 2.44 (ddd, J = 15.5, 11.5, 2.1 Hz, 1H), 2.32 – 2.21 (m, 1H), 1.04 (s, 9H), 0.27 (s, 6H).

4,4,4-trifluoro-1-(4-(6-hydroxynaphthalen-2-yl)phenyl)-3-(trifluoromethyl)butane-1,3-diol (UPR1403). Starting material (**50**) (0.20gr, 0.33 mmol) and TBAF (0.14 gr, 0.40 mmol) were dissolved in THF and stirred at room temperature for 3 hrs. The mixture is then diluted with AcOEt and washed with HCl 1M and brine. Organic layer collected and dried over sodium sulphate, filtered and solvent removed. Crude product purified by a silica gel column chromatography (hexane/AcOEe 1:1) to afford **UPR1403** as a white solid (0.12 gr,85 %). ^{1}H NMR (300 MHz, DMSO-d6) δ 9.79 (d, J = 1.2 Hz, 1H), 8.08 (d, J = 1.8 Hz, 1H), 7.93 – 7.64 (m, 5H), 7.49 (d, J = 8.1 Hz, 2H), 7.17 – 7.06 (m, 2H), 6.42 (d, J = 3.9 Hz, 1H), 5.09 (d, J = 9.4 Hz, 1H), 2.38 – 2.24 (m, 1H), 2.19 (d, J = 15.1 Hz, 1H). HPLC-MS (ESI): m/z calcd for $C_{21}H_{16}F_6O_3$ [$(M+H)^-$]: 429.09; found: 429.25.

1-(3-(6-((tert-butyldimethylsilyl) oxy) naphthalen-2-yl) phenyl) ethan-1-one (51). ((6-bromonaphthalen-2-yl)oxy)(tert-butyl)dimethylsilane (**47**) (0.50 gr, 1.5 mmol), 3-acetylphenyl boronic acid (0.30 gr, 1.8 mmol), potassium carbonate (0.88 gr, 6.3 mmol) and bis(triphenylposphine) palladium dichloride (0.5% mol) were dissolved in 20ml of 1,4-dioxane and 3 ml of water. The mixture is heated to 100°C and the reaction is stirred at reflux under nitrogen atmosphere for 5 hrs, and then is cooled to room temperature. The mixture is diluted with AcOEt and washed with NaHCO3 saturated water solution and brine. Organic layer collected and dried over sodium sulphate, filtered and solvent removed under reduced pressure. Crude residue purified by a silica gel column chromatography (toluene/hexane 10:5) to give the desired product as a white solid (350 mg, 62%). ^{1}H NMR (400 MHz, Chloroform-d) δ 8.29 (t, J = 1.8 Hz, 1H), 8.03 – 7.99 (m, 1H), 7.92 (dddd, J = 17.9, 7.8, 2.3, 1.2 Hz, 2H), 7.80 (dd, J = 8.7, 3.5 Hz, 2H), 7.71 (dd, J = 8.6, 1.9 Hz, 1H), 7.57 (t, J = 7.7 Hz, 1H), 7.23 (d, J = 2.4 Hz, 1H), 7.13 (dd, J = 8.8, 2.4 Hz, 1H), 2.69 (s, 3H), 1.04 (s, 9H), 0.27 (s, 6H).

1-(3-(6-((tert-butyldimethylsilyl) oxy) naphthalen-2-yl) phenyl)-4,4,4-trifluoro-3-hydroxy-3-(trifluoromethyl) butan-1-one (52). Methyl ketone starting material (**51**) (0.35

gr, 0.9 mmol) placed at -60°C in anhydrous THF under nitrogen atmosphere then LiHMDS (3.3 ml, 3.3 mmol) is added dropwise and stirred for 30min. In a separate two neck flask concentrated H2SO4 (10 ml) is warmed to 50 °C and linked through a cannula with the enolate flask then a trihydrate hexafluoroacetone (0.8 ml, 5.5 mmol) is dropped inside the H2SO4 and the formed gaseous HFA is cannulated inside the enolate solution. The mixture is stirred 3 hrs, and then the reaction is quenched with glacial acetic acid (few drops). Mixture diluted with AcOEt and washed with water and brine. Organic layer collected and dried over sodium sulphate, filtered and solvent removed under reduced pressure. Crude product purified by a silica gel column chromatography (hexane/Et2O 10:5) to afford the clean product as a white solid (0.15 gr,30%). ^{1}H NMR (300 MHz, Chloroform-d) δ 8.27 (t, J = 1.9 Hz, 1H), 8.06 – 7.89 (m, 3H), 7.83 (d, J = 8.7 Hz, 2H), 7.74 – 7.56 (m, 2H), 7.24 – 7.12 (m, 2H), 3.55 (s, 2H), 1.06 (s, 9H), 0.30 (s, 6H).

1-(3-(6-((tert-butyldimethylsilyl) oxy) naphthalen-2-yl) phenyl)-4,4,4-trifluoro-3-(trifluoromethyl) butane-1,3-diol (53). Ketone starting material (**52**) (80 mg, 0.15 mmol) is placed in methanol at 0°C, and then sodium boron hydride (30 mg, 0.7 mmol) is added. Mixture stirred 2 hrs, and then the reaction is quenched with NaHCO3. Mixture diluted with DCM and washed with water and brine. Organic layer collected and dried over sodium sulphate, filtered and solvent removed to afford the desired product as a white solid (70 mg, 86%). ^{1}H NMR (400 MHz, Chloroform-d) δ 7.97 – 7.92 (m, 1H), 7.79 (dd, J = 8.7, 4.5 Hz, 2H), 7.71 – 7.62 (m, 3H), 7.50 (t, J = 7.7 Hz, 1H), 7.35 (dt, J = 7.6, 1.5 Hz, 1H), 7.23 (d, J = 2.4 Hz, 1H), 7.12 (dd, J = 8.8, 2.4 Hz, 1H), 6.39 – 6.35 (m, 1H), 3.03 (s, 1H), 2.45 (dddd, J = 13.7, 11.5, 4.1, 2.0 Hz, 1H), 2.32 – 2.22 (m, 1H), 1.05 (s, 9H), 0.28 (s, 6H).

4,4,4-trifluoro-1-(3-(6-hydroxynaphthalen-2-yl) phenyl)-3-(trifluoromethyl) butane-1,3-diol (UPR1417). Starting material (**53**) (65 mg, 0.12 mmol) and TBAF (50 mg, 0.2 mmol) were dissolved in THF and stirred at room temperature for 3 hrs. The mixture is then diluted with AcOEt and washed with HCl 1M and brine. Organic layer collected and dried over sodium sulphate, filtered and solvent removed. Crude product purified by a silica gel column chromatography (toluene/Et2O 10:1) to afford **UPR1417** as a white solid (50 mg, 97%). ^{1}H NMR (300 MHz, Chloroform-d) δ 7.96 (d, J = 1.9 Hz, 1H), 7.79 (dd, J = 15.9, 8.7 Hz, 2H), 7.73 – 7.64 (m, 3H), 7.57 – 7.45 (m, 1H), 7.36 (dt, J = 7.7, 1.5 Hz, 1H), 7.21 – 7.09 (m, 2H), 6.28 (s, 1H), 5.39 (d, J = 11.4 Hz, 1H), 2.91 (s, 1H), 2.54 – 2.44 (m, 1H), 2.44 – 2.23 (m, 2H). HPLC-MS (ESI): m/z calcd for $C_{21}H_{16}F_6O_3$ [$(M+H)^-$]: 429.09; found: 429.16.

6-(4,4,5,5-tetramethyl-1,3,2-dioxaborolan-2-yl)naphthalen-2-ol (54). 6-bromonaphthalen-2-ol (**46**) (0.60 gr, 2.7 mmol), bis(pinacolato)diboron (0.77 gr, 3.0 mmol), Palladium(dppf)$_2$Cl$_2$ (110 mg, 0.1 mol) and potassium acetate (0.8 gr, 8.1 mmol) were dissolved in 1,4-dioxane and stirred at 90°C under nitrogen atmosphere. After 6 hrs

the mixture was cooled to room temperature and and diluted with AcOEt. Mixture washed with HCl 1M and brine. Solvent removed under reduced pressure and crude residue purified by a silica gel column chromatography (toluene/AcoEt 10:0.5) to give the clean product (400 mg, 55%). ^{1}H NMR (300 MHz, Chloroform-d) δ 8.29 (s, 1H), 7.79 (dd, J = 8.4, 1.4 Hz, 2H), 7.66 (d, J = 8.2 Hz, 1H), 7.16 – 7.04 (m, 2H), 1.38 (s, 12H).

Tert-butyl dimethyl((6-(4,4,5,5-tetramethyl-1,3,2-dioxaborolan-2-yl) naphthalen-2-yl) oxy) silane (55). 6-(4,4,5,5-tetramethyl-1,3,2-dioxaborolan-2-yl)naphthalen-2-ol (**54**) (0.29 gr, 1.1 mmol), TBDMSiCl (0.32 gr, 2.1 mmol) and imidazole (0.27 gr, 3.9 mmol) were dissolved in degassed DMF at 0°C. The mixture is allowed to warm to room temperature and it is stirred overnight (18 hrs). The reaction is diluted in DCM and washed with water and brine. Organic layer collected and dried over sodium sulphate, filtered and solvent removed to give the clean product as a white solid (350 mg, 83%). ^{1}H NMR (400 MHz, Chloroform-d) δ 8.29 (s, 1H), 7.81 – 7.73 (m, 2H), 7.67 (d, J = 8.2 Hz, 1H), 7.17 (d, J = 2.4 Hz, 1H), 7.06 (dd, J = 8.8, 2.4 Hz, 1H), 1.38 (s, 12H), 1.02 (s, 9H), 0.25 (s, 6H).

1-(4-bromo-3-(chloromethyl)phenyl)ethan-1-one (56). 4-bromoacetophenone (3.0 gr, 15.0 mmol) and aluminium trichloride (8.0 gr, 60.0 mmol) were placed in 30 ml of DCM at 0°C under nitrogen atmosphere then paraformaldehyde (0.7 gr, 24 mmol) was added. The mixture is heated to 45°C and stirred 24hrs. The reaction is quenched with cold water, organic layer washed with NaHCO3 and brine. Solvent removed under reduced pressure and crude residue purified by a silica gel column chromatography (hexane/AcoEt 10:1) to give the clean product (500 mg, 15%). ^{1}H NMR (400 MHz, Chloroform-d) δ 8.06 (d, J = 2.2 Hz, 1H), 7.80 – 7.67 (m, 2H), 4.74 (d, J = 1.8 Hz, 2H), 2.60 (d, J = 2.1 Hz, 3H).

1-(4-(6-((tert-butyldimethylsilyl) oxy) naphthalen-2-yl)-3-(chloromethyl) phenyl) ethan-1-one (57). Tert-butyl dimethyl((6-(4,4,5,5-tetramethyl-1,3,2-dioxaborolan-2-yl) naphthalen-2-yl) oxy) silane (**55**) (0.25 gr, 0.6 mmol), 1-(4-bromo-3-(chloromethyl)phenyl)ethan-1-one (**56**) (0.15 gr, 0.6 mmol), potassium carbonate (0.32 gr, 2.3 mmol) and bis(triphenylposphine) palladium dichloride (0.5% mol) were dissolved in 8ml of 1,4-dioxane and 0.5 ml of water. The mixture is heated to 90°C and the reaction is stirred at reflux under nitrogen atmosphere for 7 hrs, and then is cooled to room temperature and stirred overnight. The mixture is diluted with DCM and washed with NaHCO3 saturated water solution and brine. Organic layer collected and dried over sodium sulphate, filtered and solvent removed under reduced pressure. Crude residue purified by a silica gel column chromatography (hexane/ AcOEt 10:0.05) to give the desired product as a white solid (200 mg, 73%). ^{1}H NMR (400 MHz, Chloroform-d) δ 8.18 (d, J = 1.9 Hz, 1H), 7.98 (dd, J = 8.1, 1.8 Hz, 1H), 7.85 – 7.67 (m, 4H), 7.48 (dd, J = 7.4, 2.1 Hz, 2H), 7.15 (dd, J = 8.8, 2.4 Hz, 1H), 4.62 (s, 2H), 2.68 (s, 3H), 1.04 (s, 9H), 0.28 (s, 6H).

1-(4-(6-((tert-butyldimethylsilyl) oxy) naphthalen-2-yl)-3-((4-fluorophenoxy) methyl) phenyl) ethan-1-one (58). 1-(4-(6-((tert-butyldimethylsilyl) oxy) naphthalen-2-yl)-3-(chloromethyl) phenyl) ethan-1-one (**57**) (0.2 gr, 0.5 mmol), 4-fluorophenol (0.16 gr, 1.4 mmol) and potassium carbonate (0.49 gr, 3.5 mmol) were dissolved in DMF and stirred overnight at room temperature. The mixture is diluted with diethyl ether and washed with water and brine. Solvent removed under reduced pressure and crude residue purified by a silica gel column chromatography (toluene/Et2O 10:1) to give the clean product (60 mg, 25%). ^{1}H NMR (300 MHz, Chloroform-d) δ 8.24 (d, J = 1.8 Hz, 1H), 8.00 (d, J = 1.9 Hz, 1H), 7.80 – 7.64 (m, 3H), 7.53 (d, J = 8.0 Hz, 1H), 7.49 – 7.40 (m, 1H), 7.24 – 7.11 (m, 2H), 6.99 – 6.85 (m, 2H), 6.85 – 6.75 (m, 2H), 4.97 (s, 2H), 2.67 (s, 3H), 0.91 (s, 9H), 0.10 (s, 6H).

4,4,4-trifluoro-1-(3-((4-fluorophenoxy) methyl)-4-(6-hydroxynaphthalen-2-yl) phenyl)-3-hydroxy-3-(trifluoromethyl) butan-1-one (59). Methyl ketone starting material (**58**) (55 mg, 0.1 mmol) placed at -60°C in anhydrous THF under nitrogen atmosphere then LiHMDS (0.4 ml, 0.4 mmol) is added dropwise and stirred for 30min. In a separate two neck flask concentrated H2SO4 (10 ml) is warmed to 50 °C and linked through a cannula with the enolate flask then a trihydrate hexafluoroacetone (0.11 ml, 0.8 mmol) is dropped inside the H2SO4 and the formed gaseous HFA is cannulated inside the enolate solution. The mixture is stirred 3 hrs, and then the reaction is quenched with glacial acetic acid (few drops). TBAF (50 mg, 0.2 mmol) is added to the reaction and the mixture is stirred at room temperature for 3 hrs. Then the reaction is diluted with AcOEt and washed with water and brine. Organic layer collected and dried over sodium sulphate, filtered and solvent removed under reduced pressure. Crude product purified by a silica gel column chromatography (hexane/Et2O 10:5) to afford the clean product as a white solid (35 mg, 58%). ^{1}H NMR (300 MHz, Chloroform-d) δ 8.26 (d, J = 2.0 Hz, 1H), 8.02 (dd, J = 8.1, 2.0 Hz, 1H), 7.82 – 7.68 (m, 3H), 7.60 (d, J = 8.1 Hz, 1H), 7.45 (dd, J = 8.4, 1.8 Hz, 1H), 7.22 – 7.11 (m, 2H), 7.01 – 6.87 (m, 2H), 6.87 – 6.75 (m, 2H), 5.00 (s, 2H), 3.52 (s, 2H).

4,4,4-trifluoro-1-(3-((4-fluorophenoxy) methyl)-4-(6-hydroxynaphthalen-2-yl) phenyl)-3-(trifluoromethyl) butane-1,3-diol (UPR1430). Ketone starting material (**59**) (35 mg, 0.1 mmol) is placed in methanol at 0°C, and then sodium boron hydride (10 mg, 0.2 mmol) is added. Mixture stirred 1 hrs, and then the reaction is quenched with NaHCO3. Mixture diluted with AcOEt and washed with water and brine. Organic layer collected and dried over sodium sulphate, filtered and solvent removed. Crude product purified by a silica gel column chromatography (toluene/AcOEt 10:1) to afford **UPR1430** as a white solid (30 mg, 90%). ^{1}H NMR (400 MHz, Chloroform-d) δ 7.55 – 7.42 (m, 4H), 7.30 – 7.19 (m, 2H), 7.11 – 7.02 (m, 1H), 6.95 (ddd, J = 24.0, 9.1, 2.9 Hz, 2H), 6.72 (t, J = 8.6 Hz, 2H), 6.59 (dd, J = 9.1,

4.3 Hz, 2H), 6.13 (s, 1H), 5.16 (d, J = 11.4 Hz, 1H), 4.72 (s, 2H), 2.30 – 2.19 (m, 1H), 2.16 (s, 1H), 2.08 (d, J = 15.4 Hz, 1H).

Ethyl 4'-formyl-[1,1'-biphenyl]-4-carboxylate (60). Ethyl-4-iodo benzoate (1.0 gr, 3.6 mmol), 4-formylphenyl boronic acid (0.6 gr, 4.0 mmol), potassium carbonate (2.0 gr, 14.5 mmol) and bis(triphenylposphine) palladium dichloride (0.5% mol) were dissolved in 40ml of 1,4-dioxane and 5 ml of water. The mixture is heated to 100°C and the reaction is stirred at reflux under nitrogen atmosphere for 3 hrs, then is cooled to room temperature. The mixture is diluted with AcOEt and washed with water, HCl 1M and brine. Organic layer collected and dried over sodium sulphate, filtered and solvent removed under reduced pressure. Crude residue purified by a silica gel column chromatography (petroleum ether/AcOEt 10:1) to give the clean product as a white solid (0.8 gr, 87%). ^{1}H NMR (300 MHz, Chloroform-d) δ 10.08 (s, 1H), 8.20 – 8.11 (m, 2H), 8.03 – 7.94 (m, 2H), 7.83 – 7.75 (m, 2H), 7.75 – 7.66 (m, 2H), 4.42 (q, J = 7.1 Hz, 2H), 1.42 (t, J = 7.1 Hz, 3H).

Ethyl 4'-(1-hydroxyethyl)-[1,1'-biphenyl]-4-carboxylate (61). Ethyl 4'-formyl-[1,1'-biphenyl]-4-carboxylate (**60**) (0.8 gr, 3.2 mmol) was dissolved in 20 ml of anhydrous THF under nitrogen atmosphere and placed at 0°C. Then methyl magnesium bromide (1. 1 ml, 3.2 mmol) was added dropwise and the reaction was stirred for 1h. The mixture is diluted with AcOEt and washed with water, HCl 1M and brine. Organic layer collected and dried over sodium sulphate, filtered and solvent removed to give the desired product as a pale yellow powder (0.85 gr, 99%). ^{1}H NMR (300 MHz, Chloroform-d) δ 8.15 – 8.06 (m, 2H), 7.70 – 7.58 (m, 4H), 7.52 – 7.44 (m, 2H), 4.97 (q, J = 6.5 Hz, 1H), 4.40 (q, J = 7.1 Hz, 2H), 1.55 (d, J = 6.5 Hz, 3H), 1.42 (t, J = 7.1 Hz, 3H).

Ethyl 4'-acetyl-[1,1'-biphenyl]-4-carboxylate (62). Ethyl 4'-(1-hydroxyethyl)-[1,1'-biphenyl]-4-carboxylate (**61**) (0.85 gr, 3.2 mmol) was dissolved in 35 ml of toluene and placed at 0°C under nitrogen, then trimethyl aluminium (0.5 ml, 1.0 mmol) was added dropwise. The mixture is allowed to warm to room temperature then ciclohexanone (1.7 ml, 15.8 mmol) was added and the reaction was stirred at reflux at 130°C under nitrogen for 3 hrs. The reaction is quenched with NaHCO3 saturated water solution and extracted with AcOEt. Organic layer washed with HCl 1M and brine then it is dried over sodium sulphate, filtered and solvent removed. Crude residue purified by a silica gel column chromatography (petroleum ether/ AcOEt 10:3) to afford the clean product as a white solid (0.65 gr, 77%). ^{1}H NMR (300 MHz, Chloroform-d) δ 8.18 – 8.10 (m, 2H), 8.10 – 8.01 (m, 2H), 7.70 (dd, J = 9.0, 7.4 Hz, 4H), 4.41 (q, J = 7.1 Hz, 2H), 2.65 (s, 3H), 1.42 (t, J = 7.1 Hz, 3H).

Ethyl 4'-(4,4,4-trifluoro-3-hydroxy-3-(trifluoromethyl)butanoyl)-[1,1'-biphenyl]-4-carboxylate (63). Ketone starting material (**62**) (0.3 gr, 1.1 mmol) placed at -60°C in anhydrous THF under nitrogen atmosphere then LiHMDS (2.2 ml, 2.2 mmol) is added dropwise and stirred for 30min. In a separate two neck flask concentrated H2SO4 (10 ml) is warmed to 50 °C and linked through a cannula with the enolate flask then a trihydrate hexafluoroacetone (0.5 ml, 3.3 mmol) is dropped inside the H2SO4 and the formed gaseous HFA is cannulated inside the enolate solution. The mixture is stirred 3 hrs, and then the reaction is quenched with glacial acetic acid (few drops). Mixture diluted with ACOEt and washed with water and brine. Organic layer collected and dried over sodium sulphate, filtered and solvent removed under reduced pressure. Crude product purified with gel silica column chromatography (petroleum ether/AcOEt 10:1) to afford the clean product as a white solid (0.46 gr, 95%). ^{1}H NMR (300 MHz, Chloroform-d) δ 8.21 – 8.12 (m, 2H), 8.11 – 7.99 (m, 2H), 7.83 – 7.74 (m, 2H), 7.74 – 7.66 (m, 2H), 7.12 (s, 1H), 4.42 (q, J = 7.1 Hz, 2H), 3.50 (s, 2H), 1.43 (t, J = 7.1 Hz, 3H).

Ethyl 4'-(4,4,4-trifluoro-1,3-dihydroxy-3-(trifluoromethyl)butyl)-[1,1'-biphenyl]-4-carboxylate (UPR1400). The starting material (**63**) (0.45 gr, 1.1 mmol) is placed in methanol at 0°C, and then sodium boron hydride (110 mg, 3.0 mmol) is added. Mixture stirred 30 min, and then the reaction is quenched with NaHCO3. Mixture diluted with diethyl ether and washed with water and brine. Organic layer collected and dried over sodium sulphate, filtered and solvent removed. Crude residue purified by a silica gel column chromatography (petroleum ether/AcOEt 10:1) to afford **UPR1400** as a white solid (340 mg, 75%). ^{1}H NMR (300 MHz, Chloroform-d) δ 8.12 – 8.03 (m, 2H), 7.68 – 7.56 (m, 4H), 7.51 – 7.42 (m, 2H), 6.23 (d, J = 7.9 Hz, 1H), 5.36 (d, J = 11.4 Hz, 1H), 4.40 (q, J = 7.1 Hz, 2H), 2.44 – 2.34 (m, 1H), 2.29 – 2.14 (m, 1H), 1.42 (t, J = 7.1 Hz, 3H). HPLC-MS (ESI): m/z calcd for $C_{20}H_{18}F_6O_4$ [$(M+H)^-$]: 435.10; found: 435.28.

4'-(4,4,4-trifluoro-1,3-dihydroxy-3-(trifluoromethyl)butyl)-[1,1'-biphenyl]-4-carboxylic acid (UPR1402). Starting material **UPR1400** (0.3 gr, 0.7 mmol) is dissolved in 5 ml of THF then a solution of NaOH (90 mg, 2.1 mmol) in 50 ml of water is added. The reaction is stirred at room temperature overnight. Mixture diluted with HCl 1M and washed with AcOEt. Organic layer collected and and dried over sodium sulphate, filtered and solvent removed. Crude residue purified by a silica gel column chromatography (DCM + 1%AcOH) to give the clean **UPR1402** as a white solid (200 mg, 70%). ^{1}H NMR (300 MHz, DMSO-d6) δ 12.94 (s, 1H), 8.02 (d, J = 8.3 Hz, 2H), 7.83 – 7.69 (m, 4H), 7.51 (d, J = 8.1 Hz, 2H), 6.41 (d, J = 5.1 Hz, 1H), 5.09 (d, J = 9.3 Hz, 1H), 2.37 – 2.10 (m, 2H). HPLC-MS (ESI): m/z calcd for $C_{18}H_{14}F_6O_4$ [$(M+H)^-$]: 407.07; found: 407.37.

4,4,4-trifluoro-1-(4'-(hydroxymethyl)-[1,1'-biphenyl]-4-yl)-3-(trifluoromethyl)butane-1,3-diol (UPR1407). Ketone starting material (**63**) (0.45 gr, 1.1 mmol) was placed in 15 ml of THF at 0°Cunder nitrogen atmosphere then lithium aluminium hydride (2.1 ml, 2.1 mmol) was added dropwise. The mixture is diluted with NaHCO3 saturated water solution after 1 h. The product is extracted with AcOEt and the organic layer is washed eith brine then it is dried over sodium sulphate, filtered and solvent removed under reduced pressure. Crude residue purified by silica gel column chromatography (petroleum ether/ AcOEt 10:1) to afford **UPR1407** as a white solid (0.25gr , 58%). ^{1}H NMR (400 MHz, Chloroform-d) δ 7.65 – 7.54 (m, 4H), 7.44 (d, J = 7.8 Hz, 4H), 6.19 (s, 1H), 5.35 (d, J = 11.5 Hz, 1H), 4.75 (s, 2H), 2.48 – 2.37 (m, 1H), 2.25 (d, J = 15.5 Hz, 1H). HPLC-MS (ESI): m/z calcd for $C_{18}H_{16}F_6O_3$ [(M+H)$^-$]: 393.09; found: 393.41.

Ethyl 3'-acetyl-[1,1'-biphenyl]-4-carboxylate (64). Ethyl-4-iodo benzoate (0.5 gr, 1.8 mmol), 3-acetylphenyl boronic acid (0.32gr, 2.0 mmol), potassium carbonate (1.0 gr, 7.2 mmol) and bis(triphenylposphine) palladium dichloride (0.5% mol) were dissolved in 25ml of 1,4-dioxane and 5 ml of water. The mixture is heated to 100°C and the reaction is stirred at reflux under nitrogen atmosphere for 3.5 hrs, then is cooled to room temperature. The mixture is diluted with AcOEt and washed with water, HCl 1M and brine. Organic layer collected and dried over sodium sulphate, filtered and solvent removed under reduced pressure. Crude residue purified by a silica gel column chromatography (petroleum ether/AcOEt 10:1) to give the clean product as a white solid (0.4 gr, 83%). ^{1}H NMR (400 MHz, Chloroform-d) δ 8.21 (t, J = 1.8 Hz, 1H), 8.17 – 8.11 (m, 2H), 7.98 (dt, J = 7.8, 1.4 Hz, 1H), 7.82 (ddd, J = 7.7, 1.9, 1.1 Hz, 1H), 7.72 – 7.66 (m, 2H), 7.58 (t, J = 7.7 Hz, 1H), 4.42 (q, J = 7.1 Hz, 2H), 2.67 (s, 3H), 1.43 (t, J = 7.1 Hz, 3H).

Ethyl 3'-(4,4,4-trifluoro-3-hydroxy-3-(trifluoromethyl) butanoyl)-[1,1'-biphenyl]-4-carboxylate (65). Ketone starting material (**64**) (0.38 gr, 1.4 mmol) placed at -60°C in anhydrous THF under nitrogen atmosphere then LiHMDS (3.0 ml, 3.0 mmol) is added dropwise and stirred for 30min. In a separate two neck flask concentrated H2SO4 (10 ml) is warmed to 50 °C and linked through a cannula with the enolate flask then a trihydrate hexafluoroacetone (0.6 ml, 4.5 mmol) is dropped inside the H2SO4 and the formed gaseous HFA is cannulated inside the enolate solution. The mixture is stirred 3 hrs, and then the reaction is quenched with glacial acetic acid (few drops). Mixture diluted with ACOEt and washed with water and brine. Organic layer collected and dried over sodium sulphate, filtered and solvent removed under reduced pressure. Crude product purified with gel silica column chromatography (petroleum ether/AcOEt 10:1) to afford the clean product as a white solid (0.35 gr, 58%). ^{1}H NMR (300 MHz, Chloroform-d) δ 8.22 – 8.12 (m, 3H), 7.95 (tdd, J = 7.8, 2.3, 1.2 Hz, 2H), 7.72 – 7.56 (m, 3H), 7.04 (s, 1H), 4.42 (q, J = 7.1 Hz, 2H), 3.52 (s, 2H), 1.43 (t, J = 7.1 Hz, 3H).

Ethyl 3'-(4,4,4-trifluoro-1,3-dihydroxy-3-(trifluoromethyl) butyl)-[1,1'-biphenyl]-4-carboxylate (UPR1412). The starting material (**65**) (0.17 gr, 0.4 mmol) is placed in methanol at 0°C, and then sodium boron hydride (40 mg, 1.0 mmol) is added. Mixture stirred 30 min, and then the reaction is quenched with NaHCO3. Mixture diluted with diethyl ether and washed with water and brine. Organic layer collected and dried over sodium sulphate, filtered and solvent removed. Crude residue purified by a silica gel column chromatography (petroleum ether/AcOEt 10:2) to afford **UPR1412** as a white solid (160 mg, 99%). ^{1}H NMR (300 MHz, Chloroform-d) δ 8.14 – 8.06 (m, 2H), 7.68 – 7.56 (m, 4H), 7.51 (dd, J = 8.8, 7.1 Hz, 1H), 7.40 (dt, J = 7.7, 1.6 Hz, 1H), 6.20 (s, 1H), 5.39 (d, J = 11.4 Hz, 1H), 4.40 (q, J = 7.1 Hz, 2H), 2.91 (s, 1H), 2.43 (ddd, J = 15.6, 11.5, 2.1 Hz, 1H), 2.26 (d, J = 15.4 Hz, 1H), 1.41 (t, J = 7.1 Hz, 3H). HPLC-MS (ESI): m/z calcd for $C_{20}H_{18}F_6O_4$ [(M+H)$^-$]: 435.10; found: 435.11.

3'-(4,4,4-trifluoro-1,3-dihydroxy-3-(trifluoromethyl)butyl)-[1,1'-biphenyl]-4-carboxylic acid (UPR1413). Starting material **UPR1412** (0.1 gr, 0.2 mmol) is dissolved in 3 ml of THF then a solution of NaOH (70 mg, 1.7 mmol) in 20 ml of water is added. The reaction is stirred at room temperature overnight. Mixture diluted with HCl 1M and washed with AcOEt. Organic layer collected and and dried over sodium sulphate, filtered and solvent removed. Crude residue purified by a silica gel column chromatography (DCM + 1%AcOH) to give the clean **UPR1413** as a white solid (60 mg, 73%). ^{1}H NMR (400 MHz, Methanol-d4) δ 8.14 – 8.08 (m, 2H), 7.78 – 7.72 (m, 2H), 7.69 (d, J = 1.9 Hz, 1H), 7.64 (dt, J = 7.6, 1.5 Hz, 1H), 7.50 (t, J = 7.7 Hz, 1H), 7.42 (dt, J = 7.7, 1.5 Hz, 1H), 5.30 – 5.23 (m, 1H), 2.39 – 2.19 (m, 2H). HPLC-MS (ESI): m/z calcd for $C_{18}H_{14}F_6O_4$ [(M+H)$^-$]: 407.07; found: 407.07.

4,4,4-trifluoro-1-(4'-(hydroxymethyl)-[1,1'-biphenyl]-3-yl)-3-(trifluoromethyl)butane-1,3-diol (UPR1414). Ketone starting material (**65**) (0.17 gr, 0.4 mmol) was placed in 15 ml of THF at 0°Cunder nitrogen atmosphere then lithium aluminium hydride (0.8 ml, 0.8 mmol) was added dropwise. The mixture is diluted with NaHCO3 saturated water solution after 1 h. The product is extracted with AcOEt and the organic layer is washed eith brine then it is dried over sodium sulphate, filtered and solvent removed under reduced pressure. Crude residue purified by silica gel column chromatography (toluene/Et2O 10:3) to afford **UPR1414** as a white solid (0.1 gr , 70%). ^{1}H NMR (300 MHz, Methanol-d4) δ 7.65 – 7.52 (m, 4H), 7.45 (t, J = 7.6 Hz, 3H), 7.35 (dt, J = 7.7, 1.5 Hz, 1H), 5.29 – 5.20 (m, 1H), 4.65 (s, 2H), 2.33 (ddd, J = 15.1, 10.6, 1.9 Hz, 1H), 2.22 (dd, J = 15.3, 2.8 Hz, 1H). HPLC-MS (ESI): m/z calcd for $C_{18}H_{16}F_6O_3$ [(M+H)$^-$]: 393.09; found: 393.12.

Ethyl 4'-acetyl-3-methoxy-[1,1'-biphenyl]-4-carboxylate (67). Ethyl 4-iodo-2-methoxy benzoate (**66**) (0.35 gr, 1.15 mmol), 4-acetylphenyl boronic acid (0.23 gr, 1.4 mmol),

potassium carbonate (0.64 gr, 4.5 mmol) and bis(triphenylposphine) palladium dichloride (0.5% mol) were dissolved in 10ml of 1,4-dioxane and 1.5 ml of water. The mixture is heated to 100°C and the reaction is stirred at reflux under nitrogen atmosphere for 5 hrs, and then is cooled to room temperature. The mixture is diluted with AcOEt and washed with HCl 1M and brine. Organic layer collected and dried over sodium sulphate, filtered and solvent removed under reduced pressure. Crude residue purified by a silica gel column chromatography (petroleum ether/AcOEt 10:4) to give the desired product as a white solid (150 mg, 43%). ^{1}H NMR (400 MHz, Chloroform-d) δ 8.09 – 8.01 (m, 2H), 7.89 (d, J = 8.0 Hz, 1H), 7.75 – 7.65 (m, 2H), 7.26 – 7.15 (m, 2H), 4.38 (q, J = 7.1 Hz, 2H), 3.99 (s, 3H), 1.40 (t, J = 7.1 Hz, 3H).

Ethyl 3-methoxy-4'-(4,4,4-trifluoro-3-hydroxy-3-(trifluoromethyl) butanoyl)-[1,1'-biphenyl]-4-carboxylate (68). Ethyl 4'-acetyl-3-methoxy-[1,1'-biphenyl]-4-carboxylate (**67**) (0.11 gr, 0.37 mmol) placed at -60°C in anhydrous THF under nitrogen atmosphere then LiHMDS (0.6 ml, 0.6 mmol) is added dropwise and stirred for 30min. In a separate two neck flask concentrated H2SO4 (10 ml) is warmed to 50 °C and linked through a cannula with the enolate flask then a trihydrate hexafluoroacetone (0.16 ml, 1.1 mmol) is dropped inside the H2SO4 and the formed gaseous HFA is cannulated inside the enolate solution. The mixture is stirred 3 hrs, and then the reaction is quenched with glacial acetic acid (few drops). Mixture diluted with AcOEt and washed with water and brine. Organic layer collected and dried over sodium sulphate, filtered and solvent removed under reduced pressure. Crude product purified with gel silica column chromatography (petroleum ether/AcOEt 10:3) to afford the clean product as a white solid (0.1 gr,58%). ^{1}H NMR (400 MHz, Chloroform-d) δ 8.09 – 8.03 (m, 2H), 7.91 (d, J = 8.0 Hz, 1H), 7.79 – 7.71 (m, 2H), 7.23 (dd, J = 8.0, 1.6 Hz, 1H), 7.18 (d, J = 1.6 Hz, 1H), 7.10 (s, 1H), 4.39 (q, J = 7.1 Hz, 2H), 3.99 (s, 3H), 3.49 (s, 2H), 1.40 (t, J = 7.1 Hz, 3H).

Ethyl 3-methoxy-4'-(4,4,4-trifluoro-1,3-dihydroxy-3-(trifluoromethyl) butyl)-[1,1'-biphenyl]-4-carboxylate (UPR1427). Ketone starting material (**68**) (0.1 gr, 0.2 mmol) is placed in methanol at 0°C, and then sodium boron hydride (30 mg, 0.8 mmol) is added. Mixture stirred 2 hrs, and then the reaction is quenched with NaHCO3. Mixture diluted with DCM and washed with water and brine. Organic layer collected and dried over sodium sulphate, filtered and solvent removed. Crude residue purified with gel silica column chromatography (toluene/Et2O 10:0.5) to afford **UPR1427** as a white solid (60 mg, 65%). ^{1}H NMR (300 MHz, Chloroform-d) δ 7.85 (d, J = 8.0 Hz, 1H), 7.64 – 7.56 (m, 2H), 7.49 – 7.40 (m, 2H), 7.21 – 7.11 (m, 1H), 7.08 (d, J = 1.6 Hz, 1H), 6.22 (s, 1H), 5.35 (d, J = 11.5 Hz, 1H), 4.38 (q, J = 7.1 Hz, 2H), 2.91 (s, 1H), 2.38 (d, J = 13.8 Hz, 1H), 2.23 (d, J = 15.4 Hz, 1H), 1.40 (t, J = 7.1 Hz, 3H). HPLC-MS (ESI): m/z calcd for $C_{21}H_{20}F_6O_5$ [$(M+H)^-$]: 465.11; found: 465.17.

Ethyl 4'-acetyl-3-(benzyloxy)-[1,1'-biphenyl]-4-carboxylate (70). Ethyl 4-iodo-2-benzyloxy benzoate (**69**) (0.55 gr, 1.5 mmol), 4-acetylphenyl boronic acid (0.29 gr, 17 mmol), potassium carbonate (0.71 gr, 5.1 mmol) and bis(triphenylposphine) palladium dichloride (0.5% mol) were dissolved in 13ml of 1,4-dioxane and 2 ml of water. The mixture is heated to 100°C and the reaction is stirred at reflux under nitrogen atmosphere for 5 hrs, and then is cooled to room temperature. The mixture is diluted with AcOEt and washed with HCl 1M and brine. Organic layer collected and dried over sodium sulphate, filtered and solvent removed under reduced pressure. Crude residue purified by a silica gel column chromatography (petroleum ether/AcOEt 10:2) to give the desired product as a white solid (350 mg, 64%). ^{1}H NMR (400 MHz, Chloroform-d) δ 8.07 – 8.00 (m, 2H), 7.93 (d, J = 7.8 Hz, 1H), 7.67 – 7.61 (m, 2H), 7.57 – 7.50 (m, 2H), 7.44 – 7.37 (m, 2H), 7.37 – 7.31 (m, 1H), 7.28 – 7.21 (m, 2H), 5.26 (s, 2H), 4.39 (q, J = 7.1 Hz, 2H), 2.64 (s, 3H), 1.37 (t, J = 7.1 Hz, 3H).

Ethyl 3-(benzyloxy)-4'- (4,4,4-trifluoro-3-hydroxy-3- (trifluoromethyl) butanoyl)-[1,1'-biphenyl]-4-carboxylate (71). Ethyl 4'-acetyl-3-(benzyloxy)-[1,1'-biphenyl]-4-carboxylate (**70**) (0.35 gr, 0.9 mmol) placed at -60°C in anhydrous THF under nitrogen atmosphere then LiHMDS (1.4 ml, 1.4 mmol) is added dropwise and stirred for 30min. In a separate two neck flask concentrated H2SO4 (10 ml) is warmed to 50 °C and linked through a cannula with the enolate flask then a trihydrate hexafluoroacetone (0.4 ml, 2.7 mmol) is dropped inside the H2SO4 and the formed gaseous HFA is cannulated inside the enolate solution. The mixture is stirred 3 hrs, and then the reaction is quenched with glacial acetic acid (few drops). Mixture diluted with AcOEt and washed with water and brine. Organic layer collected and dried over sodium sulphate, filtered and solvent removed under reduced pressure. Crude product purified with gel silica column chromatography (petroleum ether/AcOEt 10:2) to afford the clean product as a white solid (0.4 gr,82%). ^{1}H NMR (400 MHz, Chloroform-d) δ 8.08 – 8.01 (m, 2H), 7.94 (d, J = 8.0 Hz, 1H), 7.73 – 7.67 (m, 2H), 7.56 – 7.50 (m, 2H), 7.45 – 7.37 (m, 2H), 7.37 – 7.31 (m, 1H), 7.28 – 7.20 (m, 2H), 7.11 (d, J = 1.5 Hz, 1H), 5.26 (s, 2H), 4.40 (q, J = 7.1 Hz, 2H), 3.49 (s, 2H), 1.37 (t, J = 7.1 Hz, 3H).

Ethyl 3-(benzyloxy)-4'- (4,4,4-trifluoro-1,3-dihydroxy-3- (trifluoromethyl) butyl)-[1,1'-biphenyl]-4-carboxylate (UPR1428). Ketone starting material (**71**) (0.4 gr, 0.7 mmol) is placed in methanol at 0°C, and then sodium boron hydride (90 mg, 2.2 mmol) is added. Mixture stirred 2 hrs, and then the reaction is quenched with NaHCO3. Mixture diluted with DCM and washed with water and brine. Organic layer collected and dried over sodium sulphate, filtered and solvent removed. Crude residue purified with gel silica column chromatography (toluene/Et2O 10:0.5) to afford **UPR1428** as a white solid (350

mg, 92%). ^{1}H NMR (300 MHz, Chloroform-d) δ 7.86 (d, J = 8.0 Hz, 1H), 7.58 – 7.48 (m, 3H), 7.47 – 7.29 (m, 5H), 7.20 – 7.07 (m, 2H), 6.23 (s, 1H), 5.32 (d, J = 11.4 Hz, 1H), 5.21 (s, 2H), 4.38 (q, J = 7.1 Hz, 2H), 2.97 (t, J = 2.3 Hz, 1H), 2.46 – 2.31 (m, 1H), 2.21 (d, J = 15.3 Hz, 1H), 1.37 (t, J = 7.1 Hz, 3H). HPLC-MS (ESI): m/z calcd for $C_{27}H_{24}F_6O_5$ [$(M+H)^-$]: 541.14; found: 541.17.

1-(4-bromophenyl)-4,4,4-trifluoro-3-hydroxy-3-(trifluoromethyl)butan-1-one (72). 4-bromo acetophenone (1.50 gr, 7.5 mmol) placed at -60°C in anhydrous THF under nitrogen atmosphere then LiHMDS (11.5 ml, 11.5 mmol) is added dropwise and stirred for 30min. In a separate two neck flask concentrated H2SO4 (10 ml) is warmed to 50 °C and linked through a cannula with the enolate flask then a trihydrate hexafluoroacetone (3.2 ml, 20 mmol) is dropped inside the H2SO4 and the formed gaseous HFA is cannulated inside the enolate solution. The mixture is stirred 3 hrs, and then the reaction is quenched with glacial acetic acid (few drops). Mixture diluted with DCM and washed with water and brine. Organic layer collected and dried over sodium sulphate, filtered and solvent removed under reduced pressure. Crude product purified with gel silica column chromatography (petroleum ether/Et2O 10:0.5) to afford the clean product as a white solid (1.60 gr, 58%). ^{1}H NMR (300 MHz, Chloroform-d) δ 7.87 – 7.78 (m, 2H), 7.74 – 7.65 (m, 2H), 6.95 (s, 1H), 3.42 (s, 2H).

1-(4-bromophenyl)-4,4,4-trifluoro-3-(trifluoromethyl)butane-1,3-diol (73). The ketone starting material (**72**) (1.60 gr, 4.4 mmol) is placed in methanol at 0°C, and then sodium boron hydride (0.50 gr, 13 mmol) is added. Mixture stirred 2 hrs, and then the reaction is quenched with NaHCO3. Mixture diluted with DCM and washed with water and brine. Organic layer collected and dried over sodium sulphate, filtered and solvent removed to afford the clean product as colourless oil (1.61 gr, 100%). ^{1}H NMR (400 MHz, Chloroform-d) δ 7.59 – 7.52 (m, 2H), 7.29 – 7.24 (m, 2H), 6.29 (s, 1H), 5.27 (d, J = 11.5 Hz, 1H), 3.38 (t, J = 2.4 Hz, 1H), 2.33 (ddq, J = 15.7, 11.6, 2.1 Hz, 1H), 2.18 (d, J = 15.4 Hz, 1H).

5-(4,4,5,5-tetramethyl-1,3,2-dioxaborolan-2-yl)-2,3-dihydro-1H-inden-1-one (74). 5-bromo 1-indanone (0.2 gr, 0.95 mmol), bis(pinacolato)diboron (0.27 gr, 1.1 mmol), palladium acetate (0.5% mol) and potassium acetate (0.3 gr, 3 mmol) were dissolved in DMF and stirred at reflux at 90°C under nitrogen atmosphere. After 6 hrs the mixture was cooled to room temperature and filtered on a celite pad. Organic layer diluted with DCM and washed with HCl 1M and brine. Solvent removed under reduced pressure and crude residue purified by a silica gel column chromatography (toluene/Et2O 10:3) to give the clean product (50 mg, 15%). ^{1}H NMR (400 MHz, Chloroform-d) δ 7.92 (t, J = 1.0 Hz, 1H), 7.82 – 7.69 (m, 2H), 3.13 (q, J = 5.9, 5.1 Hz, 2H), 2.72 – 2.64 (m, 2H), 1.35 (s, 12H).

5-(4-(4,4,4-trifluoro-1,3-dihydroxy-3-(trifluoromethyl)-1l3-butyl)phenyl)-2,3-dihydro-1H-inden-1-one (UPR1421). 5-(4,4,5,5-tetramethyl-1,3,2-dioxaborolan-2-yl)-2,3-dihydro-1H-inden-1-one (**74**) (50 mg, 0.2 mmol), 1-(4-bromophenyl)-4,4,4-trifluoro-3-(trifluoromethyl)butane-1,3-diol (**73**) (65 mg, 0.2 mmol), potassium carbonate (95 mg, 0.7 mmol) and bis(triphenylposphine) palladium dichloride (0.5% mol) were dissolved in 7ml of 1,4-dioxane and 1 ml of water. The mixture is heated to 100°C and the reaction is stirred at reflux under nitrogen atmosphere for 6 hrs, and then is cooled to room temperature. The mixture is diluted with DCM and washed with water, HCl 1M and brine. Organic layer collected and dried over sodium sulphate, filtered and solvent removed under reduced pressure. Crude residue purified by a silica gel column chromatography (toluene/Et2O 10:1) to give **UPR1421** as a white solid (10 mg, 15%). ^{1}H NMR (400 MHz, Methanol-d4) δ 7.79 (d, J = 7.9 Hz, 1H), 7.70 – 7.55 (m, 4H), 7.50 – 7.43 (m, 2H), 5.25 (d, J = 11.2 Hz, 1H), 3.33 (p, J = 1.7 Hz, 1H), 3.23 – 3.18 (m, 2H), 2.77 – 2.70 (m, 2H), 2.30 (t, J = 13.4 Hz, 1H), 2.21 – 2.13 (m, 1H). HPLC-MS (ESI): m/z calcd for $C_{20}H_{16}F_6O_3$ [$(M+H)^-$]: 417.09; found: 417.16.

1-(4-bromophenyl)-4,4,4-trifluoro-3-hydroxy-3-(trifluoromethyl)butyl (tert-butoxycarbonyl)-L-alaninate (75a, 75b). 1-(4-bromophenyl)-4,4,4-trifluoro-3-(trifluoromethyl)butane-1,3-diol (**73**) (0.46 gr, 1.3 mmol) N-(tert-Butoxycarbonyl)-L-alanine (0.80 gr, 1.6 mmol) and DMAP (40 mg, 0.35 mmol) were dissolved in DCM at 0°C then EDC (0.38 gr, 2.0 mmol) was added. The mixture is stirred under nitrogen atmosphere at room temperature overnight (18 hrs) then the reaction is diluted with DCM and washed with water, NaHCO3 and brine. Organic layer collected and dried over sodium sulphate, filtered and solvent removed. The diastereoisomers Xa and Xb were separate and purified by silica gel column chromatography (toluene/AcOEt 10:1) to afford clean **75a** (250 mg, 36%) and clean **75b** (80 mg, 11%). **75a**: ^{1}H NMR (300 MHz, Chloroform-d) δ 7.56 – 7.47 (m, 2H), 7.31 – 7.10 (m, 2H), 6.08 (d, J = 10.1 Hz, 1H), 5.32 (s, 1H), 4.91 (d, J = 6.0 Hz, 1H), 4.19 (p, J = 7.1 Hz, 1H), 2.71 – 2.56 (m, 1H), 2.32 (d, J = 17.0 Hz, 1H), 1.43 (s, 9H), 1.29 (d, J = 7.1 Hz, 3H). **75b**: ^{1}H NMR (400 MHz, Chloroform-d) δ 7.58 – 7.51 (m, 2H), 7.33 – 7.15 (m, 2H), 6.17 (d, J = 10.3 Hz, 1H), 5.46 (s, 1H), 4.93 (d, J = 7.1 Hz, 1H), 4.31 (t, J = 7.2 Hz, 1H), 2.66 – 2.53 (m, 1H), 2.35 (d, J = 16.1 Hz, 1H), 1.49 (d, J = 12.1 Hz, 9H), 1.41 (d, J = 7.2 Hz, 3H).

1-(4-bromophenyl)-4,4,4-trifluoro-3-(trifluoromethyl)butane-1,3-diol (76a). 1-(4-bromophenyl)-4,4,4-trifluoro-3-hydroxy-3-(trifluoromethyl)butyl (tert-butoxycarbonyl)-L-alaninate (**75a**) (0.25 gr, 0.5 mmol) is dissolve in 10 ml of methanol at 0°C under nitrogen atmosphere then metallic sodium (35 mg, 1.5 mmol) was added. Reaction stirred at 0°C 24 hrs then the mixture is diluted with DCM and washed with HCl 1M and brine. Organic layer collected and dried over sodium sulphate, filtered and solvent removed. Crude

product purified with gel silica column chromatography (petroleum ether/Et2O 10:1) to afford the clean product as a colourless oil(0.15gr,82%). ^{1}H NMR (400 MHz, Chloroform-d) δ 7.61 – 7.53 (m, 2H), 7.32 – 7.24 (m, 2H), 6.07 (s, 1H), 5.30 (d, J = 11.6 Hz, 1H), 2.68 (s, 1H), 2.35 (ddq, J = 15.6, 11.5, 2.1 Hz, 1H), 2.20 (d, J = 15.4 Hz, 1H).

1-(4-bromophenyl)-4,4,4-trifluoro-3-(trifluoromethyl)butane-1,3-diol (76b). 1-(4-bromophenyl)-4,4,4-trifluoro-3-hydroxy-3-(trifluoromethyl)butyl (tert-butoxycarbonyl)-L-alaninate (**75b**) (80 mg, 0.2 mmol) is dissolve in 5 ml of methanol at 0°C under nitrogen atmosphere then metallic sodium (15 mg, 0.5 mmol) was added. Reaction stirred at 0°C 24 hrs then the mixture is diluted with DCM and washed with HCl 1M and brine. Organic layer collected and dried over sodium sulphate, filtered and solvent removed. Crude product purified with gel silica column chromatography (petroleum ether/Et2O 10:1) to afford the clean product as colourless oil (50 mg, 91%). ^{1}H NMR (400 MHz, Chloroform-d) δ 7.60 – 7.53 (m, 2H), 7.31 – 7.25 (m, 2H), 6.08 (s, 1H), 5.30 (d, J = 11.5 Hz, 1H), 2.70 (s, 1H), 2.35 (ddq, J = 15.7, 11.5, 2.1 Hz, 1H), 2.19 (dd, J = 16.1, 1.9 Hz, 1H).

(4-(ethoxycarbonyl)phenyl)boronic acid (77). 4-carboxyphenyl boronic acid (0.3 gr, 1.8 mmol) is dissolved in 25 ml of ethanol with 0.1ml of HCl 37%. The mixture is stirred at 90°C refluxing for 8hrs. The reaction is then cooled to room temperature and the solvent is removed under reduced pressure to give the clean product as a white solid (350 mg, 100%). ^{1}H NMR (400 MHz, Methanol-d4) δ 7.97 (dd, J = 8.2, 3.5 Hz, 2H), 7.79 (s, 2H), 4.36 (q, J = 7.1 Hz, 1H), 1.39 (t, J = 7.1 Hz, 2H).

Ethyl 4'-(4,4,4-trifluoro-1,3-dihydroxy-3-(trifluoromethyl)butyl)-[1,1'-biphenyl]-4-carboxylate (UPR1422). 1-(4-bromophenyl)-4,4,4-trifluoro-3-(trifluoromethyl)butane-1,3-diol (**76a**) (0.1 gr, 0.3 mmol), (4-(ethoxycarbonyl)phenyl)boronic acid (**77**) (60 mg, 0.3 mmol), potassium carbonate (0.14 gr, 1.0 mmol) and bis(triphenylposphine) palladium dichloride (0.5% mol) were dissolved in 8ml of 1,4-dioxane and 1 ml of water. The mixture is heated to 100°C and the reaction is stirred at reflux under nitrogen atmosphere for 5 hrs, then is cooled to room temperature. The mixture is diluted with DCM and washed with water, HCl 1M and brine. Organic layer collected and dried over sodium sulphate, filtered and solvent removed under reduced pressure. Crude residue purified by a silica gel column chromatography (toluene/Et2O 10:1) to give **UPR1422** as a white solid (90 mg, 69%). ^{1}H NMR (300 MHz, Chloroform-d) δ 8.07 (dd, J = 8.3, 2.3 Hz, 2H), 7.62 (ddd, J = 9.7, 8.3, 1.4 Hz, 4H), 7.51 – 7.42 (m, 2H), 6.22 (s, 1H), 5.36 (d, J = 11.4 Hz, 1H), 4.40 (q, J = 7.1 Hz, 2H), 2.90 (s, 1H), 2.49 – 2.34 (m, 1H), 2.30 – 2.19 (m, 1H), 1.42 (t, J = 7.1 Hz, 3H). HPLC-MS (ESI): m/z calcd for $C_{20}H_{18}F_6O_4$ [$(M+H)^-$]: 435.10; found: 435.15.

Ethyl 4'-(4,4,4-trifluoro-1,3-dihydroxy-3-(trifluoromethyl)butyl)-[1,1'-biphenyl]-4-carboxylate (UPR1426). 1-(4-bromophenyl)-4,4,4-trifluoro-3-(trifluoromethyl)butane-1,3-diol (**76b**) (50 mg, 0.1 mmol), (4-(ethoxycarbonyl)phenyl)boronic acid (**77**) (30 mg, 0.2 mmol), potassium carbonate (70 mg, 0.5 mmol) and bis(triphenylposphine) palladium dichloride (0.5% mol) were dissolved in 5ml of 1,4-dioxane and 1 ml of water. The mixture is heated to 100°C and the reaction is stirred at reflux under nitrogen atmosphere for 5 hrs, then is cooled to room temperature. The mixture is diluted with DCM and washed with water, HCl 1M and brine. Organic layer collected and dried over sodium sulphate, filtered and solvent removed under reduced pressure. Crude residue purified by a silica gel column chromatography (toluene/Et2O 10:0.5) to give **UPR1426** as a white solid (20 mg, 35%). ^{1}H NMR (400 MHz, Chloroform-d) δ 8.16 – 8.08 (m, 2H), 7.70 – 7.61 (m, 4H), 7.52 – 7.46 (m, 2H), 6.25 (s, 1H), 5.39 (d, J = 11.5 Hz, 1H), 4.42 (q, J = 7.2 Hz, 2H), 2.98 (s, 1H), 2.49 – 2.38 (m, 1H), 2.31 – 2.22 (m, 1H), 1.44 (t, J = 7.2 Hz, 3H). HPLC-MS (ESI): m/z calcd for $C_{20}H_{18}F_6O_4$ [$(M+H)^-$]: 435.10; found: 435.14.

N-methoxy-N-methyloctanamide (79). Octanoic acid (**78**) (1.0 gr, 7.0 mmol) and triethylamine (2.5ml, 17.5 mmol) were placed in 15ml of DMF at 0°C then ethylchloroformate (0.75 ml, 8.0 mmol) is added dropwise. The mixture is stirred 30 min at 0°C then N,O-dimethyl hydroxylamine hydrochloride (0.82 gr, 8.5 mmol) was added. The reaction allowed to warm to room temperature then is diluted with diethyl ether. The mixture is washed with HCl 2M and brine. Organic layer collected and dried over sodium sulphate, filtered and solvent removed to give the desired product a s a yellowish oil (1.0 gr, 76%). ^{1}H NMR (300 MHz, Chloroform-d) δ 3.67 (d, J = 1.0 Hz, 3H), 3.17 (s, 3H), 2.40 (t, J = 7.6 Hz, 2H), 1.61 (td, J = 10.3, 8.9, 5.8 Hz, 2H), 1.30 (tt, J = 10.4, 4.1 Hz, 8H), 0.92 – 0.82 (m, 3H).

Nonan-2-one (80). N-methoxy-N-methyloctanamide (**79**) is placed in 15 ml of anhydrous THF at 0°C under nitrogen atmosphere then methyl lithium (8.0 ml, 12.5 mmol) is added dropwise. Reaction stirred at 0°C 20 min then is quenched with acetic acid (few drops). The mixture is diluted with diethyl ether and washed with HCl 1M and brine. Organic layer collected and dried over sodium sulphate, filtered and solvent removed. Crude product purified by a silica gel column chromatography (hexane/Et2O 10:1) to the desired product as colourless oil (700 mg, 91%). ^{1}H NMR (300 MHz, Chloroform-d) δ 2.41 (t, J = 7.4 Hz, 2H), 2.13 (s, 3H), 1.62 – 1.51 (m, 2H), 1.30 – 1.25 (m, 8H), 0.92 – 0.80 (m, 3H).

1,1,1-trifluoro-2-hydroxy-2-(trifluoromethyl)undecan-4-one (81). Nonan-2-one (**80**) (0.50 gr, 3.5 mmol) placed at -60°C in anhydrous THF under nitrogen atmosphere then LiHMDS (7.0 ml, 7.0 mmol) is added dropwise and stirred for 30min. In a separate two neck flask concentrated H2SO4 (10 ml) is warmed to 50 °C and linked through a cannula with the

enolate flask then a trihydrate hexafluoroacetone (1.5 ml, 11.0 mmol) is dropped inside the H2SO4 and the formed gaseous HFA is cannulated inside the enolate solution. The mixture is stirred 3 hrs, and then the reaction is quenched with glacial acetic acid (few drops). Mixture diluted with AcOEt and washed with water and brine. Organic layer collected and dried over sodium sulphate, filtered and solvent removed under reduced pressure. Crude product purified by a silica gel column chromatography (hexane/Et2O 10:1) to afford the product as oil (0.3 gr, 29%). ^{1}H NMR (300 MHz, Chloroform-d) δ 6.91 (s, 1H), 2.92 (s, 2H), 2.58 (t, J = 7.3 Hz, 2H), 1.68 – 1.50 (m, 2H), 1.45 – 1.24 (m, 8H), 0.89 (qd, J = 7.2, 1.9 Hz, 3H).

1,1,1-trifluoro-2-(trifluoromethyl)undecane-2,4-diol (UPR1420). Ketone starting material (**81**) (300 mg, 1.0 mmol) is placed in methanol at 0°C, and then sodium boron hydride (120 mg, 3.0 mmol) is added. Mixture stirred 3 hrs, and then the reaction is quenched with NaHCO3. Mixture diluted with DCM and washed with water and brine. Organic layer collected and dried over sodium sulphate, filtered and solvent removed. to Crude product purified by a silica gel column chromatography (hexane/Et2O 10:2) to afford the clean **UPR1420** as a colourless oil (180 mg, 58%). ^{1}H NMR (400 MHz, Chloroform-d) δ 6.27 (s, 1H), 4.24 (dd, J = 10.1, 5.4 Hz, 1H), 2.28 – 1.84 (m, 4H), 1.60 (d, J = 1.0 Hz, 1H), 1.53 (h, J = 7.0, 6.2 Hz, 2H), 1.33 – 1.26 (m, 8H), 0.97 – 0.85 (m, 3H). HPLC-MS (ESI): m/z calcd for $C_{12}H_{20}F_6O_2$ [$(M+H)^-$]: 309.13; found: 309.18.

6.2 Experimental procedures: EGFR inhibitors.

1-(4-(3-methoxy-4-nitrophenyl)piperazin-1-yl)ethan-1-one (83). 4-fluoro-2-methoxy-1-nitrobenzene (**82**) (2.00 gr, 11.7 mmol) and 1-acetyl-piperazine (1.70 gr, 13.2 mmol) were placed in a sealed round bottom flask and heated to 70°C. The mixture was stirred 8hrs then the reaction was cooled to room temperature. The mixture is diluted with toluene then the solvent is removed under reduced pressure. The crude residue is washed with hexane to give the desired product as a yellow solid (3.2 gr, 98%). ^{1}H NMR (300 MHz, Chloroform-d) δ 8.00 (d, J = 9.3 Hz, 1H), 6.41 (dd, J = 9.3, 2.6 Hz, 1H), 6.32 (d, J = 2.5 Hz, 1H), 3.96 (d, J = 2.0 Hz, 3H), 3.80 (dd, J = 6.6, 4.2 Hz, 2H), 3.66 (dd, J = 6.6, 3.9 Hz, 2H), 3.50 – 3.36 (m, 4H), 2.15 (s, 3H).

1-(4-(4-amino-3-methoxyphenyl)piperazin-1-yl)ethan-1-one (84). Starting material (**83**) (2.6 gr, 9.3 mmol), ammonium chloride (0.81 gr, 14.8 mmol) and metallic zinc (6.11 gr, 94 mmol) were placed in a round bottom flask and dissolved in 10 ml of THF. The mixture is heated to 75°C to reflux and stirred for 8 hrs then the reaction is cooled to room temperature. The mixture is filtered on a cotton pad the the solvent is removed under reduced pressure. The crude residue is purified by a silica gel column chromatography (DCM/MeOH 10:0.2) to afford the desired product as a white grey powder (1.20 gr, 52%). ^{1}H NMR (300 MHz, Chloroform-d) δ 6.61 (dd, J = 8.3, 1.6 Hz, 1H), 6.48 (dd, J = 2.5, 1.3 Hz, 1H), 6.37 (dt, J = 8.5, 2.0 Hz, 1H), 5.26 (d, J = 1.5 Hz, 2H), 3.80 (d, J = 1.6 Hz, 3H), 3.77 – 3.69 (m, 2H), 3.69 – 3.52 (m, 2H), 3.03 – 2.91 (m, 4H), 2.10 (d, J = 1.5 Hz, 3H).

2,5-dichloro-N-(3-nitrophenyl)pyrimidin-4-amine (86). 2,4,5-trichloropyrimidine (**85**) (2.89 gr, 15.8 mmol), 3-nitroaniline (1.45 gr, 10.5 mmol) and DiPEA (3.70 ml, 21.2 mmol) were dissolved in 30 ml of isopropanol. The mixture is heated to 80°C and stirred overnight (18 hrs). The reaction is diluted with AcOEt and washed with water and brine. Organic layer collected and solvent removed. Crude residue dissolved again in methanol and precipitate from water. Solid product recovered by filtration to give the product as yellow solid (2.17 gr, 72%). ^{1}H NMR (400 MHz, Methanol-d4) δ 8.64 (t, J = 2.2 Hz, 1H), 8.25 (s, 1H), 8.06 (dddd, J = 20.9, 8.2, 2.2, 0.9 Hz, 2H), 7.60 (t, J = 8.2 Hz, 1H).

1-(4-(4-((5-chloro-4-((3-nitrophenyl)amino)pyrimidin-2-yl)amino)-3-methoxyphenyl)piperazin-1-yl)ethan-1-one (87). 1-(4-(4-amino-3-methoxyphenyl)piperazin-1-yl)ethan-1-one (**84**) (1.26 gr, 5.1 mmol), 2,5-dichloro-N-(3-nitrophenyl)pyrimidin-4-amine (**86**) (2.17 gr, 7.6 mmol) and 4-toluensulphonic acid (1.92 gr, 10.1 mmol) were dissolved in isopropanol and heated to 50°C. The reaction is stirred for 18 hrs then is cooled to room temperature and the solvent is removed under reduced

pressure. The crude residue is purified by crystallization from ethanol/water (7:3) to afford the desired product (1.26 gr, 50%). ^{1}H NMR (300 MHz, Methanol-d4) δ 8.57 (dt, J = 10.1, 2.2 Hz, 1H), 8.06 (d, J = 2.1 Hz, 1H), 8.02 – 7.80 (m, 3H), 7.51 (td, J = 8.2, 1.1 Hz, 1H), 6.56 (d, J = 2.5 Hz, 1H), 6.39 (ddd, J = 8.8, 4.4, 2.5 Hz, 1H), 3.88 (d, J = 2.0 Hz, 3H), 3.81 – 3.74 (m, 2H), 3.67 (t, J = 5.2 Hz, 2H), 3.20 – 3.06 (m, 4H), 2.17 (s, 3H).

1-(4-(4-((4-((3-aminophenyl)amino)-5-chloropyrimidin-2-yl)amino)-3-methoxyphenyl)piperazin-1-yl)ethan-1-one (88). The nitro compound (**87**) (1.10 gr, 2.2 mmol) and metallic iron powder (1.24 gr, 22.2 mmol) were placed in a bottom flask and dissolved in 150 ml of ethanol (plus 0.5 ml of HCL 37%). The mixture is heated to 90°C to reflux and stirred for 2 hrs. The reaction is cooled to room temperature and filtered on a celite pad. The solvent is removed under reduced pressure and the crude residue is purified by a silica gel column chromatography (AcOEt/MeOH 10:1) to afford the desired product as a pinkish powder (0.97 gr, 93%). ^{1}H NMR (300 MHz, Chloroform-d) δ 7.73 (d, J = 8.7 Hz, 1H), 7.65 (s, 1H), 6.88 – 6.77 (m, 2H), 6.60 (ddd, J = 8.1, 2.1, 1.0 Hz, 1H), 6.33 – 6.16 (m, 3H), 3.59 (s, 3H), 3.52 – 3.43 (m, 2H), 3.43 – 3.34 (m, 2H), 2.84 (dt, J = 14.4, 5.2 Hz, 4H), 1.87 (s, 3H).

N-(3-((2-((4-(4-acetylpiperazin-1-yl)-2-methoxyphenyl)amino)-5-chloropyrimidin-4-yl)amino)phenyl) acetamide (UPR1423). Starting material (**88**) (50 mg, 0.1 mmol) is dissolved in 1 ml of pyridine and acetic anhydride (0.2 ml, 0.2 mmol). The reaction is stirred at room temperature for 30min then the cold water I added. The precipitate is recovered and is purified by crystallization from water/methanol (10:1) to afford **UPR1423** as colourless crystals (44 mg, 82%) ^{1}H NMR (300 MHz, Chloroform-d) δ 8.14 – 8.02 (m, 2H), 7.88 (s, 1H), 7.33 (dd, J = 11.1, 7.5 Hz, 3H), 7.18 (s, 1H), 7.07 (s, 1H), 6.49 (d, J = 22.0 Hz, 2H), 3.88 (s, 3H), 3.78 (t, J = 5.2 Hz, 2H), 3.62 (t, J = 5.1 Hz, 2H), 2.16 (d, J = 8.7 Hz, 6H). MS (ESI): m/z: calcd for $C_{25}H_{30}ClFN_7O_4$ [(M+H)+]: 578.17; found: 577.90. MS (ESI): m/z: calcd for $C_{25}H_{28}ClN_7O_3$ [(M+H)+]: 510.02; found: 509.93.

N-(3-((2-((4-(4-acetylpiperazin-1-yl)-2-methoxyphenyl)amino)-5-chloropyrimidin-4-yl)amino)phenyl)-2-chloroacetamide (UPR1424). 2-chloro acetic acid (0.12 gr, 1.3 mmol), DiPEA (0.17 gr, 1.32 mmol) and pivaloyl chloride (0.14 gr, 1.13 mmol) were dissolved in 2 ml THF and stirred 20 min. A suspension of aniline (**88**) (100 mg, 0.21 mmol) in toluene is then added. The reaction is stirred for 1 h at room temperature. The mixture is diluted with EtOAc and washed with water. Organic layer collected, solvent removed. Crude product purified by crystallization from ethanol/water 7:3 to afford UPR1424 (61 mg, 55%). 1H NMR (300 MHz, Methanol-d4) δ 7.98 – 7.89 (m, 2H), 7.79 (t, J = 2.0 Hz, 1H), 7.44

– 7.25 (m, 3H), 6.55 (d, J = 2.5 Hz, 1H), 6.37 (dd, J = 8.8, 2.5 Hz, 1H), 4.13 (s, 2H), 3.86 (s, 3H), 3.70 (dt, J = 22.8, 5.2 Hz, 4H), 3.10 (dt, J = 14.1, 5.2 Hz, 4H), 2.13 (s, 3H). MS (ESI):m/z: calcd for $C_{25}H_{28}Cl_2N_7O_3$ [(M+H)+]: 544.16; found: 543.86.

N-(3-((2-((4-(4-acetylpiperazin-1-yl)-2-methoxyphenyl) amino)-5-chloropyrimidin-4-yl) amino) phenyl) ethene sulfonamide (UPR1432). Aniline (**88**) (90 mg, 0.19 mmol) and triethylamine (0.6 ml, 0.43 mmol) is dissolved in pyridine (2 ml) and is placed at 0°C, then a solution of 2-bromoethane-1-sulfonyl chloride (**89**) (59 mg, 0.28 mmol) in toluene is added dropwise. The mixture is stirred under nitrogen for 24 h, then the solvent is removed. The crude product purified by silica gel column chromatography (toluene/acetone 1:1) to afford **UPR1432** as a white solid (15 mg, 14%). 1H NMR (400 MHz, Methanol-d4) δ 7.99 – 7.91 (m, 2H), 7.59 (d, J = 5.3 Hz, 1H), 7.35 – 7.07 (m, 5H), 7.01 – 6.95 (m, 1H), 6.65 – 6.54 (m, 2H), 6.49 (dd, J = 8.8, 2.5 Hz, 1H), 6.23 (d, J = 16.6 Hz, 1H), 5.92 (d, J = 9.9 Hz, 1H), 3.87 (s, 3H), 3.75 (t, J = 5.2 Hz, 2H), 3.68 (t, J = 5.1 Hz, 2H), 3.14 (dt, J = 22.4, 5.2 Hz, 4H), 2.15 (s, 3H). MS (ESI): m/z: calcd for $C_{25}H_{28}ClN_7O_4S$ [(M+H)+]: 558.17; found: 557.86.

3-((3-((2-((4-(4-acetylpiperazin-1-yl)-2-methoxyphenyl)amino)-5-chloropyrimidin-4-yl)amino)phenyl) carbamoyl) benzenesulfonyl fluoride (UPR1433). A solution of aniline (**88**) (50 mg, 0.1 mmol) in 2 ml of anhydrous THF is added dropwise to a solution of 3-(fluorosulfonyl)benzoyl chloride (**90**) (0.5 mmol) in 1ml of pyridine placed at 0°C. The reaction is stirred at 0°C for 10min then the solvent is removed under reduced pressure. The crude residue is purified by silica gel column chromatography (toluene/acetone 7:3) to afford **UPR1433** as a white solid (14 mg, 21%). ^{1}H NMR (300 MHz, Methanol-d4) δ 8.51 (t, J = 1.8 Hz, 1H), 8.32 (dt, J = 7.9, 1.4 Hz, 1H), 8.20 – 8.07 (m, 1H), 8.02 – 7.88 (m, 3H), 7.78 (t, J = 7.9 Hz, 1H), 7.59 – 7.49 (m, 1H), 7.34 – 7.29 (m, 2H), 7.20 – 6.99 (m, 2H), 3.81 (s, 3H), 3.54 (dt, J = 18.0, 5.2 Hz, 4H), 2.91 (dt, J = 20.0, 5.2 Hz, 5H). MS (ESI): m/z: calcd for $C_{30}H_{29}ClFN_7O_5S$ [(M+H)+]: 653.16; found: 653.86.

2-((3-((2-((4-(4-Acetylpiperazin-1-yl)-2-methoxyphenyl)amino)-5-chloropyrimidin-4-yl)amino)phenyl) amino) ethane-1-sulfonyl fluoride (UPR1425). Aniline (**88**) (200 mg, 0.43 mmol) is dissolved in chloroform/MeOH 1:1 (10 ml) and ESF (**91**) (120 µl, 1.45 mmol) is added. The solution is stirred at room temperature for 3 h, then is diluted with AcOEt and washed with saturated aqueous NaHCO3. The organic layer is consequently washed with water and brine, dried over Na2SO4 and concentrated under reduced pressure. Purification of the solid residue by silica gel column chromatography (toluene/EtOH95:5) affords **UPR1425** as a white solid (33 mg, 13%). 1H NMR(400 MHz, CDCl3) δ 8.08 (d, J =

8.7 Hz, 1H), 8.05 (s, 1H), 7.23 – 7.16 (m, 2H), 7.00 (d,J = 2.0 Hz, 1H), 6.90 – 6.80 (m, 1H), 6.54 (d, J = 2.5 Hz, 1H), 6.48 (dd, J = 8.8, 2.6 Hz,1H), 6.45 –6.36(m,1H), 3.87 (s, 3H), 3.81 – 3.73 (m, 4H), 3.67 – 3.55 (m, 4H), 3.11(dt, J = 12.5, 5.2 Hz, 4H), 2.15 (s, 3H). MS (ESI): m/z: calcd for $C_{25}H_{29}ClFN_7O_4S$ [(M+H)+]: 577.17; found: 577.90.

2,5-dichloro-N-(4-nitrophenyl)pyrimidin-4-amine (92). 2,4,5-trichloropyrimidine (**85**) (0.4 gr, 2.2 mmol) and 4-nitroaniline (0.30 gr, 2.2 mmol) were placed in a sealed bottom flask with 15 ml of water and 0.1 ml of HCl 37%. The mixture is heated to 100°C and stirred 7 hrs. A yellow precipitate is recovered by filtration, then is washed with water and with hexane to give the clean product (0.50 gr, 80%). ^{1}H NMR (300 MHz, Chloroform-d) δ 8.37 – 8.24 (m, 3H), 7.90 (s, 2H), 7.51 (s, 1H).

1-(4-(4-((5-chloro-4-((4-nitrophenyl)amino)pyrimidin-2-yl)amino)-3-methoxyphenyl)piperazin-1-yl)ethan-1-one (93). The chloride compound (**92**) (0.50 gr, 1.8 mmol), the aniline (**84**) (0.32 gr, 1.3 mmol) and 4-toluensulphonic acid (0.34gr, 1.8 mmol) were dissolved in 15 ml of isopropanol. The mixture is heated to 90°C to reflux and stirred overnight (18 hrs). The reaction is cooled to room temperature, solvent removed under reduced pressure. The crude residue is dissolved in DCM and washed with a saturated solution of NaHCO3 then water and brine. Organic layer collected and solvent removed under reduced pressure. The crude residue is purified by silica gel column chromatography (DCM/MeOH 10:0.2) to afford the desired product as a yellow powder (0.40 gr, 45 %). ^{1}H NMR (300 MHz, Chloroform-d) δ 8.26 – 8.17 (m, 2H), 8.15 (s, 1H), 7.98 (d, J = 8.6 Hz, 1H), 7.87 – 7.77 (m, 2H), 7.31 (d, J = 16.9 Hz, 2H), 6.60 – 6.47 (m, 2H), 3.89 (s, 3H), 3.87 – 3.76 (m, 2H), 3.71 – 3.62 (m, 2H), 3.19 – 3.11 (m, 4H), 2.16 (s, 3H).

1-(4-(4-((4-((4-aminophenyl)amino)-5-chloropyrimidin-2-yl)amino)-3-methoxyphenyl)piperazin-1-yl)ethan-1-one (94). The nitro compound (**93**) (0.10 gr, 0.2 mmol) metallic iron powder (0.34 gr, 6 mmol) were placed in a round bottom flask with 25 ml of ethanol and 1 ml of HCl 37%. The mixture is heated to 100°C to reflux and stirred 3 hrs. The mixture is filtrated on a celite pad, the ethanol is removed under reduced pressure. The crude residue is purified by a silica gel column chromatography (DCM/MeOH 10:0.5) to afford the desired aniline (40 mg, 43%). ^{1}H NMR (300 MHz, Chloroform-d) δ 8.11 (d, J = 8.8 Hz, 1H), 7.98 (s, 1H), 7.36 – 7.28 (m, 3H), 6.86 (s, 1H), 6.77 – 6.66 (m, 2H), 6.51 (d, J = 2.5 Hz, 1H), 6.42 (dd, J = 8.8, 2.5 Hz, 1H), 3.85 (s, 3H), 3.78 (t, J = 5.2 Hz, 2H), 3.65 – 3.53 (m, 2H), 3.22 – 3.02 (m, 4H), 2.14 (s, 3H).

4-(((4-((2-((4-(4-acetylpiperazin-1-yl)-2-methoxyphenyl)amino)-5-chloropyrimidin-4-yl)amino)phenyl) amino) methyl) benzenesulfonyl fluoride (UPR1444). Aniline (**94**) (60

mg, 0.1 mmol), 4-(bromomethyl) benzenesulfonyl fluoride (**95**) (35 mg, 0.13 mmol) and potassium carbonate (40 mg, 0.25 mmol) were dissolved in 3 ml of degassed DMF and stirred 2 hrs at 40°C. Then the reaction is cooled to room temperature and diluted with toluene and solvent removed under reduced pressure. The crude residue is purified by silica gel column chromatography (DCM/MeOH 10:0.2) to afford **UPR1444** as a white solid (30 mg, 35%). ^{1}H NMR (300 MHz, Chloroform-d) δ 8.12 (d, J = 8.8 Hz, 1H), 8.03 – 7.90 (m, 3H), 7.71 – 7.54 (m, 2H), 7.46 – 7.31 (m, 2H), 7.27 (s, 1H), 6.85 (s, 1H), 6.67 – 6.54 (m, 2H), 6.51 (d, J = 2.5 Hz, 1H), 6.41 (dd, J = 8.8, 2.5 Hz, 1H), 4.53 (s, 2H), 3.85 (s, 3H), 3.77 (t, J = 5.2 Hz, 2H), 3.67 – 3.57 (m, 2H), 3.07 (dt, J = 10.3, 5.2 Hz, 4H), 2.14 (s, 3H). MS (ESI): m/z: calcd for $C_{30}H_{31}ClFN_7O_4S$ [(M+H)+]: 640.18; found: 640.10.

6.3 Experimental procedures: Keap1 PPIs inhibitors.

All chemicals were purchased from chemical vendors and used without prior purification. 1H NMR and 13C NMR-spectra were recorded using a 600 MHz Bruker Avance III HD instrument equipped with a cryogenically cooled 5 mm dual probe or a 400 MHz Bruker Avance III instrument equipped with a 5 mm broad band probe. Samples were dissolved in DMSO-*d6* (VWR Chemicals, 99.80% D) or chloroform-*d* (Cambridge Isotope Laboratories, Inc., 99.8% D) and analyzed at 300 K. Chemical shifts (δ) are reported in ppm, referenced to DMSO-d6 (1H: 2.500 ppm, 13C: 39.520 ppm) or chloroform-*d* (1H: 7.260 ppm, 13C: 77.160 ppm). Coupling constants (*J*) are reported in Hz. Abbreviations for multiplicities: s, singlet; d, doublet; dd, double dou-blet; t, triplet; q, quartet; p, pentet; m, multiplet. TLC analysis was performed using TLC silica gel 60 F254 aluminum plates (Merck). LC-MS analysis was carried out using an Agilent 6410 Triple Quadrupole Mass Spectrometer instrument with elec-tron spray ionization (ESI) coupled to an Agilent 1200 HPLC system, a C18 reverse phase column (Zorbax Eclipse XBD-C18, 4.6 mm × 50 mm), autosampler and diode array detector, and a linear gradient of buffer A (milliQ H2O:MeCN:formic acid, 95:5:0.1 v/v%) to buffer B (milliQ H2O:MeCN:formic acid, 5:95:0.043 v/v%) with a flow rate of 1 mL⁄min. Normal phase flash chromatography was carried out using prepacked RediSep Rf silica flash cartridges on a CombiFlash® Rf+ apparatus. Pre-parative reverse phase HPLC was performed using an Agilent 1200 series HPLC preparative system with an Agilent Zorbax 300-SB-C18 column (21.2 x 250 mm). MW-assisted synthesis was carried out using a Biotage® Initiator+ apparatus.

Ethyl 1-(3-bromophenyl)-5-cyclopropyl-1H-pyrazole-4-carboxylate (103).
Ethyl 3-cyclopropyl-3-oxopropanoate (**102**) (2gr, 12.81 mmol) and DMF-dimethyl acetal (1.6gr, 13.43 mmol) were stirred in a microwave reactor at 130°C for 15min. The mixture was cooled to room temperature, diluted with ethanol and transferred in a bottom flask with 3-bromophenylhydrazine hydrochloride (2.80gr, 12.53 mmol) and triethylamine (4.81gr, 47.44 mmol). The mixture was stirred at room temperature for 24h then quenched with HCl 2Mol and extracted with ethyl acetate. Organic layer collected and washed with brine, dried over Na_2SO_4 filtered and solvent removed under reduced pressure. Crude mixture was purified with flash chromatography (SiO2, Hept/EtOAc) to afford **103** (2.90gr, 72.1%). LC-MS; $[M+H]^+$ found 335.1,/337.1 (1:1 signal ratio, Br). t_R: 3.84min, UV 254nm 96%.

Ethyl 5-cyclopropyl-1-(3-(phenylsulfonamido)phenyl)-1H-pyrazole-4-carboxylate (UCAB#409).

A solution of **103** (1.00gr, 2.98mmol) in degased DMF (5.5ml) was added to a dry vial previously charged with benzensulfonamide (565mg, 3.59mmol), copper iodide (115mg,

0.60mmol), N,N-dimethylglycine (65mg, 0.63mmol) and potassium phosphate (1.61gr, 7.58mmol) under nitrogen. The mixture was stirred at 160°C for 24h then was cooled to room temperature and diluted with ethyl acetate. The mixture was then washed with ammonium chloride saturated solution and brine, organic layer dried over Na2SO4 filtered and solvent removed under reduced pressure. Crude mixture was purified with flash chromatography (SiO2, Hept/EtOAc) to afford **UCAB#409** as a white solid (990mg, 80.3%). LC-MS; [M-H]- found 410.2, tR: 3.35min, UV 254nm 97%.

5-cyclopropyl-1-(3-(phenylsulfonamido)phenyl)-1H-pyrazole-4-carboxylic acid (UCAB#310).

A solution of KOH (770mg, 13.7mmol) in 4ml of water is added to a solution of **UCAB#409** (800mg, 1.9mmol) in 2ml of THF and 2ml of ethanol. The mixture is stirred overnight to completion at room temperature. Then the solvent is removed under reduced pressure and the crude is acidified with concentrated HCl and extracted with ethyl acetate. The organic layer is collected and washed with brine, dried over Na2SO4 then filtered and solvent removed under reduced pressure to give **UCAB#310** (705mg, 95%) as white solid. LC-MS; [M+H]+ found 384.1, tR: 2.67min, UV 254nm 97%.

5-cyclopropyl-1-(3-(phenylsulfonamido)phenyl)-1H-pyrazole-4-carboxamide and **5-cyclopropyl-N,N-dimethyl-1-(3-(phenylsulfonamido)phenyl)-1H-pyrazole-4-carboxamide (UCAB#419, UCAB#420).**

In a round bottom flask were dissolved HATU (650mg, 1.71mmol) and **UCAB#310** (500mg, 1.31mmol) in 4ml of DMF, then DiPEA (505mg, 3.90mmol) was added. The reaction was stirred at room temperature for 15min then ammonium chloride (140mg, 2.6mmol) was added. The reaction was stirred for 2h at room temperature then was quenched with ammonium chloride saturated water solution. The mixture is washed with ethyl acetate and the organic layer is dried over Na_2SO_4, filtered and solvent removed under reduced pressure. The crude product is purified by preparative HPLC system to afford **UCAB#419** (11mg, 78%) and **UCAB#420** as white solid (10mg, 14%, as a side product derived from dimethyl-amine impurities from DMF solvent).

LC-MS **UCAB#419**. $[M-H]^-$ found 381.2, tR: 2.44min, UV 254nm 100%. ^{1}H NMR (600MHz, DMSO d6): δ 10.60 (s, 1H), 7.89 (s, 1H), 7.79 (d, J = 7.4 Hz, 2H), 7.63 (t, J = 7.4 Hz, 1H), 7.56 (t, J = 7.6 Hz, 2H), 7.40 (t, J = 8.1 Hz, 1H), 7.36 (s, 1H), 7.26 (s, 1H), 7.23 (d, J = 7.9 Hz, 1H), 7.19 (dd, J = 8.2, 1.1 Hz, 1H), 7.13 (s, 1H), 1.88 (tt, J = 8.5, 5.5 Hz, 1H), 0.70 – 0.59 (m, 2H), 0.38 – 0.30 (m, 2H). ^{13}C NMR (151 MHz, DMSO-d6): δ 164.41, 144.69, 140.61, 140.39, 139.68, 138.64, 133.56, 130.24, 129.81, 127.11, 121.08, 119.65, 118.51, 116.7, 8.52, 7.32.

LC-MS **UCAB#420**. $[M-H]^-$ found 409.2, tR: 2.65min, UV 254nm 96,8%. ^{1}H NMR (600MHz, DMSO d6): δ 10.57 (s, 1H), 7.79 (d, J = 7.4 Hz, 2H), 7.69 – 7.60 (m, 2H), 7.56 (t, J = 7.6 Hz, 2H), 7.40 (t, J = 8.0 Hz, 1H), 7.36 – 7.27 (m, 2H), 7.18 (d, J = 8.0 Hz, 1H), 2.99 (d, J = 10.9 Hz, 6H), 1.76 (ddd, J = 13.7, 8.4, 5.4 Hz, 1H), 0.68 (dt, J = 6.1, 4.4 Hz, 2H), 0.36 (q, J = 6.0

Hz, 2H). ^{13}C NMR (151 MHz, DMSO-d6): δ 164.83, 142.44, 140.37, 139.72, 139.26, 138.72, 133.53, 130.27, 129.81, 127.10, 120.68, 119.53, 117.60, 116.45, 7.21.

5-cyclopropyl-N-hydroxy-1-(3-(phenylsulfonamido)phenyl)-1H-pyrazole-4-carboxamide (UCAB#421).

In a round bottom flask were dissolved HATU (120mg, 0.32mmol) and **UCAB#310** (100mg, 0.26mmol) in 2ml of DMF, then DiPEA (100mg, 0.77mmol) was added. The reaction was stirred at room temperature for 15min then hydroxylamine hydrochloride (37mg, 0.69mmol) was added. The reaction was stirred for 2h at room temperature then was quenched with ammonium chloride saturated water solution. The mixture is washed with ethyl acetate and the organic layer is dried over Na_2SO_4, filtered and solvent removed under reduced pressure. The crude product is purified by preparative HPLC system to afford **UCAB#421** (15mg, 15%) as white solid. LC-MS $[M-H]^-$ found 397.2, tR: 2.37min, UV 254nm 100%. 1H NMR (600 MHz, DMSO-d6) δ 10.65 (s, 1H), 10.60 (s, 1H), 7.81 – 7.74 (m, 3H), 7.66 – 7.59 (m, 1H), 7.55 (dd, J = 8.4, 7.0 Hz, 2H), 7.39 (t, J = 8.1 Hz, 1H), 7.26 (t, J = 2.1 Hz, 1H), 7.26 – 7.21 (m, 1H), 7.19 (ddd, J = 8.1, 2.2, 1.0 Hz, 1H), 1.83 (tt, J = 8.5, 5.5 Hz, 1H), 0.68 – 0.61 (m, 2H), 0.40 – 0.34 (m, 2H). 13C NMR (151 MHz, DMSO-d6) δ 160.53, 144.05, 139.82, 139.17 (d, J = 12.1 Hz), 138.21, 133.09, 129.83, 129.34, 126.62, 120.48, 119.19, 116.11, 115.53, 7.81, 6.95.

5-cyclopropyl-N-methyl-1-(3-(phenylsulfonamido)phenyl)-1H-pyrazole-4-carboxamide (UCAB#426).

In a round bottom flask were dissolved HATU (90mg, 0.24mmol) and **UCAB#310** (55mg, 0.14mmol) in 4ml of 1,4-dioxane, then DiPEA (50mg, 0.39mmol) was added. The reaction was stirred at room temperature for 15min then methylamine hydrochloride (25mg, 0.37mmol) was added. The reaction was stirred for overnight at room temperature then was quenched with ammonium chloride saturated water solution. The mixture is washed with ethyl acetate and the organic layer is dried over Na_2SO_4, filtered and solvent removed under reduced pressure. The crude product is purified by preparative HPLC system to afford **UCAB#426** (14mg, 25%) as white solid. LC-MS $[M-H]^-$ found 395.2, tR: 2.54min, UV 254nm 97%. 1H NMR (600 MHz, DMSO-d6) δ 10.59 (s, 1H), 7.86 (q, J = 4.6 Hz, 1H), 7.84 (s, 1H), 7.81 – 7.75 (m, 2H), 7.67 – 7.59 (m, 1H), 7.55 (dd, J = 8.4, 7.0 Hz, 2H), 7.39 (t, J = 8.1 Hz, 1H), 7.26 (t, J = 2.1 Hz, 1H), 7.23 (dd, J = 7.7, 2.0 Hz, 1H), 7.18 (dd, J = 8.1, 2.1 Hz, 1H), 2.73 (d, J = 4.5 Hz, 3H), 1.85 (tt, J = 8.5, 5.4 Hz, 1H), 0.69 – 0.59 (m, 2H), 0.38 – 0.28 (m, 2H). 13C NMR (151 MHz, DMSO-d6) δ 162.68, 143.79, 139.90, 139.52, 139.22, 138.18, 133.08, 129.78, 129.34, 126.62, 120.53, 119.16, 118.19, 116.18, 25.77, 7.89, 6.89.

1-(3-bromophenyl)-5-cyclopropyl-1H-pyrazole-4-carboxylic acid (104).

Intermediate **103** (120mg, 0.36mmol) dissolved in ethanol and water (2:1) then sodium hydroxide was added (100mg, 2.5mmol). Reaction stirred at room temperature overnight. Reaction acidified with HCl 37% and washed with ethyl acetate. Organic layer collected

dried over sodium sulphate, filtered and solvent removed under reduced pressure to give **104** (110mg 100%) as white solid. LC-MS $[M-H]^-$ found 305.0 + 307.0 (1:1 ratio, Br signal) , tR: 2.99min, UV 254nm 100%. Compound used without any further purification.

1-(3-bromophenyl)-5-cyclopropyl-N-methoxy-N-methyl-1H-pyrazole-4-carboxamide (105).

Compound **104** (700mg, 2.28mmol), EDC hydrochloride (650mg, 3.39mmol) and HOBt (460mg, 3.40mmol) are dissolved in degased DMF (5ml) at 0°C then DiPEA is added (1.34g, 10.35mmol). The mixture is stirred 1.5h at 0°C under nitrogen then N,O-dimethylhydroxylamine hydrochloride is added (450mg, 4.61mmol). Mixture stirred overnight at room temperature. Reaction quenched with HCl 2M and extracted with ethyl acetate. Organic layer washed with NaHCO3 and brine then dried over sodium sulphate, filtered and solvent removed. Crude mixture purified with flash chromatography (SiO2, DCM/MeOH) to afford **105** (760mg, 94%) as orange oil. LC-MS $[M+H]^+$ found 350.1 + 352.1 (1:1 ratio, Br signal), tR: 3.13 min, UV 254nm 100%.

1-(1-(3-bromophenyl)-5-cyclopropyl-1H-pyrazol-4-yl)-2,2,2-trifluoroethanone (106).

Starting material **105** (650mg, 1.86mmol) is dissolved in dry THF at 0°C with cesium fluoride (250mg, 1.7mmol), then TMS-CF3 (800mg, 5.6mmol) was added dropwise under nitrogen. Mixture stirred at room temperature 18h then 10ml of HCl 2M were added and stirred 30min at room temperature. Reaction mixture diluted with ethyl acetate, organic layer collected and dried over sodium sulphate, filtered and solvent removed under reduced pressure. Crude mixture purified with flash chromatography (SiO2, He pt/EtOAc) to afford **106** (490mg, 73%) as yellow oil. LC-MS $[M+H]^+$ found 359.0 + 361.0 (1:1 ratio, Br signal), tR: 3.97min, UV 254nm 100%.

1-(1-(3-bromophenyl)-5-cyclopropyl-1H-pyrazol-4-yl)-2,2,2-trifluoroethanol (107).

Compound **106** (80mg, 0.22mmol) is dissolved in THF (1ml +0.4ml of EtOH) at 0°C then NaBH4 is added (30mg, 0.8mmol). Mixture stirred at 0°C under nitrogen 4h then the reaction is quenched with NaHCO3 and extracted with ethyl acetate. Organic layer collected and dried over sodium sulphate, filtered and solvent removed to give **107** (70mg, 88%) of colourless oil. LC-MS $[M+H]^+$ found 361.1 + 363.1 (1:1 ratio, Br signal), tR: 2.48min, UV 254nm 96%. Compound used without any further purification.

N-(3-(5-cyclopropyl-4-(2,2,2-trifluoro-1-hydroxyethyl)-1H-pyrazol-1-yl)phenyl)benzenesulfonamide (UCAB#481).

A solution of **107** (70mg, 0.19mmol) in degased DMF (1ml) was added to a dry vial previously charged with benzensulfonamide (40mg, 0.25mmol), copper iodide (10mg, 0.05mmol), N,N-dimethylglycine (5mg, 0.05mmol) and potassium phosphate (110mg, 0.51mmol) under nitrogen. The mixture was stirred at 160°C for 4h then was cooled to room temperature and diluted with ethyl acetate. The mixture was then washed with ammonium chloride saturated solution and brine, organic layer dried over Na_2SO_4 filtered

and solvent removed under reduced pressure. . The crude product is purified by preparative HPLC system to afford **UCAB#481** (35mg, 42%) as white solid. LC-MS; $[M-H]^-$ found 436.2 tR: 3.04min, UV 254nm 100%. 1H NMR (600 MHz, DMSO-d6) δ 10.55 (s, 1H), 7.78 (dd, J = 5.2, 3.4 Hz, 2H), 7.66 – 7.59 (m, 2H), 7.55 (t, J = 7.6 Hz, 2H), 7.37 (t, J = 8.0 Hz, 1H), 7.31 – 7.22 (m, 2H), 7.21 – 7.12 (m, 1H), 5.13 (q, J = 7.4 Hz, 1H), 1.76 (tt, J = 8.4, 5.5 Hz, 1H), 0.79 (tdd, J = 8.8, 6.2, 4.4 Hz, 1H), 0.64 – 0.52 (m, 1H), 0.39 (td, J = 9.9, 5.7 Hz, 1H), 0.06 (td, J = 10.0, 5.7 Hz, 1H). ^{13}C NMR (151 MHz, DMSO-d_6) δ 141.84, 139.98, 139.26, 138.50, 138.15, 133.05, 129.66, 129.32, 126.61, 119.98, 118.73, 116.85, 115.74, 63.49 (q, *J* = 31.8 Hz), 6.33, 6.28, 5.34.

2-(1-(3-bromophenyl)-5-cyclopropyl-1H-pyrazol-4-yl)-1,1,1,3,3,3-hexafluoropropan-2-ol (108).

Intermediate **106** (490mg, 1.36mmol) is dissolved in dry THF (1.2ml) at 0°C with cesium fluoride (290mg, 1.9mmol), then TMS-CF3 (750mg, 5.3mmol) was added dropwise under nitrogen. Mixture stirred at room temperature 24h then 10ml of HCl 2M were added and stirred 1h at room temperature. Reaction mixture diluted with ethyl acetate, organic layer collected and dried over sodium sulphate, filtered and solvent removed under reduced pressure. Crude mixture purified with flash chromatography (SiO2, Hept/EtOAc) to afford **108** (350mg, 60%) as white solid. LC-MS $[M+H]^+$ found 429.1 + 431.1 (1:1 ratio, Br signal), tR: 3.77min, UV 254nm 97%. ^{1}H NMR (600 MHz, DMSO-d_6) δ 8.34 (s, 1H), 7.78 (t, *J* = 2.0 Hz, 1H), 7.68 (ddd, *J* = 8.1, 2.0, 0.9 Hz, 2H), 7.59 (ddd, *J* = 8.1, 2.1, 1.0 Hz, 1H), 7.49 (t, *J* = 8.0 Hz, 1H), 2.10 (tt, *J* = 8.5, 5.6 Hz, 1H), 0.82 – 0.73 (m, 2H), 0.43 – 0.31 (m, 2H).

N-(3-(5-cyclopropyl-4-(2,2,2-trifluoroacetyl)-1H-pyrazol-1-yl)phenyl)benzenesulfonamide (109).

A solution of **108** (200mg, 0.47mmol) in degased DMF (3ml) was added to a dry vial previously charged with benzensulfonamide (100mg, 0.64mmol), copper iodide (20mg, 0.10mmol), N,N-dimethylglycine (10mg, 0.10mmol) and potassium phosphate (280mg, 1.32mmol) under nitrogen. The mixture was stirred at 160°C for 4h then was cooled to oom temperature and diluted with ethyl acetate. The mixture was then washed with ammonium chloride saturated solution and brine, organic layer dried over Na_2SO_4 filtered and solvent removed under reduced pressure. The crude product is purified by preparative HPLC system to afford **109** (80mg, 39%) as white solid. LC-MS; $[M-H]^-$ found 434.2 tR: 3.57min, UV 254nm 100%.

N-(3-(5-cyclopropyl-4-(1,1,1,3,3,3-hexafluoro-2-hydroxypropan-2-yl)-1H-pyrazol-1-yl)phenyl) benzenesulfonamide (UCAB#506).

Intermediate **109** (80mg, 0.18mmol) is dissolved in dry THF (1.2ml) at 0°C with cesium fluoride (60mg, 0.39mmol), then TMS-CF3 (165mg, 1.16mmol) was added dropwise under nitrogen. Mixture stirred at room temperature 24h then 10ml of HCl 2M were added and stirred 1h at room temperature. Reaction mixture diluted with ethyl acetate, organic

layer collected and dried over sodium sulphate, filtered and solvent removed under reduced pressure. Crude mixture purified with preparative HPLC to afford **UCAB#506** (38mg, 41%) as white solid. LC-MS $[M-H]^-$ found 504.2, tR: 3.40min, UV 254nm 100%. ^{1}H NMR (600 MHz, DMSO-d_6) δ 10.60 (s, 1H), 8.29 (s, 1H), 7.79 (d, *J* = 7.8 Hz, 2H), 7.67 – 7.59 (m, 2H), 7.55 (t, *J* = 7.5 Hz, 2H), 7.38 (t, *J* = 8.2 Hz, 1H), 7.20 (d, *J* = 13.0 Hz, 3H), 1.97 – 1.75 (m, 1H), 0.51 (d, *J* = 8.1 Hz, 2H), 0.19 (d, *J* = 5.2 Hz, 2H). ^{13}C NMR (151 MHz, DMSO-d_6) δ 143.72, 140.28, 139.21, 138.33, 138.09, 133.11, 129.73, 129.34, 126.66, 123.04 (d, *J* = 289.4 Hz), 121.13, 119.40, 116.83, 111.42, 75.45 (p, *J* = 29.9 Hz), 8.48, 6.94.

1-(3-bromophenyl)-5-cyclopropyl-1H-pyrazole-4-carbohydrazide (110).
Intermediate **104** (200mg, 0.65mmol), EDC hydrochloride (190mg, 1.00mmol) and HOBt (135mg, 1mmol) are dissolved in degased DMF (5ml) at 0°C then DiPEA is added (420mg, 3.24mmol). The mixture is stirred 1.5h at 0°C under nitrogen then hydrazine hydrochloride is added (135mg, 1.29mmol). Mixture stirred overnight at room temperature. The reaction is diluted with NaHCO3 water solution and extracted with ethyl acetate. Organic layer washed with brine and dried over sodium sulphate, then filtered and solvent removed to afford **110** (150mg, 72%) as orange oil. LC-MS $[M+H]^+$ found 321.1, tR: 2.33min, UV 254nm 97%. Compound used without any further purification.

5-(1-(3-bromophenyl)-5-cyclopropyl-1H-pyrazol-4-yl)-1,3,4-oxadiazol-2-ol (111).
Compound **110** (100mg, 0.31mmol) is dissolved in 3ml of DCM at 0°C under nitrogen then triphosgene (140mg, 0.47mmol) is dropwise added. The mixture is stirred overnight. The reaction is diluted with ethyl acetate and washed with HCl 1M and the with brine. The organic layer is collected and dried over sodium sulphate, filtered and solvent removed. Crude mixture was purified with flash chromatography (SiO2, DCM/MeOH) to afford **111** (60mg, 54%)as a white solid. LC-MS; $[M+H]^+$ found 347.0 + 349.0 (1:1 signal ratio, Br). tR: 2.34min, UV 254nm 100%.

N-(3-(5-cyclopropyl-4-(5-hydroxy-1,3,4-oxadiazol-2-yl)-1H-pyrazol-1-yl)phenyl)-benzenesulfonamide (UCAB#482).
A solution of **111** (80mg, 0.23mmol) in degased DMF (1ml) was added to a dry vial previously charged with benzensulfonamide (45mg, 0.29mmol), copper iodide (9mg, 0.05mmol), N,N-dimethylglycine (5mg, 0.05mmol) and potassium phosphate (120mg, 0.57mmol) under nitrogen. The mixture was stirred at 160°C for 24h then was cooled to room temperature and diluted with ethyl acetate. The mixture was then washed with ammonium chloride saturated solution and brine, organic layer dried over Na_2SO_4 filtered and solvent removed under reduced pressure. . The crude product is purified by preparative HPLC system to afford **UCAB#482** (8mg, 7%) as white solid. LC-MS; $[M+H]^+$ found 424.0 tR: 2.70min, UV 254nm 100%. 1H NMR (600 MHz, DMSO-d6) δ 12.40 (s, 6H), 10.77 – 10.40 (m, 5H), 7.98 (s, 1H), 7.79 (d, J = 7.4 Hz, 2H), 7.66 – 7.59 (m, 1H), 7.59 – 7.52 (m, 2H), 7.45 – 7.37 (m, 2H), 7.30 (d, J = 7.0 Hz, 2H), 7.20 (d, J = 8.7 Hz, 1H), 1.94 – 1.85 (m, 2H), 0.75 – 0.65 (m, 2H), 0.36 – 0.26 (m, 2H). 13C NMR (151 MHz, DMSO-d6) δ 154.36,

149.69, 143.28, 139.47, 139.18, 138.79, 138.28, 133.09, 129.79, 129.34, 126.65, 120.46, 119.42, 116.06, 107.54, 7.89, 6.37.

N-(3-(4-cyano-5-cyclopropyl-1H-pyrazol-1-yl)phenyl)benzenesulfonamide (112).
UCAB#419 (100mg, 0.26mmol) is dissolved in DMF (2.5ml) at 0°C then thionyl chloride (80mg, 0.67mmol) is added dropwise. The mixture is stirred at 0°C for 30min then the reaction is quenched with NaHCO3. The mixture is extracted with ethyl acetate, the organic layer is collected and dried over sodium sulphate, filtered and solvent removed under reduced pressure to give **GM01-68** (90mg, 94%) as yellow oil. LC-MS; $[M+H]^+$ found 365.2, tR: 3.19min, UV 254nm 90%. Compound used without any further purification.

N-(3-(5-cyclopropyl-4-(1H-tetrazol-5-yl)-1H-pyrazol-1-yl)phenyl)benzenesulfonamide (UCAB#468).
Compound **112** (90mg, 0.25mmol) and TBAF (40mg, 0.15mmol) are placed in a dry bottom flask under nitrogen, then TMS-Azide (65mg, 0.56mmol) is added. The neat mixture is stirred ad 100°C overnight for 22h. The mixture is diluted with HCl 2M and washed with ethyl acetate. Organic layer collected and dried over sodium sulphate, filtered and solvent removed under reduced pressure. The crude compound is purified by preparative HPLC system to afford **UCAB#468** (30mg, 29%) as white solid. LC-MS; $[M-H]^-$ found 406.2, tR: 2.65min, UV 254nm 100%. ^{1}H NMR (600 MHz, DMSO-d_6) δ 10.63 (s, 1H), 8.07 (s, 1H), 7.83 – 7.78 (m, 2H), 7.65 – 7.60 (m, 1H), 7.59 – 7.54 (m, 2H), 7.43 (t, J = 8.0 Hz, 1H), 7.37 – 7.32 (m, 2H), 7.21 (ddd, J = 8.2, 2.1, 1.0 Hz, 1H), 2.02 (tt, J = 8.4, 5.4 Hz, 1H), 0.74 – 0.69 (m, 2H), 0.19 – 0.14 (m, 2H). ^{13}C NMR (151 MHz, DMSO-d_6) δ 143.28, 140.14 – 138.78 (m), 138.28, 133.11, 129.87, 129.35, 126.64, 120.32, 119.30, 115.93, 7.86, 6.52.

5-cyclopropyl-1-(3-(2,3,5,6-tetramethylphenylsulfonamido)phenyl)-1H-pyrazole-4-carboxylic acid (113).
A solution of **104** (650mg, 2.12mmol) in degased DMF (5.5ml) was added to a dry vial previously charged with 2,3,5,6-tetramethylbenzenesulfonamide (JP04-116: 550mg, 2.58mmol synthesised from 2,3,5,6-tetramethylbenzene-1-sulfonyl chloride treated with aqueous ammonia), copper iodide (80mg, 0.42mmol), N,N-dimethylglycine (45mg, 0.44mmol) and potassium phosphate (1.30gr, 6.12mmol) under nitrogen. The mixture was stirred at 150°C overnight for 24h then was cooled to room temperature and diluted with ethyl acetate. The mixture was then washed with ammonium chloride saturated solution and brine, organic layer dried over Na_2SO_4 filtered and solvent removed under reduced pressure. Crude mixture was purified with flash chromatography (SiO2, Hept/EtOAc) to afford **113** as a white solid (250mg, 27%). LC-MS; $[M+H]^+$ found 440.2, tR: 3.17min, UV 254nm 80%.

1-(3-(N-(2-amino-2-oxoethyl)-2,3,5,6-tetramethylphenylsulfonamido)phenyl)-5-cyclopropyl-1H-pyrazole-4-carboxylic acid (UCAB#529).
Compound **113** (250mg, 0.57mmol) is dissolved in DMF at 0°C then TBSDMSiCl and Imidazole were added. The reaction is stirred at room temperature overnight for 20h. The

mixture is then diluted with ethyl acetate and washed with brine then dried over sodium suplphate, filtered and solvent removed under reduced pressure. The crude mixture is dissolved in dry THF at 0°C then sodium hydride (35mg, 1.46mmol) is added and the reaction is stirred for 30min at 0°C under nitrogen atmosphere. Then 2-bromo-acetamide (220mg, 1.59mmol) was added and the mixture is stirred for 3h at 0°C. The reaction is then quenched with NaHCO3 and extracted with ethyl acetate. Organic layer is collected and dried over sodium sulphate, filtered and solvent removed. Crude compound purified by flash chromatography (Si_2O, DCM/MeOH eluent system) to afford **UCAB#529** (50mg, 18%) as yellow solid. LC-MS; $[M+H]^+$ found 497.2, tR: 2.89min, UV 254nm 100%. ^{1}H NMR (600 MHz, DMSO-d_6) δ 12.12 (s, 2H), 7.92 (d, *J* = 2.6 Hz, 1H), 7.54 – 7.43 (m, 3H), 7.33 (d, *J* = 7.6 Hz, 2H), 7.25 (s, 1H), 7.09 (s, 1H), 4.35 (d, *J* = 2.0 Hz, 2H), 2.31 (s, 6H), 2.18 (s, 7H), 1.94 – 1.84 (m, 5H), 0.80 – 0.63 (m, 2H), 0.49 – 0.31 (m, 2H). ^{13}C NMR (151 MHz, DMSO-d_6) δ 171.96, 168.59, 163.71, 147.04, 142.03, 139.83, 139.45, 136.39, 136.05, 135.90, 135.70, 129.23, 128.00, 125.14, 124.34, 114.24, 50.36 (d, *J* = 424.1 Hz), 21.03, 20.49, 17.53, 8.03, 6.79.

Ethyl 5-cyclopropyl-1-(3-(2,3,5,6-tetramethylphenylsulfonamido)phenyl)-1H-pyrazole-4-carboxylate (114).

A solution of **103** (650mg, 1.94mmol) in degased DMF (5ml) was added to a dry vial previously charged with 2,3,5,6-tetramethylbenzenesulfonamide (JP04-116: 550mg, 2.58mmol synthesised from 2,3,5,6-tetramethylbenzene-1-sulfonyl chloride treated with aqueous ammonia), copper iodide (77mg, 0.40mmol), N,N-dimethylglycine (50mg, 0.48mmol) and potassium phosphate (1.00gr, 4.71mmol) under nitrogen. The mixture was stirred at 150°C overnight for 24h then was cooled to room temperature and diluted with ethyl acetate. The mixture was then washed with ammonium chloride saturated solution and brine, organic layer dried over Na_2SO_4 filtered and solvent removed under reduced pressure. Crude mixture was purified with flash chromatography (SiO2, Hept/EtOAc) to afford **114** as a white solid (900mg, 99%). LC-MS; $[M+H]^+$ found 468.2, tR: 3.87min, UV 254nm 94%

Ethyl 5-cyclopropyl-1-(3-(N-(2-ethoxy-2-oxoethyl)-2,3,5,6-tetramethylphenylsulfonamido)phenyl)-1H-pyrazole-4-carboxylate (115).

Compound **114** (450mg, 0.96mmol) is dissolved in dry THF at 0°C then sodium hydride (46mg, 1.92mmol) is added and mixture stirred for 1h at 0°C under nitrogen atmosphere. Ethyl 2-bromoacetate (485mg, 2.90mmol) is then added and the reaction was stirred at room temperature overnight for 20h. Reaction quenched with NaHCO3 and extracted with ethyl acetate. Organic layer collected and dried over sodium sulphate, filtered and solvent removed. Crude compound purified by flash chromatography (Si_2O, Hept/EtOAc) to afford **115** (370mg, 70%). LC-MS; $[M+H]^+$ found 554.3, tR: 4.11min, UV 254nm 95%. ^{1}H NMR (600 MHz, DMSO-d_6) δ 7.97 (d, *J* = 2.2 Hz, 1H), 7.54 – 7.46 (m, 3H), 7.42 – 7.32 (m, 1H), 7.26 (s, 1H), 4.63 (d, *J* = 2.3 Hz, 3H), 4.24 (qd, *J* = 7.1, 2.2 Hz, 2H), 4.05 (qd, *J* = 7.2, 2.1 Hz, 3H), 2.31 (d, *J* = 2.4 Hz, 6H), 2.18 (d, *J* = 2.2 Hz, 6H), 1.94 (ttd, *J* = 8.4, 5.6, 2.2 Hz, 1H), 1.29 (td, *J* = 7.1, 2.2 Hz, 3H), 1.12 (td, *J* = 7.1, 2.2 Hz, 3H), 0.75 – 0.68 (m, 2H), 0.34 (dd, *J* = 5.6, 2.4 Hz, 2H).

1-(3-(N-(carboxymethyl)-2,3,5,6-tetramethylphenylsulfonamido)phenyl)-5-cyclopropyl-1H-pyrazole-4-carboxylic acid (UCAB#534).

Starting material **115** (370mg, 0.67mmol) dissolved in ethanol and water (2:1) then sodium hydroxide was added (115mg, 2.88mmol). Reaction stirred at room temperature overnight. Reaction acidified with HCl 37% and washed with ethyl acetate. Organic layer collected dried over sodium sulphate, filtered and solvent removed under reduced pressure. Crude mixture purified by preparative HPLC system to afford **UCAB#534** (30mg, 18%) as white solid. %). LC-MS; $[M+H]^+$ found 498.2, tR: 3.05min, UV 254nm 100%. ^{1}H NMR (600 MHz, DMSO-d_6) δ 12.64 (s, 1H), 7.92 (d, *J* = 1.7 Hz, 1H), 7.56 – 7.43 (m, 3H), 7.36 (dd, *J* = 7.5, 1.5 Hz, 1H), 7.25 (s, 1H), 4.55 (s, 2H), 2.31 (s, 6H), 2.18 (s, 6H), 1.96 – 1.82 (m, 1H), 0.80 – 0.61 (m, 2H), 0.39 (d, *J* = 5.3 Hz, 2H). ^{13}C NMR (151 MHz, DMSO-d_6) δ 169.81, 163.72, 147.04, 142.07, 139.71, 139.54, 136.44, 136.13, 135.90, 135.75, 129.39, 128.03, 125.06, 124.47, 114.32, 50.98, 20.48, 17.48, 8.02, 6.77.

1-(3-bromophenyl)-5-cyclopropyl-1H-pyrazole-4-carboxamide (116).

Compound **104** (1,00gr, 3.26mmol), EDC hydrochloride (960mg, 5.00mmol), HOBt (680mg, 5.03mmol) were dissolved in DMF (7ml) at 0°C then DiPEA (1.30gr, 10mmol) was added. Mixture stirred at 0°C for 1.5h then ammonium chloride (360mg, 6.73mmol) was added and reaction stirred at room temperature overnight for 22h. Reaction quenched with HCl 2M, and mixture extracted with ethyl acetate. Organic layer washed with NaHCO3 saturated water solution, brine and then dried over sodium sulphate, filtered and solvent removed under reduced pressure to give **116** (850mg, 85%) as pale yellow solid. LC-MS; $[M+H]^+$ found 306.0 + 308.0 (1:1 ratio, Br signal), tR: 1.96min, UV 254nm 100%. Compound used without any further purification.

1-(3-bromophenyl)-5-cyclopropyl-1H-pyrazole-4-carbonitrile (117).

Compound **116** (800mg, 2.61mmol) is dissolved in DMF (6ml) at 0°C then thionyl chloride (775mg, 6.52mmol) is added dropwise. The mixture is stirred at 0°C for 30min then the reaction is quenched with NaHCO3. The mixture is extracted with ethyl acetate, the organic layer is collected and dried over sodium sulphate, filtered and solvent removed under reduced pressure to give **117** (700mg, 93%) as yellow oil. LC-MS; $[M+H]^+$ found 288.0 + 290.0 (1:1 ratio, Br signal), tR: 3.56min, UV 254nm 10%. ^{1}H NMR (600 MHz, Chloroform-*d*) δ 7.83 (s, 1H), 7.75 (d, *J* = 2.1 Hz, 1H), 7.60 (dd, *J* = 8.0, 1.9 Hz, 1H), 7.51 (dd, *J* = 8.0, 2.1 Hz, 1H), 7.39 (t, *J* = 8.0 Hz, 1H), 1.89 (tt, *J* = 8.6, 5.3 Hz, 1H), 1.20 – 1.07 (m, 5H). ^{13}C NMR (151 MHz, Chloroform-*d*) δ 150.21, 142.97, 139.70, 132.16, 130.63, 128.53, 123.87, 122.88, 113.62, 91.43, 8.42, 7.89. Compound used without any further purification.

N-(3-(4-cyano-5-cyclopropyl-1H-pyrazol-1-yl)phenyl)-2,3,5,6-tetramethylbenzenesulfonamide (118).

A solution of **117** (610mg, 2.12mmol) in degased DMF (5.5ml) was added to a dry vial previously charged with 2,3,5,6-tetramethylbenzenesulfonamide (JP04-116: 590mg, 2.77mmol synthesised from 2,3,5,6-tetramethylbenzene-1-sulfonyl chloride treated with aqueous ammonia), copper iodide (80mg, 0.42mmol), N,N-dimethylglycine (45mg, 0.44mmol) and potassium phosphate (1.10gr, 5.18mmol) under nitrogen. The mixture was stirred at 150°C overnight for 24h then was cooled to room temperature and diluted with ethyl acetate. The mixture was then washed with ammonium chloride saturated solution and brine, organic layer dried over Na_2SO_4 filtered and solvent removed under reduced pressure. Crude mixture was purified with flash chromatography (SiO2, Hept/EtOAc) to afford **118** as a white solid (750mg, 84%). LC-MS $[M-H]^-$ found 419.2, tR: 3.71min, UV 254nm 100%. ^{1}H NMR (600 MHz, DMSO-d_6) δ 10.61 (s, 1H), 8.14 (s, 1H), 7.39 (t, *J* = 8.1 Hz, 1H), 7.26 – 7.20 (m, 2H), 7.14 (t, *J* = 2.2 Hz, 1H), 7.04 (dd, *J* = 8.3, 2.1 Hz, 1H), 2.48 (s, 6H), 2.19 (s, 6H), 1.81 (tt, *J* = 8.5, 5.3 Hz, 1H), 0.90 – 0.86 (m, 2H), 0.81 – 0.77 (m, 2H). ^{13}C NMR (151 MHz, DMSO-d_6) δ 149.72, 142.63, 138.67 (d, *J* = 5.3 Hz), 137.64, 135.78, 135.61, 134.64, 130.00, 119.43, 118.31, 114.63, 113.74, 90.74, 59.72, 20.37, 17.48, 7.17, 6.86.

Ethyl-2-(N-(3-(4-cyano-5-cyclopropyl-1H-pyrazol-1-yl)phenyl)-2,3,5,6-tetramethylphenylsulfonamido) acetate (119).

Compound **118** (350mg, 00.83mmol) is dissolved in dry THF at 0°C then sodium hydride (45mg, 1.88mmol) is added and mixture stirred for 1h at 0°C under nitrogen atmosphere. Ethyl 2-bromoacetate (420mg, 2.51mmol) is then added and the reaction was stirred at room temperature overnight for 20h. Reaction quenched with NaHCO3 and extracted with ethyl acetate. Organic layer collected and dried over sodium sulphate, filtered and solvent removed to give **119** (400mg, 95%). LC-MS; $[M+H]^+$ found 507.2, tR: 3.99min, UV 254nm 100%. ^{1}H NMR (600 MHz, DMSO-d_6) δ 8.17 (d, *J* = 1.4 Hz, 1H), 7.62 – 7.50 (m, 3H), 7.42 (dt, *J* = 7.8, 1.7 Hz, 1H), 7.26 (s, 1H), 4.63 (s, 2H), 4.15 (t, *J* = 7.1 Hz, 2H), 2.29 (s, 7H), 2.18 (s, 7H), 1.82 (tt, *J* = 8.3, 5.3 Hz, 1H), 1.21 (t, *J* = 7.1 Hz, 3H), 0.89 (dt, *J* = 8.5, 3.2 Hz, 2H), 0.82 (dt, *J* = 5.6, 3.1 Hz, 2H). ^{13}C NMR (151 MHz, DMSO-d_6) δ 168.38 (d, *J* = 3.3 Hz), 167.17, 149.90, 142.74, 139.81, 138.50, 136.18, 136.13, 135.97, 135.80, 129.89, 128.86, 125.04, 124.52, 113.69, 90.76, 61.63, 51.12, 20.44, 17.44, 13.85, 7.17, 6.78.

Ethyl 2-(N-(3-(5-cyclopropyl-4-(1H-tetrazol-5-yl)-1H-pyrazol-1-yl)phenyl)-2,3,5,6-tetramethyl-phenylsulfonamido) acetate (120).

Compound **119** (450mg, 0.89mmol) and TBAF (140mg, 0.50mmol) are placed in a dry bottom flask under nitrogen, then TMS-Azide (210mg, 1.82mmol) is added. The neat mixture is stirred ad 100°C overnight for 24h. The mixture is diluted with HCl 2M and washed with ethyl acetate. Organic layer collected and dried over sodium sulphate, filtered and solvent removed under reduced pressure. The crude compound is purified by flash chromatography (Si2O, DCM/MeOH) to afford **120** (260mg, 53%) as yellow oil. LC-MS; $[M+H]^+$ found 550.3, tR: 3.53min, UV 254nm 98%. ^{1}H NMR (600 MHz, Chloroform-*d*) δ 8.20 (s, 1H), 8.06 (s, 1H), 7.73 (d, *J* = 2.1 Hz, 1H), 7.56 – 7.52 (m, 1H), 7.41 (t, *J* = 8.0 Hz, 1H), 7.30 – 7.27 (m, 1H), 7.14 (s, 1H), 4.53 (s, 2H), 4.11 (q, *J* = 7.1 Hz, 2H), 2.39 (s, 6H), 2.22 (d, *J* = 3.5 Hz, 7H), 1.20 (t, *J* = 7.1 Hz, 3H), 1.04 – 0.95 (m, 2H), 0.35 (dt, *J* = 6.5, 3.3 Hz, 2H).

^{13}C NMR (151 MHz, Chloroform-*d*) δ 168.79, 149.48, 143.86, 140.41, 140.00, 139.85, 136.91, 136.80, 136.24, 136.16, 129.90, 129.39, 126.31, 124.76, 107.54, 61.79, 52.08, 21.18, 18.06, 14.18, 8.56, 6.70.

2-(N-(3-(5-cyclopropyl-4-(1H-tetrazol-5-yl)-1H-pyrazol-1-yl)phenyl)-2,3,5,6-tetramethylphenylsulfonamido)acetic acid (UCAB#535)

Sodium hydroxide (60mg, 1.5mmol) is added to a solution of **120** (260mg, 0.47mmol) in ethanol/water (1:1). The reaction is stirred at room temperature for 8h then the solvent is removed under reduced pressure. The crude mixture is acidified with HCl 37% and extracted with ethyl acetate. Organic layer is collected and dried over sodium sulphate, filtered and solvent removed under reduced pressure. The crude is purified by preparative HPLC to afford **UCAB#535** (35mg, 27%) as white solid. LC-MS; $[M+H]^+$ found 522.2, tR: 3.03min, UV 254nm 100%. ^{1}H NMR (600 MHz, DMSO-d_6) δ 8.10 (s, 1H), 7.63 (t, *J* = 1.9 Hz, 1H), 7.60 – 7.55 (m, 1H), 7.50 (t, *J* = 8.0 Hz, 1H), 7.35 (dd, *J* = 8.1, 1.0 Hz, 1H), 7.26 (s, 1H), 4.56 (s, 2H), 2.32 (s, 7H), 2.19 (s, 6H), 2.07 (ddd, *J* = 13.9, 8.4, 5.5 Hz, 1H), 0.80 – 0.72 (m, 2H), 0.22 – 0.13 (m, 2H). ^{13}C NMR (151 MHz, DMSO-d_6) δ 169.81, 143.43, 139.77, 139.41 (d, *J* = 4.1 Hz), 136.44, 136.13, 135.89, 135.74, 129.49, 127.85, 124.64, 123.99, 51.00, 20.47, 17.48, 7.84, 6.35.

2-(N-(3-(5-cyclopropyl-4-(1H-tetrazol-5-yl)-1H-pyrazol-1-yl)phenyl)-2,3,5,6-tetramethylphenylsulfonamido)- acetamide (UCAB#538).

UCAB#535 (50mg, 0.10mmol), EDC hydrochloride (30mg, 0.16mmol), HOBt (25mg, 0.19mmol) were dissolved in DMF (4ml) at 0°C then DiPEA (55mg, 0.42mmol) was added. Mixture stirred at 0°C for 1.5h then ammonium chloride (360mg, 6.73mmol) was added and reaction stirred at room temperature overnight for 22h. Reaction quenched with HCl 6M, and mixture extracted with ethyl acetate. Organic layer dried over sodium sulphate, filtered and solvent removed under reduced pressure. Crude mixture purified by preparative HPLC to give **UCAB#538** (20mg, 38%) as white solid. . LC-MS; $[M+H]^+$ found 521.2, tR: 2.89min, UV 254nm 100%. ^{1}H NMR (600 MHz, DMSO-d_6) δ 8.10 (s, 1H), 7.63 (t, *J* = 2.1 Hz, 1H), 7.57 (d, *J* = 8.0 Hz, 1H), 7.48 (t, *J* = 8.0 Hz, 1H), 7.35 (s, 1H), 7.32 (d, *J* = 8.0 Hz, 1H), 7.26 (s, 1H), 7.10 (s, 1H), 4.36 (s, 2H), 2.32 (s, 7H), 2.19 (s, 7H), 2.07 (td, *J* = 8.4, 4.3 Hz, 1H), 0.79 (h, *J* = 5.0 Hz, 2H), 0.19 (t, *J* = 5.6 Hz, 2H). ^{13}C NMR (151 MHz, DMSO-d_6) δ 168.63, 143.45, 139.92, 139.37 (d, *J* = 11.7 Hz), 136.42, 136.08, 135.93, 135.71, 129.36, 127.84, 124.82, 123.88, 51.84, 20.50, 17.55, 7.88, 6.40.

7 References

(1) Fischer, E.; Krebs, E. Conversion of Phorphorylase A to Phosphorylase B in Muscle Extracts. *J. Biol. Chem.* **1955**, *216*, 121–132.

(2) Manning, G.; Whyte, D. B.; Martinez, R.; Hunter, T.; Sudarsanam, S. The Protein Kinase Complement of the Human Genome. *Science (80-.).* **2002**, *298* (5600), 1912–1934.

(3) Hanks, S.; Hunter, T. The Eukaryotic Protein Kinase Supefamily: Kinase (Catalytic) Domain Structure and Classification. *FASEB J.* **1995**, *9*, 576–596.

(4) Ardito, F.; Giuliani, M.; Perrone, D.; Troiano, G.; Muzio, L. Lo. The Crucial Role of Protein Phosphorylation in Cell Signalingand Its Use as Targeted Therapy (Review). *Int. J. Mol. Med.* **2017**, *40* (2), 271–280.

(5) Hunter, T. Protein Kinases and Phosphatases: The Yin and Yang of Protein Phosphorylation and Signaling. *Cell* **1995**, *80* (2), 225–236.

(6) Hanahan, D.; Weinberg, R. A. Hallmarks of Cancer: The Next Generation. *Cell* **2011**, *144* (5), 646–674. https://doi.org/10.1016/J.CELL.2011.02.013.

(7) Cohen, P. Protein Kinases — the Major Drug Targets of the Twenty-First Century? *Nat. Rev. Drug Discov.* **2002**, *1* (4), 309–315.

(8) Daley, G.; Etten, R. Van; Baltimore, D. Induction of Chronic Myelogenous Leukemia in Mice by the P210bcr/Abl Gene of the Philadelphia Chromosome. *Science (80-.).* **1990**, *247* (4944), 824–830.

(9) Libermann, T. A.; Nusbaum, H. R.; Razon, N.; Kris, R.; Lax, I.; Soreq, H.; Whittle, N.; Waterfield, M. D.; Ullrich, A.; Schlessinger, J. Amplification, Enhanced Expression and Possible Rearrangement of EGF Receptor Gene in Primary Human Brain Tumours of Glial Origin. *Nature* **1985**, *313* (5998),

(10) Eswarakumar, V. P.; Lax, I.; Schlessinger, J. Cellular Signaling by Fibroblast Growth Factor Receptors. *Cytokine Growth Factor Rev.* **2005**, *16.*

(11) Bridges, A. J. Chemical Inhibitors of Protein Kinases. *Chem. Rev.* **2001**, *101* (8), 2541–2571.

(12) Dungo, R. T.; Keating, G. M. Afatinib: First Global Approval. *Drugs* **2013**, *73* (13), 1503–1515.

(13) Greig, S. L. Osimertinib: First Global Approval. *Drugs* **2016**, *76* (2), 263–273.

(14) Markham, A. Erdafitinib: First Global Approval. *Drugs* **2019**, *79* (9), 1017–

(15) Taylor, S. S.; Kornev, A. P. Protein Kinases: Evolution of Dynamic Regulatory Proteins. *Trends Biochem. Sci.* **2011**, *36* (2), 65–77.

(16) Madhusudan; Akamine, P.; Xuong, N.-H.; Taylor, S. S. Crystal Structure of a Transition State Mimic of the Catalytic Subunit of CAMP-Dependent Protein Kinase. *Nat. Struct. Biol.* **2002**, *9* (4), 273–277.

(17) David A. Johnson, †; Pearl Akamine, ‡; Elzbieta Radzio-Andzelm, ‡; Madhusudan, ‡ and; Susan S. Taylor*, ‡, Δ. Dynamics of CAMP-Dependent

Protein Kinase. *Chem. Rev.* **2001**, *101*, 2243–2270.
(18) Tsigelny, I.; Greenberg, J. P.; Cox, S.; Nichols, W. L.; Taylor, S. S.; Ten Eyck, L. F. 600 Ps Molecular Dynamics Reveals Stable Substructures and Flexible Hinge Points in CAMP Dependent Protein Kinase. *Biopolymers* **1999**, *50* (5), 513–524.
(19) Fabbro, D.; Cowan-Jacob, S. W.; Moebitz, H. Ten Things You Should Know about Protein Kinases: IUPHAR Review 14. *Br. J. Pharmacol.* **2015**, *172* (11), 2675–2700.
(20) Johnson, L. N.; Lowe, E. D.; Noble, M. E. .; Owen, D. J. The Structural Basis for Substrate Recognition and Control by Protein Kinases. *FEBS Lett.* **1998**, *430* (1–2), 1–11.
(21) Deminoff, S. J.; Ramachandran, V.; Herman, P. K. Distal Recognition Sites in Substrates Are Required for Efficient Phosphorylation by the CAMP-Dependent Protein Kinase. *Genetics* **2009**, *182* (2), 529–539.
(22) Henikoff, S.; Henikoff, J. G.; Eyck, L. F. Ten. Amino Acid Substitution Matrices from Protein Blocks. *Proc. Natl. Acad. Sci. U. S. A.* **1992**, *89* (22), 10915–10919.
(23) Kornev, A. P.; Haste, N. M.; Taylor, S. S.; Eyck, L. F. Ten. Surface Comparison of Active and Inactive Protein Kinases Identifies a Conserved Activation Mechanism. *Proc. Natl. Acad. Sci. U. S. A.* **2006**, *103* (47), 17783–17788.
(24) Honegger, A. M.; Kris, R. M.; Ullrich, A.; Schlessinger, J. Evidence That Autophosphorylation of Solubilized Receptors for Epidermal Growth Factor Is Mediated by Intermolecular Cross-Phosphorylation. *Proc. Natl. Acad. Sci. U. S. A.* **1989**, *86* (3), 925–929.
(25) Favelyukis, S.; Till, J. H.; Hubbard, S. R.; Miller, W. T. Structure and Autoregulation of the Insulin-like Growth Factor 1 Receptor Kinase. *Nat. Struct. Biol.* **2001**, *8* (12), 1058–1063.
(26) Till, J. H.; Becerra, M.; Watty, A.; Lu, Y.; Ma, Y.; Neubert, T. A.; Burden, S. J.; Hubbard, S. R. Crystal Structure of the MuSK Tyrosine Kinase: Insights into Receptor Autoregulation. *Structure* **2002**, *10* (9), 1187–1196.
(27) Jeffrey, P. D.; Russo, A. A.; Polyak, K.; Gibbs, E.; Hurwitz, J.; Massagué, J.; Pavletich, N. P. Mechanism of CDK Activation Revealed by the Structure of a CyclinA-CDK2 Complex. *Nature* **1995**, *376* (6538), 313–320.
(28) Filippakopoulos, P.; Kofler, M.; Hantschel, O.; Gish, G. D.; Grebien, F.; Salah, E.; Neudecker, P.; Kay, L. E.; Turk, B. E.; Superti-Furga, G.; et al. Structural Coupling of SH2-Kinase Domains Links Fes and Abl Substrate Recognition and Kinase Activation. *Cell* **2008**, *134* (5), 793–803.
(29) Yang, J.; Cron, P.; Thompson, V.; Good, V. M.; Hess, D.; Hemmings, B. A.; Barford, D. Molecular Mechanism for the Regulation of Protein Kinase B/Akt by Hydrophobic Motif Phosphorylation. *Mol. Cell* **2002**, *9* (6), 1227–1240.

(30) Schlessinger, J. Cell Signaling by Receptor Tyrosine Kinases. *Cell* **2000**, *103*, 211–225. https://doi.org/10.1016/j.cell.2010.06.011.
(31) Lemmon, M. A.; Schlessinger, J. Regulation of Signal Transduction and Signal Diversity by Receptor Oligomerization. *Trends Biochem. Sci.* **1994**, *19* (11), 459–463.
(32) Jiang, G.; Hunter, T. Receptor Signaling: When Dimerization Is Not Enough. *Curr. Biol.* **1999**, *9* (15), R568–R571.
(33) Furdui, C. M.; Lew, E. D.; Schlessinger, J.; Anderson, K. S. Autophosphorylation of FGFR1 Kinase Is Mediated by a Sequential and Precisely Ordered Reaction. *Mol. Cell* **2006**, *21* (5), 711–717.
(34) Schlessinger, J.; Lemmon, M. A. SH2 and PTB Domains in Tyrosine Kinase Signaling. *Science (80-.).* **2003**, *2003* (191), 12.
(35) Marshall, C. . Specificity of Receptor Tyrosine Kinase Signaling: Transient versus Sustained Extracellular Signal-Regulated Kinase Activation. *Cell* **1995**, *80* (2), 179–185.
(36) Lemmon, M. A.; Schlessinger, J. Cell Signaling by Receptor Tyrosine Kinases. *Cell* **2010**, *141* (7), 1117–1134.
(37) Pawson, T. Protein Modules and Signalling Networks. *Nature* **1995**, *373* (6515), 573–580.
(38) Kholodenko, B. N. Cell-Signalling Dynamics in Time and Space. *Nat. Rev. Mol. Cell Biol.* **2006**, *7* (3), 165–176.
(39) Hunter, T. The Age of Crosstalk: Phosphorylation, Ubiquitination, and Beyond. *Mol. Cell* **2007**, *28* (5), 730–738.
(40) Amit, I.; Citri, A.; Shay, T.; Lu, Y.; Katz, M.; Zhang, F.; Tarcic, G.; Siwak, D.; Lahad, J.; Jacob-Hirsch, J.; et al. A Module of Negative Feedback Regulators Defines Growth Factor Signaling. *Nat. Genet.* **2007**, *39* (4), 503–512.
(41) Futreal, P. A.; Coin, L.; Marshall, M.; Down, T.; Hubbard, T.; Wooster, R.; Rahman, N.; Stratton, M. R. A Census of Human Cancer Genes. *Nat. Rev. Cancer* **2004**, *4* (3), 177–183.
(42) Druker, B. J.; Guilhot, F.; O'Brien, S. G.; Gathmann, I.; Kantarjian, H.; Gattermann, N.; Deininger, M. W. N.; Silver, R. T.; Goldman, J. M.; Stone, R. M.; et al. Five-Year Follow-up of Patients Receiving Imatinib for Chronic Myeloid Leukemia. *N. Engl. J. Med.* **2006**, *355* (23), 2408–2417.
(43) Samuels, Y.; Wang, Z.; Bardelli, A.; Silliman, N.; Ptak, J.; Szabo, S.; Yan, H.; Gazdar, A.; Powell, S. M.; Riggins, G. J.; et al. High Frequency of Mutations of the PIK3CA Gene in Human Cancers. *Science (80-.).* **2004**, *304* (5670), 554.
(44) Hynes, N. E.; Lane, H. A. ERBB Receptors and Cancer: The Complexity of Targeted Inhibitors. *Nat. Rev. Cancer* **2005**, *5* (5), 341–354.
(45) Kaelin, W. G. The Concept of Synthetic Lethality in the Context of Anticancer Therapy. *Nat. Rev. Cancer* **2005**, *5* (9), 689–698.

(46) John (Yuan), W.; Keith, W.; Kenichi, N.; Sara, W. Recent Advances of MEK Inhibitors and Their Clinical Progress. *Curr. Top. Med. Chem.* **2007**, *7* (14), 1364–1378.
(47) Kerbel, R. S. Tumor Angiogenesis. *N. Engl. J. Med.* **2008**, *358* (19), 2039–2049.
(48) Zhang, J.; Yang, P. L.; Gray, N. S. Targeting Cancer with Small Molecule Kinase Inhibitors. *Nat. Rev. Cancer* **2009**, *9* (1), 28–39.
(49) Muhsin, M.; Graham, J.; Kirkpatrick, P. Gefitinib. *Nat. Rev. Drug Discov.* **2003**, *2* (7), 515–516. https://doi.org/10.1038/nrd1136.
(50) Zhao, G.; Li, W. -y.; Chen, D.; Henry, J. R.; Li, H.-Y.; Chen, Z.; Zia-Ebrahimi, M.; Bloem, L.; Zhai, Y.; Huss, K.; et al. A Novel, Selective Inhibitor of Fibroblast Growth Factor Receptors That Shows a Potent Broad Spectrum of Antitumor Activity in Several Tumor Xenograft Models. *Mol. Cancer Ther.* **2011**, *10* (11), 2200–2210.
(51) Kufareva, I.; Abagyan, R. Type-II Kinase Inhibitor Docking, Screening, and Profiling Using Modified Structures of Active Kinase States. *J. Med. Chem.* **2008**, *51* (24), 7921–7932.
(52) Cohen, M.; Zhang, C.; Shojat, kevan; Tauton, jack. Structural Bioinformatics-Based Design of Selective, Irreversible Kinase Inhibitors. *Sci.* **2005**, *308* (5726), 1318–1324.
(53) Garuti, L.; Roberti, M.; Bottegoni, G. Irreversible Protein Kinase Inhibitors. *Curr. Med. Chem.* **2011**, *2*, 2981–2994.
(54) Ferguson, F. M.; Gray, N. S. Kinase Inhibitors: The Road Ahead. *Nat. Rev. Drug Discov.* **2018**, *17* (5), 353–376.
(55) Tan, L.; Wang, J.; Tanizaki, J.; Huang, Z.; Aref, A. R.; Rusan, M.; Zhu, S.-J.; Zhang, Y.; Ercan, D.; Liao, R. G.; et al. Development of Covalent Inhibitors That Can Overcome Resistance to First-Generation FGFR Kinase Inhibitors. *Proc. Natl. Acad. Sci.* **2014**, *111* (45), E4869–E4877.
(56) Engel, J.; Lategahn, J.; Rauh, D. Hope and Disappointment: Covalent Inhibitors to Overcome Drug Resistance in Non-Small Cell Lung Cancer. *ACS Med. Chem. Lett.* **2016**, *7* (1), 2–5. 5.
(57) Zhou, W.; Ercan, D.; Chen, L.; Yun, C.-H.; Li, D.; Capelletti, M.; Cortot, A. B.; Chirieac, L.; Iacob, R. E.; Padera, R.; et al. Novel Mutant-Selective EGFR Kinase Inhibitors against EGFR T790M. *Nature* **2009**, *462* (7276), 1070–
(58) FAUVEL, B.; Yasri, A. Antibodies Directed against Receptor Tyrosine Kinases. *MAbs* **2014**, *6* (4), 838–851. https://doi.org/10.4161/mabs.29089.
(59) Ballantyne, A.; Dhillon, S. Trastuzumab Emtansine: First Global Approval. *Drugs* **2013**, *73* (7), 755–765.
(60) You, B.; Chen, E. X. Anti-EGFR Monoclonal Antibodies for Treatment of Colorectal Cancers: Development of Cetuximab and Panitumumab. *J. Clin. Pharmacol.* **2012**, *52* (2), 128–155.

(61) Garnock-Jones, K. P. Necitumumab: First Global Approval. *Drugs* **2016**, *76* (2), 283–289.
(62) Shirley, M. Olaratumab: First Global Approval. *Drugs* **2017**, *77* (1), 107–112.
(63) Itoh, N.; Ornitz, D. M. Fibroblast Growth Factors: From Molecular Evolution to Roles in Development, Metabolism and Disease. *J. Biochem.* **2011**, *149* (2), 121–130.
(64) Wilkie, A. O. M.; Patey, S. J.; Kan, S.; van den Ouweland, A. M. W.; Hamel, B. C. J. FGFs, Their Receptors, and Human Limb Malformations: Clinical and Molecular Correlations. *Am. J. Med. Genet.* **2002**, *112* (3), 266–278.
(65) Turner, N.; Grose, R. Fibroblast Growth Factor Signalling: From Development to Cancer. *Nat. Rev. Cancer* **2010**, *10* (2), 116–129.
(66) Basilico, C.; Moscatelli, D. The FGF Family of Growth Factors and Oncogenes. *Adv. Cancer Res.* **1992**, *59*, 115–165.
(67) Pitt, G. S.; Lee, S.-Y. Current View on Regulation of Voltage-Gated Sodium Channels by Calcium and Auxiliary Proteins. *Protein Sci.* **2016**, *25* (9), 1573–1584.
(68) Mohammadi, M.; Olsen, S. K.; Ibrahimi, O. A. Structural Basis for Fibroblast Growth Factor Receptor Activation. *Cytokine Growth Factor Rev.* **2005**, *16*, 107–137.
(69) Mohammadi, M.; Olsen, S. K.; Goetz, R. A Protein Canyon in the FGF–FGF Receptor Dimer Selects from an à La Carte Menu of Heparan Sulfate Motifs. *Curr. Opin. Struct. Biol.* **2005**, *15* (5), 506–516.
(70) Asada, M.; Shinomiya, M.; Suzuki, M.; Honda, E.; Sugimoto, R.; Ikekita, M.; Imamura, T. Glycosaminoglycan Affinity of the Complete Fibroblast Growth Factor Family. *Biochim. Biophys. Acta* **2009**, *1790* (1), 40–48.
(71) Yayon, A.; Klagsbrun, M.; Esko, J. D.; Leder, P.; Ornitz, D. M. Cell Surface, Heparin-like Molecules Are Required for Binding of Basic Fibroblast Growth Factor to Its High Affinity Receptor. *Cell* **1991**, *64* (4), 841–848.
(72) Belov, A. A.; Mohammadi, M. Molecular Mechanisms of Fibroblast Growth Factor Signaling in Physiology and Pathology. *Cold Spring Harb. Perspect. Biol.* **2013**, *5* (6).
(73) Wiedemann, M.; Trueb, B. Characterization of a Novel Protein (FGFRL1) from Human Cartilage Related to FGF Receptors. *Genomics* **2000**, *69* (2), 275–279.
(74) Stauber, D. J.; DiGabriele, A. D.; Hendrickson, W. A. Structural Interactions of Fibroblast Growth Factor Receptor with Its Ligands. *Proc. Natl. Acad. Sci. U. S. A.* **2000**, *97* (1), 49–54.
(75) Orr-Urtreger, A.; Bedford, M. T.; Burakova, T.; Arman, E.; Zimmer, Y.; Yayon, A.; Givol, D.; Lonai, P. Developmental Localization of the Splicing Alternatives of Fibroblast Growth Factor Receptor-2 (FGFR2). *Dev. Biol.* **1993**, *158* (2), 475–486.

(76) Schlessinger, J.; Plotnikov, A. N.; Ibrahimi, O. A.; Eliseenkova, A. V; Yeh, B. K.; Yayon, A.; Linhardt, R. J.; Mohammadi, M. Crystal Structure of a Ternary FGF-FGFR-Heparin Complex Reveals a Dual Role for Heparin in FGFR Binding and Dimerization. *Mol. Cell* **2000**, *6* (3), 743–750.

(77) Pellegrini, L.; Burke, D. F.; von Delft, F.; Mulloy, B.; Blundell, T. L. Crystal Structure of Fibroblast Growth Factor Receptor Ectodomain Bound to Ligand and Heparin. *Nature* **2000**, *407* (6807), 1029–1034.

(78) Kuro-o, M. Klotho and BKlotho. In *Advances in experimental medicine and biology*; 2012; Vol. 728, pp 25–40.

(79) Mohammadi, M.; Schlessinger, J.; Hubbard, S. R. Structure of the FGF Receptor Tyrosine Kinase Domain Reveals a Novel Autoinhibitory Mechanism. *Cell* **1996**, *86* (4), 577–587.

(80) Gotoh, N. Regulation of Growth Factor Signaling by FRS2 Family Docking/Scaffold Adaptor Proteins. *Cancer Sci.* **2008**, *99* (7), 1319–1325.

(81) Klint, P.; Claesson-Welsh, L. Signal Transduction by Fibroblast Growth Factor Receptors. *Front. Biosci.* **1999**, *4* (15), 165–177.

(82) Peters, K. G.; Marie, J.; Wilson, E.; Ives, H. E.; Escobedo, J.; Rosario, M. Del; Mirda, D.; Williams, L. T. Point Mutation of an FGF Receptor Abolishes Phosphatidylinositol Turnover and Ca2+ Flux but Not Mitogenesis. *Nature* **1992**, *358* (6388), 678–681.

(83) Hart, K. C.; Robertson, S. C.; Kanemitsu, M. Y.; Meyer, A. N.; Tynan, J. A.; Donoghue, D. J. Transformation and Stat Activation by Derivatives of FGFR1, FGFR3, and FGFR4. *Oncogene* **2000**, *19*, 3309–3320.

(84) Kang, S.; Elf, S.; Dong, S.; Hitosugi, T.; Lythgoe, K.; Guo, A.; Ruan, H.; Lonial, S.; Khoury, H. J.; Williams, I. R.; et al. Fibroblast Growth Factor Receptor 3 Associates with and Tyrosine Phosphorylates P90 RSK2, Leading to RSK2 Activation That Mediates Hematopoietic Transformation. *Mol. Cell. Biol.* **2009**, *29* (8), 2105–2117.

(85) Casci, T.; Vinós, J.; Freeman, M. Sprouty, an Intracellular Inhibitor of Ras Signaling. *Cell* **1999**, *96* (5), 655–665.

(86) Zhao, Y.; Zhang, Z.-Y. The Mechanism of Dephosphorylation of Extracellular Signal-Regulated Kinase 2 by Mitogen-Activated Protein Kinase Phosphatase 3. *J. Biol. Chem.* **2001**, *276* (34), 32382–32391.

(87) Tsang, M.; Friesel, R.; Kudoh, T.; Dawid, I. B. Identification of Sef, a Novel Modulator of FGF Signalling. *Nat. Cell Biol.* **2002**, *4* (2), 165–169.

(88) Monsonego-Ornan, E.; Adar, R.; Rom, E.; Yayon, A. FGF Receptors Ubiquitylation: Dependence on Tyrosine Kinase Activity and Role in Downregulation. *FEBS Lett.* **2002**, *528* (1–3), 83–89.

(89) Babina, I. S.; Turner, N. C. Advances and Challenges in Targeting FGFR Signalling in Cancer. *Nat. Publ. Gr.* **2017**, *17* (5), 318–332.

(90) Katoh, M. Fibroblast Growth Factor Receptors as Treatment Targets in

Clinical Oncology. *Nat. Rev. Clin. Oncol.* **2019**, *16* (2), 105–122..

(91) Liu, H.; Murphy, C. J.; Karreth, F. A.; Emdal, K. B.; White, F. M.; Elemento, O.; Toker, A.; Wulf, G. M.; Cantley, L. C. Identifying and Targeting Sporadic Oncogenic Genetic Aberrations in Mouse Models of Triple-Negative Breast Cancer. *Cancer Discov.* **2018**, *8* (3), 354–369.

(92) Nik-Zainal, S.; Davies, H.; Staaf, J.; Ramakrishna, M.; Glodzik, D.; Zou, X.; Martincorena, I.; Alexandrov, L. B.; Martin, S.; Wedge, D. C.; et al. Landscape of Somatic Mutations in 560 Breast Cancer Whole-Genome Sequences. *Nature* **2016**, *534* (7605), 47–54.

(93) Cihoric, N.; Savic, S.; Schneider, S.; Ackermann, I.; Bichsel-Naef, M.; Schmid, R. A.; Lardinois, D.; Gugger, M.; Bubendorf, L.; Zlobec, I.; et al. Prognostic Role of FGFR1 Amplification in Early-Stage Non-Small Cell Lung Cancer. *Br. J. Cancer* **2014**, *110* (12), 2914–2922.

(94) Hirsch, F. R.; Suda, K.; Wiens, J.; Bunn, P. A. New and Emerging Targeted Treatments in Advanced Non-Small-Cell Lung Cancer. *Lancet* **2016**, *388* (10048), 1012–1024.

(95) Jung, E.-J.; Jung, E.-J.; Min, S. Y.; Kim, M. A.; Kim, W. H. Fibroblast Growth Factor Receptor 2 Gene Amplification Status and Its Clinicopathologic Significance in Gastric Carcinoma. *Hum. Pathol.* **2012**, *43* (10), 1559–1566.

(96) di Martino, E.; Tomlinson, D. C.; Williams, S. V; Knowles, M. A. A Place for Precision Medicine in Bladder Cancer: Targeting the FGFRs. *Futur. Oncol.* **2016**, *12* (19), 2243–2263.

(97) Tanizaki, J.; Ercan, D.; Capelletti, M.; Dodge, M.; Xu, C.; Bahcall, M.; Tricker, E. M.; Butaney, M.; Calles, A.; Sholl, L. M.; et al. Identification of Oncogenic and Drug-Sensitizing Mutations in the Extracellular Domain of FGFR2. *Cancer Res.* **2015**, *75* (15), 3139–3146.

(98) di Martino, E.; L'Hôte, C. G.; Kennedy, W.; Tomlinson, D. C.; Knowles, M. A. Mutant Fibroblast Growth Factor Receptor 3 Induces Intracellular Signaling and Cellular Transformation in a Cell Type- and Mutation-Specific Manner. *Oncogene* **2009**, *28* (48), 4306–4316.

(99) Bernard-Pierrot, I.; Brams, A.; Dunois-Lardé, C.; Caillault, A.; Diez de Medina, S. G.; Cappellen, D.; Graff, G.; Thiery, J. P.; Chopin, D.; Ricol, D.; et al. Oncogenic Properties of the Mutated Forms of Fibroblast Growth Factor Receptor 3b. *Carcinogenesis* **2006**, *27* (4), 740–747.

(100) Glaser, A. P.; Fantini, D.; Shilatifard, A.; Schaeffer, E. M.; Meeks, J. J. The Evolving Genomic Landscape of Urothelial Carcinoma. *Nat. Rev. Urol.* **2017**, *14* (4), 215–229.

(101) Greenman, C.; Stephens, P.; Smith, R.; Dalgliesh, G. L.; Hunter, C.; Bignell, G.; Davies, H.; Teague, J.; Butler, A.; Stevens, C.; et al. Patterns of Somatic Mutation in Human Cancer Genomes. *Nature* **2007**, *446* (7132), 153–158.

(102) Wu, Y.-M.; Su, F.; Kalyana-Sundaram, S.; Khazanov, N.; Ateeq, B.; Cao, X.;

Lonigro, R. J.; Vats, P.; Wang, R.; Lin, S.-F.; et al. Identification of Targetable FGFR Gene Fusions in Diverse Cancers. *Cancer Discov.* **2013**, *3*, 636–647.

(103) Ha, G.-H.; Kim, J.-L.; Breuer, E.-K. Y. Transforming Acidic Coiled-Coil Proteins (TACCs) in Human Cancer. *Cancer Lett.* **2013**, *336* (1), 24–33.

(104) Gao, Q.; Liang, W.-W.; Foltz, S. M.; Mutharasu, G.; Jayasinghe, R. G.; Cao, S.; Liao, W.-W.; Reynolds, S. M.; Wyczalkowski, M. A.; Yao, L.; et al. Driver Fusions and Their Implications in the Development and Treatment of Human Cancers. *Cell Rep.* **2018**, *23* (1), 227-238.e3.

(105) Giacomini, A.; Matarazzo, S.; Pagano, K.; Ragona, L.; Rezzola, S.; Corsini, M.; Di Salle, E.; Presta, M.; Ronca, R. A Long Pentraxin-3-Derived Pentapeptide for the Therapy of FGF8b-Driven Steroid Hormone-Regulated Cancers. *Oncotarget* **2015**, *6* (15), 13790–13802.

(106) Ruotsalainen, T.; Joensuu, H.; Mattson, K.; Salven, P. High Pretreatment Serum Concentration of Basic Fibroblast Growth Factor Is a Predictor of Poor Prognosis in Small Cell Lung Cancer. *cancer Epidemiol. biomarkers Prev.* **2002**, *11*, 1492–1495.

(107) Nguyen, M.; Watanabe, H.; Budson, A. E.; Richie, J. P.; Hayes, D. F.; Folkman, J. Elevated Levels of an Angiogenic Peptide, Basic Fibroblast Growth Factor, in the Urine of Patients With a Wide Spectrum of Cancers. *J. Natl. Cancer Inst.* **1994**, *86* (5), 356–361.

(108) Lu, X.; Chen, H.; Patterson, A. V; Smaill, J. B.; Ding, K. Fibroblast Growth Factor Receptor 4 (FGFR4) Selective Inhibitors as Hepatocellular Carcinoma Therapy : Advances and Prospects Miniperspective. **2018**, *4*.

(109) Quintanal-Villalonga, A.; Ferrer, I.; Molina-Pinelo, S.; Paz-Ares, L. A Patent Review of FGFR4 Selective Inhibition in Cancer (2007-2018). *Expert Opin. Ther. Pat.* **2019**, *29* (6), 429–438.

(110) Giacomini, A.; Chiodelli, P.; Matarazzo, S.; Rusnati, M.; Presta, M.; Ronca, R. Blocking the FGF/FGFR System as a "Two-Compartment" Antiangiogenic/Antitumor Approach in Cancer Therapy. *Pharmacol. Res.* **2016**, *107*, 172–185.

(111) Allen, E.; Walters, I. B.; Hanahan, D. Brivanib, a Dual FGF/VEGF Inhibitor, Is Active Both First and Second Line against Mouse Pancreatic Neuroendocrine Tumors Developing Adaptive/Evasive Resistance to VEGF Inhibition. *Clin. Cancer Res.* **2011**, *17* (16), 5299–5310.

(112) Chae, Y. K.; Ranganath, K.; Hammerman, P. S.; Siddik, Z. H.; Mohindra, N.; Kalya, A.; Matsangou, M.; Costa, R.; Carneiro, B.; Villaflor, V. M.; et al. Inhibition of the Fibroblast Growth Factor Receptor (FGFR) Pathway: The Current Landscape and Barriers to Clinical Application. *Oncotarget* **2017**, *8* (9), 16052–16074.

(113) Man, W. Y.; Mak, J. P. Y.; Poon, R. Y. C. Dovitinib Induces Mitotic Defects and Activates the G2DNA Damage Checkpoint. *J. Cell. Mol. Med.* **2014**, *18*

(1), 143–155.
(114) Roth, G. J.; Binder, R.; Colbatzky, F.; Dallinger, C.; Schlenker-Herceg, R.; Hilberg, F.; Wollin, S. L.; Kaiser, R. Nintedanib: From Discovery to the Clinic. *J. Med. Chem.* **2015**, *58* (3), 1053–1063.
(115) Cabanillas, M. E.; Habra, M. A. Lenvatinib: Role in Thyroid Cancer and Other Solid Tumors. *Cancer Treat. Rev.* **2016**, *42*, 47–55.
(116) Hoshi, T.; Watanabe Miyano, S.; Watanabe, H.; Sonobe, R. M. K.; Seki, Y.; Ohta, E.; Nomoto, K.; Matsui, J.; Funahashi, Y. Lenvatinib Induces Death of Human Hepatocellular Carcinoma Cells Harboring an Activated FGF Signaling Pathway through Inhibition of FGFR–MAPK Cascades. *Biochem. Biophys. Res. Commun.* **2019**, *513* (1), 1–7. h
(117) Tucker, J. A.; Klein, T.; Breed, J.; Breeze, A. L.; Overman, R.; Phillips, C.; Norman, R. A. Structural Insights into FGFR Kinase Isoform Selectivity: Diverse Binding Modes of AZD4547 and Ponatinib in Complex with FGFR1 and FGFR4. *Structure* **2014**, *22* (12), 1764–1774. h
(118) Katoh, M. FGFR Inhibitors: Effects on Cancer Cells, Tumor Microenvironment and Whole-Body Homeostasis (Review). *Int. J. Mol. Med.* **2016**, *38* (1), 3–15.
(119) Gacche, R. N.; Meshram, R. J. Angiogenic Factors as Potential Drug Target: Efficacy and Limitations of Anti-Angiogenic Therapy. *Biochim. Biophys. Acta - Rev. Cancer* **2014**, *1846* (1), 161–179.
(120) Gavine, P. R.; Mooney, L.; Kilgour, E.; Thomas, A. P.; Al-Kadhimi, K.; Beck, S.; Rooney, C.; Coleman, T.; Baker, D.; Mellor, M. J.; et al. AZD4547: An Orally Bioavailable, Potent, and Selective Inhibitor of the Fibroblast Growth Factor Receptor Tyrosine Kinase Family. *Cancer Res.* **2012**, *72* (8), 2045–2056.
(121) Guagnano, V.; Furet, P.; Spanka, C.; Bordas, V.; Le Douget, M.; Stamm, C.; Brueggen, J.; Jensen, M. R.; Schnell, C.; Schmid, H.; et al. Discovery of 3-(2,6-Dichloro-3,5-Dimethoxy-Phenyl)-1-{6-[4-(4-Ethyl- Piperazin-1-Yl)-Phenylamino]-Pyrimidin-4-Yl}-1-Methyl-Urea (NVP-BGJ398), A Potent and Selective Inhibitor of the Fibroblast Growth Factor Receptor Family of Receptor Tyrosine Kinase. *J. Med. Chem.* **2011**, *54* (20), 7066–7083.
(122) Hierro, C.; Rodon, J.; Tabernero, J. Fibroblast Growth Factor (FGF) Receptor/FGF Inhibitors: Novel Targets and Strategies for Optimization of Response of Solid Tumors. *Semin. Oncol.* **2015**, *42* (6), 801–819.
(123) Zuccotto, F.; Ardini, E.; Casale, E.; Angiolini, M. Through the " Gatekeeper Door ": Exploiting the Active Kinase Conformation.*J. Med. Chem.* **2010**, 53, 2681–2694.
(124) Byron, S. A.; Chen, H.; Wortmann, A.; Loch, D.; Gartside, M. G.; Dehkhoda, F.; Blais, S. P.; Neubert, T. A.; Mohammadi, M.; Pollock, P. M. The N550K/H Mutations in FGFR2 Confer Differential Resistance to PD173074, Dovitinib, and Ponatinib ATP-Competitive Inhibitors. *Neoplasia*. **2013**, 15, 8, 975-988.

(125) Sohl, C. D.; Ryan, M. R.; Luo, B.; Frey, K. M.; Anderson, K. S. Illuminating the Molecular ,Mechanisms of Tyrosine Kinase Inhibitor Resistance for the FGFR1 Gatekeeper Mutation: The Achilles' Heel of Targeted Therapy. *ACS Chem. Biol.* **2015**, *10* (5), 1319–1329.

(126) Chell, V.; Balmanno, K.; Little, A. S.; Wilson, M.; Andrews, S.; Blockley, L.; Hampson, M.; Gavine, P. R.; Cook, S. J. Tumour Cell Responses to New Fibroblast Growth Factor Receptor Tyrosine Kinase Inhibitors and Identification of a Gatekeeper Mutation in FGFR3 as a Mechanism of Acquired Resistance. *Oncogene* **2012**, *32* (25), 3059–3070.

(127) Zhou, W.; Hur, W.; McDermott, U.; Dutt, A.; Xian, W.; Ficarro, S. B.; Zhang, J.; Sharma, S. V.; Brugge, J.; Meyerson, M.; et al. A Structure-Guided Approach to Creating Covalent FGFR Inhibitors. *Chem. Biol.* **2010**, *17* (3), 285–295.

(128) Huang, Z.; Tan, L.; Wang, H.; Liu, Y.; Blais, S.; Deng, J.; Neubert, T. A.; Gray, N. S.; Li, X.; Mohammadi, M. DFG-out Mode of Inhibition by an Irreversible Type-1 Inhibitor Capable of Overcoming Gate-Keeper Mutations in FGF Receptors. *ACS Chem. Biol.* **2015**, *10* (1), 299–309.

(129) Brameld, K. A.; Owens, T. D.; Verner, E.; Venetsanakos, E.; Bradshaw, J. M.; Phan, V. T.; Tam, D.; Leung, K.; Shu, J.; Lastant, J.; et al. Discovery of the Irreversible Covalent FGFR Inhibitor 8- (3-(4- Acryloylpiperazin-1-Yl)Propyl)-6-(2,6-Dichloro-3,5-Dimethoxyphenyl)- 2-(Methylamino)Pyrido[2,3- d]Pyrimidin-7(8H)one (PRN1371) for the Treatment of Solid Tumors. *J. Med. Chem.* **2017**, *60*, 6516–6527.

(130) Venetsanakos, E.; Brameld, K. A.; Phan, V. T.; Verner, E.; Owens, T. D.; Xing, Y.; Tam, D.; Lastant, J.; Leung, K.; Karr, D. E.; et al. The Irreversible Covalent Fibroblast Growth Factor Receptor Inhibitor PRN1371 Exhibits Sustained Inhibition of FGFR after Drug Clearance. *Mol. Cancer Ther.* **2017**, *16*, 2668–2677.

(131) Goyal, L.; Shi, L.; Liu, L. Y.; Cruz, F. F. de la; Lennerz, J. K.; Raghavan, S.; Leshchiner, I.; Elagina, L.; Siravegna, G.; Ng, R. W. S.; et al. TAS-120 Overcomes Resistance to ATP-Competitive FGFR Inhibitors in Patients with FGFR2 Fusion-Positive Intrahepatic Cholangiocarcinoma. *Cancer Discov.* **2019**, CD-19-0182.

(132) Knoepfel, T.; Furet, P.; Mah, R.; Buschmann, N.; Leblanc, C.; Ripoche, S.; Graus-Porta, D.; Wartmann, M.; Galuba, I.; Fairhurst, R. A. 2-Formylpyridyl Ureas as Highly Selective Reversible-Covalent Inhibitors of Fibroblast Growth Factor Receptor 4. *ACS Med. Chem. Lett.* **2018**, *9* (3), 215–220.

(133) Fairhurst, R. A.; Knoepfel, T.; Leblanc, C.; Buschmann, N.; Gaul, C.; Blank, J.; Galuba, I.; Trappe, J.; Zou, C.; Voshol, J.; et al. Approaches to Selective Fibroblast Growth Factor Receptor 4 Inhibition through Targeting the ATP-Pocket Middle-Hinge Region. *Medchemcomm* **2017**, *8* (8), 1604–1613.

(134) Quintanal-Villalonga, A.; Ferrer, I.; Molina-Pinelo, S.; Paz-Ares, L. A Patent Review of FGFR4 Selective Inhibition in Cancer (2007-2018). *Expert Opin. Ther. Pat.* **2007**, *29* (6), 429–438.
(135) Lu, X.; Chen, H.; Patterson, A. V.; Smaill, J. B.; Ding, K. Fibroblast Growth Factor Receptor 4 (FGFR4) Selective Inhibitors as Hepatocellular Carcinoma Therapy: Advances and Prospects. *J. Med. Chem.* **2018**, *4*.
(136) Joshi, J. J.; Coffey, H.; Corcoran, E.; Tsai, J.; Huang, C.; Ichikawa, K.; Prajapati, S.; Hao, M.; Bailey, S.; Wu, J.; et al. H3B-6527 Is a Potent and Selective Inhibitor of FGFR4 in FGF19-Driven Hepatocellular Carcinoma. *Cancer Res.* **2017**, *77*, 6999–7014.
(137) Chan, S. L.; Yen, C.-J.; Schuler, M.; Lin, C.-C.; Choo, S. P.; Weiss, K.-H.; Geier, A.; Okusaka, T.; Lim, H. Y.; Macarulla, T.; et al. Abstract CT106: Ph I/II Study of FGF401 in Adult Pts with HCC or Solid Tumors Characterized by FGFR4/KLB Expression. In *Clinical Trials*; American Association for Cancer Research, 2017; Vol. 77, pp CT106–CT106.
(138) Carmi, C.; Mor, M.; Petronini, P. G.; Alfieri, R. R. Clinical Perspectives for Irreversible Tyrosine Kinase Inhibitors in Cancer. *Biochem. Pharmacol.* **2012**, *84* (11), 1388–1399.
(139) Castelli, R.; Bozza, N.; Cavazzoni, A.; Bonelli, M.; Vacondio, F.; Ferlenghi, F.; Callegari, D.; Silva, C.; Rivara, S.; Lodola, A.; et al. Balancing Reactivity and Antitumor Activity: Heteroarylthioacetamide Derivatives as Potent and Time-Dependent Inhibitors of EGFR. *Eur. J. Med. Chem.* **2019**, *162*, 507–524.
(140) Gehringer, M.; Laufer, S. A. Emerging and Re-Emerging Warheads for Targeted Covalent Inhibitors: Applications in Medicinal Chemistry and Chemical Biology. *J. Med. Chem.* **2019**.
(141) Fumarola, C.; Bozza, N.; Castelli, R.; Ferlenghi, F.; Marseglia, G.; Lodola, A.; Bonelli, M.; La Monica, S.; Cretella, D.; Alfieri, R.; et al. Expanding the Arsenal of FGFR Inhibitors: A Novel Chloroacetamide Derivative as a New Irreversible Agent with Anti-Proliferative Activity against FGFR1-Amplified Lung Cancer Cell Lines. *Front. Oncol.* **2019**, *9*, 179.
(142) Presta, M.; Chiodelli, P.; Giacomini, A.; Rusnati, M.; Ronca, R. Fibroblast Growth Factors (FGFs) in Cancer: FGF Traps as a New Therapeutic Approach. *Pharmacol. Ther.* **2017**, *179*, 171–187. h
(143) Harding, T. C.; Long, L.; Palencia, S.; Zhang, H.; Sadra, A.; Hestir, K.; Patil, N.; Levin, A.; Hsu, A. W.; Charych, D.; et al. Blockade of Nonhormonal Fibroblast Growth Factors by FP-1039 Inhibits Growth of Multiple Types of Cancer. *Sci. Transl. Med.* **2013**, *5* (178), 178ra39-178ra39.
(144) Blackwell, C.; Sherk, C.; Fricko, M.; Ganji, G.; Barnette, M.; Hoang, B. B.; Tunstead, J.; Skedzielewski, T.; Alsaid, H.; Jucker, B. M.; et al. Inhibition of FGF/FGFR Autocrine Signaling in Mesothelioma with the FGF Ligand Trap,

FP-1039/GSK3052230. *Oncotarget* **2016**, *7* (26), 39861–39871.
(145) Tolcher, A. W.; Papadopoulos, K. P.; Patnaik, A.; Wilson, K.; Thayer, S.; Zanghi, J.; Gemo, A. T.; Kavanaugh, W. M.; Keer, H. N.; LoRusso, P. M. A Phase I, First in Human Study of FP-1039 (GSK3052230), a Novel FGF Ligand Trap, in Patients with Advanced Solid Tumors. *Ann. Oncol.* **2016**, *27* (3),
(146) Camozzi, M.; Rusnati, M.; Bugatti, A.; Bottazzi, B.; Mantovani, A.; Bastone, A.; Inforzato, A.; Vincenti, S.; Bracci, L.; Mastroianni, D.; et al. Identification of an Antiangiogenic FGF2-Binding Site in the N Terminus of the Soluble Pattern Recognition Receptor PTX3. *J. Biol. Chem.* **2006**, *281* (32), 22605–22613.
(147) Leali, D.; Bianchi, R.; Bugatti, A.; Nicoli, S.; Mitola, S.; Ragona, L.; Tomaselli, S.; Gallo, G.; Catello, S.; Rivieccio, V.; et al. Fibroblast Growth Factor 2-Antagonist Activity of a Long-Pentraxin 3-Derived Anti-Angiogenic Pentapeptide. *J. Cell. Mol. Med.* **2010**, *14* (8), 2109–2121.
(148) Ronca, R.; Giacomini, A.; Di Salle, E.; Coltrini, D.; Pagano, K.; Ragona, L.; Matarazzo, S.; Rezzola, S.; Maiolo, D.; Torrella, R.; et al. Long-Pentraxin 3 Derivative as a Small-Molecule FGF Trap for Cancer Therapy. *Cancer Cell* **2015**, *28* (2), 225–239.
(149) Colombo, G.; Margosio, B.; Ragona, L.; Neves, M.; Bonifacio, S.; Annis, D. S.; Stravalaci, M.; Tomaselli, S.; Giavazzi, R.; Rusnati, M.; et al. Non-Peptidic Thrombospondin-1 Mimics as Fibroblast Growth Factor-2 Inhibitors. An Integrated Strategy For Development Of New Antiangiogenic Compounds. *J. Biol. Chem.* **2010**, *285* (12), 8733–8742.
(150) Castelli, R.; Giacomini, A.; Anselmi, M.; Bozza, N.; Vacondio, F.; Rivara, S.; Matarazzo, S.; Presta, M.; Mor, M.; Ronca, R. Synthesis, Structural Elucidation, and Biological Evaluation of NSC12, an Orally Available Fibroblast Growth Factor (FGF) Ligand Trap for the Treatment of FGF-Dependent Lung Tumors. *J. Med. Chem.* **2016**, *59* (10), 4651–4663.
(151) Roskoski, R. The ErbB/HER Family of Protein-Tyrosine Kinases and Cancer. *Pharmacol. Res.* **2014**, *79*, 34–74. h
(152) Yarden, Y. The EGFR Family and Its Ligands in Human Cancer. Signalling Mechanisms and Therapeutic Opportunities. *Eur. J. cancer* **2001**, *37 Suppl 4*, S3-8.
(153) Normanno, N.; Bianco, C.; Strizzi, L.; Mancino, M.; Maiello, M.; Luca, A.; Caponigro, F.; Salomon, D. The ErbB Receptors and Their Ligands in Cancer: An Overview. *Curr. Drug Targets* **2005**, *6* (3), 243–257.
(154) Harris, R. C.; Chung, E.; Coffey, R. J. EGF Receptor Ligands. *Exp. Cell Res.* **2003**, *284* (1), 2–13.
(155) Ogiso, H.; Ishitani, R.; Nureki, O.; Fukai, S.; Yamanaka, M.; Kim, J.-H.; Saito, K.; Sakamoto, A.; Inoue, M.; Shirouzu, M.; et al. Crystal Structure of the Complex of Human Epidermal Growth Factor and Receptor Extracellular

Domains. *Cell* **2002**, *110* (6), 775–787.
(156) Bouyain, S.; Longo, P. A.; Li, S.; Ferguson, K. M.; Leahy, D. J. The Extracellular Region of ErbB4 Adopts a Tethered Conformation in the Absence of Ligand. *Proc. Natl. Acad. Sci.* **2005**, *102* (42), 15024–15029.
(157) Cho, H.-S.; Leahy, D. J. Structure of the Extracellular Region of HER3 Reveals an Interdomain Tether. *Science (80-.).* **2002**, *297* (5585), 1330–1333.
(158) Ferguson, K. M.; Berger, M. B.; Mendrola, J. M.; Cho, H. S.; Leahy, D. J.; Lemmon, M. A. EGF Activates Its Receptor by Removing Interactions That Autoinhibit Ectodomain Dimerization. *Mol. Cell* **2003**, *11* (2), 507–517.
(159) Burgess, A. W.; Cho, H.-S.; Eigenbrot, C.; Ferguson, K. M.; Garrett, T. P. J.; Leahy, D. J.; Lemmon, M. A.; Sliwkowski, M. X.; Ward, C. W.; Yokoyama, S. An Open-and-Shut Case? Recent Insights into the Activation of EGF/ErbB Receptors. *Mol. Cell* **2003**, *12* (3), 541–552.
(160) Cho, H.-S.; Mason, K.; Ramyar, K. X.; Stanley, A. M.; Gabelli, S. B.; Denney, D. W.; Leahy, D. J. Structure of the Extracellular Region of HER2 Alone and in Complex with the Herceptin Fab. *Nature* **2003**, *421* (6924), 756–760.
(161) Garrett, T. P. J.; McKern, N. M.; Lou, M.; Elleman, T. C.; Adams, T. E.; Lovrecz, G. O.; Kofler, M.; Jorissen, R. N.; Nice, E. C.; Burgess, A. W.; et al. The Crystal Structure of a Truncated ErbB2 Ectodomain Reveals an Active Conformation, Poised to Interact with Other ErbB Receptors. *Mol. Cell* **2003**, *11* (2), 495–505.
(162) Lemmon, M. A.; Schlessinger, J.; Ferguson, K. M. The EGFR Family: Not So Prototypical Receptor Tyrosine Kinases. *Cold Spring Harb. Perspect. Biol.* **2014**, *6* (4), a020768–a020768.
(163) Zhang, X.; Gureasko, J.; Shen, K.; Cole, P. A.; Kuriyan, J. An Allosteric Mechanism for Activation of the Kinase Domain of Epidermal Growth Factor Receptor. *Cell* **2006**, *125* (6), 1137–1149.
(164) Red Brewer, M.; Choi, S. H.; Alvarado, D.; Moravcevic, K.; Pozzi, A.; Lemmon, M. A.; Carpenter, G. The Juxtamembrane Region of the EGF Receptor Functions as an Activation Domain. *Mol. Cell* **2009**, *34* (6), 641–651.
(165) Yarden, Y.; Sliwkowski, M. X. Untangling the ErbB Signalling Network. *Nat. Rev. Mol. Cell Biol.* **2001**, *2* (2), 127–137.
(166) Wilson, K. J.; Gilmore, J. L.; Foley, J.; Lemmon, M. A.; Riese, D. J. Functional Selectivity of EGF Family Peptide Growth Factors: Implications for Cancer. *Pharmacol. Ther.* **2009**, *122* (1), 1–8.
(167) Xia, L.; Wang, L.; Chung, A. S.; Ivanov, S. S.; Ling, M. Y.; Dragoi, A. M.; Platt, A.; Gilmer, T. M.; Fu, X.-Y.; Chin, Y. E. Identification of Both Positive and Negative Domains within the Epidermal Growth Factor Receptor COOH-Terminal Region for Signal Transducer and Activator of Transcription (STAT) Activation. *J. Biol. Chem.* **2002**, *277* (34), 30716–30723.

(168) Yarden, Y.; Pines, G. The ERBB Network: At Last, Cancer Therapy Meets Systems Biology. *Nat. Rev. Cancer* **2012**, *12* (8), 553–563.
(169) Seshacharyulu, P.; Ponnusamy, M. P.; Haridas, D.; Jain, M.; Ganti, A. K.; Batra, S. K. Targeting the EGFR Signaling Pathway in Cancer Therapy. *Expert Opin. Ther. Targets* **2012**, *16* (1), 15–31.
(170) Slamon, D.; Godolphin, W.; Jones, L.; Holt, J.; Wong, S.; Keith, D.; Levin, W.; Stuart, S.; Udove, J.; Ullrich, A.; et al. Studies of the HER-2/Neu Proto-Oncogene in Human Breast and Ovarian Cancer. *Science (80-.).* **1989**, *244* (4905), 707–712.
(171) Batra, S. K.; Castelino-Prabhu, S.; Wikstrand, C. J.; Zhu, X.; Humphrey, P. A.; Friedman, H. S.; Bigner, D. D. Epidermal Growth Factor Ligand-Independent, Unregulated, Cell-Transforming Potential of a Naturally Occurring Human Mutant EGFRvIII Gene. *Cell growth Differ.* **1995**, *6* (10), 1251–1259.
(172) Fontanini, G.; De Laurentiis, M.; Vignati, S.; Chinè, S.; Lucchi, M.; Silvestri, V.; Mussi, A.; De Placido, S.; Tortora, G.; Bianco, A. R.; et al. Evaluation of Epidermal Growth Factor-Related Growth Factors and Receptors and of Neoangiogenesis in Completely Resected Stage I-IIIA Non-Small-Cell Lung Cancer: Amphiregulin and Microvessel Count Are Independent Prognostic Indicators of Survival. *Clin. cancer Res.* **1998**, *4* (1), 241–249.
(173) Sharma, S. V.; Bell, D. W.; Settleman, J.; Haber, D. A. Epidermal Growth Factor Receptor Mutations in Lung Cancer. *Nat. Rev. Cancer* **2007**, *7* (3), 169–181.
(174) Maemondo, M.; Inoue, A.; Kobayashi, K.; Sugawara, S.; Oizumi, S.; Isobe, H.; Gemma, A.; Harada, M.; Yoshizawa, H.; Kinoshita, I.; et al. Gefitinib or Chemotherapy for Non–Small-Cell Lung Cancer with Mutated EGFR. *N. Engl. J. Med.* **2010**, *362* (25), 2380–2388.
(175) Moyer, J. D.; Barbacci, E. G.; Iwata, K. K.; Arnold, L.; Boman, B.; Cunningham, A.; DiOrio, C.; Doty, J.; Morin, M. J.; Moyer, M. P.; et al. Induction of Apoptosis and Cell Cycle Arrest by CP-358,774, an Inhibitor of Epidermal Growth Factor Receptor Tyrosine Kinase. *Cancer Res.* **1997**, *57* (21), 4838–4848.
(176) Lynch, T. J.; Bell, D. W.; Sordella, R.; Gurubhagavatula, S.; Okimoto, R. A.; Brannigan, B. W.; Harris, P. L.; Haserlat, S. M.; Supko, J. G.; Haluska, F. G.; et al. Activating Mutations in the Epidermal Growth Factor Receptor Underlying Responsiveness of Non–Small-Cell Lung Cancer to Gefitinib. *N. Engl. J. Med.* **2004**, *350* (21), 2129–2139.
(177) Chan, S. K.; Gullick, W. J.; Hill, M. E. Mutations of the Epidermal Growth Factor Receptor in Non-Small Cell Lung Cancer – Search and Destroy. *Eur. J. Cancer* **2006**, *42* (1), 17–23.
(178) Brewer, M. R.; Yun, C.-H.; Lai, D.; Lemmon, M. A.; Eck, M. J.; Pao, W. Mechanism for Activation of Mutated Epidermal Growth Factor Receptors

in Lung Cancer. *Proc. Natl. Acad. Sci. U. S. A.* **2013**, *110* (38), E3595.

(179) Yun, C.-H.; Boggon, T. J.; Li, Y.; Woo, M. S.; Greulich, H.; Meyerson, M.; Eck, M. J. Structures of Lung Cancer-Derived EGFR Mutants and Inhibitor Complexes: Mechanism of Activation and Insights into Differential Inhibitor Sensitivity. *Cancer Cell* **2007**, *11* (3), 217–227.

(180) Stamos, J.; Sliwkowski, M. X.; Eigenbrot, C. Structure of the Epidermal Growth Factor Receptor Kinase Domain Alone and in Complex with a 4-Anilinoquinazoline Inhibitor. *J. Biol. Chem.* **2002**, *277* (48), 46265–46272.

(181) Park, J. H.; Liu, Y.; Lemmon, M. A.; Radhakrishnan, R. Erlotinib Binds Both Inactive and Active Conformations of the EGFR Tyrosine Kinase Domain. *Biochem. J.* **2012**, *448* (3), 417–423.

(182) Kobayashi, S.; Boggon, T. J.; Dayaram, T.; Jänne, P. A.; Kocher, O.; Meyerson, M.; Johnson, B. E.; Eck, M. J.; Tenen, D. G.; Halmos, B. EGFR Mutation and Resistance of Non–Small-Cell Lung Cancer to Gefitinib. *N. Engl. J. Med.* **2005**, *352* (8), 786–792.

(183) Pao, W.; Miller, V. A.; Politi, K. A.; Riely, G. J.; Somwar, R.; Zakowski, M. F.; Kris, M. G.; Varmus, H. Acquired Resistance of Lung Adenocarcinomas to Gefitinib or Erlotinib Is Associated with a Second Mutation in the EGFR Kinase Domain. *PLoS Med.* **2005**, *2* (3), e73.

(184) Yun, C.-H.; Mengwasser, K. E.; Toms, A. V.; Woo, M. S.; Greulich, H.; Wong, K.-K.; Meyerson, M.; Eck, M. J. The T790M Mutation in EGFR Kinase Causes Drug Resistance by Increasing the Affinity for ATP. *Proc. Natl. Acad. Sci.* **2008**, *105* (6), 2070–2075.

(185) Arcila, M. E.; Oxnard, G. R.; Nafa, K.; Riely, G. J.; Solomon, S. B.; Zakowski, M. F.; Kris, M. G.; Pao, W.; Miller, V. A.; Ladanyi, M. Rebiopsy of Lung Cancer Patients with Acquired Resistance to EGFR Inhibitors and Enhanced Detection of the T790M Mutation Using a Locked Nucleic Acid-Based Assay. *Clin. Cancer Res.* **2011**, *17* (5), 1169–1180.

(186) Giaccone, G.; Wang, Y. Strategies for Overcoming Resistance to EGFR Family Tyrosine Kinase Inhibitors. *Cancer Treat. Rev.* **2011**, *37* (6), 456–464.

(187) Oxnard, G. R.; Arcila, M. E.; Chmielecki, J.; Ladanyi, M.; Miller, V. A.; Pao, W. New Strategies in Overcoming Acquired Resistance to Epidermal Growth Factor Receptor Tyrosine Kinase Inhibitors in Lung Cancer. *Clin. Cancer Res.* **2011**, *17* (17), 5530–5537.

(188) Kwak, E. L.; Sordella, R.; Bell, D. W.; Godin-Heymann, N.; Okimoto, R. A.; Brannigan, B. W.; Harris, P. L.; Driscoll, D. R.; Fidias, P.; Lynch, T. J.; et al. Irreversible Inhibitors of the EGF Receptor May Circumvent Acquired Resistance to Gefitinib. *Proc. Natl. Acad. Sci.* **2005**, *102* (21), 7665–7670..

(189) Jeff B. Smaill, †; Brian D. Palmer, †; Gordon W. Rewcastle, †; William A. Denny, *, †; Dennis J. McNamara, ‡; Ellen M. Dobrusin, ‡; Alexander J. Bridges, ‡; Hairong Zhou, ‡; H. D. Hollis Showalter, ‡; R. Thomas Winters, ‡;

et al. 4-(Phenylamino)Quinazoline and 4-(Phenylamino)Pyrido[d]Pyrimidine Acrylamides as Irreversible Inhibitors of the ATP Binding Site of the Epidermal Growth Factor Receptor. *J. Med. Chem.* **1999**, *42* (10), 1803–1815.

(190) Smaill, J. B.; Rewcastle, G. W.; Loo, J. A.; Greis, K. D.; Chan, O. H.; Reyner, E. L.; Lipka, E.; Showalter, H. D. H.; Vincent, P. W.; Elliott, W. L.; et al. Irreversible Inhibitors of the Epidermal Growth Factor Receptor: 4-(Phenylamino)Quinazoline- and 4-(Phenylamino)Pyrido[3,2- *d*]Pyrimidine-6-Acrylamides Bearing Additional Solubilizing Functions. *J. Med. Chem.* **2000**, *43* (7), 1380–1397.

(191) Yang, J. C.-H.; Shih, J.-Y.; Su, W.-C.; Hsia, T.-C.; Tsai, C.-M.; Ou, S.-H. I.; Yu, C.-J.; Chang, G.-C.; Ho, C.-L.; Sequist, L. V; et al. Afatinib for Patients with Lung Adenocarcinoma and Epidermal Growth Factor Receptor Mutations (LUX-Lung 2): A Phase 2 Trial. *Lancet Oncol.* **2012**, *13* (5), 539–548.

(192) Sequist, L. V; Besse, B.; Lynch, T. J.; Miller, V. A.; Wong, K. K.; Gitlitz, B.; Eaton, K.; Zacharchuk, C.; Freyman, A.; Powell, C.; et al. Neratinib, an Irreversible Pan-ErbB Receptor Tyrosine Kinase Inhibitor: Results of a Phase II Trial in Patients with Advanced Non-Small-Cell Lung Cancer. *J. Clin. Oncol.* **2010**, *28* (18), 3076–3083.

(193) Sos, M. L.; Rode, H. B.; Heynck, S.; Peifer, M.; Fischer, F.; Klüter, S.; Pawar, V. G.; Reuter, C.; Heuckmann, J. M.; Weiss, J.; et al. Chemogenomic Profiling Provides Insights into the Limited Activity of Irreversible EGFR Inhibitors in Tumor Cells Expressing the T790M EGFR Resistance Mutation. *Cancer Res.* **2010**, *70* (3), 868–874.

(194) Lu, X.; Yu, L.; Zhang, Z.; Ren, X.; Smaill, J. B.; Ding, K. Targeting EGFRL858R/T790M and EGFRL858R/T790M/C797S Resistance Mutations in NSCLC: Current Developments in Medicinal Chemistry. *Med. Res. Rev.* **2018**, *38* (5), 1550–1581.

(195) Song, Z.; Ge, Y.; Wang, C.; Huang, S.; Shu, X.; Liu, K.; Zhou, Y.; Ma, X. Challenges and Perspectives on the Development of Small-Molecule EGFR Inhibitors against T790M-Mediated Resistance in Non-Small-Cell Lung Cancer: Miniperspective. *J. Med. Chem.* **2016**, *59* (14), 6580–6594.

(196) Chen, L.; Fu, W.; Zheng, L.; Liu, Z.; Liang, G. Recent Progress of Small-Molecule Epidermal Growth Factor Receptor (EGFR) Inhibitors against C797S Resistance in Non-Small-Cell Lung Cancer. *J. Med. Chem.* **2018**, *61* (10), 4290–4300. https://doi.org/10.1021/acs.jmedchem.7b01310.

(197) Finlay, M. R. V.; Anderton, M.; Ashton, S.; Ballard, P.; Bethel, P. A.; Box, M. R.; Bradbury, R. H.; Brown, S. J.; Butterworth, S.; Campbell, A.; et al. Discovery of a Potent and Selective EGFR Inhibitor (AZD9291) of Both Sensitizing and T790M Resistance Mutations That Spares the Wild Type Form of the Receptor. *J. Med. Chem.* **2014**, *57* (20), 8249–8267.

(198) Walter, A. O.; Sjin, R. T. T.; Haringsma, H. J.; Ohashi, K.; Sun, J.; Lee, K.; Dubrovskiy, A.; Labenski, M.; Zhu, Z.; Wang, Z.; et al. Discovery of a Mutant-Selective Covalent Inhibitor of EGFR That Overcomes T790M-Mediated Resistance in NSCLC. *Cancer Discov.* **2013**, *3* (12), 1404–1415.

(199) Lee, K.-O.; Cha, M. Y.; Kim, M.; Song, J. Y.; Lee, J.-H.; Kim, Y. H.; Lee, Y.-M.; Suh, K. H.; Son, J. Discovery of HM61713 as an Orally Available and Mutant EGFR Selective Inhibitor. In *Experimental and Molecular Therapeutics*; American Association for Cancer Research, 2014; Vol. 74, p LB-100-LB-100.

(200) Thress, K. S.; Paweletz, C. P.; Felip, E.; Cho, B. C.; Stetson, D.; Dougherty, B.; Lai, Z.; Markovets, A.; Vivancos, A.; Kuang, Y.; et al. Acquired EGFR C797S Mutation Mediates Resistance to AZD9291 in Non-Small Cell Lung Cancer Harboring EGFR T790M. *Nat. Med.* **2015**, *21* (6), 560–562.

(201) Callegari, D.; Ranaghan, K. E.; Woods, C. J.; Minari, R.; Tiseo, M.; Mor, M.; Mulholland, A. J.; Lodola, A. L718Q Mutant EGFR Escapes Covalent Inhibition by Stabilizing a Non-Reactive Conformation of the Lung Cancer Drug Osimertinib. *Chem. Sci.* **2018**, *9* (10), 2740–2749.

(202) Chabon, J. J.; Simmons, A. D.; Lovejoy, A. F.; Esfahani, M. S.; Newman, A. M.; Haringsma, H. J.; Kurtz, D. M.; Stehr, H.; Scherer, F.; Karlovich, C. A.; et al. Circulating Tumour DNA Profiling Reveals Heterogeneity of EGFR Inhibitor Resistance Mechanisms in Lung Cancer Patients. *Nat. Commun.* **2016**, *7* (1), 11815.

(203) Patel, H.; Pawara, R.; Ansari, A.; Surana, S. Recent Updates on Third Generation EGFR Inhibitors and Emergence of Fourth Generation EGFR Inhibitors to Combat C797S Resistance. *Eur. J. Med. Chem.* **2017**, *142*, 32–47.

(204) Ke, E.; Wu, Y.-L. EGFR as a Pharmacological Target in EGFR -Mutant Non-Small-Cell Lung Cancer: Where Do We Stand Now? *Trends Pharmacol. Sci.* **2016**, *37* (11), 887–903.

(205) Nie, K.; Zhang, Z.; Zhang, C.; Lan, K.; Ji, Y. Effect of EGFR C797S/G Mutation on Osimertinib Resistance in Chinese Patients with Non-Small-Cell Lung Cancer. *J. Clin. Oncol.* **2018**, *36* (15_suppl), e21171–e21171.

(206) Ou, S.-H. I.; Agarwal, N.; Ali, S. M. High MET Amplification Level as a Resistance Mechanism to Osimertinib (AZD9291) in a Patient That Symptomatically Responded to Crizotinib Treatment Post-Osimertinib Progression. *Lung Cancer* **2016**, *98*, 59–61.

(207) Planchard, D.; Loriot, Y.; André, F.; Gobert, A.; Auger, N.; Lacroix, L.; Soria, J. C. EGFR-Independent Mechanisms of Acquired Resistance to AZD9291 in EGFR T790M-Positive NSCLC Patients. *Ann. Oncol.* **2015**, *26* (10), 2073–2078.

(208) Thress, K. S.; Paweletz, C. P.; Felip, E.; Cho, B. C.; Stetson, D.; Dougherty, B.; Lai, Z.; Markovets, A.; Vivancos, A.; Kuang, Y.; et al. Acquired EGFR C797S

Mutation Mediates Resistance to AZD9291 in Non-Small Cell Lung Cancer Harboring EGFR T790M. *Nat. Med.* **2015**, *21* (6), 560–562.

(209) Zhao, Q.; Ouyang, X.; Wan, X.; Gajiwala, K. S.; Kath, J. C.; Jones, L. H.; Burlingame, A. L.; Taunton, J. Broad-Spectrum Kinase Profiling in Live Cells with Lysine-Targeted Sulfonyl Fluoride Probes. *J. Am. Chem. Soc.* **2017**, *139* (2), 680–685.

(210) Anscombe, E.; Meschini, E.; Mora-Vidal, R.; Martin, M. P.; Staunton, D.; Geitmann, M.; Danielson, U. H.; Stanley, W. A.; Wang, L. Z.; Reuillon, T.; et al. Identification and Characterization of an Irreversible Inhibitor of CDK2. *Chem. Biol.* **2015**, *22* (9), 1159–1164.

(211) Huang, W.-S.; Liu, S.; Zou, D.; Thomas, M.; Wang, Y.; Zhou, T.; Romero, J.; Kohlmann, A.; Li, F.; Qi, J.; et al. Discovery of Brigatinib (AP26113), a Phosphine Oxide-Containing, Potent, Orally Active Inhibitor of Anaplastic Lymphoma Kinase. *J. Med. Chem.* **2016**, *59* (10), 4948–4964.

(212) GOLDSTEIN, D. M.; GONG, L.; MICHOUD, C.; PALMER, W. S.; SIDDURI, A. BENZOTRIAZOLE KINASE MODULATORS. WO2008028860, March 13, 2008.

(213) Marvel, C. S.; Sparberg, M. S. SODIUM 2-BROMOETHANESULFONATE. *Org. Synth.* **1930**, *10*, 96.

(214) Grimster, N. P.; Connelly, S.; Baranczak, A.; Dong, J.; Krasnova, L. B.; Sharpless, K. B.; Powers, E. T.; Wilson, I. A.; Kelly, J. W. Aromatic Sulfonyl Fluorides Covalently Kinetically Stabilize Transthyretin to Prevent Amyloidogenesis While Affording a Fluorescent Conjugate. *J. Am. Chem. Soc.* **2013**, *135* (15), 5656–5668.

(215) Dong, J.; Krasnova, L.; Finn, M. G.; Barry Sharpless, K. Sulfur(VI) Fluoride Exchange (SuFEx): Another Good Reaction for Click Chemistry. *Angew. Chemie - Int. Ed.* **2014**, *53* (36), 9430–9448.

(216) Hayes, J. D.; Dinkova-Kostova, A. T. The Nrf2 Regulatory Network Provides an Interface between Redox and Intermediary Metabolism. *Trends Biochem. Sci.* **2014**, *39* (4), 199–218.

(217) Rushmore, T. H.; Morton$, M. R.; Pickett, C. B. The Antioxidant Responsive Element . **1991**, *266* (18), 11632–11639.

(218) Motohashi, H.; Yamamoto, M. Nrf2-Keap1 Defines a Physiologically Important Stress Response Mechanism. *Trends in Molecular Medicine*. November 2004, pp 549–557.

(219) Nioi, P.; Nguyen, T.; Sherratt, P. J.; Pickett, C. B. The Carboxy-Terminal Neh3 Domain of Nrf2 Is Required for Transcriptional Activation. *Mol. Cell. Biol.* **2005**, *25* (24), 10895–10906.

(220) Canning, P.; Sorrell, F. J.; Bullock, A. N. Structural Basis of Keap1 Interactions with Nrf2. *Free Radical Biology and Medicine*. Elsevier Inc. 2015, pp 101–107.

(221) McMahon, M.; Thomas, N.; Itoh, K.; Yamamoto, M.; Hayes, J. D.

Dimerization of Substrate Adaptors Can Facilitate Cullin-Mediated Ubiquitylation of Proteins by a "Tethering" Mechanism: A Two-Site Interaction Model for the Nrf2-Keap1 Complex. *J. Biol. Chem.* **2006**, *281* (34), 24756–24768.

(222) Cullinan, S. B.; Gordan, J. D.; Jin, J.; Harper, J. W.; Diehl, J. A. The Keap1-BTB Protein Is an Adaptor That Bridges Nrf2 to a Cul3-Based E3 Ligase: Oxidative Stress Sensing by a Cul3-Keap1 Ligase. *Mol. Cell. Biol.* **2004**, *24* (19), 8477–8486.

(223) Tong, K. I.; Katoh, Y.; Kusunoki, H.; Itoh, K.; Tanaka, T.; Yamamoto, M. Keap1 Recruits Neh2 through Binding to ETGE and DLG Motifs: Characterization of the Two-Site Molecular Recognition Model. *Mol. Cell. Biol.* **2006**, *26* (8), 2887–2900.

(224) Baird, L.; Swift, S.; Llères, D.; Dinkova-Kostova, A. T. Monitoring Keap1-Nrf2 Interactions in Single Live Cells. *Biotechnology Advances*. Elsevier Inc. 2014, pp 1133–1144.

(225) Yamamoto, M.; Kensler, T. W.; Motohashi, H. The KEAP1-NRF2 System: A Thiol-Based Sensor-Effector Apparatus for Maintaining Redox Homeostasis. *Physiol. Rev.* **2018**, *98* (3), 1169–1203.

(226) Cuadrado, A.; Rojo, A. I.; Wells, G.; Hayes, J. D.; Cousin, S. P.; Rumsey, W. L.; Attucks, O. C.; Franklin, S.; Levonen, A. L.; Kensler, T. W.; et al. Therapeutic Targeting of the NRF2 and KEAP1 Partnership in Chronic Diseases. *Nat. Rev. Drug Discov.* **2019**, *18* (4), 295–317.

(227) Adibhatla, R. M.; Hatcher, J. F. Lipid Oxidation and Peroxidation in CNS Health and Disease: From Molecular Mechanisms to Therapeutic Opportunities. *Antioxid. Redox Signal.* **2010**, *12* (1), 125–169.

(228) Magesh, S.; Chen, Y.; Hu, L. Small Molecule Modulators of Keap1-Nrf2-ARE Pathway as Potential Preventive and Therapeutic Agents. *Med. Res. Rev.* **2012**, *32* (4), 687–726.

(229) Lapchak, P. A. . Z. J. H. *Neuroprotective Therapy for Stroke and Ischemic Disease | Paul A. Lapchak | Springer*; 2017.

(230) Pallesen, J. S.; Tran, K. T.; Bach, A. Non-Covalent Small-Molecule Kelch-like ECH-Associated Protein 1-Nuclear Factor Erythroid 2-Related Factor 2 (Keap1-Nrf2) Inhibitors and Their Potential for Targeting Central Nervous System Diseases. *J. Med. Chem.* **2018**, *61* (18), 8088–8103.

(231) Wilson, A. J.; Kerns, J. K.; Callahan, J. F.; Moody, C. J. Keap Calm, and Carry on Covalently. *J. Med. Chem.* **2013**, *56* (19), 7463–7476.

(232) Linker, R. A.; Lee, D.-H.; Ryan, S.; van Dam, A. M.; Conrad, R.; Bista, P.; Zeng, W.; Hronowsky, X.; Buko, A.; Chollate, S.; et al. Fumaric Acid Esters Exert Neuroprotective Effects in Neuroinflammation via Activation of the Nrf2 Antioxidant Pathway. *Brain* **2011**, *134* (Pt 3), 678–692.

(233) Lo, S.-C.; Li, X.; Henzl, M. T.; Beamer, L. J.; Hannink, M. Structure of the

Keap1:Nrf2 Interface Provides Mechanistic Insight into Nrf2 Signaling. *EMBO J.* **2006**, *25* (15), 3605–3617.

(234) Tong, K. I.; Padmanabhan, B.; Kobayashi, A.; Shang, C.; Hirotsu, Y.; Yokoyama, S.; Yamamoto, M. Different Electrostatic Potentials Define ETGE and DLG Motifs as Hinge and Latch in Oxidative Stress Response. *Mol. Cell. Biol.* **2007**, *27* (21), 7511–7521.

(235) Tran, K. T.; Pallesen, J. S.; Solbak, S. M. Ø.; Narayanan, D.; Baig, A.; Zang, J.; Aguayo-Orozco, A.; Carmona, R. M. C.; Garcia, A. D.; Bach, A. A Comparative Assessment Study of Known Small-Molecule Keap1−Nrf2 Protein–Protein Interaction Inhibitors: Chemical Synthesis, Binding Properties, and Cellular Activity. *J. Med. Chem.* **2019**, *62* (17), 8028–8052.

(236) Davies, T. G.; Wixted, W. E.; Coyle, J. E.; Griffiths-Jones, C.; Hearn, K.; McMenamin, R.; Norton, D.; Rich, S. J.; Richardson, C.; Saxty, G.; et al. Monoacidic Inhibitors of the Kelch-like ECH-Associated Protein 1: Nuclear Factor Erythroid 2-Related Factor 2 (KEAP1:NRF2) Protein-Protein Interaction with High Cell Potency Identified by Fragment-Based Discovery. *J. Med. Chem.* **2016**, *59* (8), 3991–4006.

(237) Winkel, A. F.; Engel, C. K.; Margerie, D.; Kannt, A.; Szillat, H.; Glombik, H.; Kallus, C.; Ruf, S.; Güssregen, S.; Riedel, J.; et al. Characterization of RA839, a Noncovalent Small Molecule Binder to Keap1 and Selective Activator of Nrf2 Signaling. *J. Biol. Chem.* **2015**, *290* (47), 28446–28455.

(238) Wager, T. T.; Chandrasekaran, R. Y.; Hou, X.; Troutman, M. D.; Verhoest, P. R.; Villalobos, A.; Will, Y. Defining Desirable Central Nervous System Drug Space through the Alignment of Molecular Properties, in Vitro ADME, and Safety Attributes. *ACS Chem. Neurosci.* **2010**, *1* (6), 420–434.

(239) Lu, M. C.; Tan, S. J.; Ji, J. A.; Chen, Z. Y.; Yuan, Z. W.; You, Q. D.; Jiang, Z. Y. Polar Recognition Group Study of Keap1-Nrf2 Protein-Protein Interaction Inhibitors. *ACS Med. Chem. Lett.* **2016**, *7* (9), 835–840.

(240) Lassalas, P.; Gay, B.; Lasfargeas, C.; James, M. J.; Tran, V.; Vijayendran, K. G.; Brunden, K. R.; Kozlowski, M. C.; Thomas, C. J.; Smith, A. B.; et al. Structure Property Relationships of Carboxylic Acid Isosteres. *J. Med. Chem.* **2016**, *59* (7), 3183–3203.

(241) Ballatore, C.; Huryn, D. M.; Smith, A. B. Carboxylic Acid (Bio)Isosteres in Drug Design. *ChemMedChem* **2013**, *8* (3), 385–395.